A distributed parsimonious event-based model for flood forecasting in Mediterranean catchments : efficiency of the model and spatial variability of the parameters

Quoc Son Nguyen

THÈSE POUR OBTENIR LE GRADE DE DOCTEUR DE L'UNIVERSITÉ DE MONTPELLIER

En Sciences de l'Eau

École doctorale GAIA

Unité de recherche : Laboratoire Hydrosciences Montpellier

Application du modèle distribué événementiel SCS-LR pour la prévision des crues méditerranéennes : performances du modèle et variabilité spatiale des paramètres

Présentée par Quoc Son NGUYEN

Le 4 juillet 2019

Sous la direction de Dr. Christophe BOUVIER

Devant le jury composé de

Sandrine ANQUETIN, Directrice de Recherche CNRS, IGE, Grenoble	Rapporteure
Hélène ROUX, Maître de Conférences INPT, IMFT, Toulouse	Rapporteure
Patrick ARNAUD, Ingénieur de Recherche IRSTEA, Aix en Provence	Examinateur
Roger MOUSSA, Directeur de Recherche INRA, LISAH, Montpellier	Examinateur, Président du jury
Olivier PAYRASTRE, Ingénieur Divisionnaire TPE, IFSTTAR, Bouguenais	Examinateur
Christophe BOUVIER, Directeur de Recherche IRD, HSM, Montpellier	Directeur de thèse

UNIVERSITÉ DE MONTPELLIER

Acknowledgments

I would like to express my sincere appreciation and thanks to my supervisor Dr. Christophe Bouvier for the continuous support of my study. I would like to thank you for encouraging my research and for allowing me to grow as a research scientist. Your advice on both research as well as on my career have been invaluable.

I would like to thank the rest of my thesis committee: Dr. Roger Moussa, Dr. Ludovic Oudin, Dr. Lea Garandeau and Dr. Patrick Arnaud for their insightful comments and for the question which incented me to widen my research from various perspectives. I would also be thankful to Dr. Sandrine Anquetin, Dr. Hélène Roux, Dr. Roger Moussa, Dr. Patrick Arnaud, and Dr. Olivier Payrastre to accept to be in my jury.

I am also grateful for the Vietnam International Education Development, University of Science and Technology of Hanoi, Campus France, and SCHAPI for providing the financial support to stay in France and pursue this Ph.D. study.

I would especially like to thank the University Montpellier and HSM and IRSTEA to provide all the supports in terms of workspace, computers, data and facilitating all the paper works that allow my researches, as well as my stay in France.

I am also thankful to Dr. Valérie Borrell Estupina for giving me the opportunity to come to France and pursuing my studies in Hydrology, as well as giving me valuable support during my first day here.

I am also thankful for my fellow labmates: Aubin Allies, Camille Jourdan and others for the stimulating discussions, for all the help and all the fun we have had in the last three years; to Madame Catherine Marchand to help me with the administration. Also, I thank all my Vietnamese friends in Marseille and Montpellier for all the supports in life.

Last but not least, I would like to thank my family: my parents, my brother, my beloved wife and my expected daughter for supporting me spiritually throughout writing this thesis and my life in general.

Résumé

Les modèles pluie-débit sont des outils essentiels pour de nombreuses applications hydrologiques, notamment la prévision des crues. L'objet de cette thèse est d'examiner les performances d'un modèle événementiel distribué, dont l'intérêt est de résumer la représentation des processus à la phase de crue, et la condition initiale à un indice de saturation du bassin facilement observable ou accessible. Ce dernier dispense de modéliser la phase inter-crue, et simplifie la paramétrisation et le calage du modèle. Le modèle étudié combine une fonction de production type SCS et une fonction de transfert type lag and route, appliquées à une discrétisation du bassin en mailles carrées régulières.

Le modèle est d'abord testé sur le bassin versant du Real Collobrier. Ce bassin méditerranéen est suivi depuis plus de 50 ans par l'IRSTEA, et dispose d'une exceptionnelle densité de mesures de pluies et de débits. Cet environnement favorable permet de limiter les incertitudes sur l'estimation des pluies et d'évaluer les performances intrinsèques du modèle. Dans ces conditions, les crues sont bien reconstituées à l'aide d'un jeu de paramètres unique pour l'ensemble des épisodes testés, à l'exception de la condition initiale du modèle. Celle-ci apparaît fortement corrélée avec l'humidité du sol en début d'épisode, et peut être prédéterminée de façon satisfaisante par le débit de base ou l'indice w_2 fourni par le modèle SIM de Météo-France. Les performances du modèle sont ensuite étudiées en dégradant la densité des pluviomètres, et rendent compte du niveau de performances du modèle dans les cas que l'on rencontre le plus souvent.

La variabilité spatiale des paramètres du modèle est étudiée à l'échelle de différents sous-bassins du Real Collobrier. La comparaison a permis de mettre en évidence et de corriger un effet d'échelle concernant l'un des paramètres de la fonction de transfert. Les relations entre la condition initiale du modèle et les indicateurs d'humidités des sols en début d'épisode restent bonnes à l'échelle des sous-bassins, mais peuvent être significativement différentes selon les sous-bassins. Une seule relation ne permet pas de normaliser l'initialisation du modèle sur l'ensemble des sous-bassins, à une échelle spatiale de quelques km^2 ou dizaines de km^2. Dans le cas de l'indice d'humidité du sol w_2, une explication possible est que cet

indice ne prend pas en compte suffisamment finement les propriétés des sols. Enfin, la variabilité spatiale des paramètres du modèle est étudiée à l'échelle d'un échantillon d'une quinzaine de bassins méditerranéens de quelques centaines de km^2, associés à des paysages et des fonctionnements hydrologiques divers. La comparaison montre qu'à cette échelle, le lien entre les indicateurs de saturation du bassin et la condition initiale peut rester stable par type de bassin, mais varie significativement d'un type de bassin à l'autre. Des pistes sont proposées pour expliquer cette variation.

En conclusion, ce modèle événementiel distribué représente un excellent compromis entre performances et facilité de mise en œuvre. Les performances sont satisfaisantes pour un bassin donné ou pour un type de bassin donné. L'analyse et l'interprétation de la variabilité spatiale des paramètres du modèle apparaît cependant complexe, et doit faire l'objet du test d'autres indicateurs de saturation des bassins, par exemple mesures in situ ou mesures satellitaires de l'humidité des sols.

Mots clés : Méditerranée, modèle pluie-débit, variabilité spatiale, les crues éclair

Abstract

Rainfall-runoff models are essential tools for many hydrological applications, including flood forecasting. The purpose of this thesis was to examine the performances of a distributed event model for reproducing the Mediterranean floods. This model reduces the parametrization of the processes to the flood period and estimates the saturation of the catchment at the beginning of the event with an external predictor, which is easily observable or available. Such predictor avoids modeling the inter-flood phase and simplifies the parametrization and the calibration of the model. The selected model combines a distributed SCS production function and a Lag and Route transfer function, applied to a discretization of the basin in a grid of regular square meshes.

The model was first tested on the Real Collobrier watershed. This Mediterranean basin has been monitored by IRSTEA for more than 50 years and has an exceptional density of rainfall and flow measurements. This favorable environment made it possible to reduce the uncertainties on the rainfall input and to evaluate the actual performances of the model. In such conditions, the floods were correctly simulated by using constant parameters for all the events, but the initial condition of the event-based model. This latter was highly correlated to predictors such as the base flow or the soil water content w_2 simulated by the SIM model of Meteo-France. The model was then applied by reducing the density of the rain gauges, showing loss of accuracy of the model and biases in the model parameters for lower densities, which are representative of most of the catchments.

The spatial variability of the model parameters was then studied in different Real Collobrier sub-basins. The comparison made it possible to highlight and correct the scale effect concerning one of the parameters of the transfer function. The catchment saturation predictors and the initial condition of the model were still highly correlated, but the relationships differed from some sub-catchments. Finally, the spatial variability of the model parameters was studied for other larger Mediterranean catchments, of which area ranged from some tenth to hundreds of square kilometers. Once more, the model could be efficiently initialized by the base flow and the water content w_2, but significant differences were found

from a catchment to another. Such differences could be explained by uncertainties affecting as well as the rainfall estimation as the selected predictors. However, the relationships between the initial condition of the model and the water content w_2 were close together for a given type of catchment.

In conclusion, this distributed event model represents an excellent compromise between performance and ease of implementation. The performances are satisfactory for a given catchment or a given type of catchment. The transposition of the model to ungauged catchment is less satisfactory, and other catchment saturation indicators need to be tested, e.g. in situ measurements or satellite measurements of soil moisture.

Keywords: Mediterranean, rainfall-runoff model, spatial variability, flash floods

Résumé étendu

Introduction

L'eau est l'un des éléments essentiels de la vie, sans laquelle les humains ne pourraient pas survivre. Cependant, les phénomènes d'origine hydrique peuvent également avoir de graves conséquences, par exemple les inondations, qui peuvent en effet endommager lourdement les biens et entraîner des pertes de vies humaines. Parmi les différents types d'inondations, les crues éclair sont l'un des types les plus cruciaux en raison de leurs caractéristiques d'événement rapide.

Les crues éclair causent de nombreux dommages aux communautés et aux infrastructures, et représentent la cause de la mortalité la plus élevée si on se réfère à une évaluation mondiale des victimes des inondations (Jonkman, 2005). En France, la région méditerranéenne est la région la plus touchée par les crues éclair pour plusieurs raisons : les pluies très intenses et concentrées dans le temps de la Méditerranée; la petite superficie des bassins méditerranéens, limitée à quelques centaines de kilomètres carrés (Camarasa-Belmonte, 2016; Creutin et al., 2009), avec des réponses hydrologiques rapides (généralement moins de 6 heures de retard entre l'intensité maximale des précipitations et le débit maximal en aval); la faible perméabilité ou la faible profondeur des sols, et les pentes abruptes des régions montagneuses de l'arrière-pays méditerranéen.

Pour faire face aux inondations en général et aux crues éclair en particulier, l'une des méthodes les plus efficaces consiste à mettre en place des systèmes de prévision, basés sur des modèles pluie-débit. Les performances des modèles doivent être évaluées par leur capacité à simuler les crues observées, et par leur aptitude à être transposés à des bassins non jaugés. Ce dernier point correspond au concept de régionalisation, proposé pour faciliter la prévision dans les zones pour lesquelles les données ne sont pas disponibles (Blöschl et Sivapalan, 1995). Ce concept exprime la possibilité de transfert d'un ou de plusieurs modèles particuliers de modèles pluie-débit, du bassin versant déjà modélisé au nouveau bassin (c'est-à-dire celui pour lequel il n'existe pas de données observées). Le

processus de régionalisation comprend deux étapes principales. La première étape consiste à sélectionner un modèle pluie-débit suffisamment performant pour simuler les crues éclair. La recherche des meilleurs modèles est encore un objectif important en hydrologie. La deuxième étape consiste à comprendre la variabilité spatiale des paramètres, ce qui permet d'appliquer la régionalisation. Plusieurs études portant sur la régionalisation ont été réalisées en France (Perrin, 2000 ; Oudin et al., 2010 ; Vannier et al., 2014 ; Garambois et al., 2016 ; Aubert et al., 2014). Notre travail vise à compléter ces travaux antérieurs en analysant la variabilité spatiale des paramètres de ruissellement dans les bassins versants de petites et de grandes superficies (de quelques kilomètres à quelques centaines de kilomètres carrés).

Le bassin versant de Real Collobrier est un site idéal pour tester les modèles pluie-débit. Ce bassin est étudié depuis plus de 50 ans par IRSTEA (Folton et al., 2018) et de nombreuses données sont directement disponibles par Internet. Dix-sept pluviomètres ont été installés sur le plus grand bassin versant (70 km^2), et les débits ont été mesurés aux exutoires de onze sous-bassins, ce qui permet de comparer la calibration du modèle à l'échelle de quelques kilomètres carrés ou dizaines de kilomètres carrés dans une zone géographique réduite et d'évaluer la variabilité spatiale des paramètres. Dans cette étude, nous avons retenu 4 sous-bassins versants: Pont de Fer (70 km^2), Rimbaud (1,5 km^2), Maurets (8,4 km^2) et Malière (12,4 km^2) pour étudier également la variabilité spatiale des paramètres du modèle. Ces sous-bassins ont fait l'objet de nombreuses études et ont permis de mieux comprendre ce qui a permis de répondre à de nombreuses questions. (Taha et al., 1997 ; Gresillon et al., 1995)

Les performances du modèle peuvent être soigneusement estimées, tant en termes de capacité à reproduire les crues qu'en termes de variabilité spatiale des paramètres. En outre, les performances du modèle peuvent également être évaluées pour différentes densités de pluviomètres, ce qui donne une estimation des poids des incertitudes liées aux précipitations et des limites du modèle. L'objectif de cette thèse était d'appliquer un modèle pluie-débit distribué spécifique pour étudier les points suivants: (i) la capacité d'un modèle événementiel distribué, à simuler les crues éclair en climat méditerranéen, (ii) les règles de variabilité spatiale et temporelle des paramètres du modèle (iii) la capacité de modèle à être appliqué à des bassins non jaugés. L'étude a porté non seulement sur les bassins versants

de Real Collobrier, mais également sur d'autres bassins versants de la Méditerranée (Figure 1), afin d'envisager une autre échelle de bassins dont la superficie couvre des centaines de kilomètres carrés et d'obtenir un échantillon cohérent de bassins pour la comparaison des performances et des paramètres du modèle. Sept bassins versants supplémentaires ont été étudiés (Gardon à Anduze, Ardèche à Vogüe, Allier à Langogne, Tarnon à Florac, Vidourle à Sommières, Verdouble à Tautavel, Aille à Vidauban). Des données sur ces bassins ont déjà été traitées dans la base de données de bassins versants de la plate-forme de modélisation ATHYS (www.athys-soft.org).

Différents modèles ont été testés en zone méditerranéenne : TOP MODEL (Piñol et al., 1997, Blöschl et al., 2008; Durand et al., 1992; Saulnier et Le Lay, 2009); MARINE (Estupina-Borrell et al., 2006; Roux et al., 2011). Le modèle événementiel distribué SCS-LR a été sélectionné dans notre étude, en raison de son caractère parcimonieux et de sa structure extrêmement simplifiée.

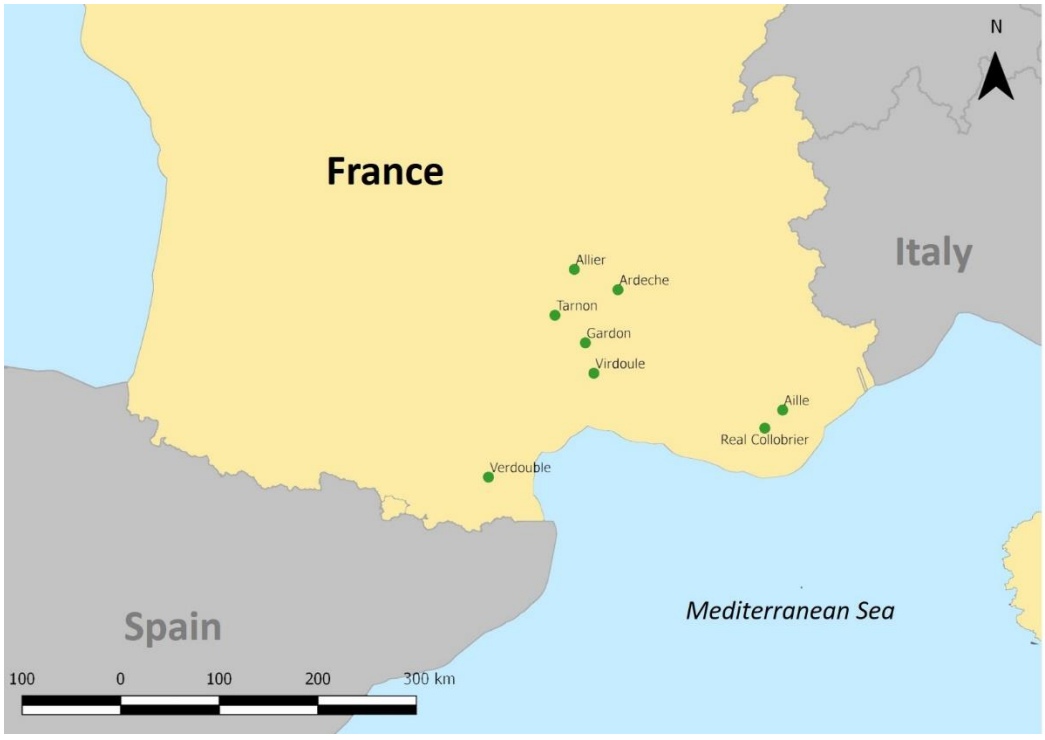

Figure 1 : Localisation des bassins versants sélectionnés dans la région Méditerranéenne

Principaux résultats

Calibration du modèle SCS-LR sur le bassin du Real Collobrier à Pont de Fer

Une étude de sensibilité préalable montre que le modèle SCS-LR comporte 2 paramètres principaux : S, la capacité maximale de stockage en eau au débit de l'épisode, et K_0 un coefficient réglant la diffusion de la crue au cours du transfert (ou dans certains cas, V_0 la vitesse de transfert). À Pont de Fer, la calibration a été effectuée sur la base de 34 événements pluie-débit. Les paramètres du modèle ont été optimisés pour chaque événement. Avec les paramètres optimisés, l'erreur commise sur la simulation des débits variait de 0.27 à 0.99 au sens du critère de Nash-Sutcliffe (NS) pour l'ensemble des événements (médiane = 0.96, quartile inférieur = 0.87). Les plus faibles valeurs de NS correspondaient à des événements se produisant dans les conditions de sol initiales les plus sèches. Dans ces cas, les valeurs de faible débit ont été surestimées, alors que les valeurs de débit de pointe ont été sous-estimées.

Relation avec les conditions initiales

Après la calibration du modèle, il est apparu que S était le paramètre le plus variable et le plus influent pour les simulations. S correspond au déficit en eau au début de l'événement, de sorte qu'il devait être fortement dépendant des événements précédents et de l'état initial de saturation du sol. Nous avons donc essayé de trouver des relations entre S et deux indices supposés exprimer la teneur en eau initiale: le débit de base et la teneur en eau volumétrique w_2 au début de l'événement simulé. Pour le bassin du Real Collobrier à Pont de Fer, les deux indices ont donné lieu à une corrélation relativement forte avec la rétention d'eau maximale, avec un coefficient de corrélation R^2 =0.85 entre S et $log_{10}Qb$ et 0.77 entre S et w_2.

Score prédictif du modèle

Ces relations peuvent être utilisées pour évaluer la précision réelle du modèle en mode projet. La précision réelle du modèle doit en effet être estimée par le NS calculé avec les valeurs prédites de S, au lieu des valeurs optimisées de S. On calcule dans ce cas de NS prédictif (pour tous les événements, la valeur médiane de K_0 a été utilisée). Le NS prédictif médian était de 0.83 en utilisant la relation entre S et le débit de base et de 0.77 en utilisant

la relation entre S et la teneur en eau w_2 (au lieu 0.94 pour le NS médian calculé avec les valeurs optimales de S et de la valeur médiane de K_0).

Incertitude des précipitations

De plus, le grand nombre de postes pluviométriques installés sur le Real Collobrier nous a permis de tester l'effet de la densité de pluviomètres sur la calibration et la qualité du modèle. Les résultats ont montré que la réduction de la densité des pluviomètres influait à la fois sur la fonction d'erreur NS du modèle et sur l'évaluation des paramètres du modèle. Lorsqu'on utilise un seul pluviomètre pour la calibration du modèle, les estimations de S peuvent varier de 250 à plus de 600 mm pour les sols initialement secs et de 50 à plus de 150 mm pour les sols initialement humides, en fonction du pluviomètre sélectionné. Les scores prédictifs NS du modèle évoluent entre 0.44 et 0.81 lorsqu'on ne considère qu'un seul des 17 pluviomètres sur le bassin.

Calibration du modèle sur les sous-bassins du Real Collobrier

Le modèle a ensuite été calibré sur trois sous-bassins supplémentaires du Real Collobrier : Rimbaud, Maurets, Malière. Les performances du modèle sont légèrement moindres que sur le bassin du Real à Pont de Fer, mais restent comparables. Les valeurs médianes de S diminuent avec les coefficients de ruissellement médians. On note toutefois que le bassin de Maurets présente un coefficient médian supérieur aux autres bassins et un S médian également supérieur. Les régressions entre S et les descripteurs w_2 et débit de base sont très voisines pour Pont de Fer et Rimbaud d'une part, et Maurets et Malière d'autre part. Les différences de Rimbaud avec Malière et Maurets pourraient être dues au fait que Rimbaud est représentatif de versants amont pentus productifs, alors que Malière et Maurets comprennent à la fois les mêmes versants pentus que Rimbaud à l'amont, et des unités peu productives à l'aval. La variabilité spatiale du paramètre K_0 a été attribuée à un effet d'échelle affectant la version initiale du modèle, qui a été corrigé.

Variation spatiale du paramètre S dans les bassins méditerranéens

La calibration du modèle a finalement été étendue à des bassins méditerranéens de plus grandes superficies. La valeur médiane de S variait d'un bassin à l'autre (Figure 2). La valeur la plus élevée de S appartenait à l'Allier, alors que le bassin versant d'Aille avait la valeur la plus faible. L'une des raisons de la valeur élevée du paramètre S dans le bassin de l'Allier

pourrait être due au fait que les sols de ce bassin sont très perméables. Ils peuvent donc absorber une forte proportion de précipitations et alimenter des aquifères profonds. Le bassin versant de l'Aille est un bassin, dont la géologie est différente de celle des autres: on sait que ces grès du Permien génèrent des sols peu perméables de couleur rouge, comme dans la région de Lodève et Salagou, dans le département de l'Hérault (Brunet et Bouvier, 2017).

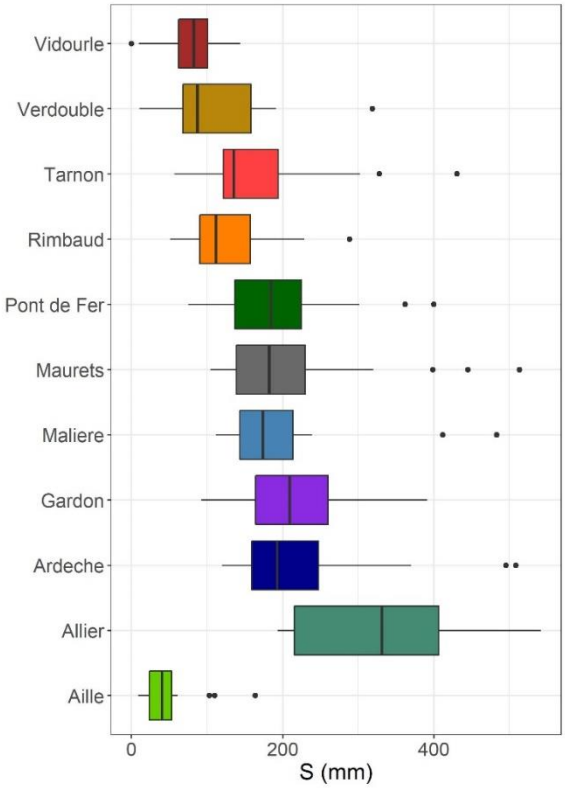

Figure 2 : Variabilité du paramètre S sur 11 bassins versants

La comparaison de la valeur S médiane et du coefficient de ruissellement médian pour chaque bassin montre cependant que ces variables sont peu corrélées. Cela pourrait s'expliquer par le fait que le coefficient de ruissellement intègre la réponse rapide et la réponse lente du bassin, tandis que S n'exprime que la réponse rapide du bassin. Par exemple, les bassins versants de l'Allier et de l'Aille ont un coefficient de ruissellement élevé similaire, mais pour des raisons différentes: les sols du bassin de l'Allier étaient supposés avoir une grande capacité de stockage de l'eau, mais aussi une grande capacité à produire de l'écoulement retardé par drainage des sols, alors que les sols peu perméables du bassin de l'Aille génèrent principalement du ruissellement superficiel ; ils ne peuvent stocker

beaucoup d'eau en raison de leur imperméabilité, et par conséquent ne libèrent que peu d'écoulement retardé. Ceci souligne le rôle de la contribution des écoulements souterrains dans la simulation des débits. Nous avons donc conclu que l'interprétation S devait tenir compte du type de ruissellement dans le bassin versant.

Afin de prendre en compte des facteurs secondaires spécifiques sur les bassins, notamment les conditions initiales de saturation des sols et leur impact sur la variabilité spatiale de S, nous avons ensuite considéré la variabilité spatiale des régressions entre S et les prédicteurs de la saturation des sols, débit de base et indice Hu2 (équivalent à w_2).

Indice Hu2/w_2

Les régressions entre les indices S et Hu2 de tous les événements sont significatives pour chaque bassin versant. Pour preuve, 9 des 11 bassins varient un coefficient de corrélation R^2 supérieur à 0.5. La comparaison des droites de régression pour l'ensemble des bassins (Figure 3) montre des divergences de pentes et d'intercepts. Les régressions semblent être divisées en 2 groupes:

Allier, Maurets et Malière ont des pentes similaires, plus fortes que les autres. Les intercepts sont cependant différents.

Les autres bassins versants ont des pentes similaires, avec toutefois des intercepts différents, la valeur minimale étant obtenue pour le bassin de l'Aille, et la valeur maximale pour le bassin de l'Ardèche.

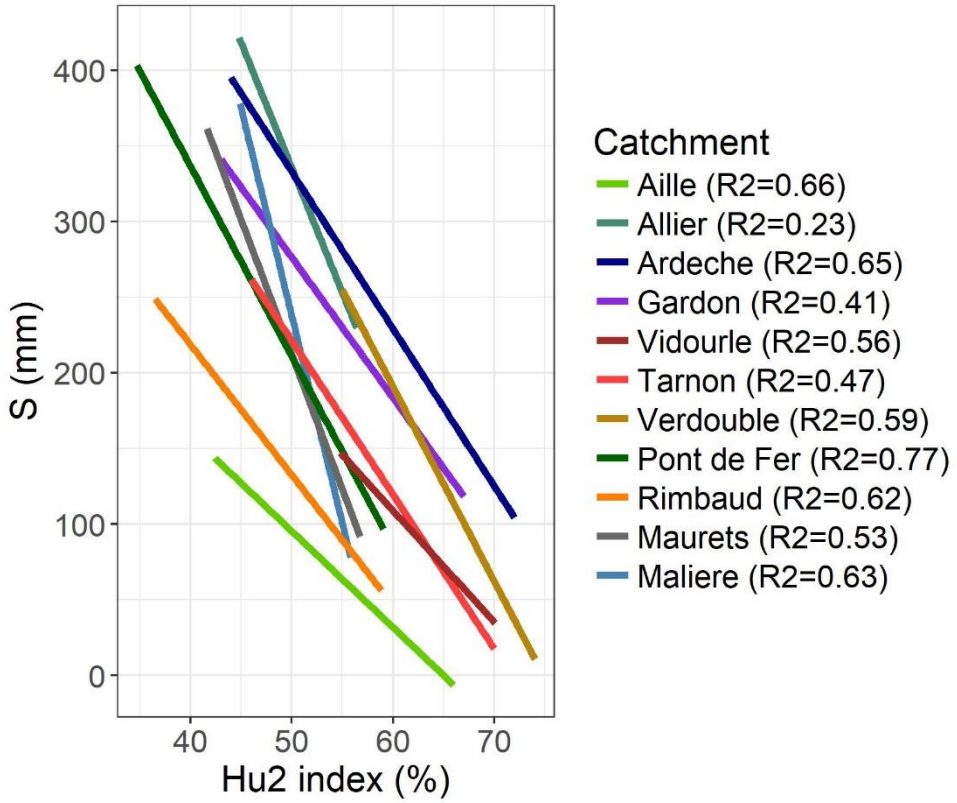

Figure 3 : Comparaison des régressions S-Hu2pour l'ensemble des bassins versants.

Débit de base

Le débit de base peut être considéré comme un autre indice pour expliquer la variabilité des événements du paramètre S. Les corrélations entre S et le débit de base sont généralement significatives, mais médiocres dans certains cas, notamment le bassin du Vidourle (R2=0). Les meilleurs scores ont été obtenus pour les bassins versants du Real Collobrier (0.61 à 0.86), alors que les autres bassins versants de la Méditerranée avaient un R^2 inférieur à 0.5. La comparaison des régressions sur l'ensemble des bassins (Figure 4) montre que les relations peuvent être très différentes d'un bassin à l'autre, et ne font pas apparaître un schéma régional (même si Allier, Gardon et Ardèche sont géographiquement proches et montrent des régressions similaires). Pour tenir compte des différentes superficies des bassins, le débit de base a été rapporté à la superficie du bassin, et désigne donc le débit spécifique de base.

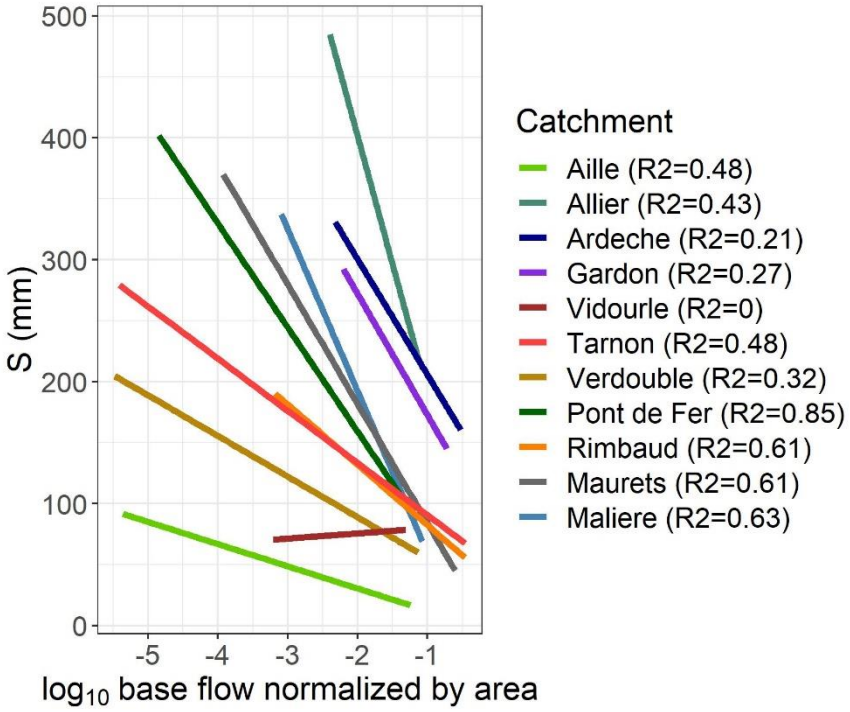

Figure 4 : Comparaison des régressions S-Qb pour l'ensemble des bassins versants

D'autres tentatives ont été faites pour utiliser un débit de base normalisé en divisant par le débit de base moyen, sans pour autant permettre de faire clarifier le schéma régional.

Discussion et conclusion

Le présent travail a permis une analyse détaillée des performances du modèle SCS-LR sur un ensemble de bassins méditerranéens, tant sur le plan de la capacité du modèle à simuler les crues que sur la variabilité spatiale des paramètres du modèle. Pour répondre aux questions énumérées dans les parties objectives du chapitre 1, nous présentons ici les principales conclusions et résultats, en premier lieu, pour le bassin versant de Real Collobrier:

1) Les résultats de notre étude ont prouvé que le modèle SCS-LR pouvait simuler une crue éclair en Méditerranée avec une grande précision. Le modèle ne nécessite qu'un petit nombre de paramètres et peut être calibré avec des données facilement accessibles. La calibration du modèle sur le Real Collobrier et d'autres bassins méditerranéens a donné des résultats positifs avec des valeurs élevées de NS ainsi que des valeurs élevées de R^2 pour la

corrélation entre S et les prédicteurs de la saturation initiale du bassin dans la plupart des cas.

2) les données de précipitations denses sur le Real Collobrier, nous ont permis de tester l'effet de la densité des pluviomètres sur les résultats de la simulation. Les résultats ont montré que la réduction de la densité des pluviomètres influait à la fois sur la régression avec les conditions initiales et sur les paramètres calibrés du modèle. La diminution du nombre de pluviomètre a entraîné le changement des paramètres du modèle et la diminution du coefficient de corrélation R^2. Ce résultat conduit à la conclusion que la comparaison des performances du modèle d'un bassin à l'autre peut être faussée lorsque les densités pluviométriques sont différentes

3) La variabilité spatiale du paramètre de transfert K_0 dans le modèle initial était initialement due à un effet d'échelle. La solution proposée a consisté à modifier la relation entre le temps de propagation T_m et le temps de diffusion K_m du modèle Lag et Route. La variabilité spatiale de K_0 apparaît ainsi considérablement diminuée, et peut finalement être reliée à la pente du bassin versant.

4) pour les bassins versants du Real Collobrier, la variabilité spatiale du paramètre de production S dans a été jugée cohérente avec la variabilité spatiale du coefficient de ruissellement. Cette relation n'a pas été vérifiée pour tous les bassins méditerranéens, et a conduit à penser que l'interprétation de S est dépendante du type de ruissellement généré dans le bassin.

5) La variation spatiale des régressions entre S et Hu2/w_2 (ou débit de base) a conduit à la conclusion qu'il était difficile de régionaliser ces régressions. Cet échec peut trouver son origine dans de multiples raisons :

- les incertitudes associées au prédicteur Hu2/w_2, qui pourraient être dues au fait que les mailles du modèle SIM sont trop grandes pour représenter les spécificités de petits bassins, ou au fait que les propriétés du sol utilisées dans SIM ne sont pas vraiment appropriées ou suffisamment précises pour représenter les propriétés réelles du sol.
- La mauvaise qualité de la mesure des débits de base, compte tenu de l'éventualité de mouvements des lits des rivières et de détarages fréquents de la courbe d'étalonnage des débits en basses-eaux, que des jaugeages trop peu nombreux ne permettent pas de suivre.

- De même, l'extrapolation de la courbe de tarage vers les débits de hautes-eaux est susceptible de générer sur certains bassins une forte incertitude, qui affecte directement l'estimation du paramètre S. Dans certains cas en effet (Gardon et Ardèche, par exemple), seulement quelques jaugages ont été utilisés pour établir la courbe de tarage.
- La raison peut aussi être liée aux incertitudes des précipitations. À l'exception du Real Collobrier, les autres bassins n'avaient pas une densité très élevée de pluviomètres. La variation de toutes les pentes et intercepts des régressions S-Hu2 ou S-Qb pour les bassins méditerranéens est assez similaire à celle des régressions établies en n'utilisant qu'un seul pluviomètre sur le Real Collobrier à Pont de Fer.
- La calibration des paramètres secondaires du modèle peut aussi être un problème. L'utilisation de Ia/S = 0.2, l'utilisation de paramètres constants, l'utilisation de S uniforme pour tout le bassin peuvent également conduire à une erreur lors de la calibration du paramètre S, puis affaiblir la corrélation entre S et les conditions initiales.

En conclusion et perspective, la calibration du modèle SCS-LR à l'aide d'observations pluies et débits permet de simuler les crues méditerranéennes avec une efficacité qui dépend de la densité des postes pluviométriques présents sur le bassin. La variabilité spatiale des paramètres du modèle reste difficile à interpréter, dans l'état des connaissances que nous avons des pluies, des débits et des caractéristiques hydrologiques des bassins versants. Les pistes d'amélioration consistent à tester de nouveaux indicateurs ou de mieux caractériser les propriétés des sols pour estimer la saturation initiale du bassin, à intégrer l'apport du radar météorologique pour la mesure des pluies, et à tester différentes spatialisations du paramètre S au sein des bassins.

List of abbreviations

Abbreviation	Full name
ATHYS	L'ATelier HYdrologique Spatialisé
CLC	Corine land cover
CN	Curve Number
DEM	Digital Elevation Model
EM-DAT	Emergency Events Database
IRD	Institut de Recherche pour le Développement
IRSTEA	Institut National de Recherche en Sciences et Technologies pour l'Environnement et l'Agriculture
LR	Lag & Route
NSE	Nash–Sutcliffe Efficiency
RR	Rainfall Runoff
SCHAPI	Service Central d'Hydrométéorologie et d'Appui à la Prévision des Inondations
SCS	Soil Conservation Services – Lag & Route
SIM	SAFRAN-ISBA-MODCOU
UT	Universal Time

Table of contents

General introduction

Water is one of the essential elements of life, which without it humans cannot survive. However, the water-originated phenomena can also cause huge consequences, e.g. floods. Indeed, floods can severely damage both human lives and properties. This natural disaster is also inevitable, as currently there has not been any perfect way yet to prevent floods from occurring. Among different types of floods, flash flood is one of the most crucial types because of its characteristics of fast occurring.

According to the USA National Weather Service, "Flash flood is a flood caused by heavy or excessive rainfall in a short period of time, generally less than 6 hours. Flash floods are usually characterized by raging torrents after heavy rains that rip through river beds, urban streets, or mountain canyons sweeping everything in front of them. They can occur within minutes or a few hours of excessive rainfall. They can also occur even if no rain has fallen, for instance after a levee or dam has failed, or after a sudden release of water by a debris or ice jam" (https://www.weather.gov/mrx/flood_and_flash)

Flash flood causes many damages to the communities and the infrastructure (Gruntfest and Handmer, 2001). This type of natural phenomena has been shown to cause the highest mortality in a global assessment of flood-related casualties (Jonkman, 2005). In order to deal with floods in general and flash floods in particular, one of the most effective methods is to build the prediction systems. Many efforts have been invested in generating the database for flood researches and prediction. For instance, the Hydrometeorological Data Resources and Technologies for Effective Flash Flood Forecasting (HYDRATE) project was established in 2006 to understand better the hydro-meteorological processes leading to flash floods, which involves a multidisciplinary team of 17 organizations from 10 EU countries, China, USA, and South Africa. This project was also associated with the publicly accessible European Flash Flood Database, which aggregated all hydrometeorological data from the project (Borga et al., 2011). Moreover, the Hydrological Cycle in Mediterranean Experiment (HyMeX) program is a 10-year experimental effort (from 2010 to 2020) aiming to improve our understanding of the Mediterranean water cycle and its variability at different scales, which specially

focuses on hydro-meteorological extreme events and the associated social and economic vulnerability in the Mediterranean region (Drobinski et al., 2013). This program involves more than 400 scientists working in atmospheric sciences, hydrology, oceanography and social sciences from over 20 countries. An important part of the Hymex project - the Cévennes-Vivarais Mediterranean Hydro-meteorological Observatory aims to improve the knowledge and capabilities of hydrological risk prediction, which involves scientists from various disciplines, including meteorology, hydrology, geophysics, geography, applied mathematics and social sciences (Boudevillain et al., 2011). In addition, the EuroMedeFF dataset has collected flash flood hydrometeorological and geographical data, including high-resolution radar rainfall estimates and flood hydrographs from 49 high-intensity flash floods in the western and central Mediterranean, the Alps region and Continental Europe (Amponsah et al., 2018).

In spite of many efforts, current knowledge in flash flood prediction and risk assessment are still limited, which is mainly due to the lack of effective monitoring. Another inconvenience is the fact that the rain and stream gauges can be damaged when floods happen, which causes difficulties in maintaining the continuity of collected data, thus affecting the performance of flood simulating model. Moreover, the most vulnerable areas by flash floods are often where there is no data observed.

Thus, the concept of regionalization was proposed to help the prediction in the areas without available data (Blöschl and Sivapalan, 1995). This concept relies on the transfer of one or more particular parameters flood models from the catchment that have been already modeled to the new catchment (i.e. the one that lacks observed data). The regionalization process consists of two main steps. The first step is selecting a flood model which is sufficient for flash flood prediction. The possibility of improving this model should not be neglected. The second step is applying the selected model to at least one catchment to test their performance. The most important thing is the understanding of the variability of the parameters, thereby we can apply the regionalization. Several studies dealing with regionalization have been performed in France : Perrin, 2000 aimed to automatically calibrate several models over more than 1000 catchments, and relate the parameters to the catchments main characteristics (Perrin, 2000); Oudin et al., tested the performances of several regionalization methods such as geographical proximity, hydrological similarity and

multi-linear relationships with the catchment characteristics (Oudin et al., 2010); Vannier et al., dealt with the regionalization of the recession curves in Mediterranean catchments (Vannier et al., 2014); Garambois et al. compared the regionalization methods used by Oudin in a small set of Mediterranean catchments (Garambois et al., 2016). Besides, The SHYREG method (Aubert et al., 2014) which is a flood frequency analysis method was applied to 1605 basins in the French metropolitan territory for flood risk management. Our work intends to complete these previous works by analyzing the spatial variability of the runoff parameters in catchments of small and large areas (from a few to hundreds of square kilometers).

Several models have been developed to study flash floods at various scales which was reported in (Javelle et al., 2018; Roux et al., 2011). However, there is still a debate on the question of which model is preferable, and which is not: continuous or event-based, empirical or physically-based, lumped or distributed models. As pointed out by (Oudin et al., 2010), a major concern about regionalization is due to equifinality of the parameters (Bardossy and Singh, 2008), that is a multiplicity of parameters satisfying to the goodness of the model. Equifinality can result from over parametrization of the model, thus it will be preferable to use parsimonious models when aiming to regionalization objectives. In addition, many uncertainties affect the input data used by the rainfall-runoff models, and can possibly originate artificial biases in the estimation of the model parameter, and their comparison from a catchment to another. So that each model would have to be tested and evaluated in highly documented sites where input and output data are observations are available and reliable, and where the uncertainties can be reduced as far as can be. It allows estimating in the one hand the actual performances of the model, and in the other hand simulating the impact of rainfall uncertainties for lower rain gauges density, which are representative of most of the catchments.

As a matter of fact, The Real Collobrier catchment is such a convenient site for modeling workbench. This catchment has been studied for more than 50 years by IRSTEA (Folton et al., 2018), and a lot of data are directly available from a website. Seventeen rain gauges have been settled over the larger catchment (70 km^2). The discharges have been monitored in eleven sub-catchments, which allows comparing the model calibration at the scale of some square kilometers or dozen of square kilometers in a reduced geographical area and assess the spatial variability of the parameters. In such case, the performances of the model can be

carefully estimated, as well in terms of ability to reproduce the floods as in terms of applying the model in ungauged catchments. In addition, the performances of the model can also be compared for different dense rain gauges device, which gives an estimation of the weights of the rainfall uncertainties and the limitations of the model. The objective of this Ph.D. was to study a specific event-based distributed model in firstly the Real Collobrier to answer the following questions (i) how appropriate is an event-based distributed, but parsimonious model for flash flood prediction in Mediterranean climate, (ii) what is the impact of the uncertainty to the model calibration and (iii) how to explain the variability of these model's parameters? The study dealt not only with the Real Collobrier catchments but also with other Mediterranean catchments, in order to consider another scale of catchments of which area covers hundreds of square kilometers and to obtain a consistent sample of catchments for the comparison of the model performances and parameters. 7 additional catchments have been considered (Gardon at Anduze, Ardèche at Vogüe, Allier at Langogne, Tarnon at Florac, Vidourle at Sommières, Verdouble at Tautavel, Aille at Vidauban. Data of these catchments have already been processed in the catchment database of the ATHYS platform www.athys-soft.org.

To fulfill the above objectives, the works are defined and described in this Ph.D. document is the composition of the following chapters:

Chapter 1 is a review of the literature and theoretical concepts on which the Ph.D. thesis is based. It introduces the water cycle's processes, flood processes and the main factor that can affect flood. This chapter also mentions about Mediterranean flash floods and these consequences. Moreover, the hydrological model is described: the rainfall-runoff classification, modeling process and examples of rainfall-runoff model dealing with Mediterranean flash floods.

Chapter 2 provides the methodology of a parsimonious event-based rainfall-runoff model Soil Conservation Services – Lag & Route (SCS-LR) which are selected in the study. It also brings out the sensitivity test, the method of parameters assessment of the model.

Chapter 3 presents the Real Collobrier catchment and the results of the calibration of the model on the Pont de Fer sub-catchment. The chapter deals with various aspects: how the initial condition of the event-based model has to be set for each event, what is the actual performance of the model when using the predicted initial condition, what are the effects of

a reduction of the rain gauge density on the performances of the model as well as the parameters assessment.

Chapter 4 presents the spatial variability of the parameters at the sub-catchment scale. The results of the sub-catchments in Real Collobrier such as Pont de Fer, Rimbaud, Maurets, Malière are used. The range of area allows to test the hypothesis if the parameters are stable or not at this scale of the catchment, and if not, how can be explained the differences, for example in terms of numerical effects or hydrological effects.

Chapter 5 described the spatial variability of the parameters of the models at a higher scale, between Mediterranean catchments of which area extends from tenth to hundreds of square kilometers. The possibility of using predictors for applying the model in ungauged catchments is judged.

The document ends with a general conclusion and further perspectives.

1 Introduction

This chapter presents the theoretical background and state of the art underpinning this work. The issue of the hydrological processes is reviewed in Section 1.1. In Section 1.2, the overview of the flood is indicated with the flood processes and the main factors affecting flood process. Then, the part of the model in general, hydrological model, model's operation and the scaling issues and spatial-temporal variabilities is presented in Section 1.3. The following Section 1.4 reviews the knowledge about Mediterranean floods, as well as several previous studies about floods modeling in this region and the concept of regionalization.

1.1. Theoretical background: hydrological processes in the drainage area

It has been well-known that the total mass of water on Earth does not significantly change over time (Skinner and Murck, 2011). However, the distribution of water into different forms and reservoirs is greatly variable, which mostly depends on the changes in climatic conditions. Indeed, water continuously moves and transforms between different reservoirs on Earth, including rivers, oceans, and atmospheres, via different physical processes, at the same time it transforms between different physical forms: liquid, solid and vapor. The continuous movement of water around the surface of the Earth is described by a concept called the water cycle. The water cycle involves the exchange of mass and energy and is also essential for the maintenance of all lives and ecosystems on this planet.

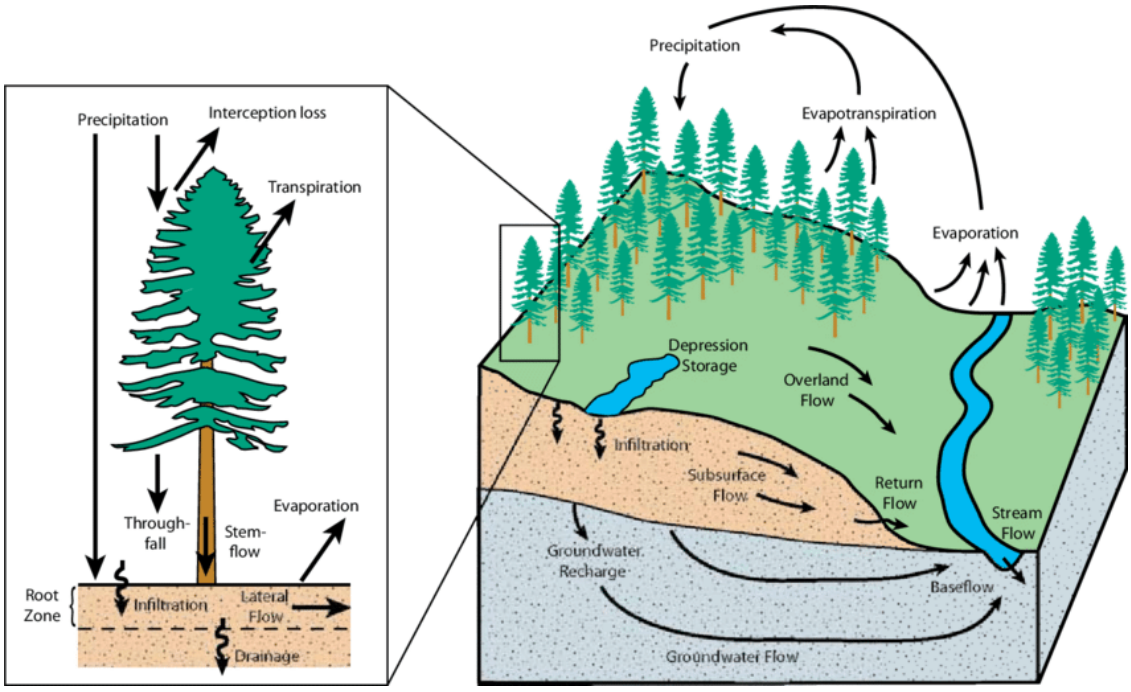

Figure 1.1: The water cycle on the catchment scale (From Winkler et al. 2010).

The different physical processes involved in the water cycle include precipitation, interception, evapotranspiration, condensation, infiltration, and percolation (Figure 1.1). Firstly, precipitation is the falling of any product of the condensed atmospheric water vapor under gravity (Deodhar, 2008), which occurs under the saturation of the atmosphere portion with water vapor. Precipitation can be divided into different categories based on the state of the water that falls off, including rain, drizzle, and snow (UNESCO and World Meteorological Organization, 1999). There are three mechanisms in which precipitation can occur, which differs in the direction of air movement, intensity, and duration, including convective, stratiform and orographic rainfall (Anagnostou, 2004; Dore et al., 2006).

However, only a part of precipitated water can reach the ground directly, while the rest is intercepted by vegetation and other surfaces. Interception is the interruption of movement of water from precipitation to stream channels, and it slows down the effect of precipitation. The precipitation that reaches the ground is called net precipitation. The part of the water that does not reach the ground directly can subsequently slide or drip from these surfaces to the ground, or it can be lost through evaporation. A part of water can fall to the forest floor

(through fall), run down branches and stems (stem flow), be absorbed by the vegetation, or remain on the surface of the foliage and branches and evaporate after the storm. The rain interception depends on storm intensity and duration, weather conditions (wind speed, air temperature, humidity), and amount and type of vegetation present (Crockford and Richardson, 2000).

The amount of precipitated water that reaches the ground directly or indirectly can be infiltrated into the soil. Infiltration is the movement of water through the boundary between the atmosphere and the soil, which is largely dependent on the soil surface conditions (Maidment, 1993). In particular, the porosity of the soil and the permeability of the soil affects the transfer of water. The infiltration rate also depends on the impact of the raindrops, the texture and structure of the soil, the initial soil moisture content. The maximum rate at which water can infiltrate into the soil is called the infiltration capacity (Winkler et al., 2010).

Infiltrated and stored water in the soil can later become subsurface runoff and contribute to streamflow. Streamflow is the flow or discharge of water along a defined natural channel. Streamflow is generated by a combination of runoff from the upstream watershed and return flow from the groundwater aquifer. Streamflow reflects the volume of the supplying water to a watershed (can be accounted by precipitation, evapotranspiration, infiltration) and also changes in the volume of other storages (lakes, aquifers, soil moisture). The streamflow rate at a particular point in time and space integrates all the hydrologic processes and storages upstream of that point. It depends on the sequence and size of rainfall events; seasonal distribution and nature of precipitation; the extent, type, and transpiration of covered vegetation; the soil infiltration capacity; and the topography of the watershed. (Maidment, 1993).

Infiltrated water can also percolate into deeper soil and rock layers through different layers of the soil due to gravity and capillary forces, then go to the groundwater. Groundwater is the water in the zone of saturation and completely fills the pores (Meinzer, 1923). Groundwater not only contributes to the stream base flow but also buffers peak flow when the bank sediments are sufficiently permeable (Winter et al., 2003). Depending on the relative water level, water can move from the groundwater to the stream or vice versa. The discharge of groundwater moving to the streams is commonly called base flow. This type of

flow occurs during the dry time of the year without specific storm events and seasonal phenomena.

The other part of precipitated water which is not infiltrated can directly contribute to stream flow or can also be stored in various type of water bodies such as lakes, swamps, ponds, and icebergs. A part of groundwater can also be considered as stored water.

The water which is infiltrated, stored, intercepted, and free in streamflow can return to the atmosphere by evapotranspiration in the form of water vapor. Evapotranspiration contains two main processes, evaporation and transpiration. Evaporation is the movement of water from intercepted rain and snow, as well as water bodies such as ponds, lakes, streams and even bare soil. Different important conditions are required for evaporation including (i) the availability of water, (ii) the humidity at the evaporative surface must be higher than that of the surrounding air, (iii) the energy to evaporate the water and (iv) the movement, or transfer, of water vapor away from the evaporative surface (Winkler et al., 2010). Therefore, the evaporation rate will increase when factors that induce those conditions occur, such as increasing solar radiation, air temperature, wind speed and decreasing atmospheric humidity (Condie and Webster, 1997). Transpiration accounts for the transfer of water from plant leaves through the stomata. The rate of this process depends strongly on the stomata, thus different plant species have different ability to regulate water loss. For example, trees usually have higher stomatal resistance to water loss than shrubs and grass (Kelliher et al., 1995). It is worth to note that transpiration rates decrease during rainfall due to the decreased vapor pressure gradient.

The amount of water that comes back to the atmosphere in the form of vapor can transform back to the liquid state by a process called condensation, forming dew, fog or clouds (McNaught and Wilkinson, 1997). Condensation occurs when the temperature of the air decreases or the amount of vapor increases up to its saturation points. This process releases an amount of heat which is previously required for evaporation. The most active particles forming clouds are sea salts, the atmospheric ions caused by lightning and the combustion products containing sulfurous and nitrous acids. These condensed water waits for the ideal condition to contribute to the water cycle as precipitation.

1.2. Overview of floods

1.2.1. Floods process

Extreme hydrological phenomena, including floods, are partly caused by the unequal geographical and geological distribution and movement of water. To decrease the damage of flood to humanity, the understanding of flood processes is very important. Initially, the definition of flood is expressed as the temporary rise in the level of a river. The flooding process can be explained below:

There are several mechanisms involved in the generation of runoffs (Figure 1.2). Each mechanism responds differently to rainfall in the flood variables: runoff volume, peak discharge and the timing of stream flow's contributions in the channel. Climate, geology, topography, soil characteristic, vegetation, land use, and the intensity of events can also affect the relative dominance of each process.

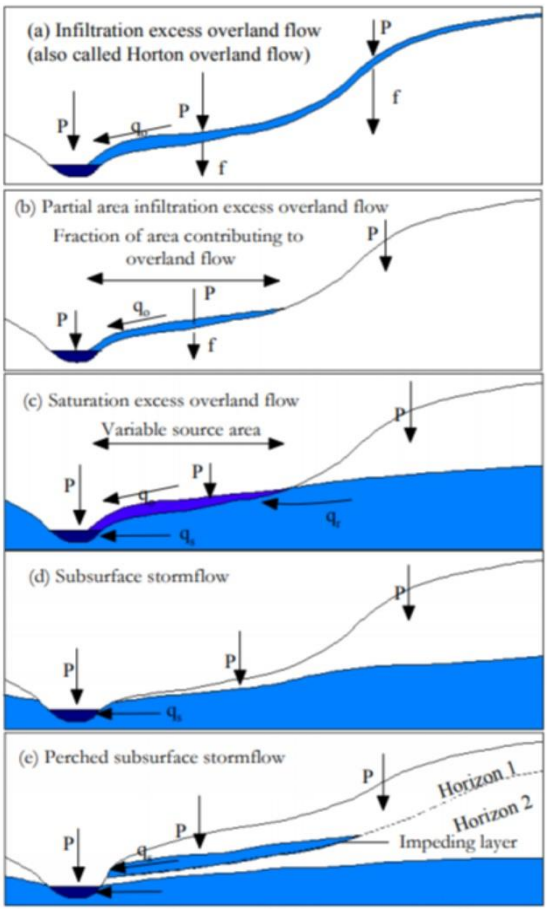

Figure 1.2: Classification of runoff generation mechanisms (Beven, 2012)

1.2.1.1. Infiltration excess overland flow

Firstly, we have to mention the infiltration excess overland flow mechanism (Figure 1.3a). This mechanism is also called Hortonian overland flow because it was referred to by Robert E. Horton, one of the quantitative hydrology's founding father in 1933. It was claimed that there is a maximum limiting rate for the soil in a given condition can absorb surface water input, so-called infiltration capacity. The excess water of the surface water input firstly accumulates on the soil surface and fills small depressions when it exceeds infiltration capacity. This part of water will evaporate or infiltrate later, thus it does not contribute directly to the overland runoff. However, if the surface water input continues to increase, the depression storage will also be filled, and the amount of water accumulated on the soil will start moving downslope, contributing to the overland runoff.

Infiltration excess runoff does not necessarily happen over a whole drainage basin area. Due to the spatial variability of the rainfall and soil properties, the area which contributed to infiltration excess runoff can only be a small part of the watershed (Betson, 1964). This concept is known as the partial-area infiltration excess overland flow.

The infiltration excess overland flow can occur anywhere that the water input excesses the infiltration capacity, most frequently in the area with having thin of devoid of plant cover. We can also see this process where the soil has been compacted or topsoil removed and in an urban area.

1.2.1.2. Saturation excess overland flow

In the place where infiltration capacity is very high, and the water input does not exceed infiltration capacity, overland flow can still occur by the water input on the area that is already saturated. Such mechanism is referred to as saturation excess overland flow (Figure 1.3b). This mechanism occurs when the infiltrated water has completely saturated the soil, or due to the rising of the water table, which make all surface water input become overland flow runoff.

Saturation excess overland flow is not restricted to near stream saturated zone although it is the most critical area. Saturation excess overland flow can also occur:

- where soil layers conducting subsurface flow are thin

- where there are slope concavities which subsurface flow converge, thus water flows in faster than it can be transmitted downslope
- where the hydraulic gradient that induces subsurface flow in upslope is greater than that inducing downslope transmission
- where percolated water accumulates above the low-conductivity soil layers, forming perched zones of saturation due to decreasing hydraulic conductivity gradually with depth

1.2.1.3. Subsurface flow

The subsurface flow was mentioned above in the part of saturation excess overland flow. So, what is subsurface flow? Subsurface flow comes from the subsurface hydrologic processes, which are very complicated and unable to observe directly. The subsurface hydrologic processes are driven by many factors that influence the paths and rates of water movement. Therefore, subsurface flow is the major source of uncertainty in hydrologic models (Beven, 2012).

Subsurface flow occurs when water moves down a hillslope through soil layers or permeable bedrock to contribute to the runoff (Figure 1.3c-g). This process requires that the hydraulic lateral conductivity of the environment is larger than the vertical conductivity. Besides, subsurface flow is favored by the presence of impermeable shallow soil layers.

Subsurface flow can play the key role of flood runoff in humid environments and steep terrain with conductive soils (Anderson and Burt, 1990). We can see the subsurface flow in most upland terrain, and it may be dominant in humid regions with vegetal covering and well-drained soils. Meanwhile, this process can occur only under certain extreme conditions in lowland regions and in drier climates, for example, under high rainfall and high antecedent soil moisture.

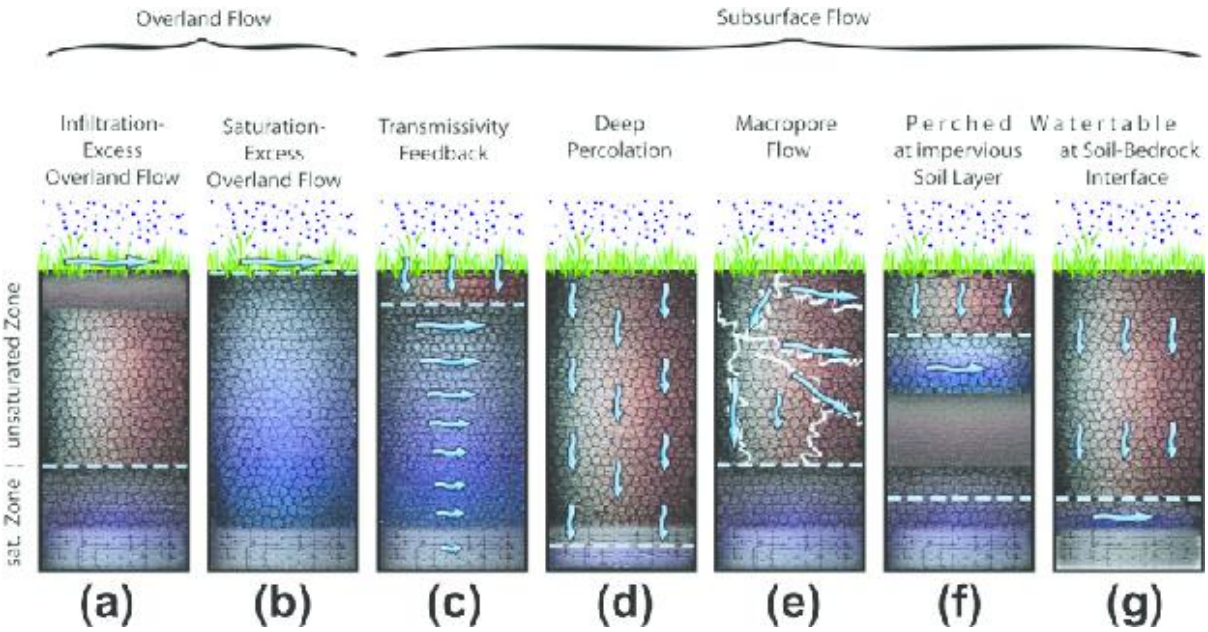

Figure 1.3: (Rinderer et al., 2012) Different types of surface and subsurface runoff processes. (a) Overland flow is generated when the infiltration capacity of the soil layers at or near the surface is exceeded; (b) Overland flow can also be generated when the storage capacity of the soil layers at or near the surface is exceeded, (c) Lateral subsurface runoff increases when ground water rises into more transmissive soil layers, (d) Groundwater table tends to be low and soil water can percolate deep down into the soil or bedrock when the soil has coarse and highly permeable texture, (e) The flow rates toward the nearest stream channel can be high and subsurface runoff is generated when there are horizontal macropores, (f) A perched water table will form leading to lateral subsurface flow within the saturated soil layer when there exists water restricting layer in the soil profile, (g) lateral subsurface flow can also occur when there are water-restricting layers at the soil-bedrock interface.

The subsurface flows can accompany these mechanisms:

Piston effect: The piston effect assumes that water that falls on a slope is transmitted downstream with a quasi-instantaneous pressure wave. It may cause a sudden exfiltration on the watershed.

Gravitational subsurface flow in macropores

Subsurface flow may be carried through macro pores which lead the water to unsaturated areas. Macropores are pores in which the capillarity phenomena do not exist. We can distinguish four types of macropores:

- Natural macropores: these macropores appear due to high initial hydraulic conductivity.

- Pores which formation is the result of micro soil fauna: these pores normally locate in the superior soil layer (0-100 cm) with a dimension of 1-50 mm.
- Pores which formation is due to vegetation roots. These pores normally become free when the plants die. Therefore, the structure of the macropores network of this type will depend on both the type of vegetation and its growing state.
- Cracks.

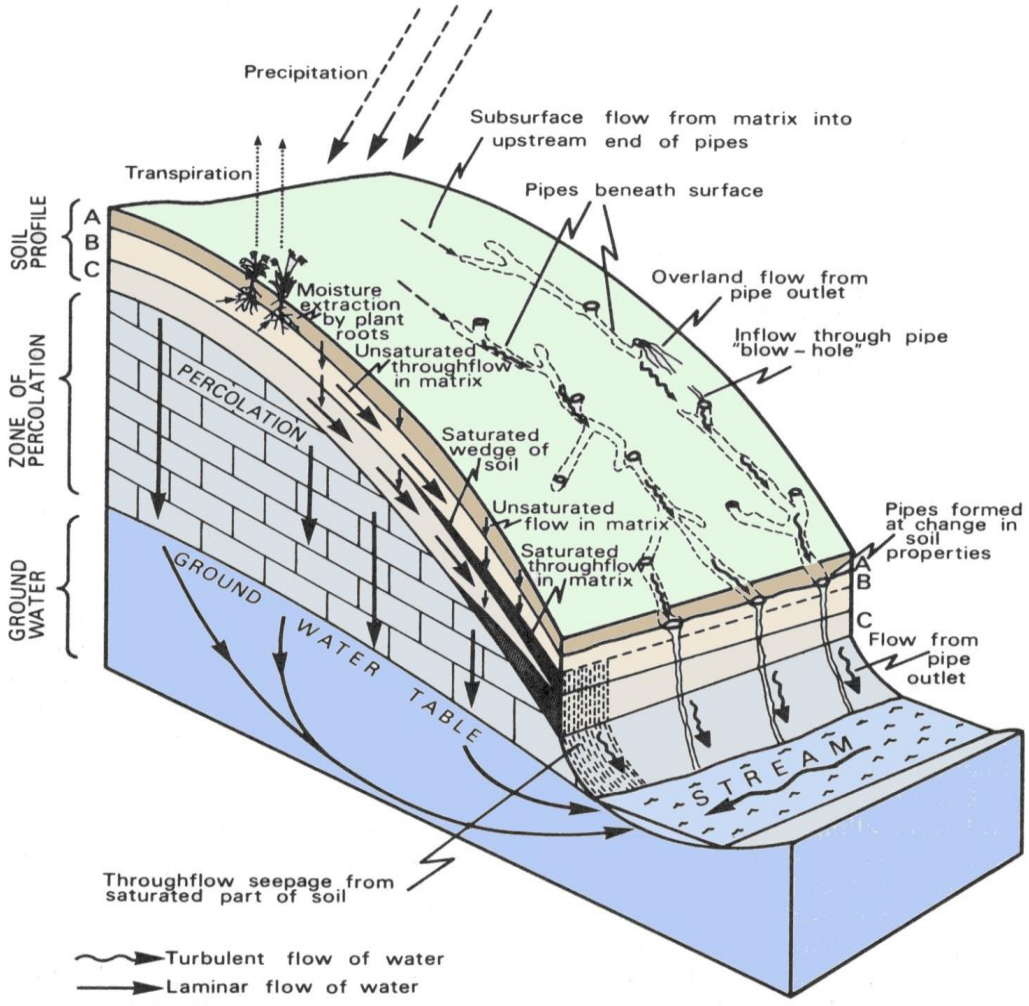

Figure 1.4: Pathways followed by a subsurface runoff on hillslopes (Kirkby, 1978)

Detailed cross-section through a hillslope that exposes in the pathways infiltrated water may follow as described in Figure 1.4. Infiltrated water may flow through the structural voids in the soil matrix, which are either small or large (macropores), including the opened passage in the soil caused by decaying roots and animals. Among these passages, subsurface

flow is favored by macropores. The different permeability of the horizontal soil matrix may lead to the build-up of a saturated wedge above a soil horizon interface. Water can either flow laterally from these saturated wedges through the soil matrix or enter the macropores in the soil, before going to the stream. Both processes mentioned above result in the subsurface flow called interflow.

Pipe flow

Another mechanism of subsurface flow is pipe flow. Pipe flow leads water to an unsaturated environment. This mechanism is similar to macro-pore to some extent, however, pipes are considered to be larger and more connective than macropores, as they can form a continuous network in the soil.

Transmissivity feedback

Subsurface flow can also occur by a mechanism called transmissivity feedback (Weiler and McDonnell, 2004). This phenomenon happens when water infiltrates rapidly along preferential pathways. This leads to the rapid rising of groundwater, reaching the highly permeable soil layers or macro-pore networks. As a consequent, water is then transmitted downslope (Figure 1.5).

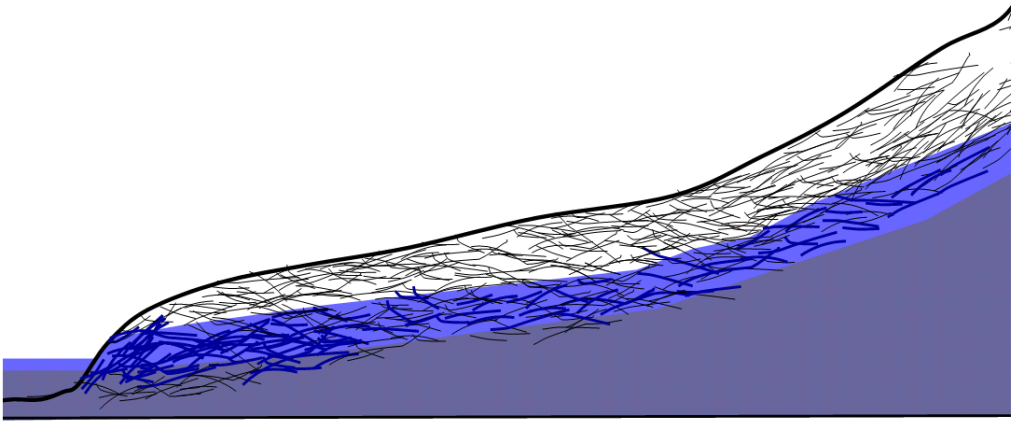

Figure 1.5: (Tarboton, 2003) Schematic illustration of the macropore network being activated due to the rise in groundwater resulting in rapid lateral flow

Rapid lateral flow at the soil-bedrock interface

Another mechanism of subsurface flow, called lateral flow at the soil-bedrock interface (Weiler and McDonnell, 2004), occurs in regions with steep terrain, low permeability

bedrock and thin soil cover (Figure 1.6). In these regions, water can move rapidly through the thin soil layer and perch at the soil-bedrock interface. The addition of only a small amount of rainfall is enough to produce saturation at the soil-bedrock or soil-impeding layer interface because moisture content near the bedrock interface is often close to saturated.

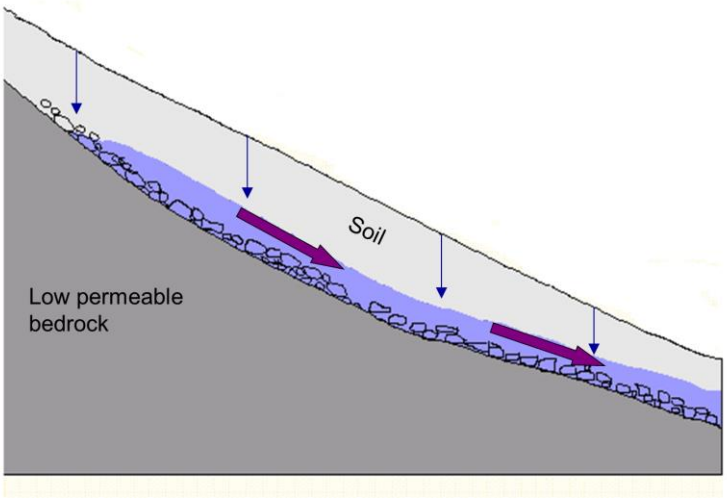

Figure 1.6: Rapid lateral flow at the soil-bedrock interface (Tarboton, 2003)

Subsurface stormflow by groundwater ridging

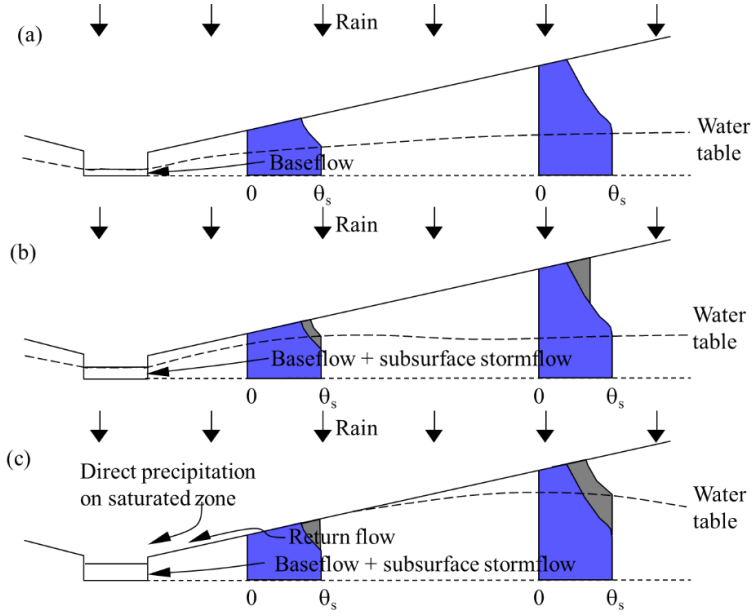

Figure 1.7: Groundwater ridging subsurface stormflow processes in an area of high infiltration (Tarboton, 2003). The shaded areas represent graphs of soil moisture at the base, middle and near the top of the hillslope (a) before the onset of rainfall; (b) as an initial response to rainfall; and (c) after continuing rainfall.

The processes involved in the generation of subsurface stormflow by groundwater ridging are illustrated in Figure 1.7. Before the onset of rainfall, the water table slopes slightly towards the channel to maintain the base flow of the stream (Figure 1.7a). When the rain starts, initially the water input leads the water table to rise near the stream but keep further upslope unchanged (Figure 1.7b). This leads to the increase of hydraulic gradient between groundwater and stream, resulting in the subsurface flow into the stream. As the rain continues, the water table rises to the surface over the lower part of the hillslope and the saturated area is expanding uphill. The water arises from this saturated area and runs downslope called return flow (Figure 1.7c). In this case, there is also direct precipitation onto the saturated zone which forms saturation excess runoff.

1.2.2. Main factors affecting flood process

It is widely recognized that the two most important climate variables influencing runoff generation during floods are rainfall and initial condition. Therefore, in the following section, rainfall and soil moisture will be discussed in detail.

1.2.2.1. Rainfall

1.2.2.1.1. Rainfall characteristic

The most important factor that drives flood is precipitation. Flood properties have been shown that be influenced by a combination of precipitation characteristics including the amount, intensity, duration, and spatial distribution. Moreover, the time of the rains and the area covered by the rain are also essential. The importance of each factor is not easy to separate and evaluate.

Rainfall intensities are one of the important factor leading to flooding generation in all catchment sizes (Costa, 1987; Pitlick, 1994; Schick, 1988). The higher rainfall intensity likely leads to higher potential runoff. Short and intense storms can generate the highest channel discharge, despite low total rainfall and storms with long durations or with greatest total rainfalls in the condition of uniform spatial distributions tended to produce moderate discharge events (Martín-Vide et al., 1999). However, it was reported that floods can be related to the total rainfall occurring than to intensity of an event (Bracken et al., 2008).

The spatial distribution of rainfall can affect flood at any scale catchments (Arnaud et al., 2002). It influences runoff volume, peak flow and also the time shift of hydrograph (Dawdy and Bergmann, 1969; Krajewski et al., 1991; Troutman, 1983; Wilson et al., 1979). Even for very small catchments (5 ha), rainfall variability must be taken into account because it is not always representative to use the information from a single measuring point (Faurès et al., 1995). However, it was also found that in the case in which the rainfall volume at each time interval is preserved, spatial rainfall variability does not significantly influence the flood response for basin areas up to about 3500 km^2 (Nicótina et al., 2008).

The effects of spatial rainfall can be assessed by comparison of rainfall–runoff responses between events within a catchment (Bell and Moore, 2000; Cole and Moore, 2008) or between catchments covering different hydrological regimes (Smith et al., 2012). Besides, implementing observed rainfall data through models representing idealized catchments or implementing realizations of synthetic rainfall patterns through a calibrated hydrological model can also help to investigate spatial rainfall effects (Arnaud et al., 2002).

The spatial rainfall-runoff relationship varies significantly for different climatic regimes. In arid and semi-arid regions, the sensitivity of runoff to the spatial-temporal characteristics of the rainfall event was tested at various catchment scales (Syed et al., 2003), with the conclusion that the sensitivity being decreased for frontal compared to convective precipitation (Koren et al., 1999; Vischel and Lebel, 2007).

The spatial rainfall-runoff relationship can also be affected by catchment perviousness and antecedent catchment conditions (Pechlivanidis et al., 2017). This study showed that spatial rainfall is less sensitive to runoff volume and peak flow in less impermeable catchments. In addition, the runoff prediction errors are generally considerably lower for wet than for dry conditions (Zehe et al., 2005).

1.2.2.1.2. Rainfall measurement

The precipitation can be measured with the help of devices: rain-gauges, radar, and satellite. Rain gauges are popular from the beginning of hydrological science. Rain gauges provide a direct and most accurate measurement (relative to other sensors), however, they are associated with small sampling area. Moreover, they can be damaged or suffered from errors depend on the wind, temperature, and type of precipitation (rain or snow), etc. It is

difficult to accurately measure the dynamics of a flash flood-inducing storms that are highly localized and spatially and temporally variable because of the usually low density of rain gauge networks, especially over complex terrain areas (Creutin and Borga, 2003). However, nowadays, with the development of space and information technologies, rainfall can be measured by radar or satellite.

Weather radar technology was developed as an outcome of the intensive work on radar technology during World War II. This technology is useful in addressing the coverage and in monitoring precipitation, as it provides continuous and spatially distributed rainfall fields at high resolution (Nikolopoulos et al., 2012). For instance, the network used by the UK Met Office includes 13 weather radars. This network provides 2x2 km gridded radar data at the 5-minute interval and a real-time extrapolation based on radar data every 30 minutes. It also provides precipitation forecasts every 6 hours (Sun et al., 2000). A national river forecasting system has been operated by the US Weather Bureau since the early 1990s. This system combines weather forecasts with flood prediction models to give warnings for floods (Sun, 2005). These improvements enhance notably the flood warning systems, and the predictive understanding of flash floods (Borga et al., 2007; Delrieu et al., 2005; Ogden et al., 2000; Vivoni et al., 2007).

The idea of using satellite rainfall for flood modeling has been implemented since the late 1970s (Scofield and Oliver, 1977). The direct use of satellite rainfall estimations into hydrologic models can be apply in large basin scale with daily to monthly time scales (Artan et al., 2007; Behrangi et al., 2011; Bitew and Gebremichael, 2010; Collischonn et al., 2008; Grimes and Diop, 2003; Guetter et al., 1996; Su et al., 2008; Tsintikidis et al., 1999; Wilk et al., 2006; Wu et al., 2012) and small-scale basins (100–1200 km^2) with 1–3-h time scales (Bitew et al., 2011; Gourley et al., 2011; Nikolopoulos et al., 2010, 2012).

The relationship between precipitation inputs and flood outputs has been described differently in different studies. However, these differences may be caused by the differences in climate and drainage basin area. It was pointed out that there is no direct relationship between runoff production and connected channel flow (Sharma, 1998). There are many different factors that could result in this variability, including the heterogeneity existing in surface crusting and roughness (Auzet et al., 1995; Helming et al., 1998; Singer and Le

Bissonnais, 1998) and within soils themselves (Fitzjohn et al., 1998), the density and type of vegetation (Bergkamp et al., 1996; Imeson et al., 1992), the catchment morphometry (Yair and Raz-Yassif, 2004), the rock exposures (Yair and Kossovsky, 2002), the transmission losses in tributaries and main channels (Reid and Frostick, 1997) and land use (Bull et al., 2000; Lasanta et al., 2000).

1.2.2.1.3. Rainfall uncertainty

The rainfall observation can be affected by many partial uncertainties which depend on the type of measurement (Stransky et al., 2007).

The rainfall observation by rain gauge uncertainty can be caused by random and systematic errors. Random errors mainly derive from a mechanical and electrical disturbance in the gauge, data transmission, and tipping bucket clogging. Meanwhile, systematic errors are mainly the results of wind, wetting of internal walls, splashing, evaporation, and rain gauge design. These errors can cause underestimation of the rainfall volume of about 3% to 30% (Rauch et al., 1998).

Using radar leads to a number of error sources which relate to radar calibration, atmospheric attenuation, the variability of the relationship between radar reflectivity and rainfall rate, ground clutter, vertical reflectivity profile, and beam blockage effect (Krajewski and Smith, 2002). The errors affect extremely in radar observations over complex terrain areas and in real-time radar-rainfall applications (Gourley et al., 2011). Error in remotely sensed precipitation data would be transmitted, leading to the uncertainty in associated with hydrological model structure and parameters(Chen et al., 2016).

There are also two types of uncertainties associated with satellite precipitations products: the systematic and random errors. There are different factors that affect these errors, including the sensor observation, the algorithms that produce the rain estimated from the observations and the sampling process. The random errors are mainly resulted from the sensor sampling design, while the systematic errors can derive from problems such as the inclusion of gauge information (Huffman, 1997). However, the complete removal of both systematic and random errors is impossible due to the lack of high-quality reference datasets to estimate these uncertainties, despite current efforts in that direction(Maggioni et al., 2016).

1.2.2.2. Initial condition

1.2.2.2.1. Soil moisture

Soil moisture has great effects on hydrological and meteorological processes; in particular, it controls the process of partitioning rainfall into runoff and infiltration. The magnitude of the flood event is strongly influenced by the initial soil moisture conditions of the catchment (Tramblay et al., 2010). Thus, it is necessary to accurately estimate soil moisture for a range of hydrological applications, including floods and drought forecasting and assessment. The content of water in the first active meters of soil plays a central role in the regulation of the hydraulic and energy transfers between the soil, the surface and the atmosphere (Vischel et al., 2008). Thus, it is very important to have a realistic representation of the spatial variability of near-surface soil moisture to represent the hydrological fluxes in the subsurface at various scales (Zehe and Blöschl, 2004) and to link between hydrological and atmospheric processes (Montaldo and Albertson, 2003; Ronda et al., 2002).

However, it is challenging to obtain an accurate estimation of soil moisture due to its high spatial and temporal variability (Western and Blöschl, 1999). In small scale, among other factors, this variability mainly depends on topography, soil type, precipitation and vegetation (Western et al., 2002). Besides, the spatial variability of soil moisture also strongly controls the runoff. In particular, the dominant flow path varies under different soil moisture conditions, which in turn affects the runoff peaks and response time (Patil et al., 2014; Penna et al., 2011).

Information about soil moisture with increasing temporal and spatial resolutions (Wagner et al., 2007) are currently available from different sources, including the in situ measurements (for example the International Soil Moisture Network ISMN (Dorigo et al., 2011)), satellite sensors information (for example the Advanced Microwave Scanning Radiometer for Earth observation AMSRE (Owe et al., 2008), the Advanced SCATterometer ASCAT (Bartalis et al., 2007), the Soil Moisture and Ocean Salinity Mission SMOS (Kerr et al., 2010)), and from land surface models (for example, the ERA-Interim/Land data set (Balsamo et al., 2015)).

Soil moisture can also be used as a proxy to assess the wetness state of the catchment to predict flood hydrographs. Many studies have been investigating the assimilation of soil

moisture observations into rainfall-runoff (RR) modeling (Brocca et al., 2008; Javelle et al., 2016; Massari et al., 2014; Tramblay et al., 2012). Besides, Yu et al. used the output of the daily SWAT continuous model embedded in an event-based sub-daily SWAT model (Yu et al., 2018). Field monitoring of soil moisture was also used (Tramblay et al., 2010) and satellite soil moisture data were suggested (Tramblay et al., 2012). At this point, the relationship between the initial condition of the model and the external predictors remains however little known and needs further exploration.

Among the others, the SIM model is one of the French models which can produce soil moisture daily data (Habets et al., 2008; Quintana Seguí et al., 2009).

SIM model

The SIM model is the combination of three independent models: SAFRAN which provides atmospheric forcing analysis, IBSA which computes the surface water and energy budgets, and MODCOU which computes the evolution of the aquifer and the river flow. The SIM model system was firstly tested for France catchment in 1999. It was extended for all over France since 2002 and has been used operationally at Meteo-France to monitor the near real-time water resources since 2003.

For the ISBA model which give the output of the soil moisture, most of the parameter is defined by the soil and vegetation classification except the subgrid runoff parameter and the subgrid drainage parameter. The soil classification derived from ECOCLIMAP database (Champeaux et al., 2005). The vegetation classification based on CLC 1990 database, associated with a climate map. It is claimed that quite correct for the forested areas, vineyards, and urban area but not distinguish the various crops that are aggregated into a single class (Habets et al., 2008).

The information of soil which the origin comes from FAO-UNESCO soil map of the word gave the three qualitative properties of soil: soil color (light, medium, dark), soil texture (fine, medium, coarse) and drainage (free, medium, impeded). Soil depth is related to the root zone of the plant, which derived from the type of vegetation.

The SIM model supplied output indexes once a day at 6 UT, over an 8x8 km^2 grid mesh of France, for three layers (Boone et al., 1999): the surface layer (1cm deep), the root layer and the deep layer (depths depending on the type of vegetation).

1.2.2.2.2. Base flow

Another initial condition index we can consider is base flow. Base flow is generated by the amount of precipitation that infiltrates through the subsurface and discharges to the streams. Various basin characteristics, including catchment geology, climate, soils, topography and land cover, can affect the amount of base flow that discharges to the streams. High rates of infiltration, recharges and groundwater storage can increase base flow, while high rates of evapotranspiration and runoff can reduce base flow (Brutsaert, 2005). The subsurface storage and drainage network structures are strongly dependent on the geological characteristics (Price et al., 2011), while the rate of infiltration, hydraulic conductivity, and groundwater recharge depend on soil characteristics (Pirastru and Niedda, 2013). Besides, the topographic characteristics can also influence base flow by affecting the movement of water across the surface and subsurface, which in turn can influence the infiltration, flow process and rates of water transmission (McGuire et al., 2005). Moreover, the vegetation can also affect the base flow by changing the rate of interception, evapotranspiration, infiltration, and recharge of subsurface storage (Nie et al., 2011). Last but not least, temperature, precipitation, and other climatic factors can have impacts on base flow as they can change the rate of evaporation, infiltration, and recharge. These climatic factors can also cause snowmelt runoff, which can also alter the base flow (Tague and Grant, 2009).

Information about baseflow can be obtained by inferring from field measurements of different characteristics, including temperature, tracer concentrations and flow by seepage meters which are installed in the stream beds (Becker et al., 2004). However, these techniques are often challenging to be applied over an entire catchment. Baseflow is thus often estimated using different baseflow separation methods. The estimation of baseflow can be based on either the linear storage-discharge relationship between aquifer and stream (Barnes, 1939; Hall, 1968) or nonlinear storage-discharge relationship (Wittenberg, 2003; Wittenberg and Sivapalan, 1999), depending on the characteristics of the catchments. Besides, baseflow can also be estimated using hydrological reasoning without physically-based mathematical framework, including four main categories of methods: (i) graphical separation (Sloto and Crouse, 1996), (ii) conceptual models (Eckhardt, 2005; Huyck et al.,

2005) (iii) recession analysis (Tallaksen, 1995) and (iv) recursive digital filters (Arnold and Allen, 2007; Nathan and McMahon, 1990).

1.3. Hydrological model

Nowadays, with the development of hydrological science and information technology, flash floods, and floods, in general, can be simulated and predicted by models. It helps people in the understanding flood and most importantly, reducing damages of floods.

1.3.1. Definition – why we need models

A model is a representation of one or more concepts that may be realized in the physical world (Friedenthal et al., 2014). Consequently, a model always describes the basic and most important components of a complex system. Modeling supports the conceptual exploration of the behavior of object or process and their interaction. Modeling is a mean of better understanding and generating hypotheses; it also supports the experiments in which hypotheses can be tested, and the outcomes can be predicted (Gregory, 1998). Modeling is also a good way to reproduce data which are difficult to measure (e.g. floods) from data which are more easily available (rainfalls, catchment geography).

The hydrologic real-word system can be simplified and characterized using a RR model. By modeling runoff, we can better understand the hydrologic phenomena, as well as how those phenomena affect the hydrological cycle (Xu, 2002). RR models also help to reproduce floods in any situation which cannot be observed, or which is difficult to observe: for example, extrapolation to extreme floods, floods in ungauged catchments, forecast of floods.

A runoff model can be defined as a set of equations which helps estimate the amount of rainfall that turns into runoffs (Devia et al., 2015). These equations involve input variable (e.g. rainfall, slopes, etc.), output variable (here, various characteristics of the flood: runoff volume, peak flow, rising time, etc.), and parameters which describe the watershed. A variable in a hydrological system is understood to be a characteristic which may be measured, which assumes different values when measured at different times. Daily rainfall, runoff, evaporation, temperature, infiltration, soil moisture, etc. are some of the examples (Xu, 2002). A parameter is a quantity characterizing a system. The parameter is internal to the model and it can be estimated from data. It may or may not remain constant in time.

Since the first runoff prediction model appeared in the 19th century, RR models continued to develop until now. The major development of RR models is made thank to the availability of the learning data sets which were used to calibrate the nonlinear behavior of those models. Currently, a wide range of RR models are used, which applications highly depend on the purpose of modeling. Those models can be helpful in decision making by providing a means of quantitative extrapolation or prediction. RR models can be classified and divided into different types based on spatial resolution, input/output type, model simplicity, etc. Despite the different classification, not all models fit into a single category because they are normally developed for different purposes (Singh, 2012). The selection of an appropriate RR models needs to be based on the modeling purposes, for instance, to understand and answer a specific question about hydrological processes, to assess the frequency of runoff events, to estimate the runoff generated for management (Vaze et al., 2011). Choosing the most appropriate models also based on the data availability, time and budget for modeling.

The first way to classify RR models is based on the model structure, which determines how runoff is calculated, by which RR models are categorized into empirical, conceptual and physical models. Some RR models can involve a few variables while others may require a large number of interconnecting variables. The model can have the structure varying simple to complex depending on the equations. The empirical model is the simplest type, while the physical mechanistic model is the most complex type of RR model. The application of both physical and conceptual models requires an understanding of the physical process involving in the movement of surface water in the hydrological cycle (Srinivasulu and Jain, 2008). The differences between the three types of models are explained in detail in Table 1.1.

.

Table 1.1: Comparison of the basic structure for rainfall-runoff models (Sitterson et al., 2017)

	Empirical	Conceptual	Physical
Method	Non-linear relationship between inputs and outputs, black box concept	Simplified equations that represent water storage in catchment	Physical laws and equations based on real hydrologic responses
Strengths	Small number of parameters needed, can be more accurate, fast run time	Easy to calibrate, simple model structure	Incorporates spatial and temporal variability, very fine scale
Weaknesses	No connection between physical catchment, input data distortion	Does not consider spatial variability within catchment	Large number of parameters and calibration needed, site-specific
Best Use	In ungauged watersheds, runoff is the only output needed	When computational time or data are limited	Have great data availability on a small scale
Examples	Curve Number, Artificial Neural Networks[a]	HSPF[b], TOPMODEL[a], HBV[a], Stanford[a]	MIKE-SHE[a], KINEROS[c], VIC[a], PRMS[d]

[a] (Devia et al., 2015)

[b] (Johnson et al., 2003)

[c] (Woolhiser, 1989)

[d](Singh, 2012)

There is another classification system for RR models, which is based on the spatial interpretation of the model's catchment area. The spatial interpretation of the catchment area is based on input data and the way in which runoff is generated and routed over the catchment (Figure 1.8). Following this classification, RR models are categorized into lumped, semi-distributed and distributed models. These models differ in consideration of variability in geology, soils, vegetation, and topography of a catchment which affect the relationship between rainfall and runoff (Beven, 2012)

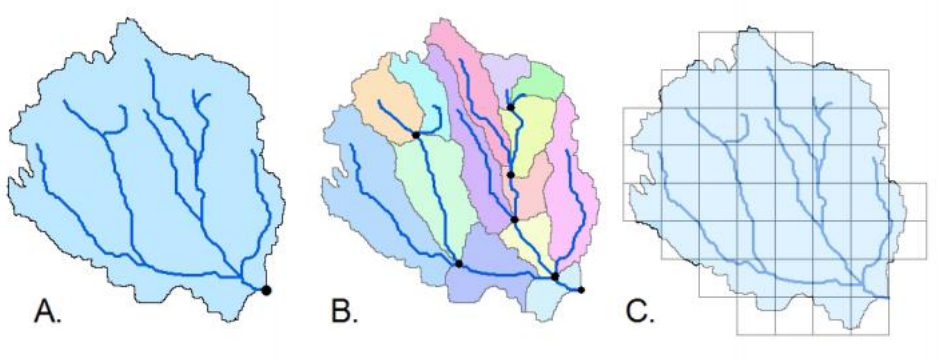

Figure 1.8: Visualization of the spatial structure in runoff models. A: Lumped model, B: Semi-Distributed model by sub-catchment, C: Distributed model by grid cell (Sitterson et al., 2017)

In particular, the lumped model does not consider the spatial variability within a catchment, while the semi-distributed model does consider some spatial variability, and distributed models consider and process spatial variability via the grid cells. In other words, different types of model consider different spatial processes and produce different output type. The detailed differences between those three types of models are presented in Table 1.2.

Table 1.2: Comparison of the spatial structures in rainfall-runoff models (Sitterson et al., 2017)

	Lumped	Semi-Distributed	Distributed
Method	Spatial variability is disregarded; entire catchment is modeled as one unit	Series of lumped and distributed parameters	Spatial variability is accounted for
Inputs	All averaged data by catchment	Both averaged and specific data by sub-catchment	All specific data by cell
Strengths	Fast computational time, good at simulating average conditions	Represents important features in catchment	Physically related to hydrological processes
Weaknesses	A lot of assumptions, loss of spatial resolution, not ideal for large areas	Averages data into sub-catchment areas, loss of spatial resolution	Data-intense, long computational time
Examples	Empirical and conceptual models,	Conceptual and some physical models,	Physically distributed models, MIKESHE[c],

machine learning	TOPMODEL[a], SWAT[b]	VELMA[d]

[a] (Devia et al., 2015)
[b] (Beven, 2012)
[c] (Singh, 2012)
[d] (McKane, R. et al., 2014)

The final classification that is mentioned in this report is continuous/event-based RR models. Depending on how the model chooses the required initial condition, hydrological models will be categorized as continuous or event-based. The continuous approach requires an initialization, or warm-up period, in which the model is run until its state reaches a value that is no longer dependent on an arbitrarily selected initial value. The duration of this initialization period depends on the memory of previous conditions of the catchment and on the model. The duration of this period may last for a few months (Kitanidis and Bras, 1980b) or for one climatic cycle, however, for certain catchments with large aquifers feed streamflow, this period needs up to several years (Le Moine, 2008). This data requirement leads to one major drawback of continuous approach in operational forecasting perspective, as it is often difficult to provide the long continuous precipitation time series up to the day of interest due to difficulties in real-time data repatriation. Thus, it is necessary to gather a sufficiently long data series before making the first forecast in a new location if the continuous approach is used.

On the contrary, event-based models use a different method to obtain the initial value of the model states. There are different methods that are used in the event-based approach. The values can be defined based on the climatology if the model states reliably represent measurable physical quantities. For instance, the event-based SCS-CN model can be integrated with soil moisture measurements for flow simulation on the small catchment (Brocca et al., 2009), however, the results should be generalized. Although continuous models have been applied a rigorous approach to estimate the initial conditions for a long time (Kitanidis and Bras, 1980a), event-based models are often preferred in real-time operational applications (Lamb and Kay, 2004). This is partly because event-based models are simpler, as they do not require all the necessary process as in continuous models, thus this type of models is more suitable to limited data. Besides, it is often challenging to look for

high time resolution series, as it is difficult to maintain and validate automatic measurements networks over a long period of time in many countries. Nalbantis once suggested the use of coarser data series (e.g. daily) to estimate fine initial conditions to overcome this challenge (Nalbantis, 1995). Furthermore, the event-based approach may be culturally favored by some people who are traditional users of hydraulic propagation methods. Due to the reasons mentioned above, event-based models are becoming more widely used by practitioners. Moreover, event-based models are useful for other purposes rather than flood forecasting, such as torrential flood modeling.

As opposed to continuous modeling which simulates streamflow over a long period (Stephens et al., 2018), the event-based approach considers each individual rainfall-runoff event separately. As precipitation and streamflow data are rarely collected at hourly or finer scales for a long period due to limited data availability, continuous hydrologic models are usually applied at daily scale. Meanwhile, event-based hydrologic models can be applied at sub-daily time scale (Yao et al., 2014), such as hourly or finer scale.

The continuous approach considers some flow components, including for example evapotranspiration and subsurface flow. Meanwhile, these flow components might be excluded to some extent or become less important in event-based approach, in which their underlying processes are not active for the considered rainfall-runoff events (Huang et al., 2016). The event-based models have advantages such as using limited data or reducing the complexity of the model and the number of parameters. However, they need to be initialized for each event, and the initial condition of the model has to be derived from an external variable, which expresses the state of the catchment at the beginning of the rain event. A comparison of event-based and continuous models was performed elsewhere (Berthet et al., 2009). It showed that both types of model were more or less equivalent. Recently, another study also compared continuous and event-based models and showed that event-based models are suitable for climate change impact (Stephens et al., 2018). However, event-based models are often the only option in many cases, when a complete series of data are not available.

1.3.2. Model's operation

1.3.2.1. Calibration of the model

Most models contain two types of parameters: physical parameters (defining the physical structure of the system) and process parameters (defining the order of the process's magnitude). Defining of the process parameters is known as calibration of the model. When the model is physically based, these process parameters can be defined by the measurement, otherwise, they are calibrated using an optimization process (Kirkby et al., 1993).

In the calibration, we must pay attention to the sensitivity of the parameters, with carefully calibrating the sensitive parameters to ensure the reliable outcomes of the model. Trial-and-error is the simplest form of model optimization. In this approach, the model parameters are changed; then a metric of model accuracy will be measured and noted. This process will be repeated until the best possible fit of prediction and observation is obtained. The selecting of the calibration parameters and techniques is depended on the purpose to which the model will be put (Wainwright and Mulligan, 2013).

Furthermore, the results obtained from model calibration depend strongly on the function and objectives. Indeed, a model that is calibrated for predicting the peak flow will be very different from that predicting total flow (Botterweg, 1995). The prior information on the range of the parameters is also essential for model calibration, thus a preliminary sensitivity or uncertainty test are usually implemented before model calibration. The range of the parameter and the agreement of the model makes a relationship called the calibration curve for that parameter. A parameter that has a significant change in error with the changing of its value is the sensitive parameter (Wainwright and Mulligan, 2013).

Model parameters are often highly interdependent in most models, which can make optimum parameterization become more challenging. Especially, in the distributed model, calibration is even more difficult due to a large number of parameters involved (Eckhardt and Arnold, 2001).

1.3.2.2. Sensitivity test

Sensitivity analysis is the process of defining how the magnitude of model output affected by changes in model input parameters. Sensitivities test often carries out before the

calibration because it can act as a check on the model logic and the robustness of the simulation and it can define the importance of the parameter. The measurement of the sensitivity test to a parameter can also help to understand the impact of the uncertainty of this parameter on the model outcomes. If sensitivities analysis show that the model has too many sensitive parameters, this may indicate over-parameterization and the need for the model simplification. Sensitivities analysis is also made for understanding the impact of parameter forcing, and its interaction/dependence (Michaelides and Wainwright, 2002).

In most sensitivity test, a single parameter is varied around its normal value when the other parameters keep unchanged (Saltelli et al., 2009). Then, the changes in model outputs in response to the changes in those parameters are recorded. Model sensitivity is defined as the proportional change in model output per unit of change of the input parameter. Besides, the sensitivity of models to a parameter could also be affected by the values of other parameters. It is important to recognize the different trend for parameter change in sensitivity analysis: to reach a threshold of value, the change of the parameter can have the other effect on the model output. In this case, it is necessary to have appropriately assessed the range of parameter variation, as well as the values of varying and non-varying parameters during the sensitivity test.

1.3.2.3. Error, uncertainty, and equifinality

All the measurements are made with error, which should be cited so that the implication can be considered during the interpretation of results. This is especially important when a secondary dataset, in which little is known about its data collection and quality control, is used. In particular, field measurements are often error-prone due to the difficulties in data collection. Indeed, specific problems can arise during the measurement of features with fractal characteristics or when the system is sensitive to initial conditions due to the lack of precision. Therefore, it is important to consider modeling requirements to decide the precision of measurement.

Error leads to the uncertainty in modeling. Zimmerman (2000) defines six causes of uncertainty in the modeling process: lack of information, an abundance of information, conflict evidence, ambiguity, measurement, and belief (Zimmermann, 2000). Lack of information demands to collect more information, but it is worth to know the quality of this

information. The abundance of information relates to our inability to perceive a large amount of complex information, and it requires the simplification of information. Conflicting information need the application to evaluate and control the quality of information, and to find the source of conflict that comes from errors or the wrong use of the model. Ambiguity may result in confusion during the reporting of information. Measurement uncertainty can be reduced by the involvement of more precise techniques. Uncertainty can also be caused by beliefs in data interpretation, as the different outcome can arise from the same starting point.

Errors are considered as an important part of modeling, which must be integrated into the framework and uncertainty evaluation of all realistic modeling approach. The uncertainty is needed to concern in all modeling cases; it has significant impacts on model applications (Beck, 1987). The implication of error and uncertainty is that we need to improve the basic inputs into the model as much as possible, not only the quantity but the quality of the data.

The main operation to deal with uncertainty is parameter identifiability. When a given model with a set of data can constrain the parameters, we can identify the maximum likelihood values of the parameters which means that those parameters are identifiable. Inversely, there is an issue of equifinality in data assimilation (Beven, 2006). Equifinality means that different models, or different parameter values of a model, maybe equally well-fitted to the data without the ability to distinguish which models or parameter values are better than others (Luo et al., 2009).

In hydrological models, equifinality arises when many different parameter sets are equally good at reproducing an output signal. This normally happens with distributed models with a large number of parameters which are quite good at describing hydrological behavior but are unable to predict what will happen if certain characteristics of the catchment change (Savenije, 2001).

To deal with errors, uncertainties and equifinality, the validation step is needed to check the quality of a model.

1.3.2.4. Validation

Validation is the process to test the model output to confirm the results that should be produced for the same inputs in reality (Fishman and Kiviat, 1968). The dataset for the validation must be independent of the dataset which is used for the calibration. Rykiel (1996) distinguishes validation into three types: (i) operational or whole- model validation (correspondence of model output with real-world observation); (ii) conceptual validation (evaluation of underlying theories and assumption); and (iii) data validation (evaluation of the data to test the model) (Rykiel, 1996). There also are many sorts of the procedure can be applied for the validation, and all of these procedures provides the support for the model acceptant. The more tests a model can successfully pass, the more confidence we can have for the model. The model test aims to assess (i) the simplifications upon which the model is based, (ii) the optimal set of parameters obtained and (iii) the level of similarities between model output and test data. The evaluation process should be iterative throughout the modeling.

1.3.3. Scaling issues and spatial-temporal variabilities

1.3.3.1. Scaling issues

The scaling issues have been previously summarized by Zhang et al. (2013). Briefly, the scaling issues arise from the variation due to space, time or other dimensions in the real world. Following this concept, finite and discrete measurements are used to understand the infinite variables and the continuous system. Thereby, information about environmental features can be stored, recalled and analyzed. There are three types of scale: operation scale, measurement scale, and modeling scale. An operation scale is a scale which concerns the operation of a physical process in a natural environment. A measurement scale concerns the spatial resolution used to determine an object. There are two extents of a measurement scale for a data set: spatial (the space between samples) and temporal (the integration time).

Besides, a modeling scale relates to both the natural process and the applied models. A modeling scale can involve four different extents, including geographic scale (the research area), temporal scale (the time period of research), measurement scale of parameters (the resolution of input data) and the model scale (the temporal and spatial scale when a model

was established). The spatial scales can be local or plot scale (~1m), hillslope or research scale (~100m), catchment scale (~10km) and regional scale (~1000km), while the temporal scales can be event scale (~1 day), seasonal scale (~1 year) or long-term scale (~100 years).

There are many causes leading to scaling problem (Harvey, 2000; Heuvelink, 1998). The most common and fundamental cause is the existence of spatial heterogeneity and relevant process nonlinearities. Indeed, the spatial scale depends on both climatic input data and land-surface parameters, which are in turn derived from various measurements including temperature, precipitation, topography, land uses, soil physical and chemical properties and other hydrological properties. Thus, it is difficult to aggregate large-scale behavior from local processes. The second reason is that the predominant processes can differ in different scales. The correlations derived at one scale might not be applicable to another scale. Therefore, more processes need to be considered by the scaling method. The third cause is the cross-scale interactions between small-scale and large-scale parameters, suggesting that scaling should be only applied over a limited range of scales and specific context. Another cause for scaling problems is the lack of information on process linkages in a dynamic environment.

The alterations of the scale measurement can significantly influence the variability of model parameters. The physical meaning of model parameters is associated with its corresponding processed. If a parameter is estimated at its process scale, its value will be able to approximate the reality. Otherwise, its value will be less realistic if the measurement scale is larger or smaller than the process scale.

1.3.3.2. The temporal variability

The temporal variability of hydrological phenomena can be caused by climatic and human factors. There are different types of temporal variability, including the diurnal, annual, inter-annual or irregular temporal variations. Among those, diurnal and seasonal characteristics are the important source of variations that affect directly the flood process.

The diurnal variability of hydrological phenomena can result in changes in river pattern, for example, due to snowmelt, evaporation or water management operations. The diurnal variability can influence the behavior of discharges in terms of timing, relative magnitude, and shape (Lundquist and Cayan, 2002). For example, in rivers where water is added diurnally, the discharges will be characterized by daily sharp runoff rise and gradual decline.

Meanwhile, in rivers where water is removed diurnally, the discharges will be characterized by daily gradual runoff rise and sharp decline.

The seasonal variability of hydrological phenomena can differ across different area. In particular, this type of variability also depends on climatic factors, for example, on seasonal snow accumulation and release, or seasonal rainfall changes. The inter-annual variability is also caused by climatic phenomena, such as the atmospheric-ocean phenomena like El Nino or Pacific Decadal Oscillation (Woods, 2006).

Another important type of spatial variability is caused by irregular phenomena, including storms and floods (Woods, 2006). These extreme weather phenomena can affect the streamflow directly. Especially, this type of temporal variability is now becoming more important nowadays, due to the more frequent extremes foreseen under the climate change conditions.

1.3.3.3. The spatial variability

The spatial variability of hydrological phenomena are the results of spatial patterns in climate, land use, topography, geology, and soil characteristics.

Climate factors are indeed an important cause of spatial variability. Climate conditions vary across different regions, which strongly affect hydrological processes. For example, rainfall accumulation tends to be higher in the high mountainous area than in the downhill area. Climate conditions can also vary within a specific region. For instance, rainfall accumulation can be greatly different between the upwind and downwind side of the mountains, due to differences in air moisture (Woods, 2006).

Geological and soil characteristics are characterized by complex spatial variability. This type of variability can affect hydrogeological characteristics such as porosity and permeability, which in turn affect the rate of infiltration and water movement throughout soil layers. The variation of topography within and across the region can also affect hydrological processes, as it can influence the streamflow direction and velocity. Last but not least, vegetation is also an important source of spatial variability, as it can affect water transport, evapotranspiration, soil water content. The presence of plants in different regions also reflect the climatic conditions.

1.4. Mediterranean flash floods

1.4.1. Characteristics of Mediterranean flash floods

The Mediterranean region is a large area with more than 4,000 km along from the west to the east and 1,500 km from the south to the north. The distribution in climatic patterns and population densities in this region are very spatially variable (Gaume et al., 2016).

Flood is one of the most dangerous meteorological hazards affecting the Mediterranean countries. Floods in some Mediterranean regions such as southern France, Italy; eastern Spain; and the west of the Balkan Peninsula, are such frequent enough to be considered as a component of the local climate (Llasat et al., 2010). These regions have widespread and intense economic activity and high population densities. Thus, the frequency and the impact of floods on the entire Mediterranean region are not homogeneous over the entire area.

The Mediterranean floods are mostly fast floods, often called "flash floods" which are induced by short duration (less than one hour to 24 hours) and caused by the very intense and concentrated in time Mediterranean rains (typically 100 mm or more rainfall accumulated over a few hours) (Creutin et al., 2009). Moreover, the Mediterranean basins are often small which limited to a few hundred square kilometers (Camarasa-Belmonte, 2016; Creutin et al., 2009), with rapid hydrological responses (generally less than 6 hours of delay between the peak rainfall intensity and the peak discharge downstream) is also one of the conditions for flash flood. The most important floods usually occur in autumn, when the Mediterranean Sea is still warm and liable to evaporate humid and unstable water bodies towards the continental surfaces (Anquetin et al., 2004; Pensieri et al., 2018).

Besides, the Mediterranean basins are often characterized by low permeability, highly erodible soils and steep slopes that are susceptible to landslides. Thus, the fast response runoff of these basins considerably favors the formation of flash floods (Creutin et al., 2009). Flash floods can cause huge damage for the Mediterranean regions not only because it can bring a high content of solid materials (e.g. mud, debris, and timber) from the riverbed and soil slips, but also due to the high population density of the coastal regions. It is very difficult to predict the area that will be affected by flash floods with high accuracy, even when there is more precise weather forecasting for civil protection purposes.

1.4.2. Recent flash flood events

Flash floods have caused billions of euros of damages and several dozens of casualties in the South of France near the Mediterranean Sea over the last two decades (Gaume et al., 2004). In September 1992, a flash flood occurred in Vaucluse, Vaison-la-Romaine causing 32 deaths (Rebora et al., 2013). A flash flood took place in Aude, Languedoc-Roussillon leading to the death of 35 people in November 1999 (Bechtold and Bazile, 2001). In addition, another flash flood happened in Gard, Languedoc-Roussillon in September 2002 causing 22 deaths (Delrieu et al., 2005). Moreover, in the flash flood in June 2010, after a storm hitting South-East France, The casualties list were 25 people (Javelle et al., 2016).

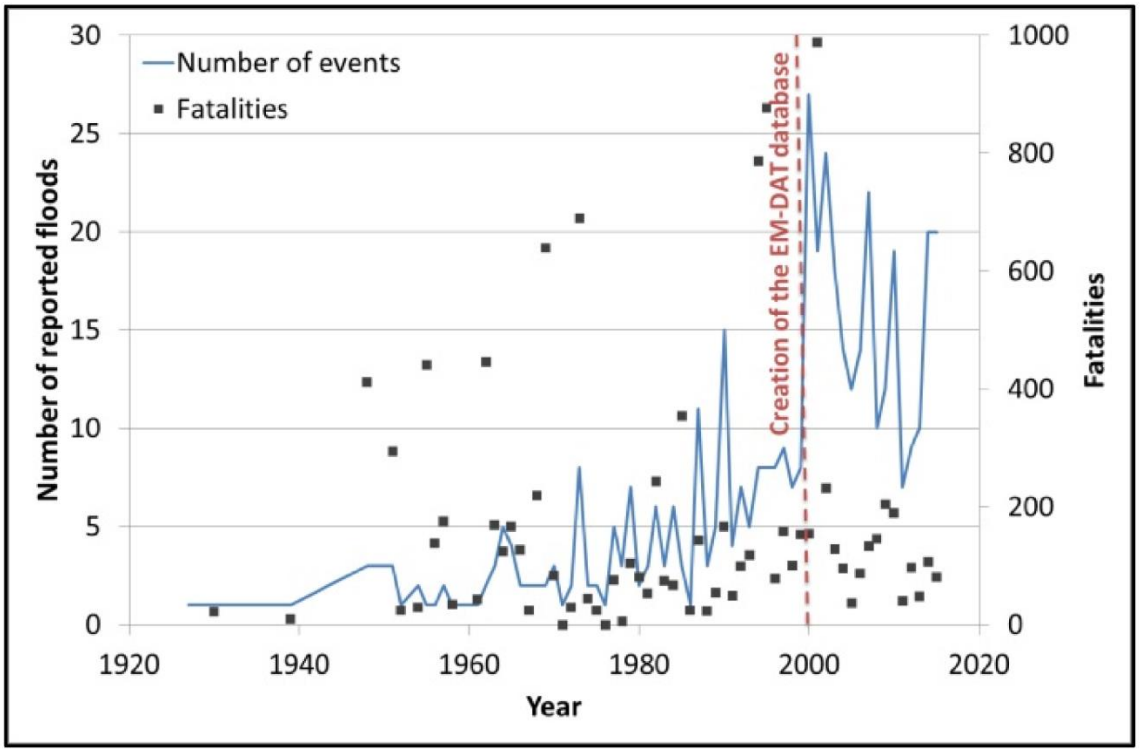

Figure 1.9: Changes in the number of damaging floods and the number of fatalities in the countries in the Mediterranean regions documented in the EM-DAT database (source: emdat.be)

Several floods database were created in recent years (Figure 1.9). For example, the Emergency Events Database EM-DAT collects information on disastrous events, including floods, which meet one of the following criteria: at least ten deaths, 100 people affected, a declaration of a state of emergency and whether there was a call for international assistance.

The number of floods documented by this database has increased since its creation. However, the total number of reported annual fatalities does not increase over time. This inconsistency suggests that there might be a large number of moderate floods included in the databases since the start of data collection by EM-DAT, and the number of catastrophic events does not significantly change.

Table 1.3: The contents of the database of most notable Mediterranean flash flood events for the period 1940-2015 based on their estimated discharges or to the number of deaths. When no estimated discharge was available, events with more than ten deaths were selected, except for Greece for which a larger dataset was available (Gaume et al., 2016).

Country	Number of events	With discharge estimates	Sources
Algeria	20	1	(Recouvreur, 2005; Sardou et al., 2016), press
Egypt	3	0	Internet and press
France	40	38	Hydrate, recent surveys by the authors, press
Greece	22	5	Hydrate, press, (Diakakis and Deligiannakis, 2017; Papagiannaki et al., 2013)
Israel	11	11	(Tarolli et al., 2012)
Italy	46	36	Hydrate, (Anselmo, 1985), (Barredo, 2007), recent surveys, press
Lebanon	1	0	Press
Morocco	7	7	Hymex database
Portugal	1	0	Press
Slovenia	1	1	Survey by (Gaume et al., 2016)
Spain	16	11	Hydrate, (Llasat et al., 2013), (Barredo, 2007)
Tunisia	3	2	Press and technical reports
Turkey	1	0	Press
Total	172	112	

As a type of flood, a flash flood is also mainly sensitive to rainfall accumulation, intensities, the shape and position of the maximum rainfall within the episode, to the previous rainfall that conditions the basin response. Besides, the total rainfall amounts, land use, soil, and

bedrock types and the initial soil moisture content strongly affect the responses of the catchments to heavy rainfall events, especially their runoff rates (which is defined as the estimated proportion of the incident rainfall contributing to the observed stream discharges). During flash floods, runoff rates can reach 100% in some rare cases, especially when the watersheds are saturated due to large cumulated rainfall amounts (Marchi et al., 2010). The complex interaction between the characteristics of the rainfall events (in terms of maximum intensities, duration, spatial extent) and the factors that control the response of the catchments (e.g. rainfall rates) has resulted in the observed variability of flood frequencies and discharge magnitudes.

1.4.3. Flash flood modeling applications and the concept of regionalization

1.4.3.1. Flash flood modeling applications

Many scientists have also researched this kind of phenomena in the previous time, and they also pointed out that there are many problems to solve. PiÑOl et al. used TOP MODEL to simulate the hydrological event in Spanish catchments and they realized that the spatial soil depth heterogeneity, as well as the characteristics and the localized nature of downslope flows of water in the soil, are the most difficult to be described in the model (Piñol et al., 1997). They also pointed out that models with very large numbers of parameters would not be easy to calibrate. Many applications using TOP MODEL have been made in the Mediterranean area and lead to promising data and results although there is a need for improvement for wetting up period or extreme events such as storm (Blöschl et al., 2008; Durand et al., 1992; Saulnier and Le Lay, 2009).

Another study has claimed that flash flood forecasting could not be characterized via only the deterministic and mechanistic approach, due to the complicated processes involved in its generation and propagation (Montz and Gruntfest, 2002). Many other applications of real-time flash flood forecasting have been proposed to describe the flood process. Indeed, a more recent research has introduced a semi-distributed model with empirical SCS concept on a hill slope and a Muskingum scheme (reservoir-type model) in the river into presenting flash

flood, in which the key parameters are derived from topographic conventional data, land cover maps and field surveys (Foody et al., 2004).

Another application is proposed using a spatially distributed model base in the physical process of the water cycle and flood genesis (Moussa and Chahinian, 2009). When the surface runoff is dominated in the hydrology process, this model is well-adapted; however, in the results, it is shown that the performance of the model decreases without the intense flood events. Thus, there is a question for the model to be well-represented for hydrological processes during both drought and flood periods.

Because of numerous and complex processes involved in a flash flood, the notion of the model framework including different concepts for each process of generation and propagation in flash flood was suggested to use. Each model can be a simplified hydrological physically-based model taking into account the spatial variability of different processes combines with the runoff process over hill-slopes derived from the kinematic wave approximation. The built model called MARINE stands for Model of Anticipation of Runoff and INondations for Extreme events (Estupina-Borrell et al., 2006; Roux et al., 2011).

1.4.3.2. The concept of regionalization

Although rainfall-runoff models are crucial tools for prediction and flood forecast, they must still be improved in order to gain for temporal and spatial extrapolation. Regionalization aims to transpose models from gauged catchments to ungauged one, and many regionalization studies have been performed up to now (McIntyre et al., 2005; Merz and Blöschl, 2004; Oudin et al., 2008; Young, 2006). Several methodologies can be used for regionalization:

Regionalization based on regression: it allows for defining a posteriori relationship between catchment attributes and model parameters at gauged catchments. After determination of these relationships, one can define parameters in ungauged catchments based on its physio-climatic characteristics.

Regionalization based on spatial proximity: this approach considers that the same parameter values can be associated with geographic neighbors with an assumption that physio-climatic characteristics of the explored region are homogeneous.Regionalization based on physical similarity: This type of regionalization approach represents the

combination of the previous two. It is based on a hydrologic similarity between an ungauged and gauged site where parameter transfer is not geographically based but rather in terms of similar catchment descriptors behavior.

However, previous studies revealed a poor efficiency of the models when transposed to ungauged catchments (Aubert et al., 2014; Bastola et al., 2008; Lee et al., 2005; Norbiato et al., 2009; Viviroli et al., 2009). The failure of regionalization may be mainly attributable to the equifinality, which makes that several sets of parameters can be accepted for modeling rainfall-runoff relationship; and makes difficult the spatial comparison and the interpretation of those parameters. Another difficulty in regionalization is due to the lack of appropriate descriptors of the catchment properties (mainly the soil properties) when using methods such as multivariable relationships (Oudin et al., 2010). In addition, scaling problems can interact with the interpretation of the parameters: scaling means that the parameters are not independent of the size of the catchment, for several possible reasons: heterogeneity of the surface (and possibly subsurface) features, change in the dominant processes, inadequacy of the equations at different scales, mismatch between the local field data and the aggregated parameters (Blöschl, 2001; Gentine et al., 2012; Vinogradov et al., 2011). Thus, further researches are needed to improve the performance of the regionalization.

1.5. Conclusion

The hydrological processes, flood processes, an overview of the model, Mediterranean floods and the applications of several models on Mediterranean floods have been described in this chapter, which provided the theoretical background for our study. In the next chapter, we will detail the methodology which is applied for Mediterranean flood forecasting. It is the combination of two widely-used models SCS production model and LR routing model.

2. Description of the SCS-LR model

This chapter describes the SCS-LR model used for the study. After a brief justification of the selection of the model, the main part of this chapter gives the information about the overview, previous application as well as the formulation of each function of the model. We also describe the main steps for using SCS-LR and the ATHYS platform, where SCS-LR was run within.

2.1. Introduction

The previous chapter showed that RR rainfall-runoff models are essential for flood forecasting or other hydrological applications, but that there were many RR models. The selection of the model was made from several considerations:

- The idea was not only reproducing floods, but also comparing the parameters in different catchments, over parametrization and equifinality must be avoided as far as can be, and the model must be parsimonious.
- Due to the poor knowledge about soil properties or other physical properties of the catchments, the model should be more conceptual than physically-based, which could be said in other terms that it is not worth to integrate additional wrong or uncertain data if not necessary.
- Distributed models are potentially more efficient than lumped models, but we should consider a reasonable level of distribution for not increasing too much the number of parameters. Accounting for the spatial distribution of the rainfalls is for example recommended, because it does not add complexity to the model parametrization; it would not be the case when using soil spatial distribution, which would bring additional model parameters.
- Because of the objective aims at flood forecasting, an event-based structure could be preferable, easier-to-use and easier-to-calibrate.

- Popular or widely used models could be better in order to the benefit of the previous experience relative to the model performance as well as the estimation of the parameters.

The SCS-LR model filled all the above criteria and was thus selected to be used as the reference model in this study.

2.2. State of the art of the SCS model

The SCS model was proposed in the mid-1950s by the United State Department of Agriculture. The model was designed from numerous infiltrometer experiments led during the 1930-40' in the USA. This model aims to demonstrate and evaluate the design and construction of soil and water conservation project. The method quickly became widely applied in hydrologic practice in the US and other countries due to its simplicity, predictability, stability.

Initially, the equation of the SCS model was:

Equation 1:

$$Q = \frac{(P - I_a)^2}{P - I_a + S}$$

where Q denotes the cumulated runoff at the event scale, P the cumulated precipitation at the event scale, Ia the initial ponding losses before the runoff starts, *S* the potential maximum retention or storage.

The SCS model relies on the concept that the ratio of the cumulated runoff Q and the cumulated precipitation P-Ia equals the ratio of the cumulated infiltration F to the maximum potential retention S:

Equation 2:

$\frac{Q}{P-I_a} = \frac{F}{S}$Equation 1 was obtained by combining Equation 2 with the equation of the budget:

Equation 3:

$$P = I_a + Q + F$$

Equation 1 turns into Equation 4:

$$Q = \frac{(P - 0.2S)^2}{P + 0.8S}$$

when considering that

Equation 5:

$$I_a = 0.2S$$

Equation 2 is an empirical equation which involves variables having physical meaning. SCS thus appears like a conceptual model.

From the beginning, the SCS model considered only one parameter, in which the potential maximum retention of post-initial abstraction retention S is determined from the scaled values of CN derived from the tables of the National Engineering Handbook. The Curve Number CN was computed as a function of S (expressed in mm):

Equation 6:

$$CN = \frac{25400}{S + 254}$$

This CN values depend on the soil type, land use, initial abstraction, antecedent moisture condition, hydrologic condition, climate and the characteristics of the rainfall, including intensity, duration, and turbidity.

(Mockus, 1964) defined S as being equivalent to the maximum differences between P and Q ($P - Q$). This difference corresponds to the maximum possible infiltration capacity of the soil, ignoring other losses including initial abstractions. (Yu, 1998) defined S as the product of the spatially averaged infiltration rate and storm duration during the attempt to theoretically justify the basis of the SCS hypothesis. (McCuen, 2002) defined S as the representation of volumetric retention, distinguished from in the filtration rate.

(Collis-George, 1977) described S by the relations of negative pressure-moisture content and hydraulic conductivity-moisture content, which characterize the moisture movement in unsaturated porous soil. These relations also represented the physical characteristics of the soil-vegetation-land use complex. According to this definition, the physical significance of S was explained by the linear Fokker-Planck equation for infiltration. This equation related S to the storage and transmission properties of the soil.

Since its first formulation, the SCS model was widely developed:

- As the SCS model was initially working with the cumulated runoff and rainfall at the event scale, several studies have pointed out the fact that this method did not consider any expression of time, so that it ignored the impact of rainfall intensity and its temporal distribution. Further formulations made it possible to predict infiltration rates and build runoff hydrograph (Aron et al., 1977; Gaume et al., 2004).
- The SCS was originally built as a lumped model which aggregated spatial and temporal variation into the total infiltration depth's calculation for a given storm and a watershed. However, since it was developed as an infiltration loss model, it can be distributed as well. The distributed model can describe local and/or instantaneous infiltration rates, by that a total infiltration depth can be obtained by appropriate integration in time and space.
- (Hawkins, 1993) noted that CN values could vary in a given catchment, according to the cumulated rainfall of the event. He explained that catchments could have three different types of asymptotic behavior: (i) complacent behavior: observed CN decline steadily with increasing rainfall depth. In this case, no constant value can be found for the curve numbers; (ii) standard behavior: it is the most common behavior which observing CN declines with increasing storm size. In this case, the CN approach maintains a near – constant value with the increasing of storm size and (iii) violent behavior: CN rise suddenly and asymptotically approach and apparent constant value. Thus, the watersheds are classified with their asymptotic behavior. SCS seemed to fail with some kind of watersheds, which have a complacent situation.
- Although widely used, the value 0.2 of the proportion between Ia and S has been frequently questioned (Hawkins et al., 2002). The value of 0.3 was recommended to use for most regions of India by (Central Unit for Soil Conservation, 1972). (Aron et al., 1977) and (Golding, 1979) suggested many other values for urban watersheds. Value of 0.2 was reported as not appropriate for both arid and humid watersheds and needed caution in use for other watersheds (Springer et al., 1980). Ia/S = 0 was the best fit to the dataset of (Cazier and Hawkins, 1984), and (Bosznay, 1989) suggested to treat a random value of Ia. (Chen, 1982) expressed Ia/S as the square root of the ratio of initial and final infiltration rates, and it could vary from 0 to 1.(Mishra and Singh, 2003) described Ia/S as the degree of atmospheric saturation and did not use

a proportional relationship between Ia and S. (Mishra et al., 2006) proposed different formulations of Ia/S depending of the soil type or the antecedent conditions.

- Initially, the SCS-CN method was developed and best performed in the computation of the amount of direct surface runoff (or rainfall excess) from a given storm rainfall which occurs on agriculture sites (Ponce and Hawkins, 1996) and urban environments (SCS, 1975). Steenhuis et al., (1995) proposed an interpretation of the SCS model in terms of runoff generated by variable source area processes.
- Michel et al., (2005) reformulated the time-dependent SCS model by directly relating the runoff coefficient to the level in a soil reservoir. This improvement allowed using the SCS model as a continuous model. It also made easier the integration of soil drainage.
- Theoretically, the SCS-CN method is applicable to catchments in any size as long as the measured runoff corresponds to the observed rainfall amount. However, in the large catchment (e.g. more than 250 km^2), there is a need to couple with routing model which plays an important role in converting the rainfall-excess to the surface runoff hydrograph produced at the outlet of the basin (Ponce and Hawkins, 1996).
- Using theoretical arguments, the SCS-CN method can be applied for long-term hydrologic simulation (Mishra and Singh, 2013). The SCS models have been applied in long-term hydrologic simulation in different studies with varying degrees of success (Hawkins, 1978; Knisel, 1980; Williams and LaSeur, 1976; Woodward and Gburek, 1992).
- One weakness of the method was due to the fact that only 3 discontinuous AMC (antecedent moisture condition) were used for estimating *S* or CN values. In addition, the classical criteria that determine these AMC were based on rainfall amounts during the five previous days, which were found to be inefficient in many cases (Huang et al., 2007). (Durbude et al., 2011) indicated that a continuous AMC could be more efficient to predict CN. (Tramblay et al., 2010) also related continuously the *S* or CN values to measurements or estimations of the water content. (Coustau et al., 2012) used piezometric levels to constrain *S* values.
- (Coustau et al., 2012) integrated drainage of the cumulated rainfall, resulting in a decrease of the runoff coefficient within a dry period. They also considered a delayed

runoff as a fraction of the drainage of the soil reservoir, increasing the accuracy of the recession of the floods.

2.3. SCS model formulation

The model that we used was the formulation of the SCS given by Michel et al., (2005), in which were added the drainage and delayed runoff proposed by Coustau et al., (2012) (Fig 2.1). The model can be applied in both event-based and continuous mode. The model was run within the ATHYS platform modeling www.athys-soft.org.

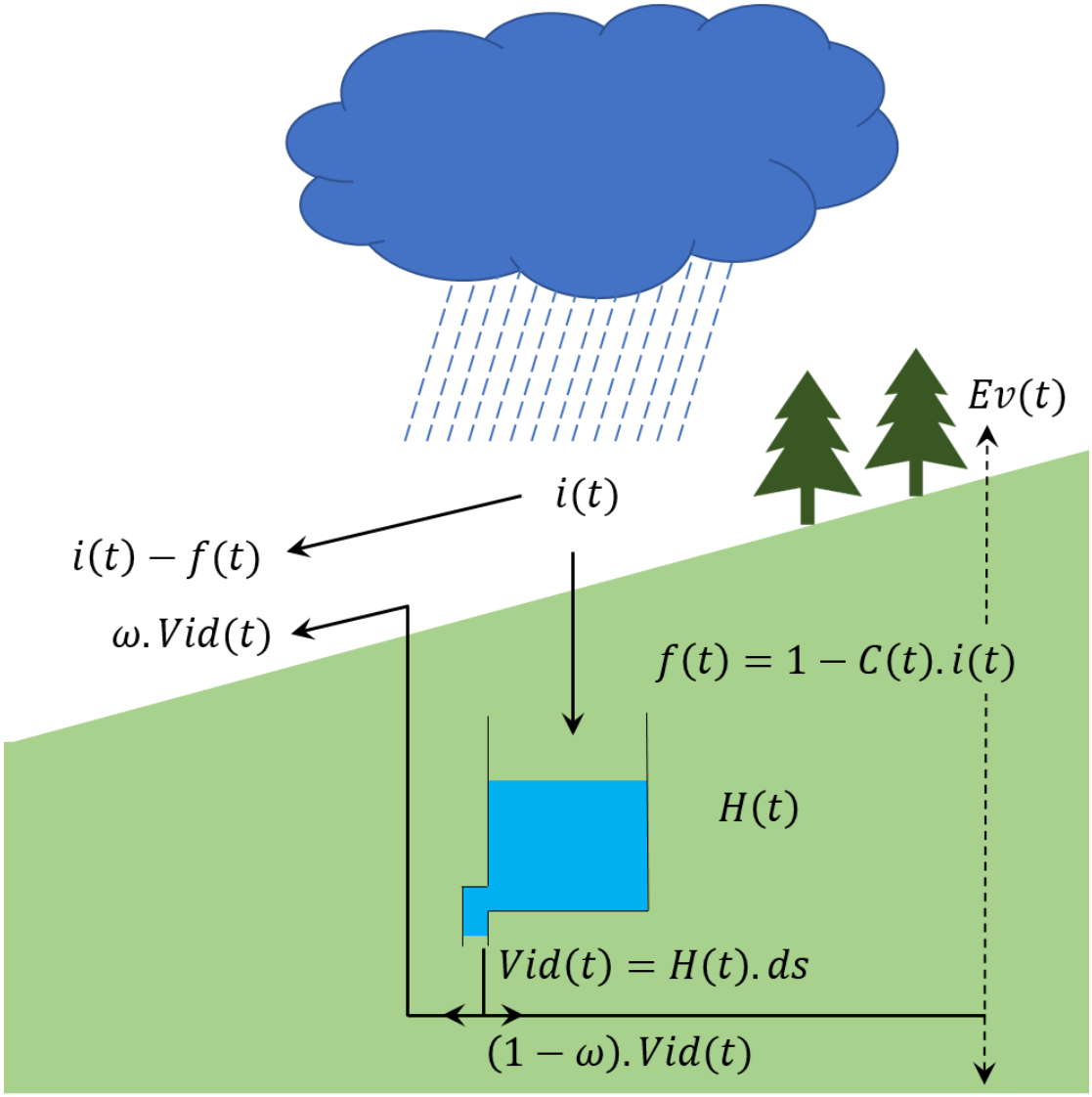

Figure 2.1: Scheme of adjusted Soil Conservation Service (SCS) model operating for each mesh of the basin.

The effective rainfall (or runoff) intensity $R(t)_{[L/T]}$ at a given time t can be calculated as followed:

Equation 7: $$R(t) = C(t).i(t)$$

in which, $i(t)$ [L/T] denotes the rain intensity at time t, and $C(t)$ [-] is the runoff coefficient, as (Michel et al., 2005):

Equation 8: $$\begin{cases} C(t) = \frac{H(t)-Sa}{S}.\left(2 - \frac{H(t)-Sa}{S}\right) when\ S(t) > Sa \\ C(t) = 0 \text{ otherwise} \end{cases}$$

In the equation above, t is the time, $H_{[L]}$ denotes the level of the soil reservoir; $S_{[L]}$ the maximum water capacity of the reservoir; $S_{a[L]}$ the Michel's initial abstraction, equal to the sum of the initial water level in the soil reservoir $H_{0[L]}$ and the $I_{a[L]}$ abstraction in the classical SCS:

Equation 9: $$S_a = H_0 + I_a$$

S_a should be independent of the event, which means that I_a is event-dependent, and that the variability of I_a is compensated by the variability of H_0.

The water level in the soil reservoir is governed by the infiltration and the drainage: the infiltration fills the reservoir, and the drainage makes that the runoff coefficient decreases when it does not rain (due to water evaporation near the soil surface, lateral subsurface flow or deep drainage at lower layers). The infiltration $f(t)$ equals:

Equation 10: $$f(t) = \big(1 - C(t)\big).i(t)$$

The drainage $Vid(t)_{[L/T]}$, so-called "the vertical flow", is assumed to be a linearly dependent on the level $H(t)$ in the reservoir:

Equation 11: $$Vid(t) = ds.H(t)$$

where $ds_{[1/T]}$ is a proportionality coefficient.

The level of the reservoir is finally computed by:

Equation 12: $$\frac{dH(t)}{dt} = f(t) - Vid(t)$$
$$H(t_0) = H_0$$

Moreover, a delayed runoff provided by subsurface runoff or exfiltration is generated as a part of the drainage of the soil reservoir. This runoff, *Exf(t)* [L/T], so-called the "lateral flow", is assumed to be a constant fraction ω of the drainage:

Equation 13: $$Exf(t) = \omega . Vid(t)$$

Thus, the total runoff *Rtot(t)*[L/T] produced by a cell at time *t* is given by:

Equation 14: $$Rtot(t) = R(t) + Exf(t) - Ev(t)$$

Ev(t) is the function of evapotranspiration of the selected catchment. However, when using the event-based model, the evapotranspiration is not important comparing to other abstractions and can be neglected (Rossi et al., 2012; Xie et al., 2019).

Finally, the SCS model operates in distributed mode over a grid mesh of regular cells Figure 2.2. Each cell is thus able to produce runoff, according to the selected parameters *S*, ω and *ds* which can vary for each cell, or not.

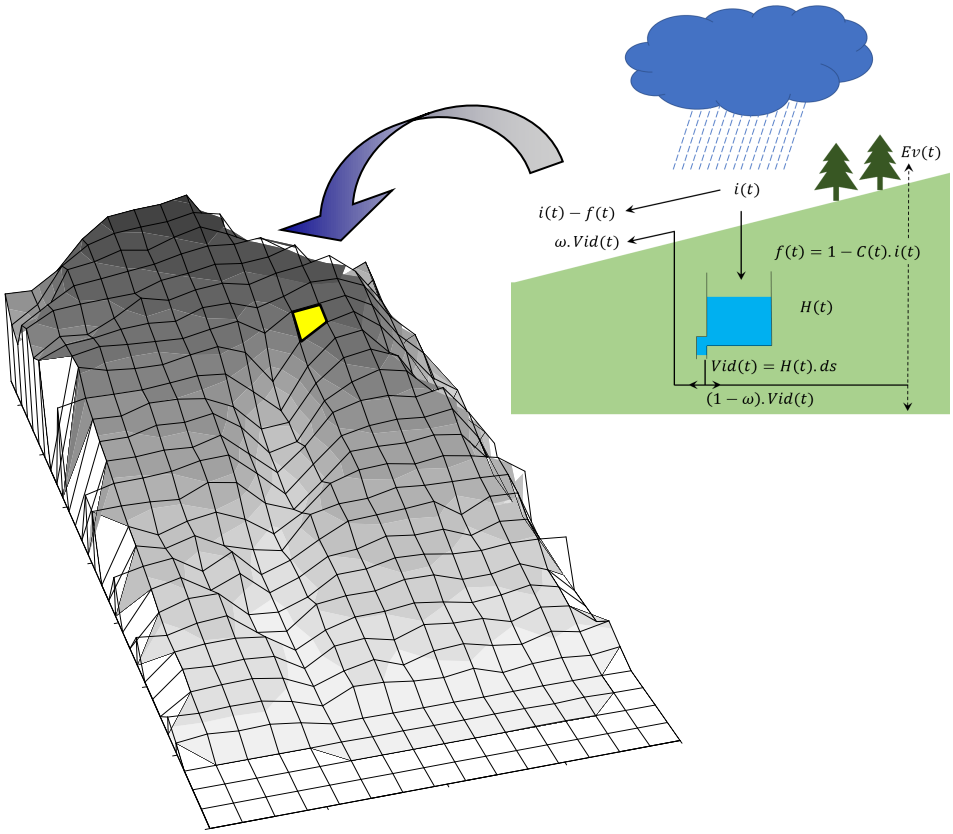

Figure 2.2: Distributed SCS model over a grid mesh of regular cells

(Coustau et al., 2012) pointed out an important point concerning the drainage. They argued that using the same reservoir discharge *ds* before and after the rain was not convenient, because the discharge mostly comes from the groundwater before the flood, from the near-surface layers during the recession of the flood. The corresponding discharge rates are supposed to be different, slow before the flood, fast during the recession. Thus, the drainage should be differentiated before and after the rain/flood. For event-based models, several solutions can be proposed to represent the dual discharge of the soil reservoir, such as considering two *ds* coefficients instead of one or introducing a threshold of the amount of the rain or the level in the reservoir, which activated either the slow or the fast drainage. Finally, the adopted solution was here to consider as (Coustau et al., 2012) that the initial storage H_0 was always 0 at the beginning of the event, making that the drainage is null before the rainfall started and the reservoir filled up. The hypothesis that there is no drainage of the soil reservoir before the rain starts seems to be convenient in most cases. This hypothesis also makes it possible to reduce the number of parameters of the model by removing H_0, whereas the other solutions require additional parameters. Consequently, according to the hypothesis $H_0 = 0$, i) S is no longer the maximal storage capacity of the reservoir soil, but the initial water deficit of the reservoir, which should vary from an event to another, ii). S_a is similar to I_a, which is set as a function of S: $I_a = 0.2S$.

(Coustau et al., 2012) also indicated that ω and S were linked by linear regression, with a negative slope. That means the higher S, the lower ω. In other terms, the delayed runoff was low when the soil was initially dry, and high when the soil was initially wet. This is coherent with the fact that free water in the soil depends on the water content. In order to reduce the equifinality, it was thus decided to express ω as the ratio of a water storage threshold $\omega'_{[L]}$ and the S water storage capacity of the soil at the beginning of the event, $\omega = \omega'/S$ when $S > \omega'$, and $\omega = 1$ when $S < \omega'$. The ω' parameter substituted to the ω parameter in the calibration of the model and was expected to be uniform for all the events.

2.4. Coupling SCS and Lag and Route model

For the transfer of flow from each cell to the outlet, in this study, we used the Lag and Route (LR) model. The LR model was built with two components: the translation (route) and diffusion (lag) through a reservoir. The reservoir can be a linear reservoir or a quadratic

reservoir (see Bentura and Michel, 1997). These components are conceptual tools which are acceptable and popular among hydrologists.

The LR model operated as a cell-based model, implemented by dividing the catchment into equal cells, which are connected. The specific algorithm routes the water from one cell to another and finally to the outlet of the watershed. Using the cell-to-cell model, a watershed can be represented as a single cell, a cascade of n equal cells, or a network of n equal cells (Singh, 1988). Working as a system, all the cells represent the flow pattern of this catchment.

The digital elevation model (DEM) is the product of digital mapping technique. It can automatically extract from raster elevation data topographic variables, such as basin geometry, stream networks, slope, flow direction, etc. (Jain et al., 2004). In three schemes of DEM data structuring as triangulated irregular networks, grid networks and vector or contour based networks (Moore and Grayson, 1991), the most widely used is the grid network.

For grid network model operation, the catchment is separated into cell or grid areas. For each cell of the catchment, besides the information about the topography, we can also integrate other information such as soil, land use, etc. with the help of GIS. The cell represents an area with an average of all properties. Flow from one cell to other neighbor cell is identified by using the eight-direction pour point algorithm which chooses the direction of the steepest descent among the eight permitted choices. When the flow of all the cells are determined, a unique cell-to-cell flow path is established to the catchment outlet (Maidment, 1993).

There are several applications that use both grid/cell approach and GIS (Beven and Freer, 2001; Grayson et al., 1992; Wang and Hjelmfelt, 1998; Watson et al., 1998) which are highly evaluated with the capability of quantifying the effect on runoff of variability in physical characteristics of the catchment.

The LR model was used in several studies for flood simulating (Bouvier and Delclaux, 1996; Coustau et al., 2012; Lhomme et al., 2004). Similar models have also been proposed by (Maidment, 1993; Olivera and Maidment, 1999; Zech et al., 1994).

The LR model was applied for each cell of the catchment (Figure 2.3).

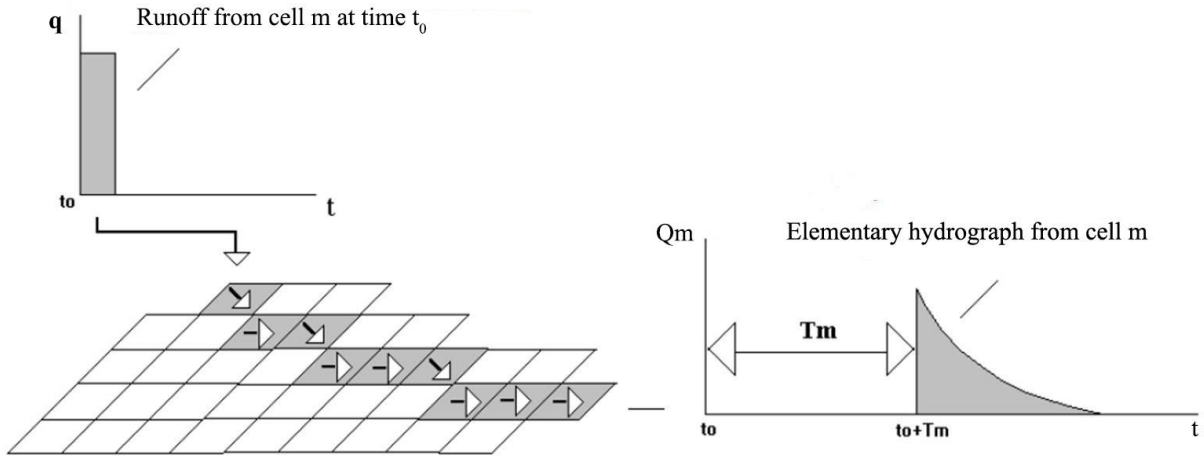

Figure 2.3: Scheme of Lag-and-Route model operating for each mesh of the basin.

From each cell *m*, the runoff at time t_0 generated an elementary hydrograph $Q_m(t)$ at the outlet of the catchment. The lag process operates through a linear reservoir model, of which the diffusion time K_m is the parameter so that the elementary hydrograph at the outlet may be expressed as:

Equation 15:
$$Q_m(t) = \begin{cases} \frac{q(t_0)}{K_m} exp\left(-\frac{t-(t_0+T_m)}{K_m}\right) * A \; when \; t \leq t_0 + T_m \\ 0 \; when \; t > t_0 + T_m \end{cases}$$

where $q(t_0)$ denotes the runoff from the cell at the date t_0, T_m and K_m represent respectively the travel time (route) and the diffusion time (lag) of the initial input along the travel paths, and A is the area of the cell (Figure 2.3).

The travel time T_m was computed by

Equation 16:
$$T_m = \Sigma_k \frac{l_k}{V_0}$$

in which, l_k is the length of the k^{th} cells between the cell m and the outlet; V_0 denotes the velocity of travel, which was considered here as uniform over the whole catchment. Note that the distributed LR model performs a linear transformation of the effective rainfall, in the sense that the velocities may vary for each cell, but do not vary in time at the event scale.

The diffusion time K_m was assumed to be proportional to the travel time T_m, with the slope equal to K_0, as follows:

Equation 17:
$$K_m = K_0 . T_m$$

The diffusion increases linearly with the travel time means that the flow moving from one cell to another cell is equal to the flow routing between these two cells through an intermediate cell.

Finally, all the elementary hydrographs derived from any time and any cell were added to obtain the total hydrograph (Olivera and Maidment, 1999). The model, although not physically based, has several advantages: short computation times, slight dependence on the spatial resolution (because it does not rely on cells slopes), possibility to give a physical interpretation to the parameters. However, the concept only retrieves the hydrograph at the outlet of the catchment, but not the internal flows at the cell scale. This is due to the fact that the elementary hydrographs are only added at the outlet of the catchment, but not in the upstream cells. For this reason, the model cannot work for any storage in the cells, which requires an actual budget at any time in the given cells.

2.5. Model calibration

As mentioned above, we opt to use the combination of the SCS production model and the LR routing model to simulate a flood. The complete event-based SCS-LR model finally dealt with three parameters for the production function: S (initial water deficit), ds (drainage coefficient of the reservoir), ω' (related to the fraction $\omega = \omega'/S$ of the drainage corresponding to the delayed runoff), and two parameters for the transfer function: V_0 (velocity of travel), K_0 (coefficient of the linear relationship between the travel time and the diffusion time). However, the effect of each parameter to the hydrograph is different. Thus, the sensitivity test is initially needed for the understanding of each parameter's role.

2.5.1. Sensitivity test

Calibrating too many model parameters can generate non-uniqueness and uncertainties of the estimated parameters. Indeed, quantifying the level of uncertainties in model parameters calibration has become an important issue recently (Abbaspour et al., 2004; Beven and Binley, 1992; Gupta et al., 2003; Yapo et al., 1998). Thus, we will not definitely

calibrate all of the parameters. Through the sensitivities test, we can detect the most influent or independent parameters which will be calibrated for each event.

The sensitivity test is implemented as we investigate how the simulation of our hydrological model would be affected when each parameter varied while the others were kept unchanged. The most sensitive parameters, in other words, were the one which modification affected the greatest on the model simulation should be focused during the calibration stage.

2.5.2. Model calibration

After the sensitivity test, we move to the calibration. In this step, some parameters were kept constant for all the events, whereas others were allowed to vary from one event to another, depend on the decision made for the sensitivity test. The calibration will compare the observed flow and the simulated flow through the quality of Nash–Sutcliffe Efficiency (NSE, Nash and Sutcliffe, 1970) value. The calibration of the model was driven event-by-event, aiming to maximize the NSE value for each event:

Equation 18: $$NSE = 1 - \frac{\sum_{t=1}^{T}(Q_0^t - Q_c^t)^2}{\sum_{t=1}^{T}(Q_0^t - \overline{Q_0})^2}$$

where $\overline{Q_0}$ is the mean of observed discharges during the event, Q_c^t is the calculated discharge and Q_0^t is the observed discharge at time t during the event.

Nash–Sutcliffe efficiency can take values from $-\infty$ to 1. An efficiency of 1 ($NSE = 1$) implies a perfect match of modeled discharge to the observed data. The value of 0 ($NSE = 0$) indicates that the model predictions are as accurate as the mean of the observed data, whereas the negative value (NSE < 0) occurs when the observed mean during the event is a better predictor than the model or, in other words, when the residual variance is larger than the data variance. Essentially, the closer the value of NSE is to 1, the more accurate the prediction is. Note that NSE was computed only for the time steps corresponding strictly positive observed discharge during the event (after subtraction of the base flow). The algorithm used for the maximization of NSE was the simplex algorithm (Rao, 2009).

2.5.3. Model efficiency

When using an event-based model, the calibration of the model event-by-event leads to the optimal NSE of the model, i.e. the NSE obtained with the optimal values of the calibrated parameters. But the predictive score of the model must account either for the best adjustment of the simulated floods to the observed one and for the better adjustment of the relationship between the initial condition of the model and the external predictors. In other terms, the predictive NSE of the model should be the NSE constrained by the predicted value of the initial condition of the model. The so-called predictive NSE indeed assesses the accuracy of the event-based model. The goodness of the model will be thus expressed by the quartiles (upper, median, lower) of the predictive NSE values of all the events, the initial condition being predicted by the relationship with the external predictors (base flow, the output of the SIM model). The model efficiency will also be controlled by split-sample cross-validation, in order to check the stability of both the calibration and goodness of the model. For the event-based models, note that the split-sample cross-validation needs to compare the predictive NSE of both calibration and validation samples.

2.5.3.1. Base flow

The base flow here in the model is the "memory" of the catchment, due to the previous rainfalls, before the event. In the SCS-LR event-based model used as above, no base flow could be simulated, because the initial water level in the reservoir was 0 so that the drainage and delayed runoff were also null until the rainfall begins during the event. The simulated flow was only due to the rainfall of the event. Thus, the simulated discharges must be compared to the total observed discharges, minus the base flow. This base flow was estimated by fitting an exponential decrease with time, between the first discharge of the event Q_0 and the last continuously decreasing discharge Q_i (i.e. Q_i such as $Q_k<Q_{k-1}$, for any 1<k<i), before the rising of the flood: $Q_k=Q_0.exp(-\alpha(t_i-t_0))$, with $\alpha = Ln((Q_i-Q_0)/(t_i-t_0))$. The base flow was then computed with this exponential decrease for the whole event, and subtracted to the observed discharge, to be compared to the simulated discharge.

2.5.3.2. Water content predictors/ Soil moisture index

In addition to the base flow, the *w* volumetric water content or the soil moisture index output of the SIM model (Habets et al., 2008; Quintana Seguí et al., 2009) was used as another predictor of the initial condition of the model.

The volumetric water content is calculated according to the soil hydraulic properties (water content at saturation w_{sat}, water content at the wilting point, w_{wilt}, and water content at field capacity w_{fc}). w_{sat} is the maximum amount of water that a given soil can hold (Clapp and Hornberger, 1978). Field capacity w_{fc} is the soil water content at which gravitational drainage effectively ceases, corresponding to a hydraulic conductivity of 0.1 mm/day (Wetzel and Chang, 1987). The wilting point w_{wilt} is the soil water content below which it is assumed that plants are unable to pump water from the root zone to stomatal cells, calculated as water potential of -15 bar.

The percentage of soil saturation is calculated by

Equation 19

$$Hu = \frac{\theta}{\theta_S} 100\%$$

where θ denotes the soil moisture and θ_S the saturated volumetric soil moisture (Marchandise and Viel, 2009).

In the scope of this study, we only considered the indicator from the second soil layer, w_2/Hu2, because of the shallow depth of the soils in the catchment and because it is a priori the most representative moisture index of the superficial deposits (Coustau et al., 2012). The values used for w_2/Hu2 correspond to the average of all the pixels that comprise the Real Collobrier basin.

2.6. ATHYS platform

ATHYS is a modeling platform that the French Institut de Recherche pour le Développement (IRD) have been developing since 1995 with the aim of "bringing together in a friendly and homogenous environment a set of hydrological models associated with hydrodynamic data processing climate and geography". With the basic principle as a hydrological environment for distributed modeling, ATHYS contains a series of models

(production and transfer), DEM processing, hydrological and rainfall data, and geographical display, spatial data interpolation.

ATHYS consists of four modules to prepare the geometric and hydro-meteorological data and format them as required by the rain-flow model:

- The MERCEDES module "Square Regular Elemental Mesh for the Study of Superficial Flows" is a space-based modeling platform designated for the study of rain-flow transformation. Its advantage is that it is applicable to the basin of different sizes.
- VISHYR module "Visualization of Hydrological Data" which gathers a set of pre and post-data processing of hydro-climatic stations such as correction, calculation, management, and visualization operations.
- The VICAIR module "Visualization of Raster Cards and Images" which groups together a set of pre and post-processing spatialized spatial data such as correction, analysis, and visualization operations.
- The SPATIAL is a module for spatial interpolation of rain.

The MERCEDES menu gives the possibility to use the pair of the production model and transfer model to simulate floods. Among many available combinations, the SCS-LR model was selected due to its wide application and its ability to forecast Mediterranean floods.

Figure 2.4: ATHYS interface

2.7. Conclusion

This chapter helps to understand the history, the development and how the model works for this study. For the production model, the SCS is selected due to its simplicity, popularity and its ability to forecast floods which were proved in many other studies. We also adjusted it following another suggesting of (Michel et al., 2005) among many solutions to use the model. This adjustment enhanced the model that it can be more physically interpreted. For the transfer model, we directly use a model which was successfully used to simulate floods with ease in many other studies: the Lag and Route model.

After selecting and adjusting the appropriate model, we will apply it to simulate Mediterranean floods, firstly in Real Collobrier catchment. The results will be presented in the next chapter.

3. Calibration of the model on Real Collobrier catchment

This chapter describes the Mediterranean Real Collobrier. The Real Collobrier has been studying for more than 50 years by IRSTEA and supplies an ideal rainfall and runoff database, which will be used to study the performance of the SCS-LR model as well as the impact of the uncertainties of the rainfall estimation on the model performance and parametrization. The Real Collobrier at Pont de Fer was considered here, as the larger catchment of the nested device of rainfall and runoff data. The catchment and the previous studies in Real Collobrier are first described in section 3.1, the event database is then presented and analyzed from a hydrological point of view in section 3.2, section 3.3 summarizes the calibration of the model and the relationships existing between the model parameters and the characteristics of the catchment or the events initial conditions, calibration of the model, and section 3.4 analyzes the impact of the reduction of rain gauges density on the performances and the parametrization of the model.

3.1. Introduction

Real Collobrier site consists of a nested device of sub-catchments, of which area range from 1.5 to 70.4 km^2. The site has been studying for more than 50 years by IRSTEA so that it is one of the most well-documented sites which can be found in the Mediterranean area. Real Collobrier was the object of numerous studies in the past or recent years:

As a long period of observation is now available, Real Collobrier was investigated for detecting trends of the impact of the climate change on rainfalls and floods (Folton et al., 2018),

Real Collobrier catchments were used as a benchmark for several models. Obled et al. (1994) applied a semi-distributed version of TOPMODEL using an hourly time step and a series of independent events, Parkin et al., used a physically-based, distributed catchment modelling system named SHETRAN (1996), which quantified the uncertainty of four different predicted features, including continuous hydrograph, peak flow rates, monthly and total runoff, then compared the

observed with predicted features. Andréassian et al. (2001) used Real Collobrier data to test three model, including a three-parameter GR3J model and six-parameter TOPMODEL and IHACRES models at daily time step, Taha et al. (1997) developed a two dimensional unsaturated – saturated model of the hillslope-channel cross-section profile to explain the high proportion of storm discharges coming from old water. Nevertheless, such studies were limited to the local scale or intended no more than calibrating exercise, so that it still lacks a complete modeling framework of the Real Collobrier.

Real Collobrier was also tested for assessing the impact of the density of the rain gauges on the calibration and the performances of models. Andréassian et al., (2001) proposed an approach to analyze the sensitivity of RR models to the lack of rainfall data input, by comparing between the efficiency ratings, the values of model parameters and the quality of rainfall input estimations. Obled et al. (1994) also assessed the performance of their models on the comparison of two different densities of networks, which includes a different number of gauges.

Hydrological processes were investigated at various scales. Gresillon et al. (1995) showed that runoff was locally generated by saturation of the vertical profile of the soil. Marc et al. (1995) used geochemical tracers to differentiate the generation of runoff in Maurets and Rimbaud catchments. Travi et al. (1994) also used geochemical tracers for estimating the impact of the fire in Rimbaud catchment. Martin et al., (2004) measured and compared the floods in the upstream and downstream part of the Maurets catchment, proving that the upstream part supplied the main contribution to the flood.

All these studies helped a lot to understand the behavior of the Real Collobrier and brought the possibility to improve the physical meaning of the model parameters.

3.2. Real Collobrier catchment

3.2.1. Location

Real Collobrier is a Southern French basin which includes 11 sub-basins (Figure 3.1). It is about 16 km long and 9.6 km wide. The general axis of flow is east-west oriented, beginning in the reliefs on the eastern edge of the basin. The altitudes decrease from the east (770m maximum) to the west (80m at the outlet). The highest peaks of the Massif (770 m at the top of the Sauvette) are located in the northern ridge, which is higher than the southern one. The

largest catchment in Real Collobrier is controlled by the Pont de Fer steam gauge and covers 70 km².

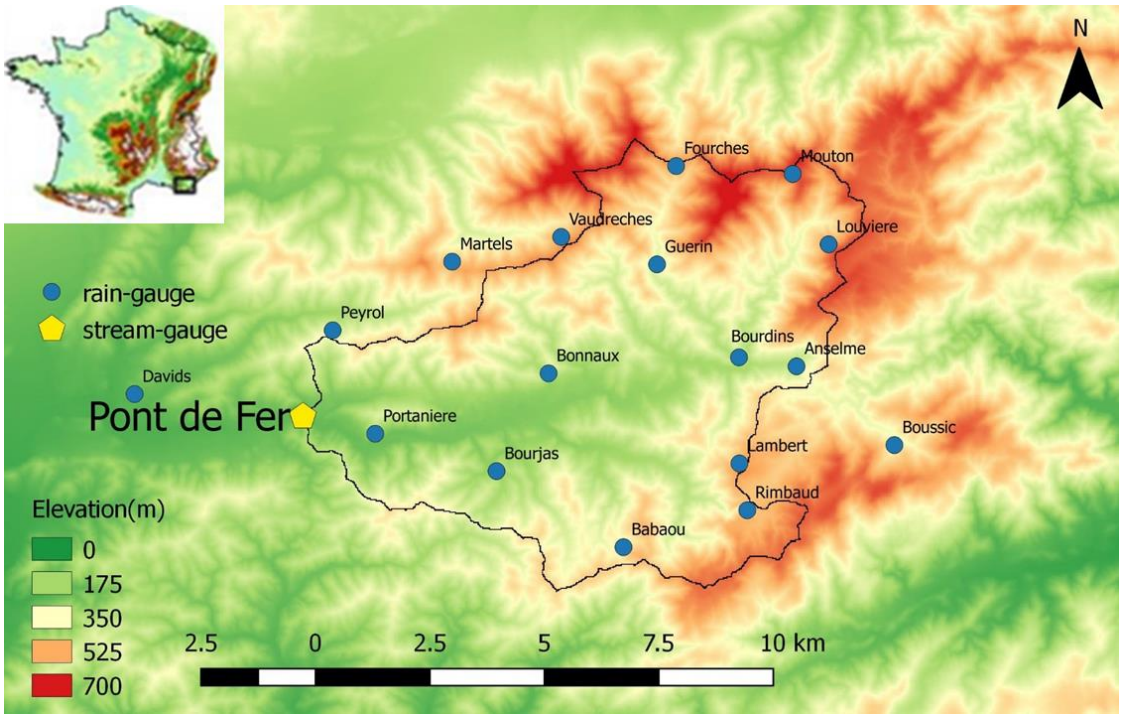

Figure 3.1: Maps of the Real Collobrier catchment. Relief (from IGN ALTI database at 25m spatial resolution) and rain gauges location.

3.2.2. Geology and soil

The geological formations are mainly crystalline, with metamorphism increasing from east to west: gneiss, schists, phyllites (Folton et al., 2012). Alluvial deposits are limited to the western part of the plain of Real Collobrier. Soils have sandy clay characteristics, more or less pebbly, with their thickness varying dependently on the bedrock and topography: the gneiss soils are shallow, the phyllites-soils are thicker, and the alluvium soils can reach several meters. Some bare rock areas appear at particularly high altitude.

The average proportions in sand and clay in Real Collobrier are 633 g/kg and 162 g/kg (Figure 3.2 and Figure 3.3) (from Geosol https://webapps.gissol.fr/geosol/). Parkin et al. (1996) gave a description of the soil in the Rimbaud sub-catchment: the soils are generally sandy, and contain a significant proportion of gravel and broken rock; there is considerable local variation in soil depth from nothing (at bedrock outcrops) to a meter or more in bedrock depressions, but depths are generally less than 1 m; the deepest and most

homogeneous soils occur in the chestnut plantation near the catchment outlet, where soil depths may reach 2 m; plant roots generally extend over the full depth of the shallow soils. The shallow soils seem to have high hydraulic conductivities at saturation, up to 100 $mm.h^{-1}$ (Parkin et al., 1996), and low water retention (Taha et al., 1997).

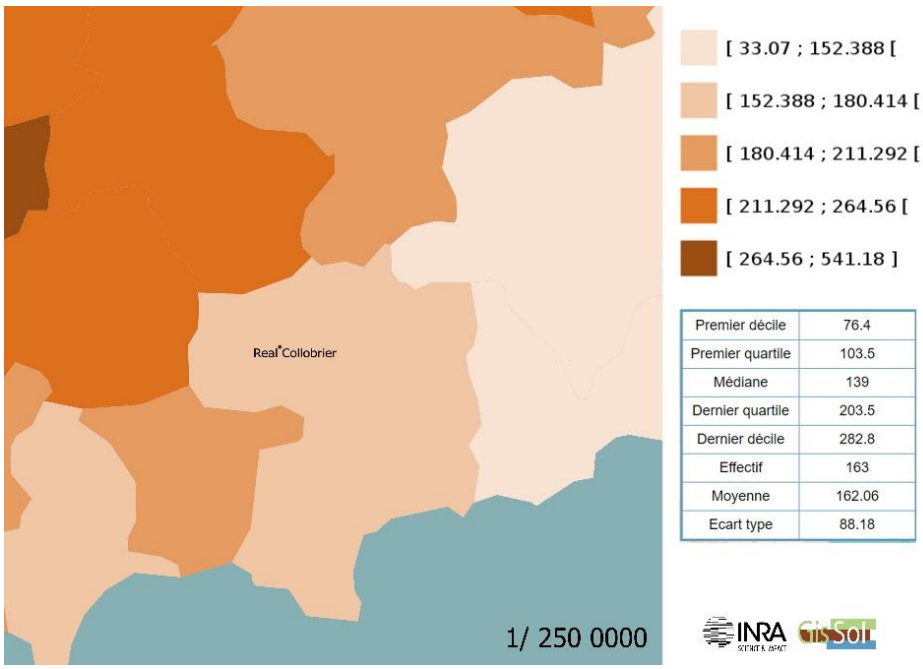

Figure 3.2: Map of clay in Real Collobier catchment

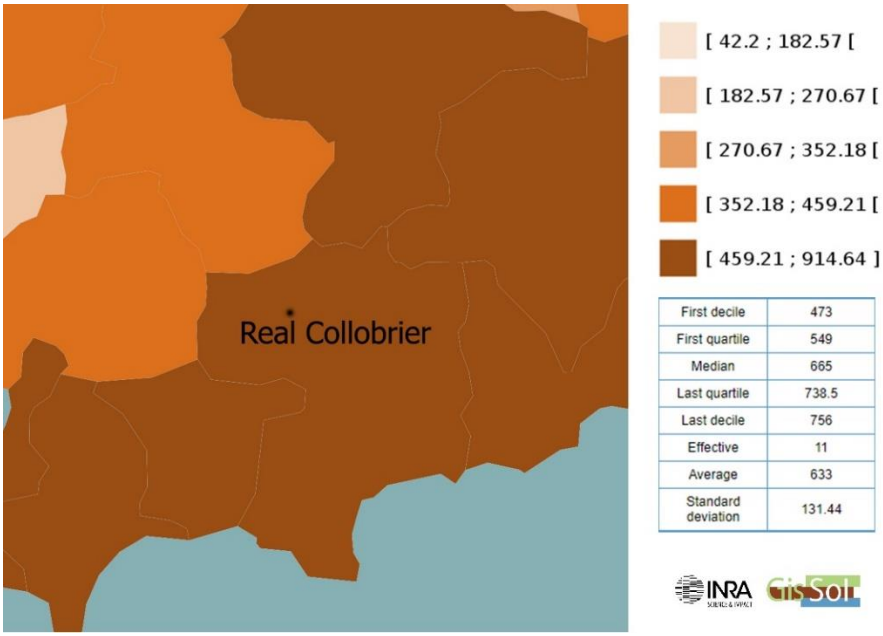

Figure 3.3: Map of sand in Real Collobier catchment

3.2.3. Land use

As the geological components are crystalline, the vegetation is essentially calcifuge, such as chestnut and cork oaks. In a small portion of the surface in the plain Real Collobrier, vineyards are grown. The land use map of Real Collobrier is presented in Figure 3.4.

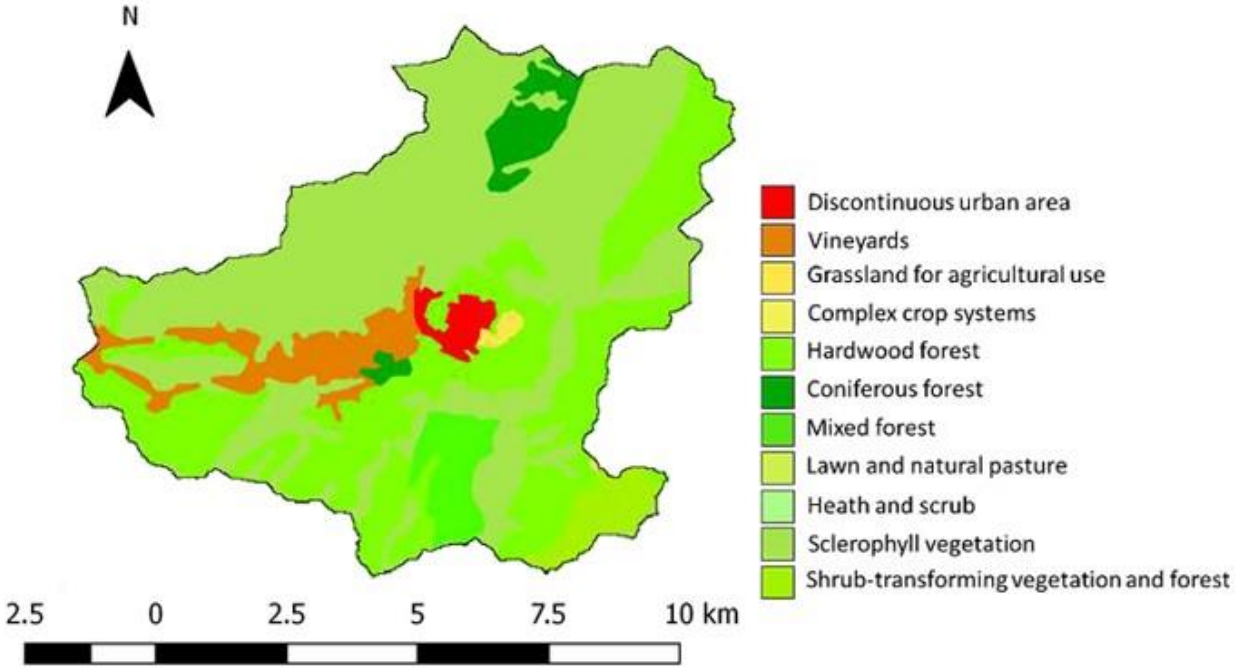

Figure 3.4: Maps of the Real Collobrier catchment: Land use (from Corine Land Cover database).

3.2.4. Climate

The climate in this area is the humid Mediterranean type with a remarkable dry period, autumn with strong intensity of rainfall, and rainy spring. The eastern topographic boundary of the basin has a predominant role on the spatial distribution of rainfall, which generally orderly decreases from the east to the west. The annual average rainfall ranges from 750 mm to 1200 mm.

The general characteristics strongly fluctuate annually. The strong fluctuation of the annual average rainfall is not caused by the lengthening of the rainy season, but by the increase of the average rain intensity. It is also found that there is the same spatial distribution for daily rainfall. Rainfalls observed in summer usually accompany with a storm event. The most intense rainfall (up to 100 mm per hour) happens in the fall season. The

spatial distribution of rainfall infers a high variability in the runoff, although rainfall only partly contributes to the fluctuating flows. Other reason can be due to descriptive physical characteristics also strongly influences the hydrological basins.

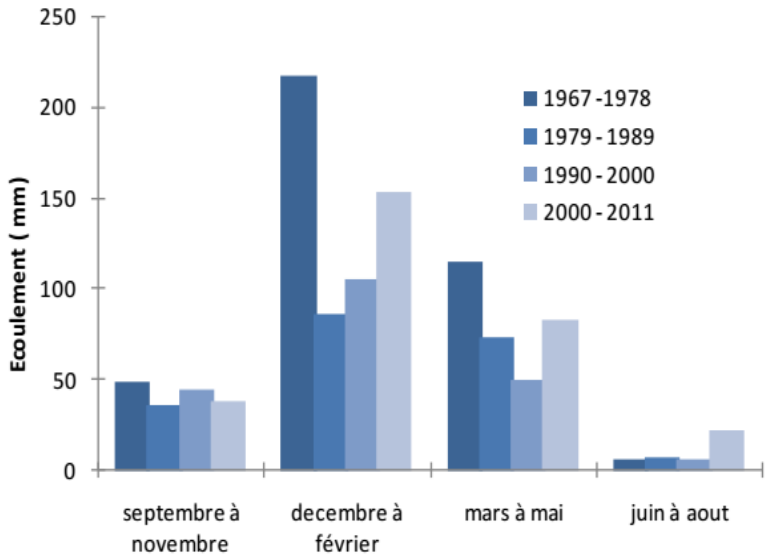

Figure 3.5: Average seasonal flow in station Pont de Fer. (Folton et al. 2012)

Flow in Real Collobrier is coupled with seasonal variability. Figure 3.5 showed the average seasonal flow in station Pont de Fer in four periods of time: 1967-1978; 1979- 1989; 1990-2000; 2000-2001. We can see in all the periods, the winter months seemed to have the strongest average flows, while the summer month (from June to August) had flowed nearly 0.

3.2.5. The measuring device

The initial measuring device in 1966 included 25 tipping bucket rain gauges and 11 flow monitoring stations. It was downgraded in 1989, and the number of rain gauges was reduced to 17, distributed up- and downstream of each basin. On average, one rain station covers 5 km^2, of the Real Collobrier at Pont de Fer, which makes it a quite dense system. To date, the hydrological data measured in Real Collobrier catchment are one of the most comprehensive datasets collected in France.

3.2.6. Rainfall-runoff events

Both rainfall and runoff data were obtained from IRSTEA (https://bdoh.irstea.fr/REAL-COLLOBRIER/) and were used with 30 minutes time step. We considered here the discharges at Pont de Fer station, which controls a catchment of 70 km^2. In this catchment, 17 rain gauges were available for the rainfall data. The events were delimited by considering several conditions: i) a new event was defined when occurred a period of 48 hours without amount exceeding 0.5 mm during a 30minutes-time step; a 48 hours period was enough to consider that discharge came back to the initial value before the rain, ii) the rainfall during the event had to exceed 50 mm in at least one rain gauge; ; the threshold 50 mm was found necessary for flood triggering, iii) the peak flow during the event had to exceed 30 m^3/s, which corresponded to the 1-year return period peak flow.

The method led to select 34 events from 1968 to 2006 (Table 3.1). All the rain gauges did not always work together, as shown in Table 3.1, but 31 out of 34 events have more than 12 rain gauges working together. The cumulated mean areal rainfall of the events ranged from 49 to 318 mm, with an average of 166 mm. The spatial variability of the rainfall during the event was expressed by the coefficient of variation CV (ratio of the spatial standard deviation and the spatial average) of the cumulated rainfalls at the rain gauges, CV's varying from 0.11 to 0.84. The ratio between the maximal and the minimal cumulated rainfalls at the rain gauges were more than 2 for 25 events out of 34, more than 3 for 10 events out of 34. The correlation coefficients between the cumulated rainfalls of the events at the different gauges ranged from 0.14 to 0.97 (Table 3.2). They regularly decreased with the distances between gauges (Figure 3.6), but gauges 6 and 8 were less correlated to some others. As a matter of fact, these gauges are located in the upper northeastern part of the catchment and seem to be sensitive to local orographic effects. As an example of a median case, the correlation coefficient between the cumulated rainfalls at gauges Mouton (gauge 5) and Portaniére (gauge 12) was r = 0.69, the distance between the gauges being 10.7 km.

e

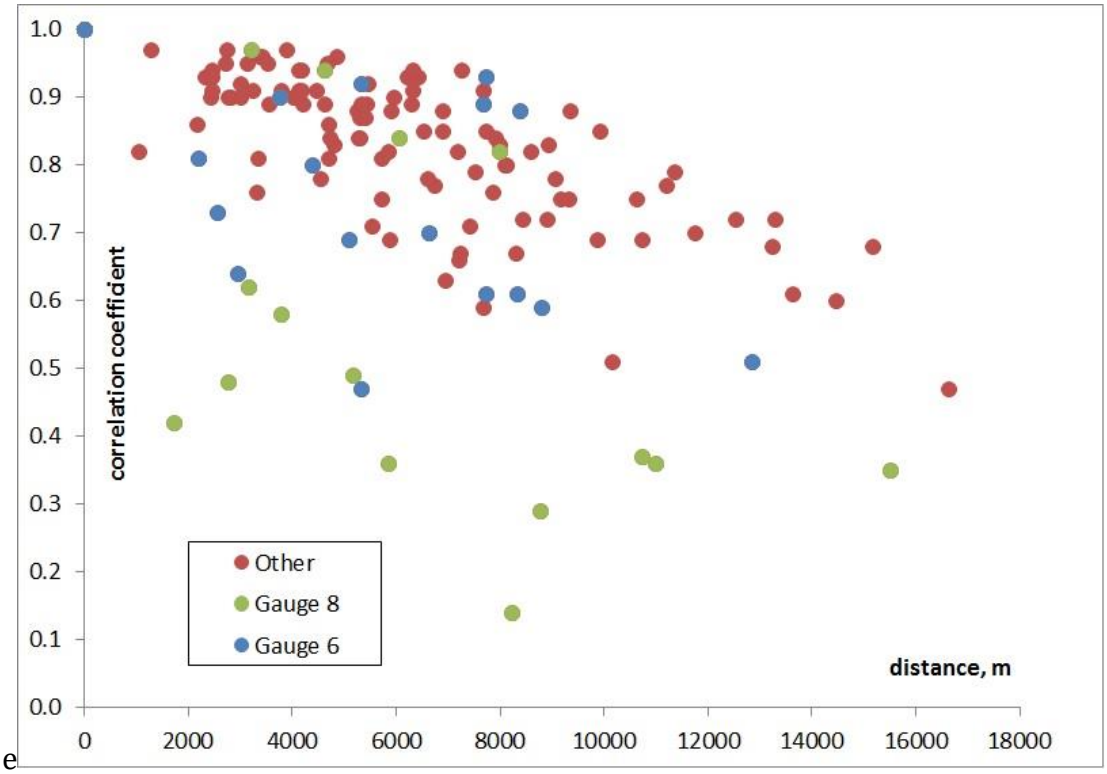

Figure 3.6: Correlation coefficients between the rainfall amounts measured for the 34 events at each rain gauge. Gauges 6 and 8 were the worst correlated gauges to the other ones.

The maximal peak flow was 91 m^3/s. The response time was computed for some single-peak floods and ranged between 1 and 2 hours, considering the time between the main rainfall intensity and the peak flow. The runoff coefficients (Rc) ranged between 4 and 56%, 34% on average. The lowest runoff coefficients (≤10%) corresponded to the events which occurred right after long dry periods. In spite of their low runoff coefficients, these events gave high peak flow, e.g. the maximum value 91 m^3/s on the 13/09/1968. The initial moisture of the catchment was expressed for each event either by the base flow and the volumetric water content at the second soil layer, w_2.

Table 3.1: Main characteristics of the rainfall-runoff events in Pont de Fer. # gauges: Number of gauges in the considered catchment; P: cumulated precipitation; CV: coefficient of spatial variation of the precipitation; Vr: runoff volume; Rc: runoff coefficient; Imax: maximal rainfall intensity during one-time step; w_2*: volumetric water content of the root layer.*

Event	Starting date	Finishing date	P (mm)	# gauges	CV	Vr ($10^3.m^3$)	Rc (%)	Imax ($mm.h^{-1}$)	Peak flow ($m3.s^{-1}$)	w_2 ($cm^3.cm^{-3}$)	Base flow ($m^3.s^{-1}$)
1	12/4/1968	17/04/1968	142.4	16	0.27	2082.7	17	11.3	30.4	0.21	0.06
2	13/09/1968	15/09/1968	177.2	14	0.18	1025.3	9	64.9	91.4	0.19	0.02
3	2/1/1972	5/1/1972	68.5	11	0.29	1961.5	36	11.6	39.6	0.25	2.33
4	1/2/1972	7/2/1972	125.1	16	0.40	3948.3	37	8.9	40.1	0.23	0.77
5	17/02/1972	23/02/1972	207.8	15	0.25	8864.3	56	13.7	60.7	0.23	1.64
6	13/02/1973	23/02/1973	168.2	15	0.84	3850.8	36	12.5	39.1	0.22	0.44
7	13/10/1973	15/10/1973	104.9	15	0.21	1512.7	19	29.7	45.7	0.22	0.06
8	26/01/1974	5/2/1974	247.8	13	0.32	8920.6	40	12.4	76.6	0.22	0.43
9	12/2/1974	21/02/1974	212.6	13	0.25	8286.4	46	10.6	59.8	0.23	1.22
10	26/02/1974	7/3/1974	163.6	16	0.16	7321.0	53	8.9	63.1	0.24	1.88
11	18/09/1974	22/09/1974	123.6	15	0.27	373.5	4	44.2	44.8	0.15	0
12	5/2/1975	9/2/1975	160.1	12	0.18	3395.4	27	8.1	40.8	0.22	0.12
13	29/01/1976	8/2/1976	260.3	15	0.15	5095.0	22	16.9	39.8	0.21	0.16
14	15/04/1976	19/04/1976	145	12	0.35	4288.4	37	15.4	77.4	0.22	0.31
15	24/10/1976	31/10/1976	318.7	15	0.31	11191.6	44	14.9	68.3	0.24	0.50
16	1/1/1977	3/1/1977	49.1	13	0.25	1966.9	46	7.2	31.5	0.24	3.30
17	6/12/1977	11/12/1977	178.1	13	0.11	3142.4	22	17.5	43.3	0.23	0.13
18	11/1/1978	19/01/1978	244.1	13	0.30	10043.5	49	12.3	77.5	0.23	0.20
19	8/2/1978	13/02/1978	125.9	15	0.26	5467.2	52	8.1	41.6	0.22	0.76
20	25/10/1979	31/10/1979	191.8	12	0.13	6182.4	41	13.6	50.7	0.23	0.21
21	30/11/1984	4/12/1984	77.9	13	0.22	1488.4	22	17.9	31.9	0.23	0.41
22	28/01/1986	7/2/1986	280.5	13	0.23	7037.4	30	13.1	53.7	0.21	0.06
23	13/01/1988	17/01/1988	116.4	14	0.37	3325.5	33	11.1	73.4	0.23	0.30
24	20/04/1993	4/5/1993	221.2	10	0.16	6106.0	31	25.4	38.7	0.21	0.25
25	5/1/1994	9/1/1994	109.6	14	0.16	2400.7	23	15.9	33.5	0.21	0.12
26	1/2/1994	8/2/1994	131.8	15	0.12	4192.2	33	19.3	31.1	0.22	0.64
27	10/1/1996	19/01/1996	147.9	14	0.28	5646.6	54	14.6	48.7	0.24	1.62
28	20/01/1996	31/01/1996	209.4	14	0.29	8816.0	50	12.6	58.3	0.24	1.50
29	6/1/1997	13/01/1997	97.1	13	0.27	3266.7	44	10.2	59.9	0.25	4.05
30	13/11/2000	28/11/2000	176.9	13	0.23	4388.0	29	21.5	29.9	0.24	0.37
31	24/12/2000	29/12/2000	134.6	14	0.22	4107.1	37	21.7	44.1	0.22	0.39
32	24/01/2001	31/01/2001	88.3	13	0.19	2749.5	22	9.2	33.4	0.23	0.83
33	5/9/2005	12/09/2005	231.4	8	0.35	2541.8	10	64.2	60.9	0.15	0.003
34	26/01/2006	1/2/2006	202.7	13	0.32	5760.2	34	16.7	34.5	0.22	0.15

Table 3.2: Correlation matrix calculated with rain-gauge data of events. NA = not available when there is no common event at both gauges.

Gauge	1	2	3	4	5	6	7	8	9	10	11	12	13	14	15	16	17
1	1.00																
2	0.91	1.00															
3	0.92	0.89	1.00														
4	0.93	0.96	0.91	1.00													
5	0.83	0.88	0.89	0.89	1.00												
6	0.88	0.92	0.69	0.81	0.73	1.00											
7	0.95	0.89	0.94	0.86	0.93	0.70	1.00										
8	0.82	0.77	0.48	0.58	0.42	0.90	0.49	1.00									
9	0.94	0.97	0.76	0.91	0.59	0.47	0.91	0.14	1.00								
10	0.91	0.90	0.63	0.81	0.75	0.61	0.87	0.29	0.95	1.00							
11	0.84	0.83	0.51	0.67	0.75	0.61	0.88	0.36	0.92	0.84	1.00						
12	0.90	0.90	0.75	0.82	0.69	0.59	0.83	0.37	0.94	0.90	0.91	1.00					
13	0.90	0.84	0.76	0.75	0.71	0.89	0.82	0.84	0.72	0.71	0.69	0.67	1.00				
14	0.85	0.90	0.69	0.86	0.88	0.64	0.89	0.36	0.93	0.84	0.87	0.88	0.66	1.00			
15	0.96	0.94	0.97	0.95	0.91	0.80	0.93	0.62	0.78	0.82	0.72	0.80	0.81	0.81	1.00		
16	0.77	0.78	0.60	0.70	0.68	0.51	0.72	0.35	0.79	0.80	0.78	0.89	0.61	0.85	0.68	1.00	
17	0.91	0.85	0.97	0.85	0.94	0.93	0.96	0.94	NA	NA	0.72	0.79	0.95	0.82	0.97	0.47	1.00

Gauge 1 – Babaou, 2 – Bonnaux, 3 – Anselme, 4 – Guerin, 5 – Mouton, 6 – Fourches, 7 – Lambert, 8 – Louviere, 9 – Martels, 10 – Bourjas, 11 – Peyrol, 12 – Portaniere, 13 – Rimbaud, 14 – Vaudreches, 15 – Bourdins, 16 – Davids, 17 – Boussic

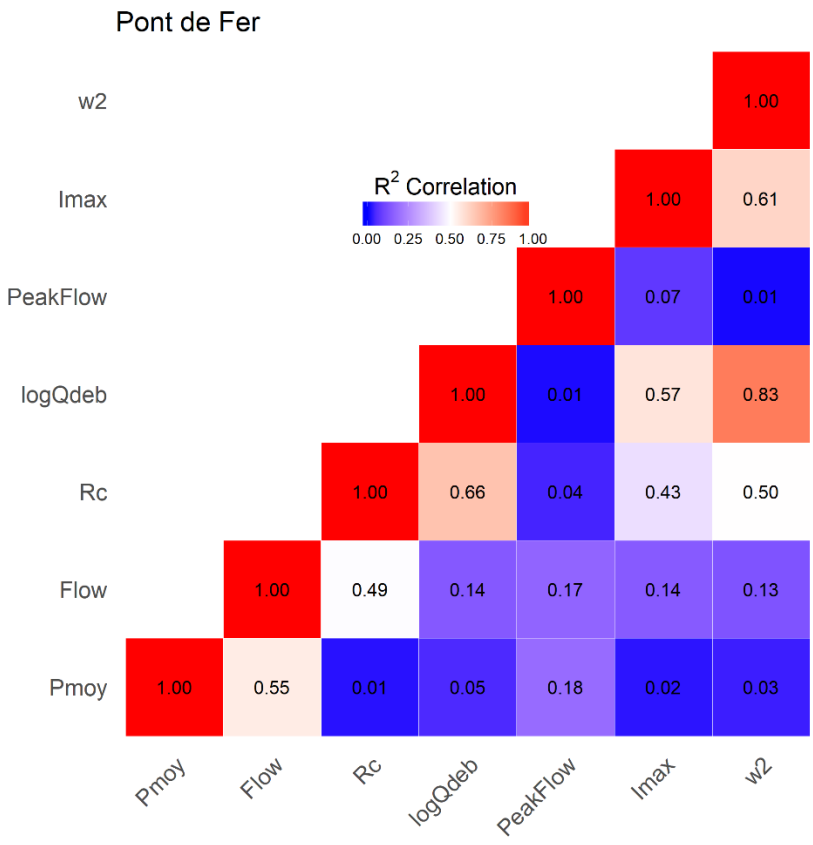

Figure 3.7: Correlation between each pair of indexes in the Pont de Fer catchment. Pmoy: average areal cumulated precipitation (mm); Flow: runoff volume ($10^3.m^3$); Rc: runoff coefficient (%); w_2: volumetric water content of the root layer ($cm^3.cm^{-3}$); logQdeb: log_{10} base flow (log_{10} $m^3.s^{-1}$); Imax: Maximum rainfall intensity ($mm.h^{-1}$); PeakFlow: peak flow ($m^3.s^{-1}$)

We tried to find the correlation between the runoff coefficient and the other hydrological indexes of the catchments. As we can see in Figure 3.7, the correlation coefficient R^2 from the regression between Rc and these indexes showed that Rc was very little correlated with P and peak flow, but much more with the initial condition w_2 and base flow. More information was shown in Figure A 1 to Figure A 5 in the Appendix. Thus, the runoff coefficient can be influenced by the initial condition more than the rainfall.

3.3. Calibration and goodness of the model when using all the rain gauges

3.3.1. The sensitivity of the model to the parameters

Sensitivity tests were performed in order to detect the most influential or independent parameters as said in the methodology section. The sensitivity analysis aimed to investigate how the simulation of our hydrological model would be affected when each parameter varied while the others were kept unchanged. The most sensitive parameters, in other words, were the one which modification affected the greatest on the model simulation should be focused during the calibration stage. The event n°5 has been selected for this test, as a multi-peak event. The *a priori* values and boundaries of the parameters for this event have been set as far as possible from physical or empirical methods. The reference set of parameters used for the sensitivity test was finally S =140 mm, ω'=60 mm, ds = 0.4 d^{-1}, V_0= 2.5 $m.s^{-1}$, K_0 = 3, which led to a good simulation of the observed flood.

S parameter

S is equivalent to CN as usual, $S_{(mm)} = 25400/CN - 254$ and can be derived from the Soil Conservation Service (SCS) National Engineering Handbook Section 4: Hydrology (NEH-4) and Technical Release 20 (TR-20). CN is known to be related to the land use, the hydrologic condition, the type of soil and the antecedent moisture condition. However, as shown in further discussion, the optimal values of S - or CN can be very different than those supplied by the SCS Handbook. The sensitivity analysis was performed by using S = 75 mm and S = 400 mm as probable boundaries of the S parameter in the Mediterranean area. The model was very sensitive to the range of variation of S (Figure 3.8), so this parameter was calibrated for each event. Changes in S mainly affected the peak height in the hydrograph. Specifically, decreases in the value of S increased the height of the peaks, which means higher flow rates in flood events.

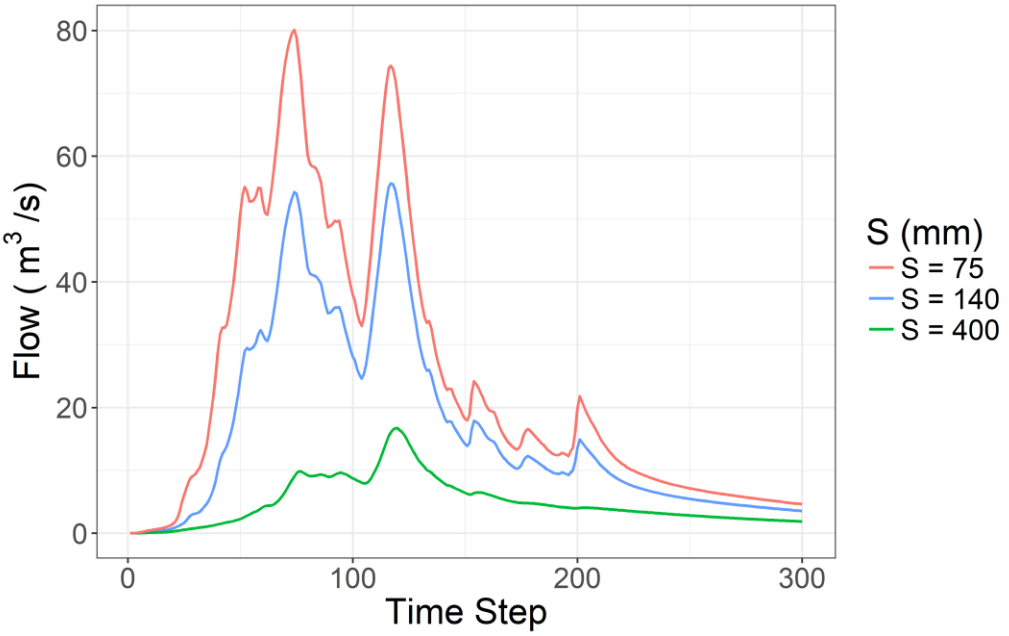

Figure 3.8: Sensitivity test of S *parameter*

ds parameter

As a mathematical property of the model, the discharge coefficient of the reservoir, *ds*, is equivalent to the recession coefficient α used in the Maillet's law:

Equation 20 $$Q(t) = Q_0.e^{-\alpha * t}$$

where α is the drainage coefficient and Q_0 initial base flow. The recession coefficient *ds* was calculated for all the events, fitting an exponential recession on the terminal part of the floods (See Equation 20) The mean value was 0.4 d^{-1}, with a 0.1 d^{-1} standard deviation. The min and max values were respectively 0.2 and 0.7 d^{-1}. The sensitivity test was thus performed with the reference set of parameters, by using *ds* = 0.2, 0.4, 0.7 d^{-1}. The first peak was not sensitive to *ds* (<1%) but the second one was much more (more than 20% between the min and max). That showed that the *ds* parameter was important in case of multiple peaks flood (Figure 3.9), but most of the events exhibit single peak, so the *ds* parameter was set constant in first approximation, *ds* = 0.4 d^{-1}.

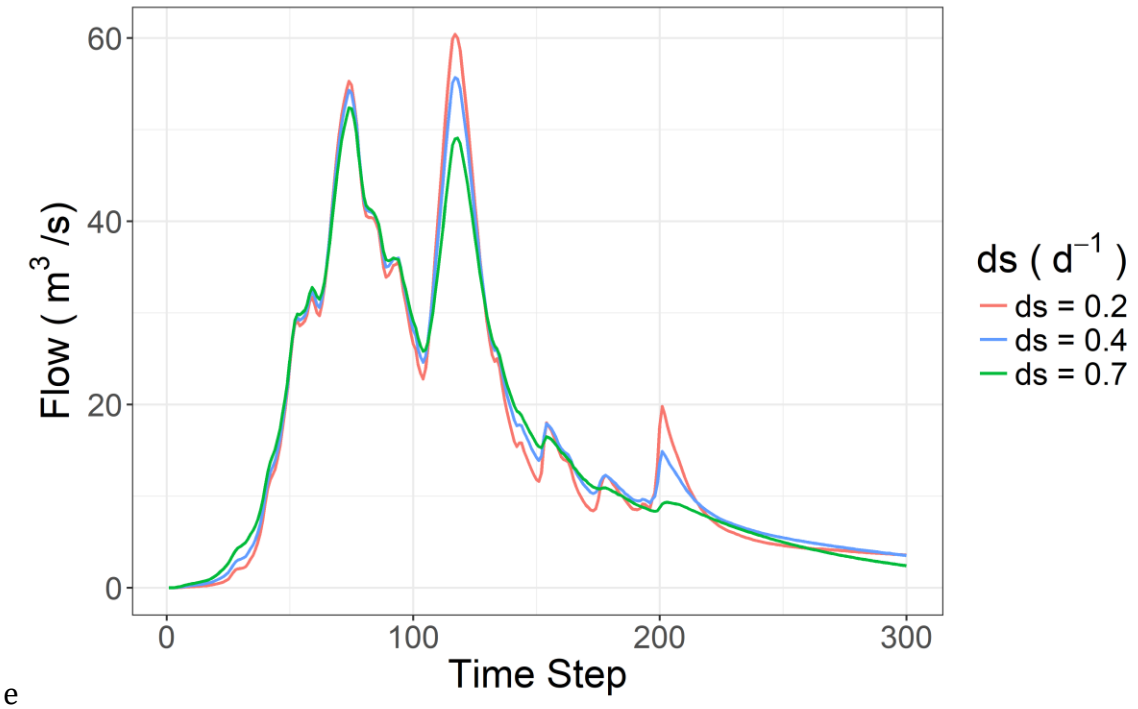

e

Figure 3.9: Sensitivity test of the ds parameter

We can see in Figure 3.9, modifying *ds* did not change either the height of the peaks or the height of the recession, but it slightly altered the slope of the recession

V_0 and K_0 parameter

The V_0 parameter should be interpreted as the maximal velocity in a cross-section. Thus, V_0 can be derived from the slope, friction and hydraulic radius of the streams or channels. Although the velocity in a cross section is far to be constant in space (and time) at a small scale, it is not unrealistic to assume that V_0 is globally constant over the catchment: roughly speaking, it results from the fact that the slopes are steep and the hydraulic radius low upstream, whereas the slopes are low and the hydraulic radius high downstream. In other terms, the variability of the slopes compensates the variability of the hydraulic radius for stabilizing the velocity values. In addition, V_0 was used to compute the travel time *Tm* between a given cell and the outlet of the catchment (Equation 17) and must be seen as a mean value along this trajectory: this is another reason why the hypothesis of V_0 uniform in space could be reasonable.

The transfer parameters V_0 and K_0 were found to be strongly dependent (Figure 3.10). In this example (event n°5), it can be seen that there is a very wide range of pairs (V_0, K_0) which

satisfy *NSE* > 0.8, the other parameters being S = 140 mm, ω' = 60 mm, ds = 0.4 d^{-1}. Thus, it is necessary to set one of these two parameters to avoid their artificial variation. As the V_0 parameter was somewhat more physically-based, we chose to set V_0 = 2.5 $m.s^{-1}$: this is indeed close to the value that would give the Manning-Strickler formula used in a rectangular cross-section with a Strickler friction coefficient 20 $m^{1/3}.s^{-1}$, a slope 0.015 $m.m^{-1}$, a width 20 m, a water level 1 m high, which seems to be realistic according to the available observations.

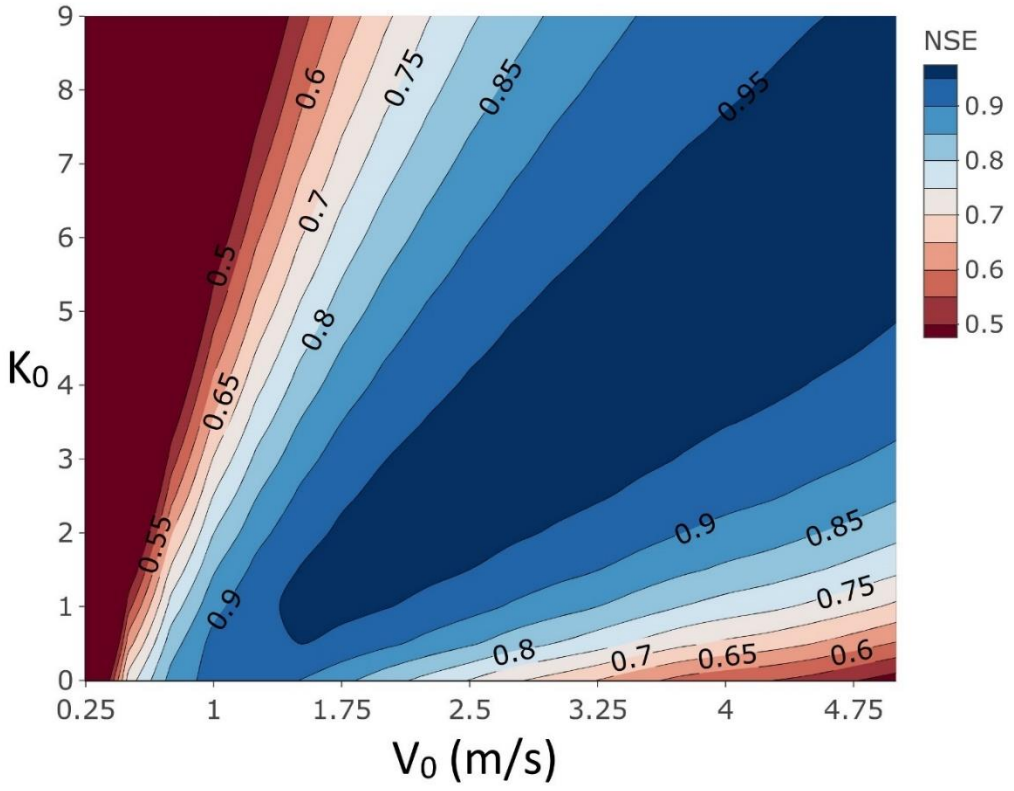

Figure 3.10: NSE values depending on V_0 and K_0 (the other parameters were S *= 140 mm,* ω' *= 60 mm,* ds *= 0.4 d^{-1}), event n°5. The wide area where NSE > 0.8 showed a high dependency between V_0 and K_0 parameters.*

The K_0 parameter governs the relationship between the translation time T_m and the diffusion time K_m. The diffusion time K_m displays a complex role and serves both as a real diffusion since the velocity through a cross-section is not uniform, and as an artificial way to make the real velocity varies in time, whereas V_0 does not. Therefore, there is no physical evidence to set *a priori* the K_0 value, and it was necessary to calibrate K_0. To know more about

the influence of K_0, the sensitivity test was performed with the reference set of parameters, by using K_0 = 0, 2.4 and 4.5, which were respectively the a posteriori minimal, median and maximal values of the calibrated K_0 (Figure 3.11). K_0 mainly acted in the reduction of the peak flow, and to some extent, in the time position. However, despite the modification of K_0 influenced both peak height and the recession of the hydrographs, the sensitivity of the model to K_0 seemed to be less than the sensitivity to *S*.

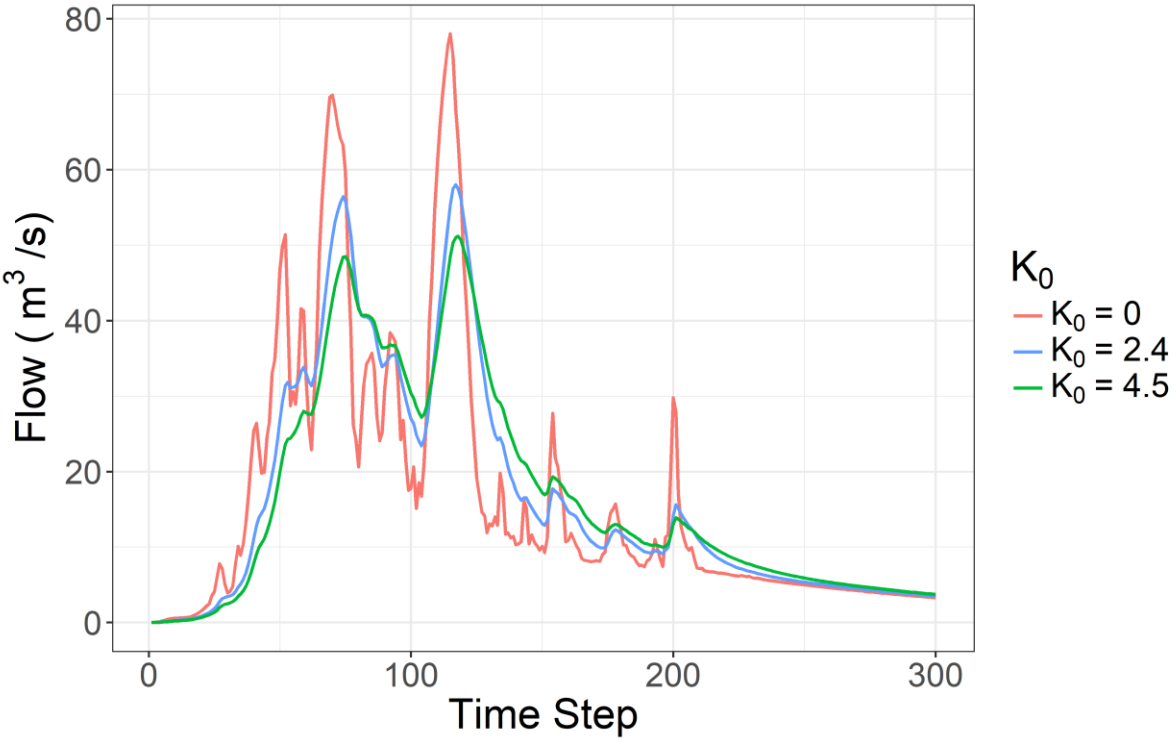

Figure 3.11: Sensitivity test of K_0 parameter

ω parameter

There is no physical evidence for the ω parameter. Then, the other parameters S, ω and V_0 had first to be calibrated for the 34 events. An optimized set of values was found for each event, by optimization of the NSE computed with the observed and computed discharges (Figure 3.12):

- S parameter ranged from 80 to 420 mm with the average approximately equal to 180 mm,
- K_0 value was mainly between 1 and 6 with an average of about three except for some special events.

- ω fluctuated from 0 to about 1, and the average was approximately 0.3
- NSE average value was 0.9, ranging from 0.3 to 1.

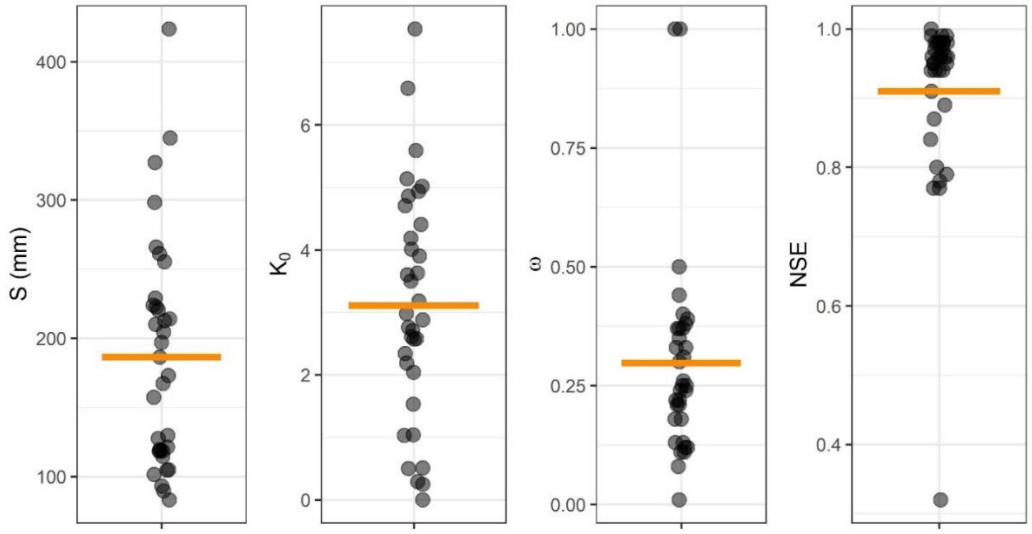

Figure 3.12: Variations of the calibrated values of S, K_0, ω, and NSE for the events

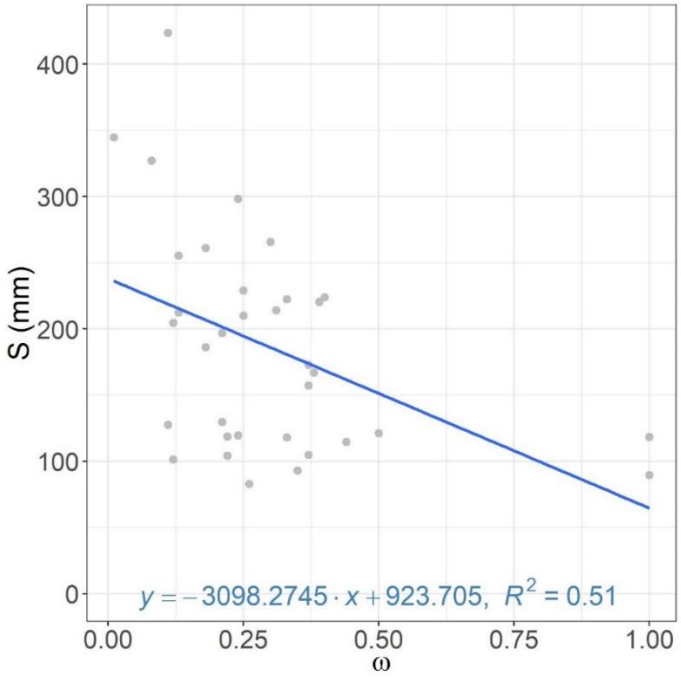

Figure 3.13: Relationship between S and ω

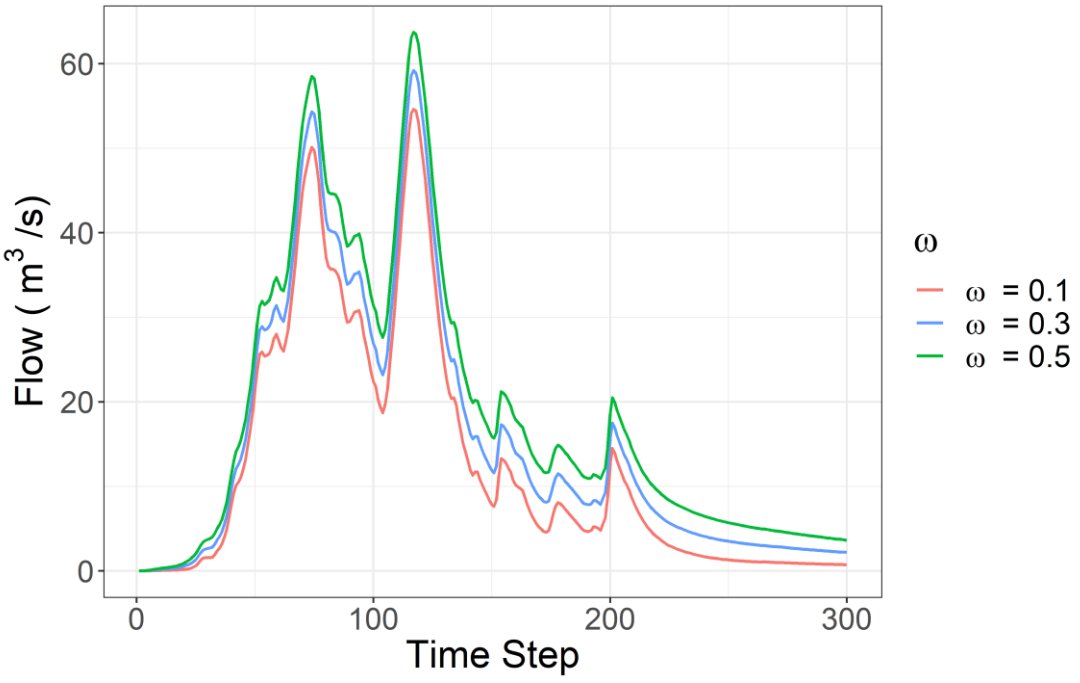

Figure 3.14: Sensitivity test of the ω parameter

ω and S were significantly dependent as already pointed out by Coustau et al. (2012). In our case, ω and S were linked by linear regression (R^2 = 0.51, Figure 3.13). That means that the higher S, the lower ω. In other terms, the delayed runoff is low when the soil is initially dry, and high when the soil is initially wet. This is coherent with the fact that free water in the soil depends on the water content. We can also see that due to Figure 3.12 and Figure 3.14, the variation of ω appeared not to greatly affect the height of the peaks, however, it affected the height of the recession.

In order to reduce the equifinality, it was thus decided to express ω as the ratio of a water storage threshold ω' and the S maximal water storage capacity of the soil at the beginning of the event, $\omega = \omega'/S$ of $S > \omega'$, $\omega = 1$ if not. The ω' parameter (in mm) substituted to the ω parameter in the calibration of the model and was expected to be uniform for all the events. The ω' parameter was set as the product of the median value of ω (0.3) and the median value of S (190 mm), thus ω' was approximately 60 mm.

Modeling with ω'/S did not perform worse than with optimized ω. The median NSE value improved for most of the case especially the events which were in dry condition whether calibrating S and K_0 with ω and or with ω'/S. The values of the S and K_0 parameters did not

change much: when calibrating *S* and V_0 with *ω'*/S instead of calibrating S, *ω* and K_0, *S* values reduced in an average of 10 %, and K_0 values almost kept the same (Figure 3.15).

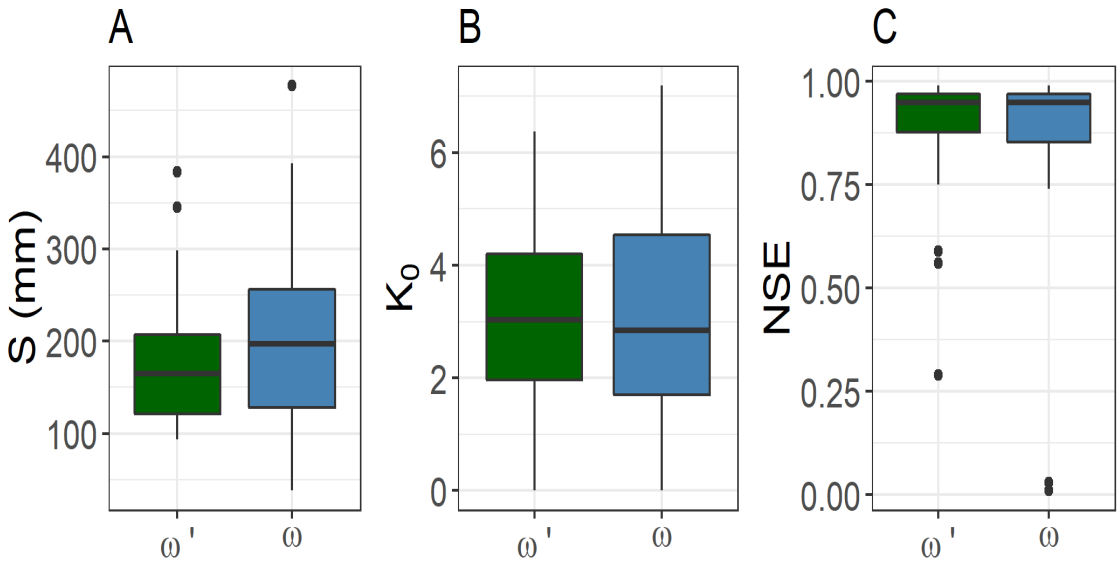

Figure 3.15: Comparison of S, K_0, and NSE between using ω and ω'. The box plots feature median, upper and lower quartiles, (Q3 and Q1, respectively), minimum and maximum values without outliers, and outliers (outliers are defined as data points that fall out of the range [Q1-1.5(Q3-Q1), Q3+1.5*(Q3-Q1)] (Tukey, 1977)*

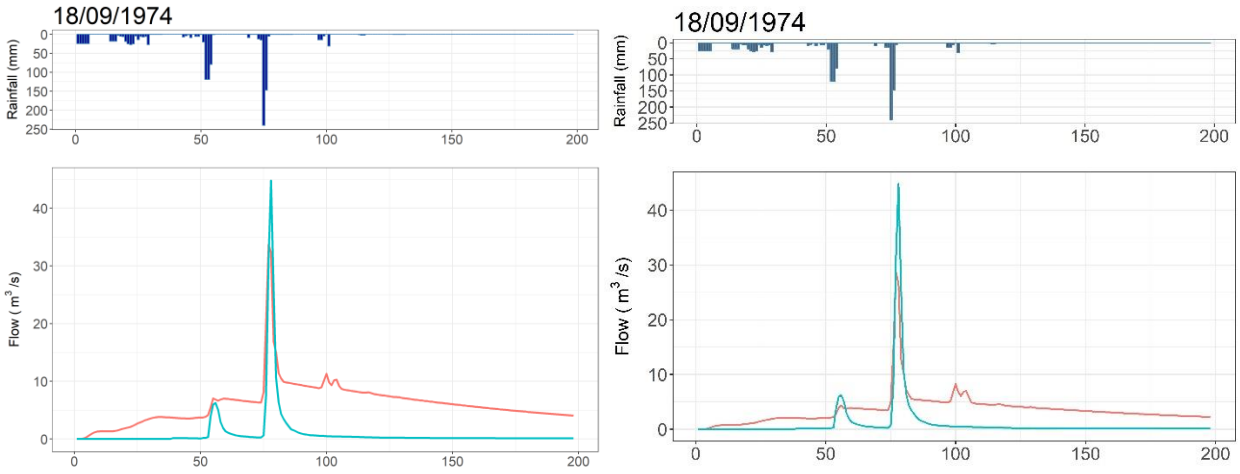

Figure 3.16: Result of simulation for episode 11 with y-axis is flow discharge in m^3/s and x-axis is 30 minutes time step with the use of ω (left) and ω' (right). In the flow plots, blue lines represent observed flow, and the red line represents flow simulated using the model with the corresponding values of ω and ω'. The plotted rainfall corresponds to the rainfall measured in gauge 4 (Guérin) located near the center of the catchment.

Moreover, modeling with ω'/S improved significantly the NSE value of the special events which happened in dry condition. Figure 3.16 describes both cases where we used ω and ω', apply for a special event. It is shown that the use of ω' decreased the peak of the simulated flow, but it made the total hydrograph fit better with the observation.

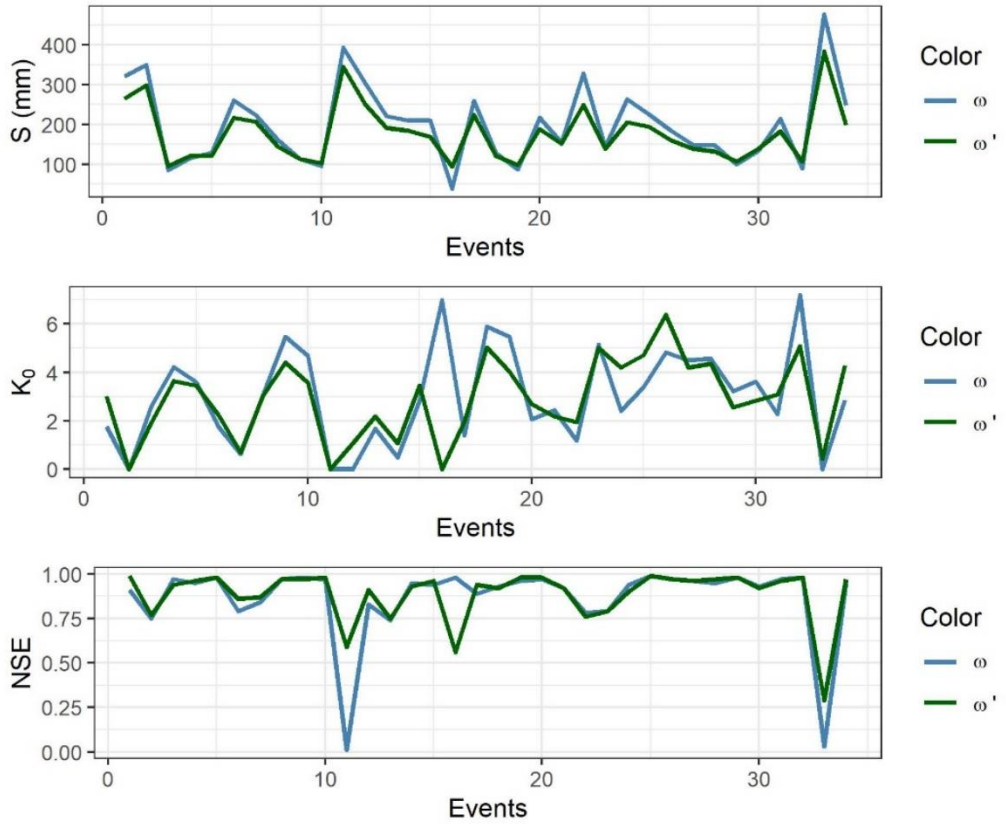

Figure 3.17: Comparison between using ω and ω' for all events

The comparison of using ω and ω' for all the events was described in Figure 3.17, led to the conclusion that the use of ω' is better for the simulation. Finally, the ω'= 60 mm were finally kept for the calibration and now the model ran with two parameters calibrated.

3.3.2. Model calibration

The parameters S and K_0 had to be calibrated for the 34 events. An optimized set of values was found for each event, by optimization of the NSE computed with the observed and computed discharges (Figure 3.18). The S calibrated parameter values ranged from 75 to 400 mm (median = 181 mm), K_0 between 0 and 4.5 (median =2.4), and the NSE ranged from 0.27 to 0.99 (median = 0.96, lower quartile = 0.87) (Figure 3.18). The simulated hydrographs

indeed proved to be very similar to the observed one (Figure A 9). The two worst values of NSE corresponded to events occurring in the driest initial soil conditions (18/09/74 and 05/09/2005). In these cases, the low flow values were overestimated, whereas the peak flow values were underestimated.

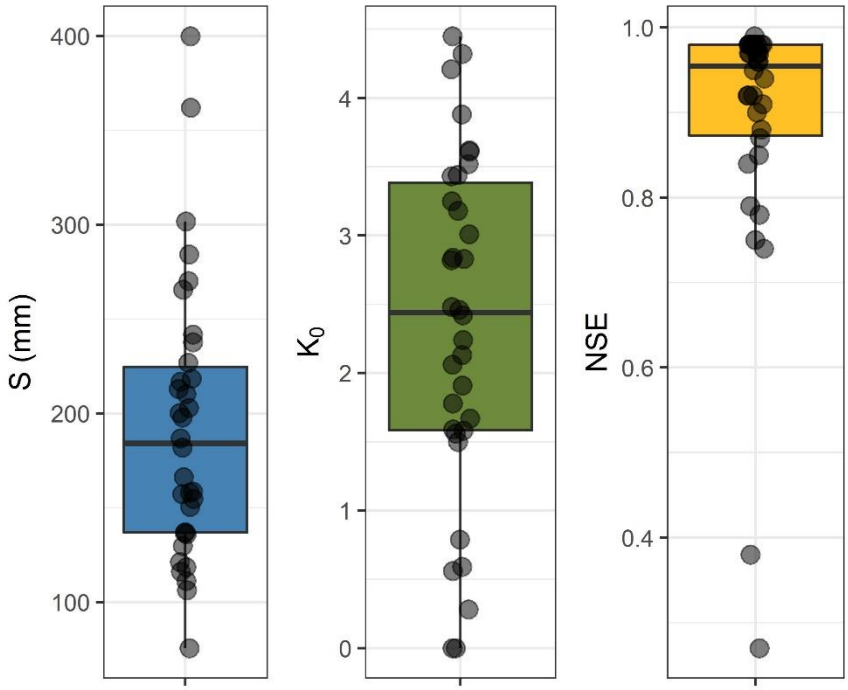

Figure 3.18: Calibrated values of S and K_0 and corresponding NSE for the events.

The sensitivity test performed above gave an idea of the impact of such variabilities, and the model was supposed to be more sensitive to *S* than to K_0, at the event scale. It is, however, worth to note that the K_0 low value normally appears in dry condition (high value of *S*) while the high value of K_0 is often in wet condition (low value of *S*) (Figure 3.19). In dry initial condition, the shape of the flood would be sharper because the delayed runoff should be smaller; thus, K_0 will tend to be reduced in order to fit the shape of the flood. Finally, the fact that the model was not very sensitive to K_0 made that we could use the median value to simulate floods without significant loss of accuracy.

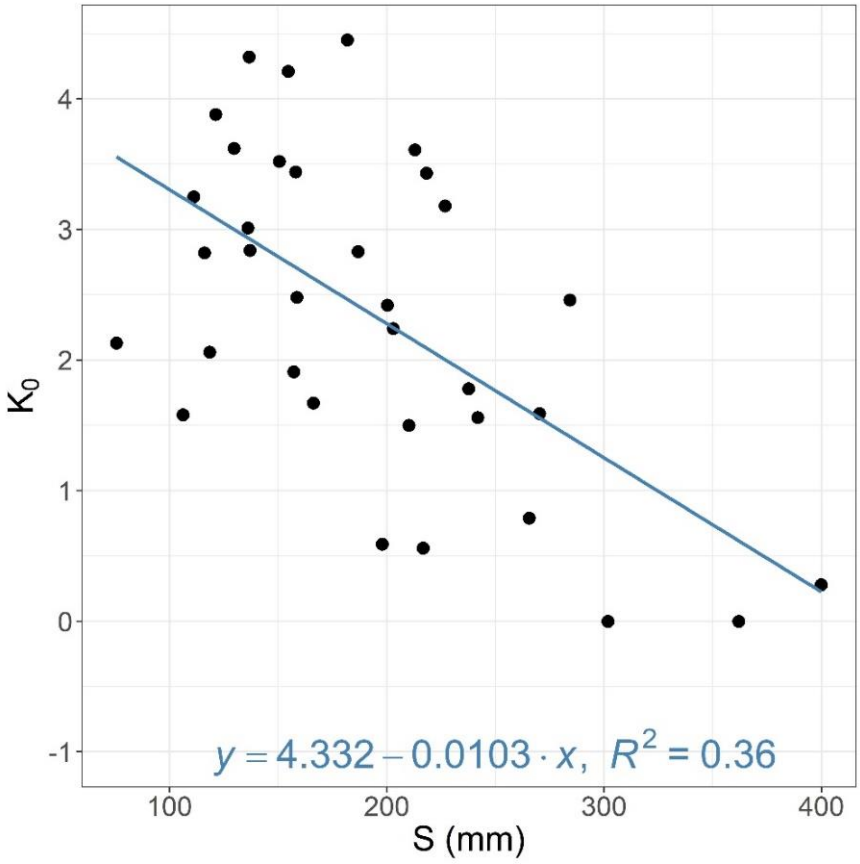

Figure 3.19: Relationship between S *and* K_0.

3.3.2.1. Event variability of the K_0 parameter

In the parameter sensitivity section above, we saw it clearly that the part of recession which mainly contributed by the subsurface flow was controlled by the two main parameters ω (for the height of the recession) and *ds* (for the slope of the recession). However, because of the variability of the K_0 parameter, we can see the role of the K_0 parameter with the subsurface flow could be more than the production parameters in the case of the dry condition. Thus, the K_0 was related to initial conditions. However, the results show that the K_0 was not strongly correlated with these indexes ($R^2 \sim 0.3$, Figure 3.20). For events that are not in the dry condition, we can still have the varied K_0 value.

K_0 was also tried to correlate with all the internal characteristics of the storm events, however, we did not find any strong correlation with any index (Figure A 10 to Figure A 12 in the Appendix)

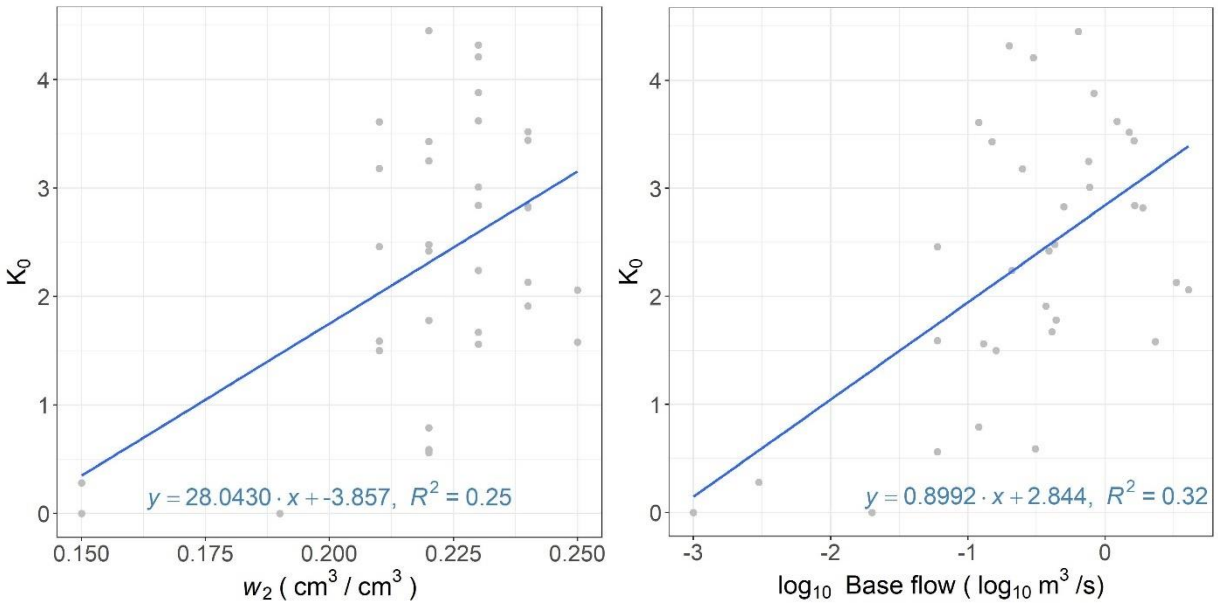

Figure 3.20: Correlation between K_0 and external characteristics of the events.

As S and K_0 were found to be more or less dependent, another test was performed to answer the question of the actual impact of the parameter's variability over the whole range of the events. The analysis was led by using the median value of each parameter (S then K_0) and by recalibrating the other parameters of the model (Figure 3.21). For each calibration, the loss in NSE and the differences in S or K_0 expressed the sensitivity of the model to a given parameter. The highest loss in NSE was found when using the median S parameter and calibrating K_0: in this case, the median NSE decreased to 0.78 instead of 0.96 when calibrating both S and K_0, and the median K_0 increased to 3 instead of 2.4.

Meanwhile, using the median of parameter K_0 resulted in marginal changes of the median NSE (0.94 instead of 0.96) and median S (178 instead of 181 mm). Thus, the parameter S can be considered as the key parameter of the model, of which the variability at the event scale must be accounted for. The variability of the K_0 parameter seemed to have less impact on the flood simulations, although the impact could be important for some events.

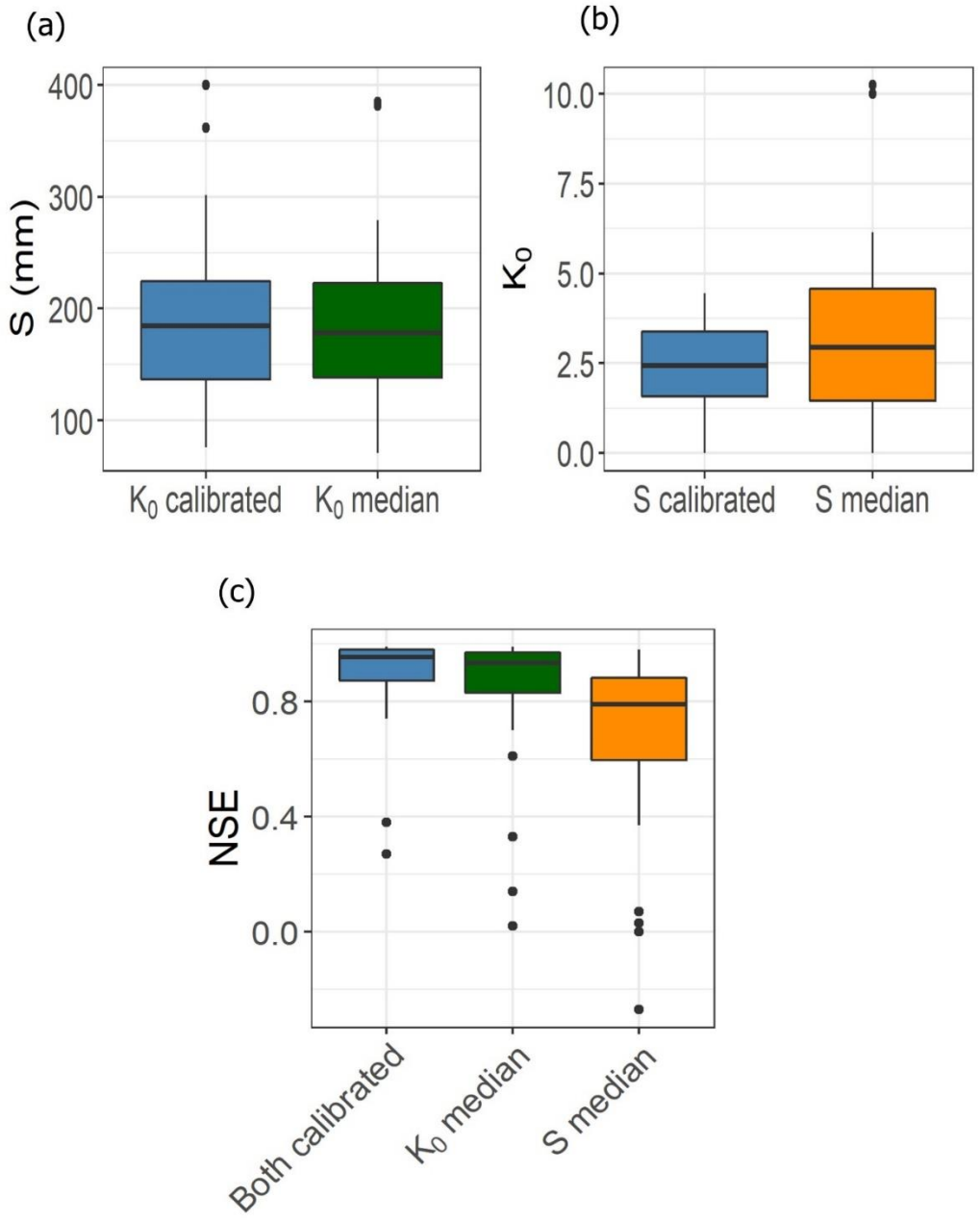

Figure 3.21: Sensitivity of the model to the variability of each parameter. (a): change in calibrated S *when using either median or calibrated* K_0*, (b): change in calibrated* K_0 *when using either median or calibrated S, (c): changes in NSE when two parameters calibrated and using one median.*

More details were shown at the event scale, comparing the calibrated values of S using either median or calibrated K_0, or the calibrated values of K_0 using either median or calibrated S (Figure 3.22). The calibrated S values were found to be stable when using median K_0, whereas the calibrated values changed a lot. Thus, the variability of K_0could be

neglected and using the median value would be enough, as well for the model score than for the *S* parameter estimation.

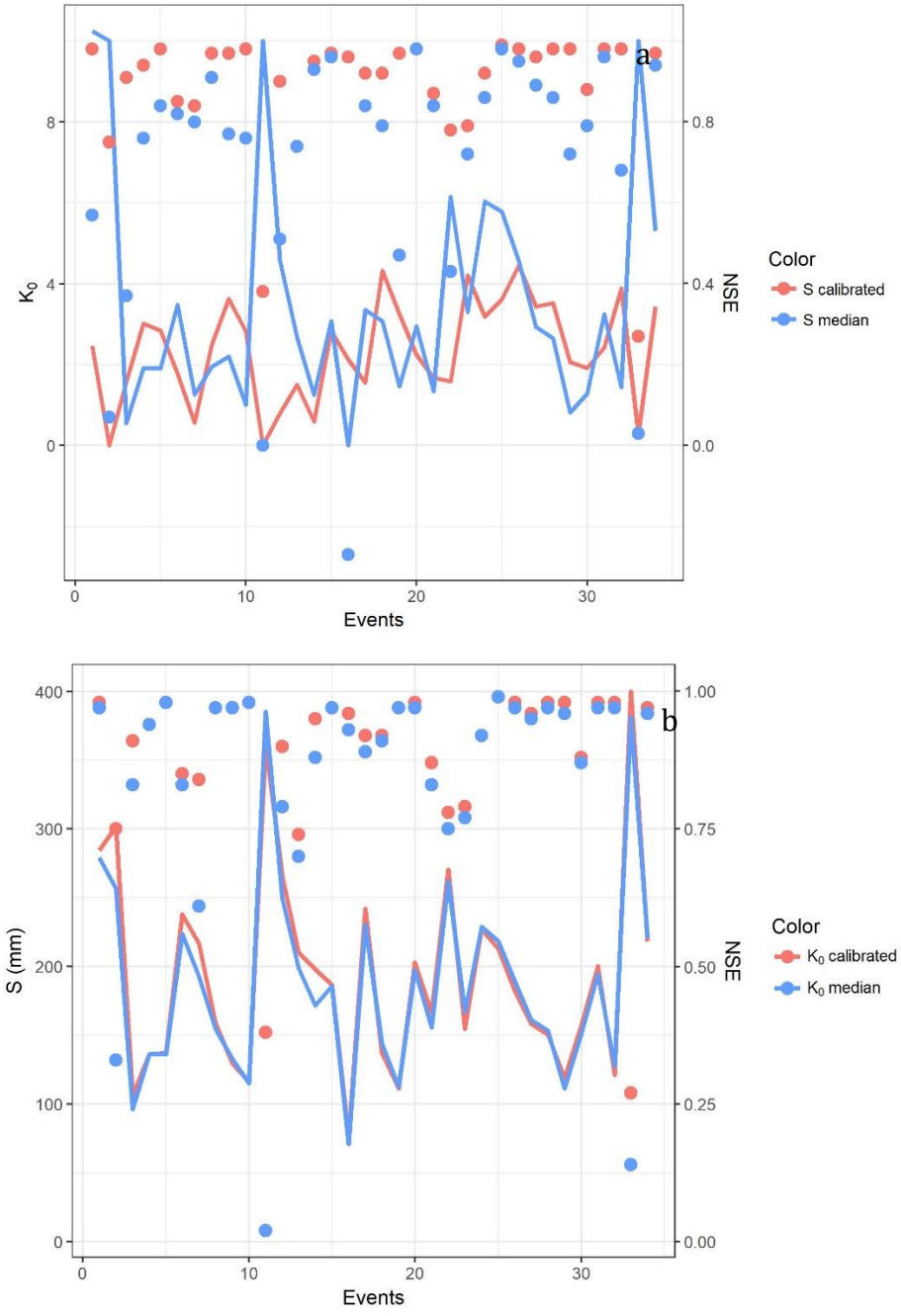

Figure 3.22: Sensitivity of the model to the variability of each parameter: (a) changes in NSE and calibrated K_0 when using either median or calibrated S;(b) changes in NSE and calibrated S *when using either median or calibrated K_0. Lines represent the values of* S *in mm, while points represent the value of NSE in each event.*

3.3.2.2. Event variability of *S* parameter

After the calibration of the model, it appeared that *S* was the most variable and most influent parameter for the simulations. Firstly, the calibrated *S* is related to the internal characteristics of the storm events such as the mean areal rainfall and the runoff coefficient. As we can see from the results (reported in Figure A 6 to Figure A 8 in the Appendix), the event variability of the *S* parameter was not correlated with either mean areal rainfall (Figure A 6) or peak flow (Figure A 8), with $R^2 \sim 0$ but had a moderate positive relationship with the runoff coefficient (Figure A 7, $R^2 = 0.58$). Moreover, *S* corresponds to the water deficit at the beginning of the event, so that it is expected to be highly dependent on the previous events and the initial state of saturation of the soil. Therefore, we tried to find relationships between *S* and two indexes supposed to express the initial water content: the base flow and the w_2 volumetric water content at the beginning of the simulated event.

Both indexes gave rise to a relatively strong correlation with maximum water retention, presented by the correlation coefficient R^2 (0.85 between *S* and $log_{10}(Qb)$ and 0.77 between *S* and w_2, Figure 3.23). To allow the computation of the logarithms, the null base flows were changed to 0.001 m^3/s.

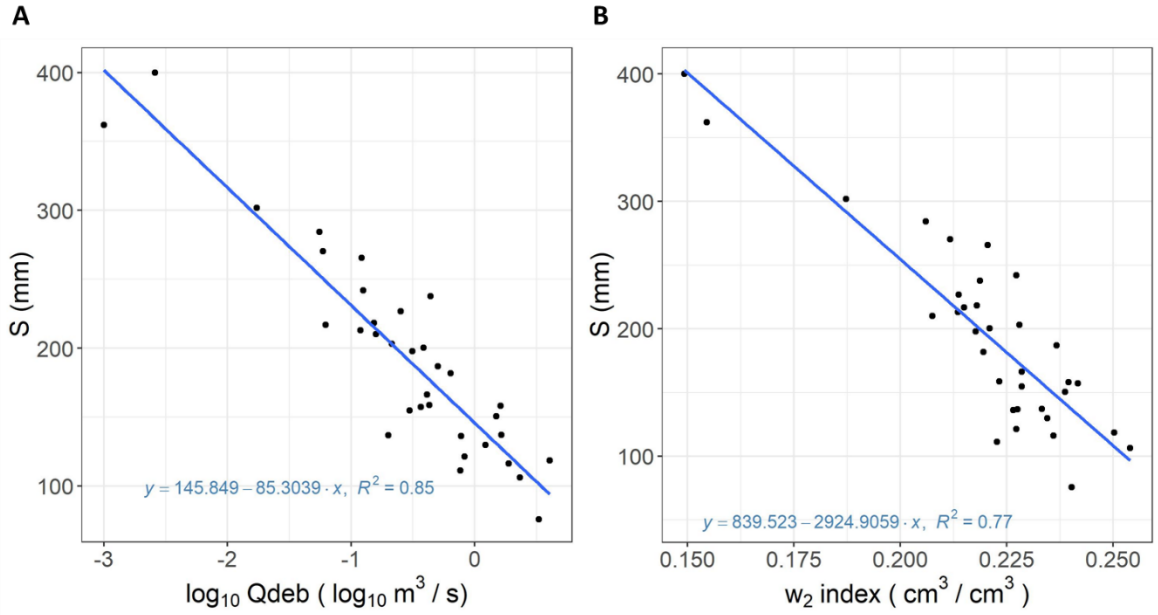

Figure 3.23: Relationship between maximum water retention and base flow (A) and volumetric water content (B).

These relationships should be used to assess the actual accuracy that could have the model in calibration mode. The actual accuracy of the model should be indeed estimated by the NSE computed with the predicted values of S instead of the optimized values of S, i.e. the predictive NSE. Figure 3.24 showed that using the predicted values of S instead of the optimized one reduced the NSE values (for all the events, the median value of K_0 was used): the median predictive NSE was 0.83 when using the relationship between S and the base flow and 0.77 when using the relationship between S and the water content w_2 (instead of 0.94 for the median optimal NSE, derived from optimal values of S and median value of K_0). This shows that the S-base flow relationship performs better than the S-w_2 relationship, in order to simulate the flood.

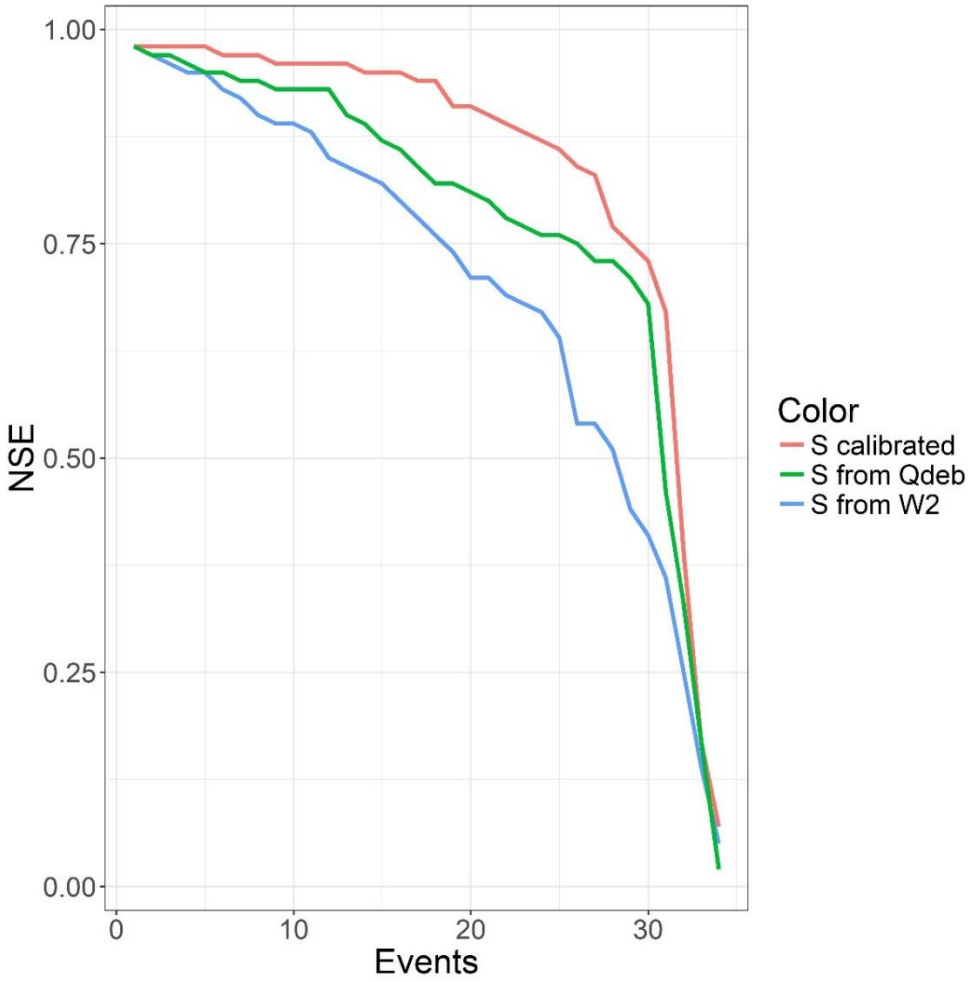

Figure 3.24: NSE value when using either S *calibrated,* S *derived from the* w_2 *index or from the base flow. The NSE values are sorted in descendant order for the 34 events.*

3.3.3. Validation of the model

The validation of the model was performed using cross-validation. Firstly, all the events were split into three samples: sample 1 included the 11 first events; sample 2 contained the events 12 to 22 and sample 3 was constituted of the 12 remaining events. For each predictor (w_2 or base flow), the model was first calibrated (S and K_0) on the set containing the calibration events, and the regression between S and two predictors was designed from the calibrated values of S. Then the model was applied on the set containing the remaining events (Table 3.3), by using the S values derived from the regression previously designed in the calibration phase and the median value of K_0 obtained with the calibration sample. The median predictive NSE was finally computed for both calibration and validation events (the median value of K_0 was also used for the calibration sample to calculate the median predictive NSE).

Table 3.3: Results of the split sample tests performed with the two predictors (w_2 *index, base flow Qb). "a", "b" and "*R^2*" are respectively the slope, the intercept and the determination coefficient of the regression designed between the initial condition* S *and the given predictor using the events of the calibration sample.*

Predictors	Calibration events	Validation events	a	b	R^2	Median predictive NSE for calibration	Median predictive NSE for validation
w_2	1-22	23-34	-2429.9	835	0.71	0.78	0.83
	1-11,23-34	12-22	-2740.2	797.45	0.90	0.88	0.76
	12-34	1-11	-2680.4	788.36	0.69	0.71	0.71
Log_{10}Qdeb	1-22	23-34	-81.77	140.73	0.85	0.89	0.76
	1-11,23-34	12-22	-77.49	153.51	0.87	0.9	0.78
	12-34	1-11	-88.91	146.05	0.83	0.81	0.92

The correlation coefficient R^2 was the highest for the second sample (0.9 for w_2 and 0.87 for base flow). One possible reason is that this sample contains all the dry events (i.e. events that occurred in dry soil conditions), and the corresponding extremely low values of S could artificially increase the correlation coefficient R^2. However, the other R^2 values were also very good (≥0.69), which showed a good correlation between the S parameter and the predictors. The coefficients a and b of the relationships did not differ a lot and were also very

close to those obtained for the whole sample of events, meaning that a stable relationship could be used for estimating S whatever the calibration sample was. The median predictive NSE were closed for the calibration and the validation samples, even sometimes higher for the validation sample than for the calibration sample. There was no significantly better sample for the comparison of the median predictive NSE for calibration and validation. Besides, the median predictive NSE were better for the base flow than the w_2, for both the calibration and the validation samples. Finally, to summarize, these results gave acceptable confidence for the performance and the robustness of the model, and for the possibility to apply it for other events than those used in this study.

3.4. The sensitivity of the model to rain gauges density

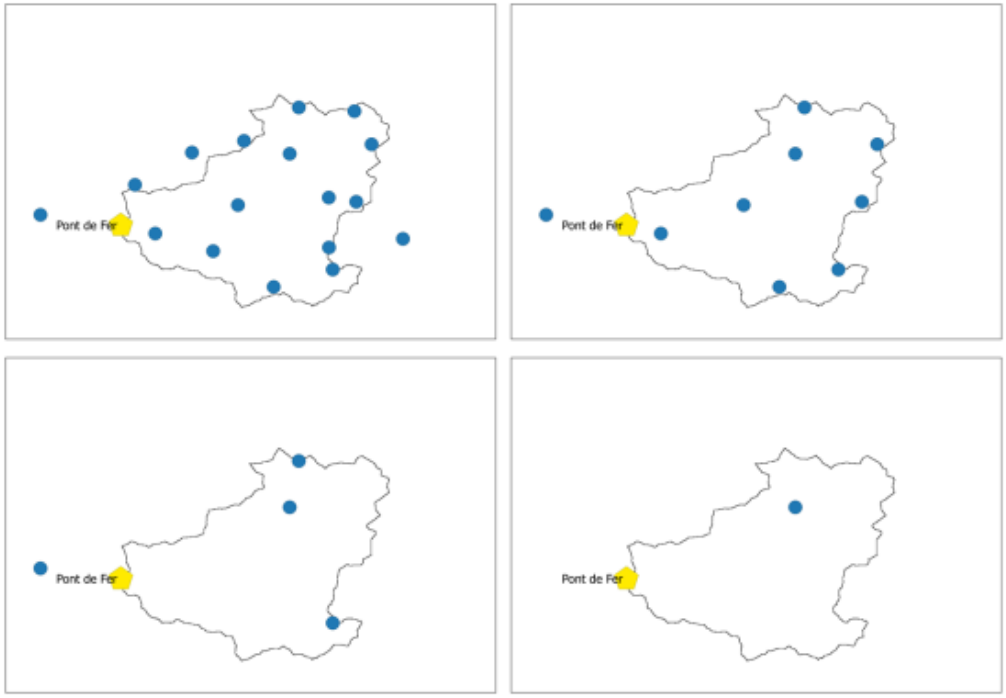

Figure 3.25: Maps of rain gauges that were selected for the test of data contribution. The density of gauges was one in 4 km², one in 8 km², one in 18 km² and one in 70 km², corresponding to 100%, 53%, 23% and 6% of the total gauges, respectively.

As mentioned above, the Real Collobrier catchment is one of the most-documented catchments in France. In other catchments, however, much fewer data are available.

Therefore, to assess how the model would perform for these less documented catchments, we decreased the density of gauges for calibrating the model: instead of all the rain gauges, we used 9, 4 and only one rain gauges. The gauges were selected in order to respect the optimal coverage of the catchment (Figure 3.25). We also considered the quality of the gauges, i.e. when we have gauges close together, the chosen gauge is the one which has more data available. The calibration of the model was carried out following the method above (S and K_0 were the parameters to be calibrated, whereas was kept ω'= 60 mm). When the number of rain gauges decreased from all the gauges to one single gauge, the median of both the initial water deficit S and K_0 did not change remarkably while the median NSE criteria decreased from 0.95 to 0.91, the R^2 between S and the base flow decreased from 0.85 to 0.62 (Figure 3.26), and the R^2 between S and the soil water content w_2 decreased from 0.77 to 0.59 (Figure 3.27). It was consistent with the fact that a higher number of rain gauges could improve the performance of the model, in other words, more rain data would help the model become more predictive. As seen above, insufficient data mainly affected the relationships between water retention and the external parameters (soil wet condition, base flow, etc.). Nevertheless, the parameters of the model stayed robust in spite of the decrease of the rain gauge density.

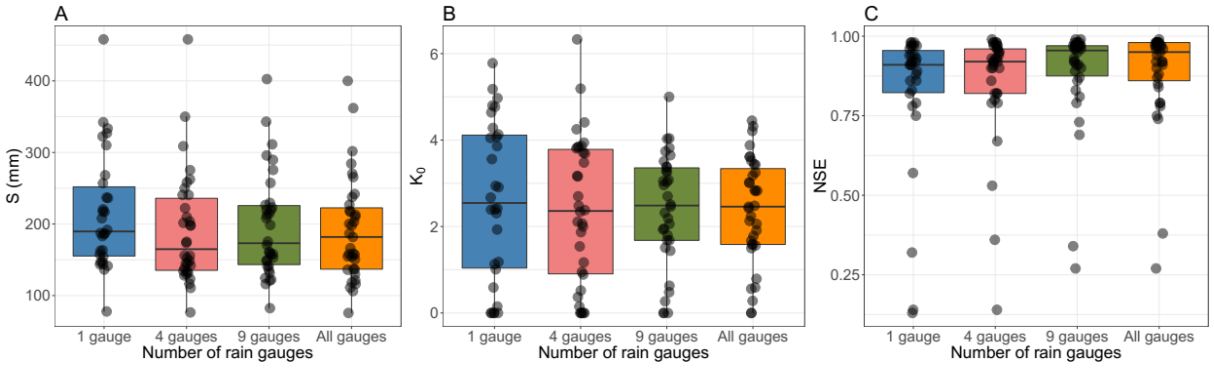

Figure 3.26: Distribution of the maximum water retention (a), the velocity of travel (b) and NSE (c) calculated from SCS-LR calibration with different number of rain gauges

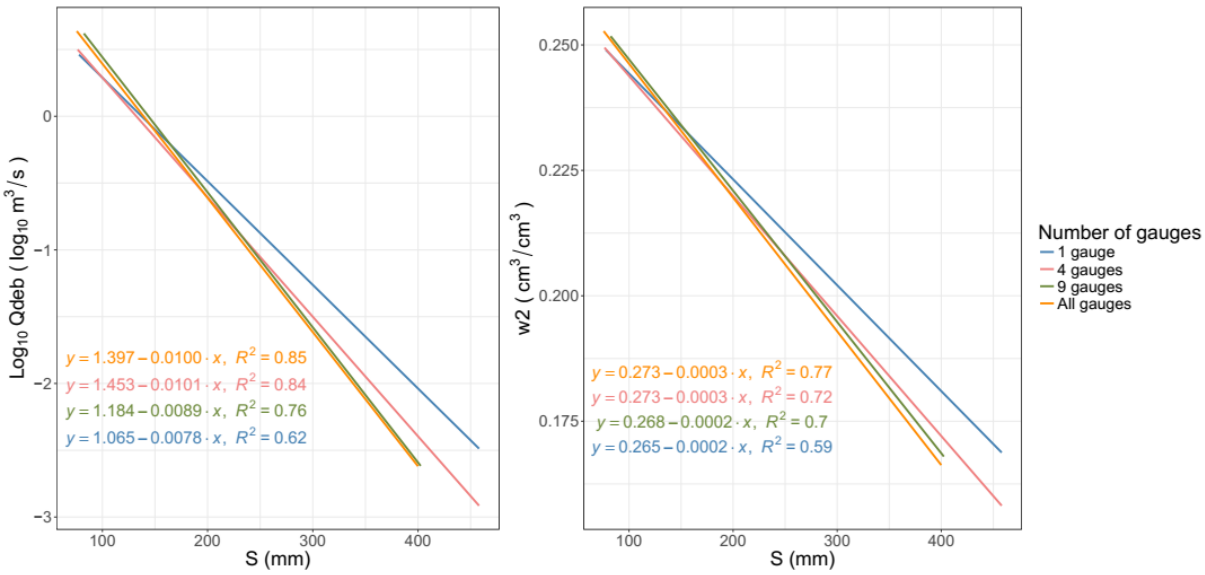

Figure 3.27: The coefficient of determination (R^2) between maximum water retention and base flow (left) and soil water content (right) when using all, 9, 4 and 1 gauges, respectively

Moreover, we can also test the effect of the spatial rainfall distribution by testing the calibration of the model when using each gauge. The density of rain gauge when we used 9 or 4 gauges was still more than what we usually had in most of the cases. Thus, in the case of Real Collobrier, we should test further the effect or each rain gauge to the output of the model.

The rainfall uncertainty was then tested by using only one gauge at a time for model calibration. We implemented the calibration of the model following the method mentioned above (S and K_0 were the parameters to be calibrated for each event, whereas we kept ω' = 60 mm, ds = 0.4 d^{-1}, V_0 = 2.5 $m.s^{-1}$). The results were given in Table 3.4, in which the regression and the predictive score were calculated for two predictors (w_2 and base flow).

Table 3.4: Results of using each rain gauge performed with the three predictors (w_2 *index, base flow* Qb*). "a", "b" and "R2" are respectively the slope, the intercept and the determination coefficient of the regression established between the initial condition* S *and the given predictor using the events of the calibration sample; PM is the median predicted NSE of the model.*

Gauge	# Events available	Median *S*	*W2*				Base flow			
			a	b	R^2	PM	a	b	R^2	PM
All	34	181.0	-2924.91	839.52	0.77	0.80	-85.30	145.85	0.85	0.91
Babaou	28	197.8	-2961.43	858.72	0.65	0.74	-90.49	154.05	0.76	0.79
Bonnaux	27	191.7	-3324.64	919.27	0.72	0.66	-97.20	129.07	0.79	0.72
Anselme	24	244.8	-2027.36	692.43	0.27	0.51	-64.51	207.92	0.42	0.68
Guerin	28	215.5	-2782.46	827.45	0.59	0.66	-79.37	167.31	0.61	0.70
Mouton	25	225.1	-5479.90	1465.77	0.27	0.57	-148.82	169.17	0.41	0.58
Fourches	27	197.4	-5204.81	1385.53	0.23	0.44	-135.17	156.16	0.39	0.52
Lambert	26	184.1	-2328.31	704.18	0.51	0.67	-66.07	153.42	0.63	0.74
Louviere	27	252.7	-2124.46	724.16	0.29	0.47	-68.85	215.55	0.39	0.51
Martels	15	153.6	-2421.10	683.62	0.64	0.58	-69.67	113.06	0.77	0.70
Bourjas	18	182.4	-4423.16	1152.60	0.87	0.76	-113.00	115.49	0.91	0.81
Peyrol	25	119.6	-2020.89	571.91	0.6	0.64	-55.28	95.13	0.68	0.72
Portaniére	26	143.6	-3365.36	890.62	0.71	0.64	-85.63	99.40	0.74	0.67
Rimbaud	29	221.9	-2321.87	735.02	0.41	0.60	-73.25	181.66	0.52	0.64
Vaudreches	26	136.6	-5648.03	1412.75	0.63	0.63	-140.77	79.17	0.68	0.71
Bourdins	21	233.4	-2557.44	798.06	0.41	0.69	-69.58	194.86	0.47	0.72
Davids	28	111.8	-2124.44	586.36	0.52	0.58	-59.78	83.17	0.64	0.59
Boussic	11	233.8	-2304.99	743.57	0.67	0.71	-74.80	199.50	0.69	0.71

The median *S* values ranged from 112 to 252 mm when using only one rain gauge for calibrating the model (it was 181 mm when using all the rain gauges). The R^2 of the relationship between *S* and w_2 (resp. *S* and *Qb*) ranged from 0.87 to 0.23 (resp. 0.91 to 0.39). The median predictive NSE of the model ranged from 0.76 to 0.44 (resp. 0.81 to 0.51) when estimating *S* from the relationship with w_2 (resp. with *Qb*). The results also indicated that there were differences in both slope and intercept when we considered the regression of the calibrated *S* parameter and predictors in each rain gauge and in all gauges (Figure 3.28). Figure 3.28 also showed the possible bias of the *S* parameter estimates, at a given density of rain gauges (here, 1 out of 70 km^2). It showed that for dry soil, let's say w_2 = 0.18 $cm^3.cm^{-3}$ or *Qb* = 0.01 m^3/s, the *S* estimates could range from nearly 250 mm to more than 600 mm, even

more for w_2, depending on the selected rain gauge used for the calibration of the model. For wet soil, let's say w_2 = 0.24 $cm^3.cm^{-3}$ or Qb = 10 m^3/s, the S estimates could range between nearly 50 and 150, even 200 mm.

This is consistent with the fact that a higher number of rain gauges could improve the performance of the model, in other words, more rain data would help the model become more predictive. As seen above, insufficient data affected both the performance of the model (predictive NSE) and the parameters of the model (median, dry and wet values of S).

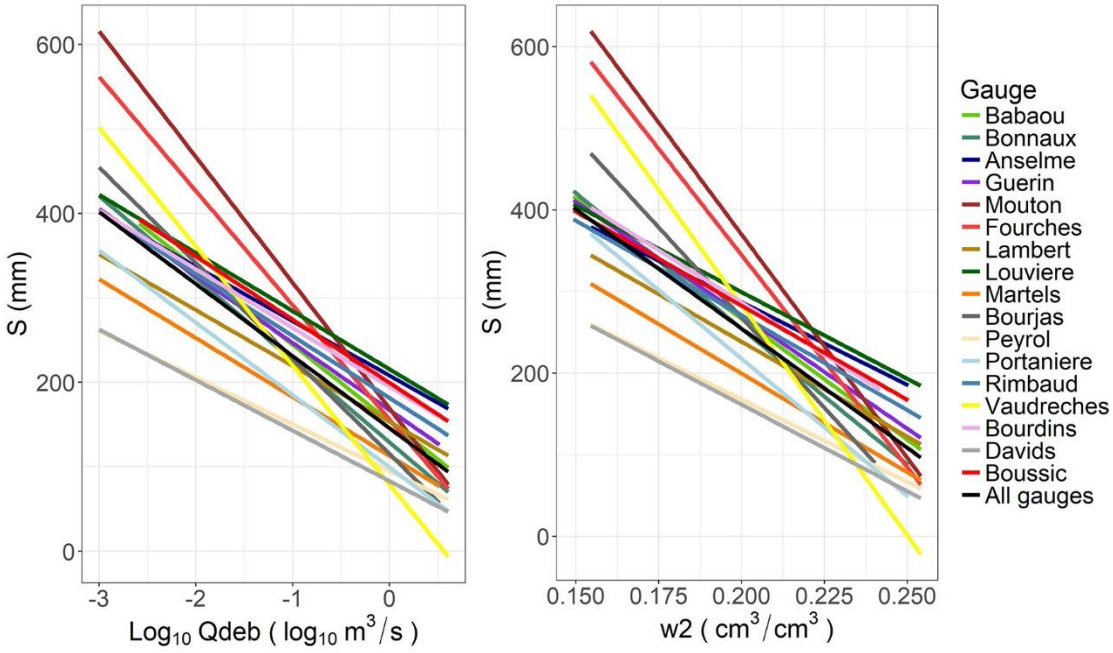

Figure 3.28: Relationship between S *and base flow (a) and between* S *and* w_2 *(b) when using all gauges or only one gauge for the model calibration. The regression obtained when using all the gauges was presented in black, while the regression obtained by using each single gauge were shown in colors.*

The effect of the rain gauges did depend on their position in the catchment so that the best R^2 were obtained for the gauges Bonnaux and Bourjas. Bonnaux can be considered as the most central gauge in the catchment. Bourjas exhibited the best R^2, probably because only half of the events could be recorded (18/34), which could artificially increase the R^2. In addition, most of the gauges led to equivalent both R^2 and slopes in the relationships between S and the saturation index (base flow or w_2), but different intercepts. This is due to the fact that all these gauges are correlated, but that rainfalls have different mean values,

probably due to orographic effects. Conversely, the worst R^2 were found for the gauges Fourches and Louviere, which were known to be poorly representative of the whole catchment (see Table 3.2 and Figure 3.6).

We can also see that when considering the relationship with the initial condition, the most different slope come from three gauges: Vaudreches, Fourches, and Mouton which are close together (Figure 3.28). The problem could possibly come from a numerical error to calibrate a special dry event (event 11) which make the excessive value of *S* parameter or the error from the gauges in differentiated places. If we remove these values of S, the regression between *S* and base flow and w_2 close with the others (Figure 3.29). Thus, these slopes should be considered to be due to the calibration uncertainty rather than to the rainfall uncertainty. Besides, we can also see the importance of the *S* calibrating of the special events to the regression with the initial condition.

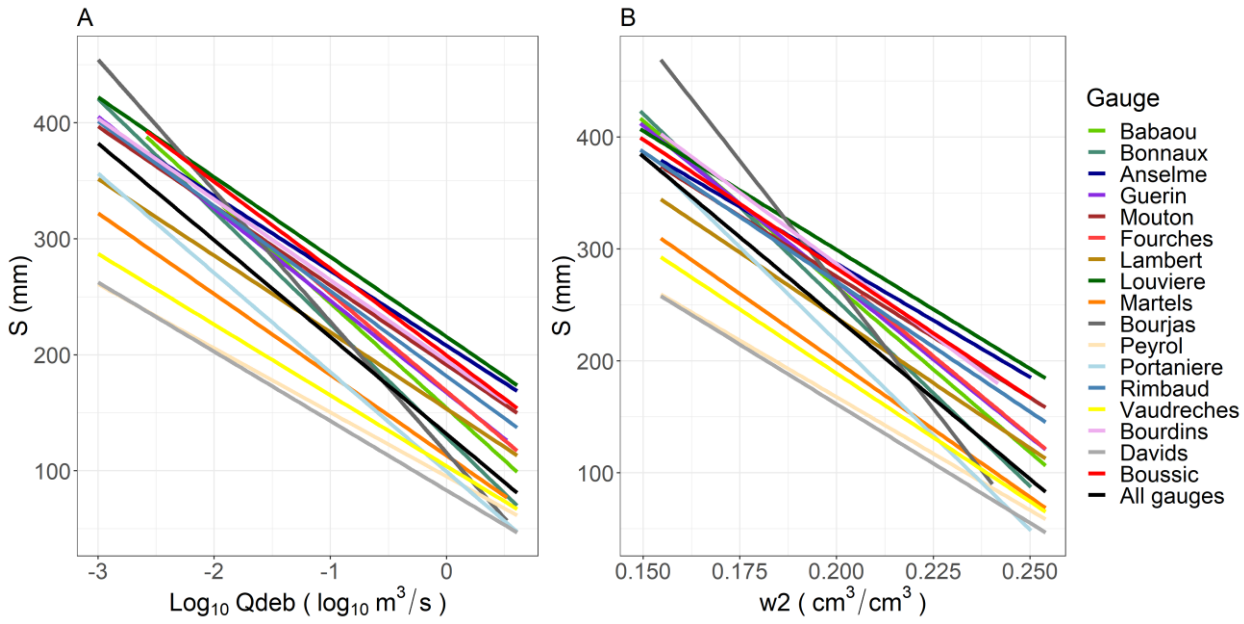

Figure 3.29: Relationship between S *and base flow (a) and between* S *and* w_2 *(b) when using all gauges or only one gauge for the model calibration, when the event with numerical error has been removed. The regression obtained when using all the gauges were presented in black, while the regression obtained by using each single gauge were shown in colors.*

3.5. Discussion

The *S* parameter was first compared to the estimated value that can be derived from the SCS Handbook. Real Collobrier can be described as mostly forestall, with pines, chestnuts, and oaks, in fair hydrologic condition. The most appropriate hydrologic soil group according to the high hydraulic conductivity of the shallow soil (> 100 $mm.h^{-1}$) was A, therefore the *S* value in medium conditions of soil moisture should be 459 mm when referring the SCS method guide. This value is far above the median calibrated value, S = 210 mm. As the calibration of *S* was shown to be robust, this difference should not result from equifinality or any other bias generated by the values of the other parameters, and there should be a more physical explanation. This is probably due to the fact that shallow soil does not have sufficient depth to allow such higher water storage capacity. The hydrological soil group D would be preferable to account for this limited capacity, but in this case, the *S* value in medium conditions of soil moisture would be 68 mm, which highly underestimates the actual calibrated *S* value.

Moreover, *S* was poorly correlated with the classical previous 5-days cumulated rainfall (Huang et al., 2007), P5D, as shown in Figure 3.30, and the large and continuous variability of the calibrated *S* also shows that the predicted values of *S* cannot be reduced to only three values corresponding to antecedent moisture conditions (AMC) AMC_I, AMC_{II}, and AMC_{III}, as proposed in the SCS guide. The above comments illustrate the difficulty of predicting *S* from the method guide.

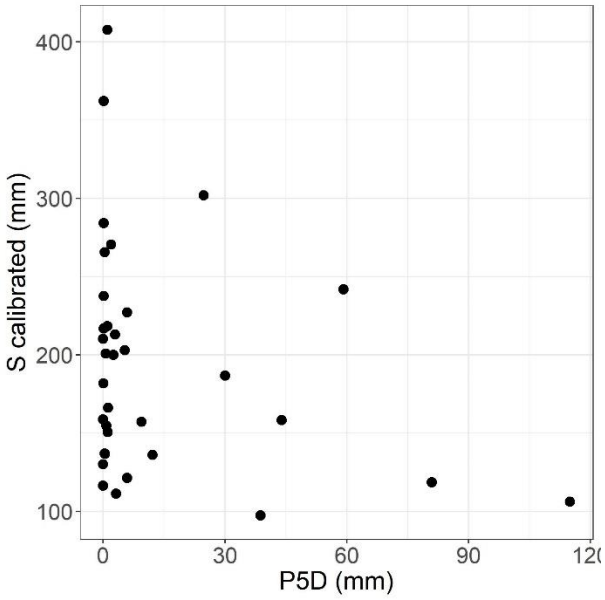

Figure 3.30: Comparison between calibrated S *values and 5-days previous rainfall amounts P5D, for the 34 events*

Similar relationships between *S* and the water content estimates have been found before when modeling floods at a sub-daily time step. In the small Mediterranean Valescure catchment (4 km², Δt = 30 minutes), Tramblay et al. (2010) found a high correlation (R^2 > 0.7) between *S* and either the field monitoring of water content, the base flow, the previous rainfalls or the output of the SIM model. In the Mdouar catchment in Morocco (635 km², Δt = 1 h), Tramblay et al. (2012) also found a high correlation (R^2 ~0.8-0.9) between *S* and either the antecedent precipitation index or the output of the GR4J daily model, whereas only four rain gauges operated over the catchment. This high correlation was probably due to the local oceanic climate, generating large-extended spatial rainfall. The correlation between the event cumulative rainfalls of 2 sites distant from 50 km was estimated to r = 0.96, which is much higher than in the Mediterranean climate. In a larger catchment such as the Wangjiaba catchment in China (30630 km², 139 operative rain gauges), under Moonson climate, Yu et al. (2018) found predictive NSE values varying between 0.66 and 0.95 for 24 flood events (Δt = 2 h), when using predicted values of S. But in several Mediterranean catchments, weak correlations or predictive NSE have been found between *S* and the water content predictors (see in the ATHYS catchment database http://www.athys-soft.org/bassins). It seems to be due to the high spatial variability of the rainfall, and the low density of rain gauges in these

catchments. As an example, the Gardon at Anduze (545 km², Δt = 1 h) indeed exhibited a weak correlation between *S* and the SIM output or the base flow ($R^2 < 0.5$). The present study indicates that it could be due to the relatively low density of rain gauges (7 rain gauges) on the catchment.

The R^2 of the relationship between *S* and w_2 or the base flow is not only affected by the rainfall uncertainties, but also by many other uncertainties, such as the ones related to the base flow, the w_2, the calibration protocol and the accuracy of the model. As the discharge at the Pont de Fer stream gauge was controlled by a downstream spillway, the low flow rating curve was assumed to be stable, and the base flow correctly measured. The calibration of the model was performed in different conditions which showed that the calibrated *S* values were stable whatever the other parameters values were. The uncertainty on the medium and high flows rating curve could also affect the *S* values, but this kind of uncertainty should generate a rather systematic than a randomized error, which should not affect the R^2 of the relationships between *S* and the base flow or w_2. Thus, it was reasonable to assume that the main uncertainty which could affect the relationships between *S* and the base flow or w_2 was due to the rainfall and that the R^2 mainly reflected this uncertainty.

3.6. Conclusion

The results of our study proved that SCS-LR model could simulate flash flood in Real Collobrier catchment with good accuracy. The calibration and the validation of the model were mainly based on the rainfall and runoff data corresponding to 34 events of Real Collobrier catchment in the period of 1968 – 2006. The sensitivity test and parameters dependency test allowed reducing the number of parameters to be calibrated. Some parameters could be set constant for all the events, by considering either numerical properties of the parameters (in case of *ds* or V_0) or empirical assumptions (for ω'). The maximum water retention *S* and diffusion time K_0 were calibrated for each event, and the variability of *S* exhibited a wider impact on the simulated flows than the variability than K_0. K_0 could be set to its median value without significant loss of quality in NSE values, nor change in *S* values. The variability of *S* was significantly correlated with the predictors of the basin wetness state: the soil water content and the base flow. The regression coefficient values (R^2) were high for both cases (0.85 and 0.77). The calibration protocol showed that

the estimated S values were robust and that the variability of these values was not dependent on the other parameters of the model. The median NSE equals 0.94 when using the optimal calibrated values and reduces to respectively 0.83 and 0.77 when using the predicted S values given by respectively the relationship with the base flow or w_2. These latter values are representative of the accuracy of the model at the event scale, as it can be expected for any further application of the model.

Moreover, the dense rainfall data gave us the possibility to test the effect of the rain gauge density on the calibration and the goodness of the model. The results proved that the reduction of the density of the rain gauges affected both the regression with the initial condition and the calibrated parameters of the model. When using a single rain gauge for the calibration of the model, the estimates of S can vary from 250 to more than 600 mm for initially dry soils, and from 50 to more than 150 mm for initially wet soils, depending on the selected rain gauge.

In the next chapter, we assess the performance of this model in other sub-catchments of the Real Collobrier, as well as study the spatial variability of the model parameters in the sub-catchment scale.

4. Spatial variability of the model parameters in the Real Collobrier sub-catchments

This chapter focuses on the spatial variability of the model parameters in Real Collobrier on four sub-catchments of the Real Collobrier: Rimbaud (1.5 km^2), Maurets (8.4 km^2), Marlière (12.4 km^2) and Pont de Fer (70 km^2). These sub-catchments are different not only in the scale but also in characteristics.

4.1. Presentation of the selected sub-catchments

4.1.1. Physio-geographical characteristics

The Pont de Fer watershed is the main catchment, which drains the other sub-catchments. For the analysis, we compared catchments of smaller areas: Rimbaud (1.5 km^2); the Maurets catchment (8.4 km^2); Malière (12.4 km^2 receiving the flows of the Rimbaud watershed) (Figure 4.1)

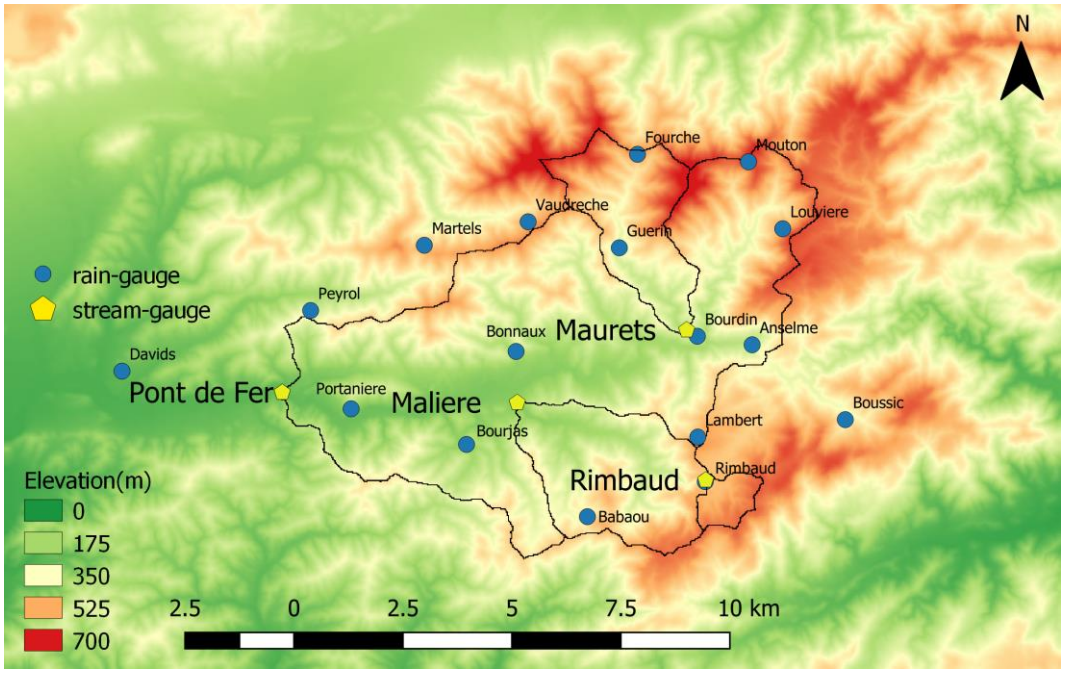

Figure 4.1: Map of the selected catchments in Real Collobrier.

4.1.1.1. Rimbaud

Rimbaud (1.5 km^2) is located in the south-east of Real Collobrier. The altitudes range between 470 and 622m. The slopes have an average value of 9-10°, but they can often exceed 20° in canyons carved out by the rivers. The basin of the Rimbaud is made up of relatively homogenous, entirely gneiss bedrock affected to a very strong dip towards the North-West (Figure 4.2A). Shallow stony soils with a sandy texture and lumpy structure belong to ranker's class. The soil is normally less than 30 cm deep, with frequent occurrence of bedrock at the surface (Figure 4.1B). The small depths of the superficial formations make that the stream of the Rimbaud reacts violently to precipitation. Before the wildfire in August 1990, the catchment was covered by a dense matorral and sparse cork-oak. The fire affected 84% of the basin watershed (Puech et al., 1991), by destroying a maquis with cork oaks and pines. A small chestnut grove, located in the downstream part, escaped the fire. The revegetation, essentially made from pine, made a fast recovery on burnt areas, and by August 1993 already covered around 50% of the catchment. The characteristics and the correlation among indexes of all events in this catchment were reported in Table A 1 and Figure A 13 in the Appendix.

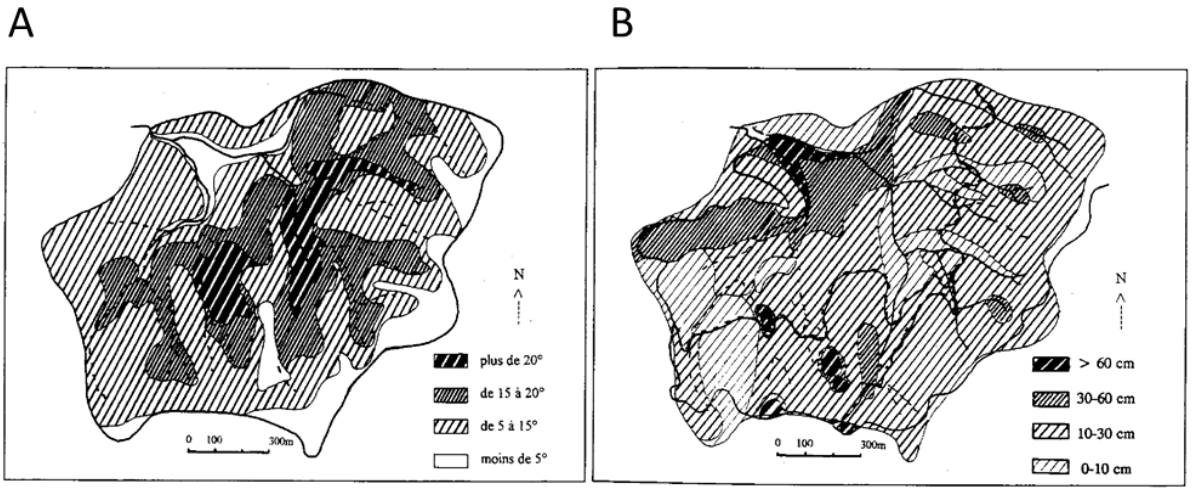

Figure 4.2: The topography of Rimbaud sub-catchment. (A) The map of slope of the area and (B) soil thickness and superficial formations (Béguin, 1993)

4.1.1.2. Maurets

Maurets (8.4 km^2) locates in the north-east of Real Collobrier. The elevation ranges from 209 m to 770 m. The average slope is greater than 10°. The topography of the basin is mixed

between high-sloped and planar structures. The highest slope in the basin can reach to more than 30° (Figure 4.3). The area is covered with forests of oaks, chestnuts, and pines. The understory soil surface in Maurets is covered with dense grassland. The basin is made up of metamorphic geological composition. The northern part composed of large outcrops of phyllites. There are two forms of phyllites in this part of Maurets: the alternating quartz and schist in the north-western part and the shales in the North-eastern part. Amphibolites, associated with leptynites, are found only in the downstream part. In this part, gneiss and mica schists are also found (Figure 4.3). Amphibolites are extremely sensitive to the weathering, whereas the phyllades are very resistant (Martin et al., 2004). The nature of the topsoil also highly varies from skeletal soil to brown soil and alluvium (with the thickness of several meters). The characteristics of all events in this catchment were reported in Table A 2 and Figure A 14 in the Appendix.

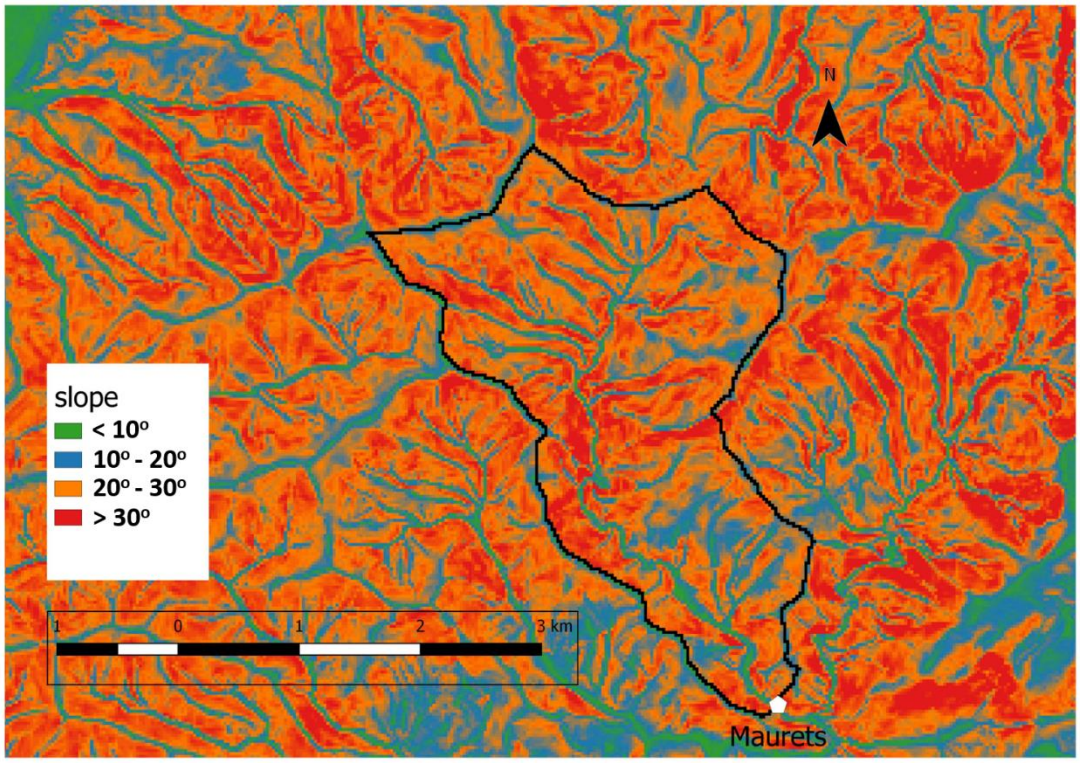

Figure 4.3: The map of slope of the Maurets sub-catchment

4.1.1.3. Malière

Malière (12.4 km^2) located in the south-east of Real Collobrier. The average elevation is 386 m. The geology included bedrock metamorphic composed of gneiss, mica-schist, amphibolite, and phyllade. The majority of the area has a slope greater than 10^o (Figure 4.4). The cover vegetation was the same with Maurets as maquis of heath, cork-oak, maritime pine and groves of chestnut. The characteristics of all events in this catchment were reported in Table A 3 and Figure A 15 in the Appendix.

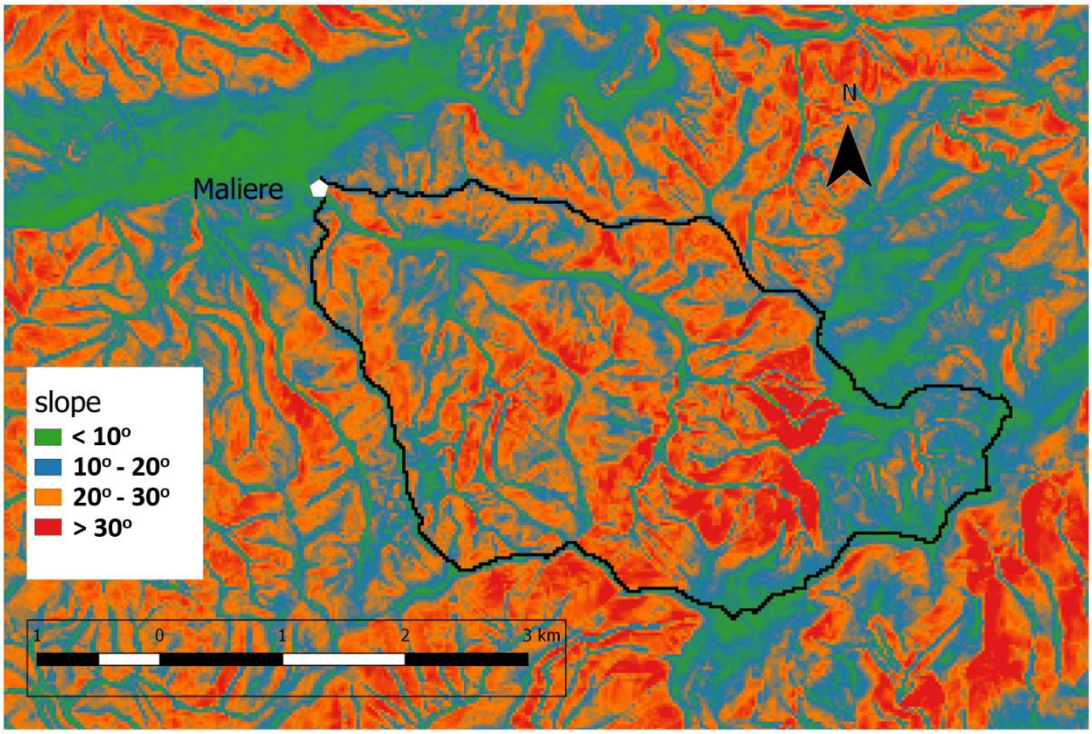

Figure 4.4: The map of slope of the Malière sub-catchment

4.1.2. Hydrological behaviors

The Rimbaud and Maurets sub-catchments have been widely studied in the past years. Soil properties have been monitored in one hillslope in the Maurets catchment. From Guelph permeameters multi-disc infiltrometers, Taha et al. (1997) found hydraulic conductivity at saturation of 100 mm.h^{-1} in average at the surface and 10-15 mm.h^{-1} in average at 60 cm deep (Figure 4.5). Soil porosity was 0.51 at the surface and 0.29 at the depth 60 cm. Head pressures ranged from some hundreds of cm to 0, according to the soil water content. Such

values were considered to lead to produce runoff by saturation of the whole vertical profile of the soil (Gresillon et al., 1995).

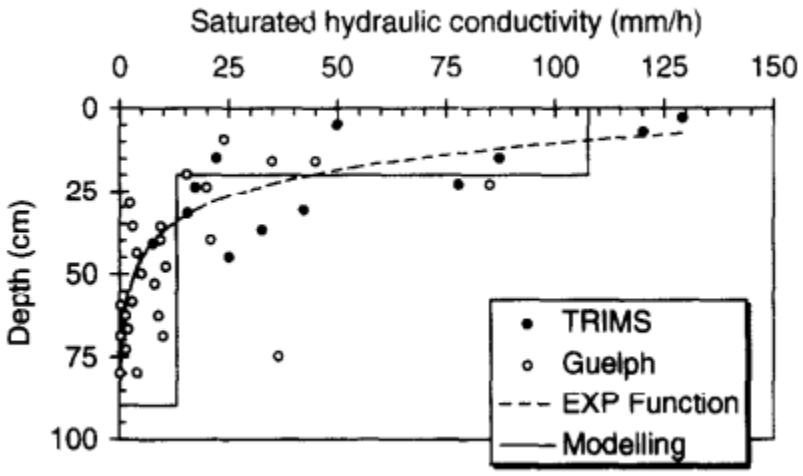

Figure 4.5: Measured hydraulic conductivity as a function of depth (Taha et al., 1997).

Marc et al. (1995) compared Maurets and Rimbaud runoff production during one flood by using geochemical tracers and stable water isotopes. They estimated that flood runoff in Maurets was due for 80% of pre-existing water (of which 60% was shallow soil water) whereas rainwater (new water) was only 20% (Figure 4.6). In Rimbaud, the contributions were significantly different, with only 40% of old water. The high percentage of old water in Maurets suggests that first, soils have a high storage capacity, and second that the infiltrated water is able to produce much runoff, as delayed runoff. Soils in Maurets thus have a much higher capacity to store water than in Rimbaud, but also higher capacity to be drained and produce runoff.

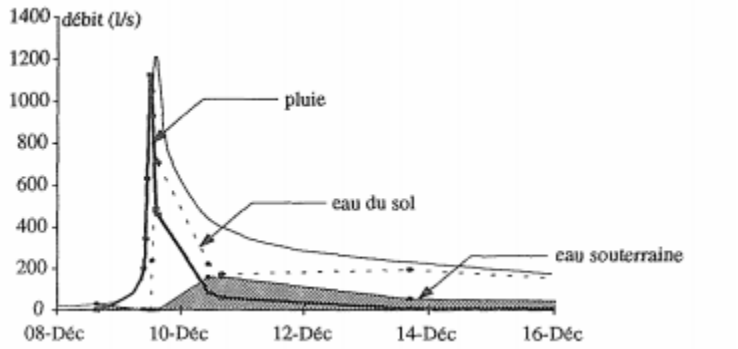

Figure 4.6: Three-component hydrograph separation in the Maurets basin (Marc et al., 1995)

The Maurets catchment was itself divided into sub-catchments during the 1992-1999 period. Four stream gauges delimited nested catchments, of which area were 0.26, 0.56, 5.75 and 8.37 km^2 (Figure 4.7). The hydrological responses of the three upstream catchments were found similar, whereas the more downstream part contributed very little to the runoff production (Figure 4.8). Both the slopes (steep in the upstream part, smooth in the downstream part) and the angles between the slopes and the planar structures of the rock could explain those differences (Martin et al., 2004).

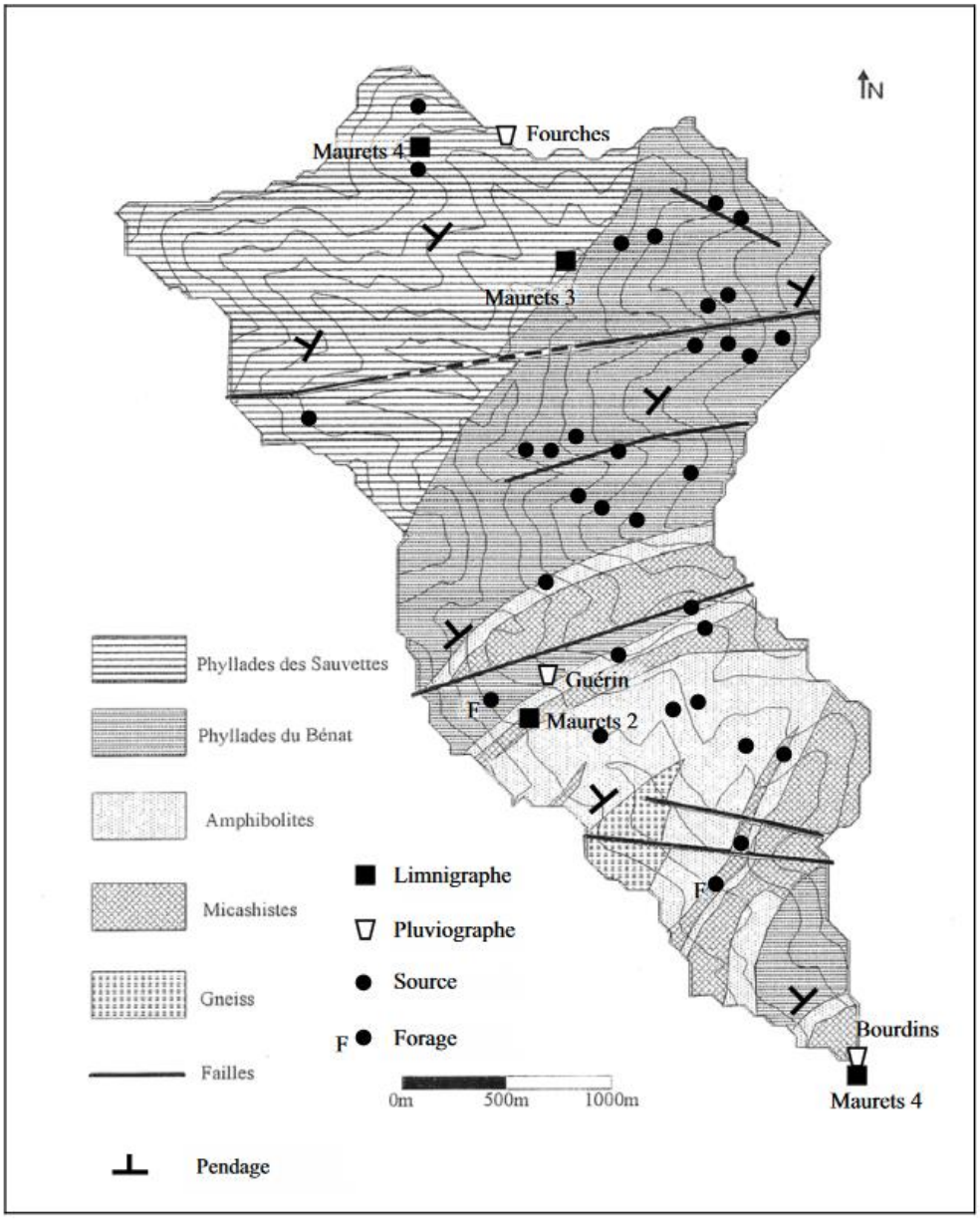

Figure 4.7: Geological map of Maurets and sub-catchment (Martin et al., 2004)

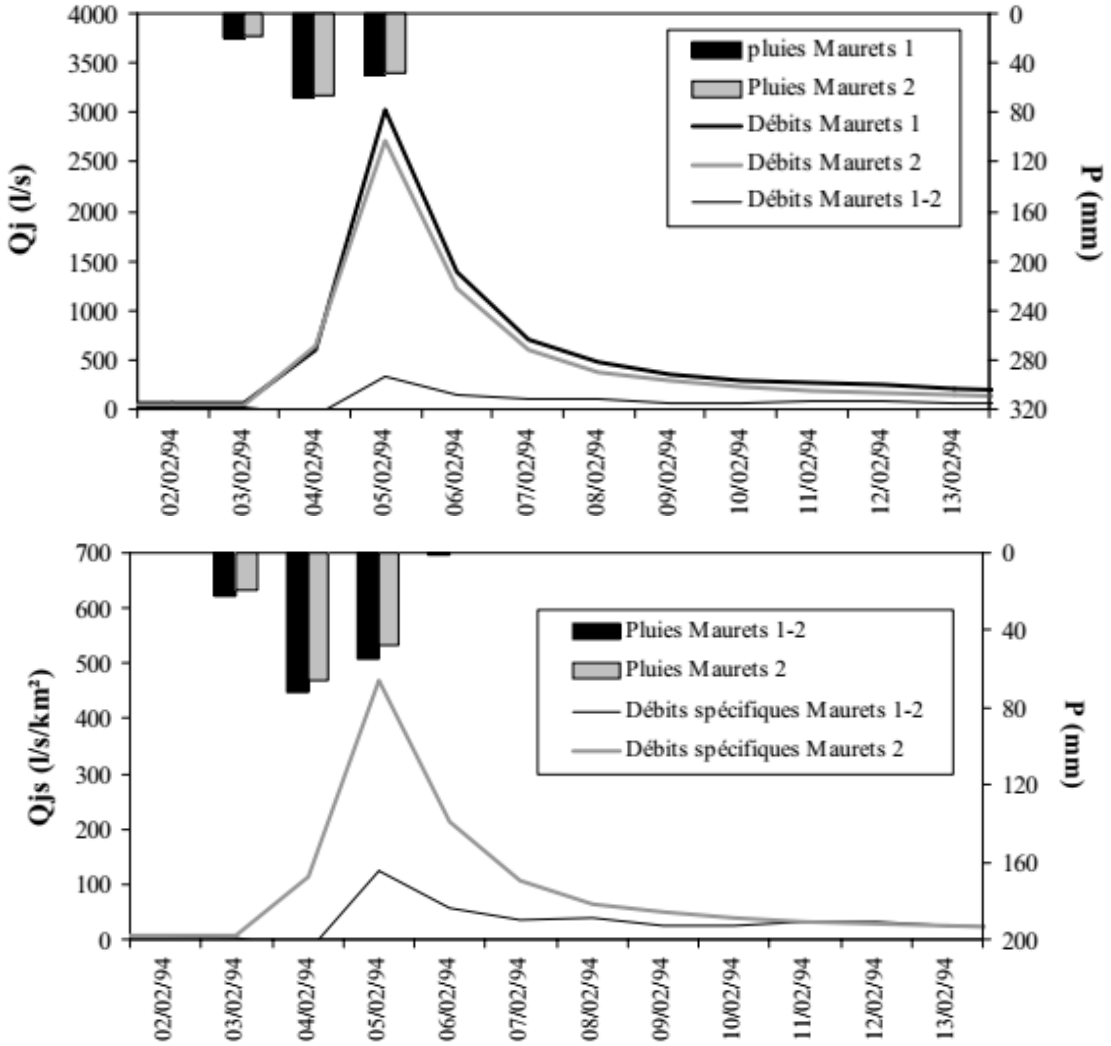

Figure 4.8: Daily flows (top) and specific daily flows (bottom) during the flood of February 5, 1994

4.1.3. Flood characteristics

The Rimbaud sub-catchment included thirty-two events from 1968 to 2002 applying the criteria: i) a new event was defined when occurred a period of 48 hours without amount exceeding 0.25 mm during a 15mn-time step, ii) the rainfall during the event had to exceed 30 mm in at least one rain gauge, iii) the peak flow during the event had to exceed 1 m^3/s. The cumulated rainfall was 73 – 365 mm, the peak flow reached 14.2 m^3/s. In this sub-catchment, the runoff coefficients ranged from 23.4 to 87% with an average of 62.3%.

Thirty-two events in the period 1970 – 2008 were obtained in Maurets sub-catchments with the same criteria than above, but the peak flow threshold was 3 m^3/s instead of 1 m^3/s in Rimbaud. The mean areal cumulated rainfall from 87 to 357 mm, the maximum peak flow was 7.8 m^3/s. The runoff coefficients ranged from 9 to 61% with an average of 37.5%.

In Malière sub-catchment, the selection method gave a series of 21 events from 1966 to 2008, with the same criteria than those used in Maurets. The cumulated rainfall ranged between 36-324 mm with the median of 165mm. The peak flow reached 25.6 m^3/s. The runoff coefficient of this sub-catchment ranged between 25 and 75%, with an average of 45%. Table 4.1 summarises the characteristics of four sub-catchments in the Real Collobrier.

Table 4.1: The hydrological and geological characteristics of four sub-catchments in Real Collobrier, including Pont de Fer, Rimbaud, Maurets, and Malière.

Catchment	Area	#events	Pmoy		Rc		Peak flow		Geology	Vegetation
			Range	Median	Range	Median	Range	Median		
Pont de Fer	70	32	49-319	162	4-56	35	30-91	44	Crystalline rocks with decreasing metamorphism from east to west (gneiss, mica-schist, phyllads)	Calcifuge vegetation (maritime pine, cork oak, chestnut, scrub) and 10% of cultivated areas (vineyard)
Rimbaud	1.5	32	73-365	166	23.4-87	62.3	2-14.2	3	A gneiss bedrock	A dense scrubland
Maurets	8.4	32	87-357	182	9-61	37.5	3-7.8	4.7	Bedrock metamorphic composed of phyllade and amphibolite	Maquis of heath, cork-oak, maritime pine and groves of chestnut
Malière	12.4	21	93-324	167	25-74	45	7.8-25.6	11.4	Bedrock metamorphic composed of gneiss, mica-schist, amphibolite and phyllad.	

It is shown that the mean areal cumulated rainfall of all the sub-catchments was almost equivalent for except a slightly higher for Maurets. Furthermore, the peak flow was logically

highest for Pont de Fer because it had the largest area. However, the highest for all of the events in Rimbaud was higher than Maurets (14.2 m^3/s to 7.8 m^3/s).

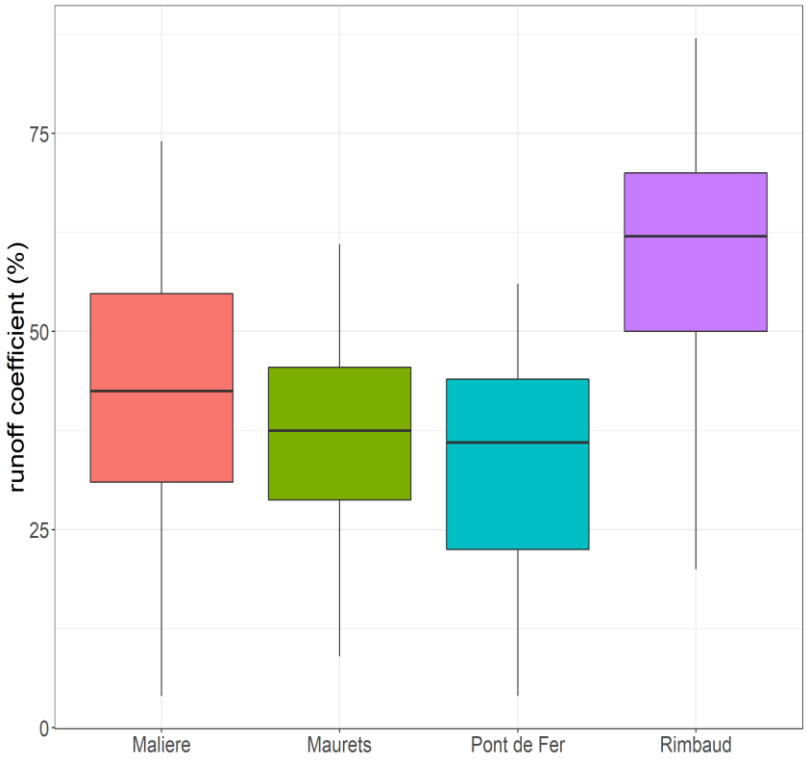

Figure 4.9: Comparison of Runoff coefficient across four selected catchments

Figure 4.9 showed a comparison of the runoff coefficient for four selected catchments. As we can see, the lowest value was for Pont de Fer although it was not so far with Maurets or Malière, whereas the runoff coefficient in Rimbaud was so far greater than the others. The reason could be due to the contrast between the higher runoff produced by the upstream areas and the lower runoff produced by the downstream areas, which originates in different soil depth, slopes, and planar rock structure. Rimbaud features a homogeneous headwater catchment, as could be the upstream part of the Maurets catchment (Martin et al., 2004), whereas parts of the other catchments seem to be much less productive, e.g. downstream area in Maurets.

Comparing the specific discharges in the catchments shows that Rimbaud catchment is more productive than the others, as well during the floods as during the recession phase (

Figure 4.10).

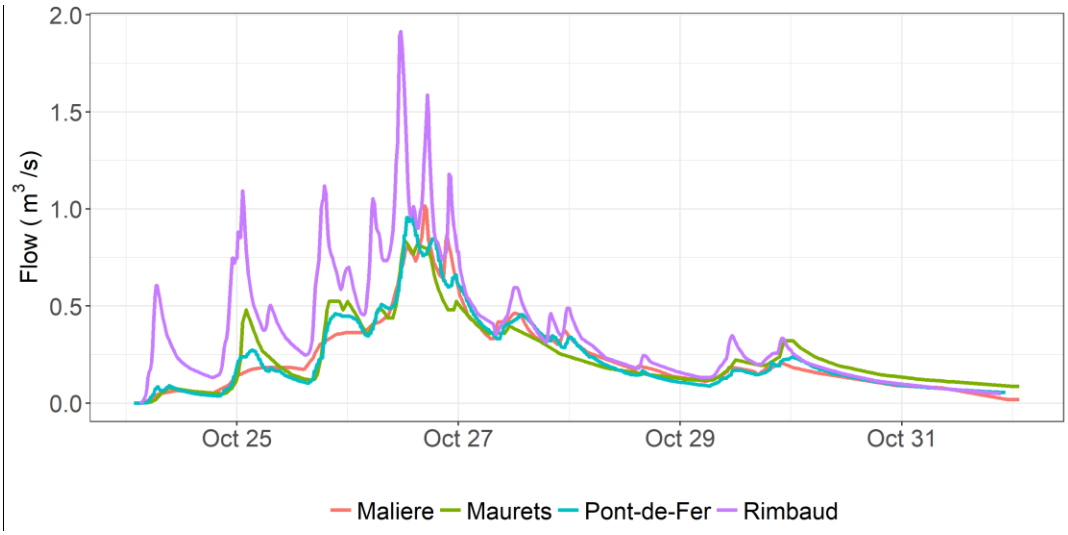

Figure 4.10: Comparison of the specific discharges among four sub-catchments of the Real Collobrier

4.2. Model calibration

The methodology was the same than used in Pont de Fer catchment. The model combined SCS distributed runoff model with LR transfer model, which counts with five parameters: S, ω', *ds*, V_0, K_0.

The *ds* parameter was derived by the analyses of the recession coefficient of all the events form each sub-catchment, as the median value of the coefficients of all the events. It is known that the model is little sensitive to the *ds* value.

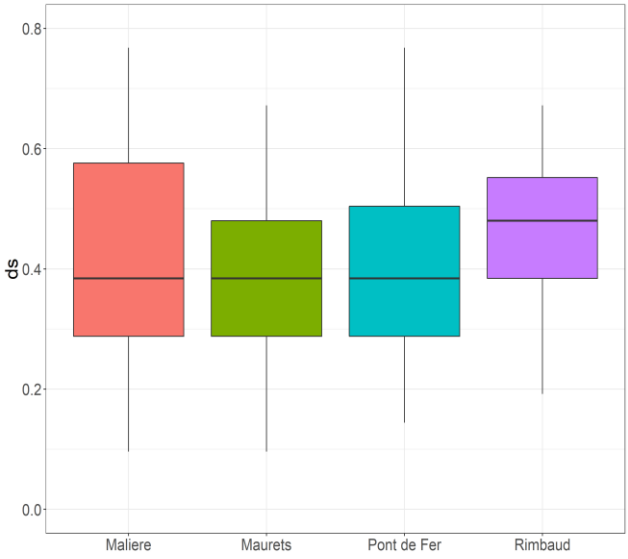

Figure 4.11: Comparison of ds *parameters across the 4 selected sub-catchments.*

As we can see in the figure, the median of the *ds* parameter was equal in Malière, Maurets, and Pont de Fer and slightly higher in Rimbaud (Figure 4.11). Due to the sensitivity test for the *ds* parameter above, the median value of *the ds* parameter could be kept for all the events. Thus, we used the value of *ds* as 0.5 for Rimbaud and 0.4 for the rest sub-catchments.

The ω' parameter was initially calibrated for each sub-catchment, it was shown that it should vary from one event to another. However, the sensitivity of the model to this parameter is quite low, at least for simulating the peak flow, and this justifies the choice of a constant value in time and space for ω'. Thus, ω' was set as the median calibrated value for each sub-catchment.

The value used for each sub-catchment was different: ω'= 70 mm for Rimbaud; ω'= 35 mm for Maurets; ω' = 90 mm for Malière. The differences will be commented later after that *S* has been estimated for each catchment.

The transfer parameter V_0 and K_0 are known to be strongly dependent (see chapter before), and one of these parameters need to be set to avoid artificial variation. As we could consider as a hypothesis of the model that the V_0 parameter is constant over the catchment, it was reasonable to keep V_0 unchanged (2.5 m/s as the same as the value used in Pont de Fer for the last chapter). The optimization was then run with the calibration of the two parameters *S* and K_0 for each catchment.

The median NSE values were 0.95 for Pont de Fer, 0.9 for Maurets and Rimbaud, and 0.88 for Malière (Figure 4.12). These high values of NSE indicated a very high predictive power of the model over all the nested sub-catchments.

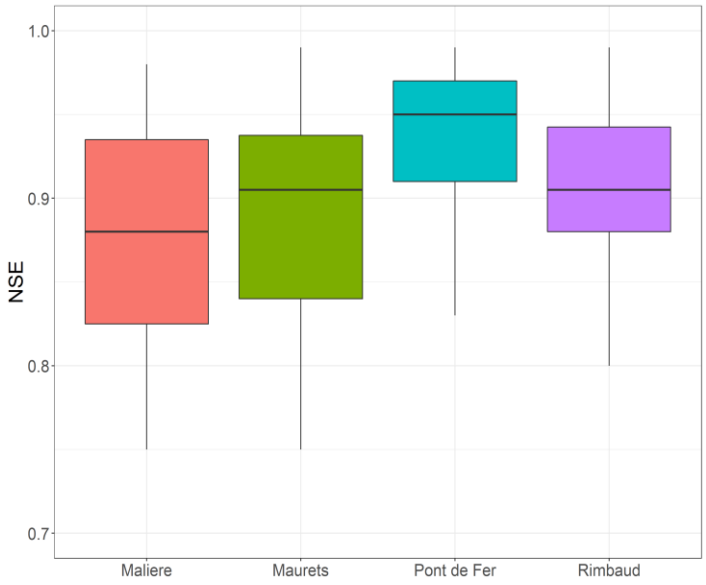

Figure 4.12: Comparison of the NSE values across the four selected sub-catchments

S parameter

The *S* parameter varied between different events and between different sub-catchments. The median *S* was the lowest in Rimbaud (115 mm); while it was higher in Pont de Fer and Maurets (180 mm), and the highest was in Malière (200 mm). The spatial variability of the median *S* values was in agreement to the calculated runoff coefficients in the case of Rimbaud: this catchment exhibited indeed higher runoff coefficients than the others. The three other sub-catchments had relatively similar runoff coefficients; however, Malière had higher *S* than Pont de Fer and Maurets (Figure 4.13). Although a difference of 20 mm could not really be significant for S, the difference could also be due to that the runoff coefficient accounts for the surface runoff as well as the delayed runoff, whereas *S* is associated only to the surface runoff. *S* and the runoff coefficient could indeed not be equivalent. As Malière exhibited the larger median runoff coefficient with a higher median value of S, it would mean that the direct runoff was less in Malière than in Pont de Fer and Maurets, but the delayed runoff was more important in Malière than in Pont de Fer and Maurets.

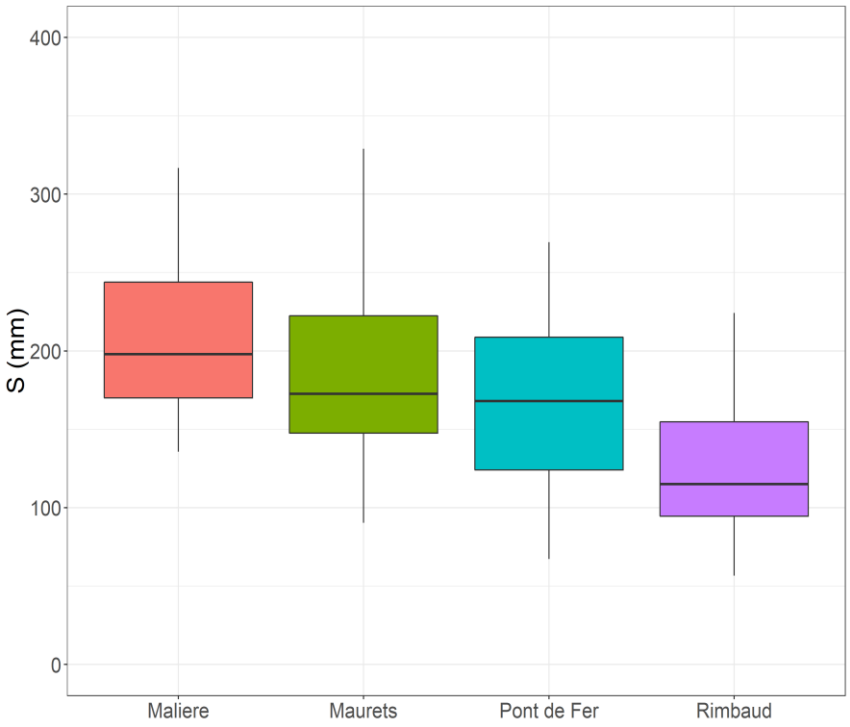

Figure 4.13: Comparison of S parameters across four selected sub-catchments

ω' parameter

The delayed runoff was expressed as a fraction $\omega = \omega'/S$ of the drainage of the soil reservoir, equaling itself a fraction *ds* of the soil reservoir level (Equation 11 and Equation 13). As *ds* soil drainage parameters and median *S* values were similar for the catchments Maurets, Malière and Pont de Fer, the delayed runoff in those catchments directly related to the ω parameter. The estimated median ω would thus be 35/180 = 0.19 in Maurets and 90/200 = 0.45 in Malière. It would be 60/180 = 0.33 in Pont de Fer (see the previous chapter). Thus, Malière seems to produce more delayed runoff than Pont de Fer and Maurets, which confirms what was found above (Figure 4.10 of the comparison of the floods in Pont de Fer, Malière, Maurets, and Rimbaud).

In Rimbaud, the estimated median ω would be 70/115 ~ 0.60. It means that more infiltrated water flows laterally in Rimbaud than in the other catchments. It could be interpreted as the fact that the Rimbaud substratum is probably less fractured or weathered than the Malière and Maurets ones, so that water cannot infiltrate deeply in Rimbaud, and

tends to drain laterally, whereas water percolates deeper Malière and Maurets, and could no more flow superficially.

K_0 parameter

The K_0 parameter was higher in Maurets and Rimbaud (29 and 18 for median K_0, respectively), while the value was much lower in Pont de Fer and Malière (median K_0 = 3 and 3.5) (*Figure 4.14*). The spatial variability of K_0 could be interpreted in different ways:

- Firstly, it could be some pure scale effect, due to the formulation of the relationship between T_m and K_m: $K_m = K_0 . T_m$, which could be inappropriate to be applied for any catchment area. The position of Maurets shows however that the catchment area is not the only factor to be considered for explaining the variability of K_0.
- It is known that the floods in Maurets and Rimbaud have different shapes, much smoother in Maurets (Marc et al., 1995). This seems to be due to deeper soils and higher water storage capacity, which also generates more subsurface flows in this catchment. Thus, in addition to numerical scale effects, there is probably also to account for dominant hydrological processes to explain the variability of K_0: subsurface flows processes are dominant at hillslope scale, so they are much more to be considered in small headwater catchments than in Pont de Fer, where subsurface flows are less influential due to the larger area of the catchment.
- The hypothesis that V_0 is constant in time and space over all the cells of the nested catchments could also not be adequate, and able to generate an artificial shift in the K_0 values.

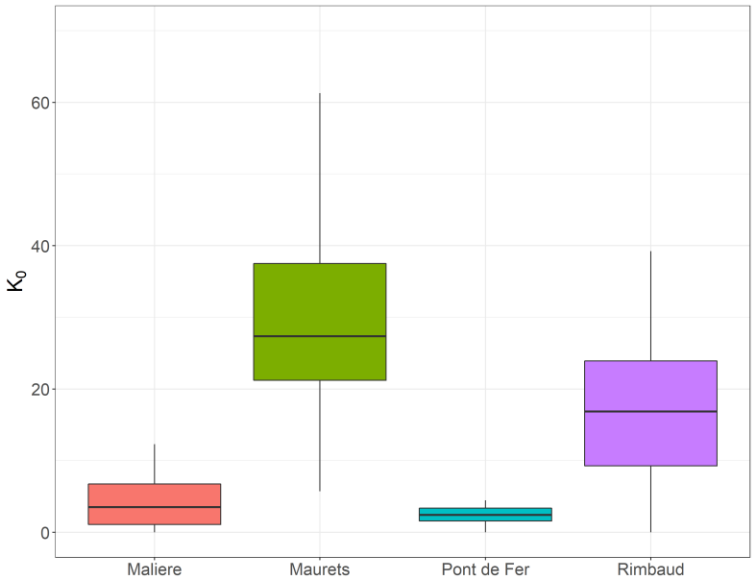

Figure 4.14: Comparison of K_0 parameters across 4 selected sub-catchments.

We mainly focused here on the first hypothesis. Thus, we performed another K_0 calibration, after having modified the relationship $K_m = K_0.T_m$ into $K_m = K_0.T_m{}^{\alpha}$, where α is a constant. After several trials, α = 0.33 led to similar K_0 values (approximately 60) in Pont de Fer, Malière, and Rimbaud, whereas Maurets had a higher value (K_0 = 150) (Figure 4.15). The use of this new relationship between K_m and T_m did not modify the other calibrated parameters.

The difference in Maurets could be due to the higher subsurface flow in this sub-catchment. This new formulation of the relationship between K_m and T_m will be checked with catchments of larger areas in the next chapter.

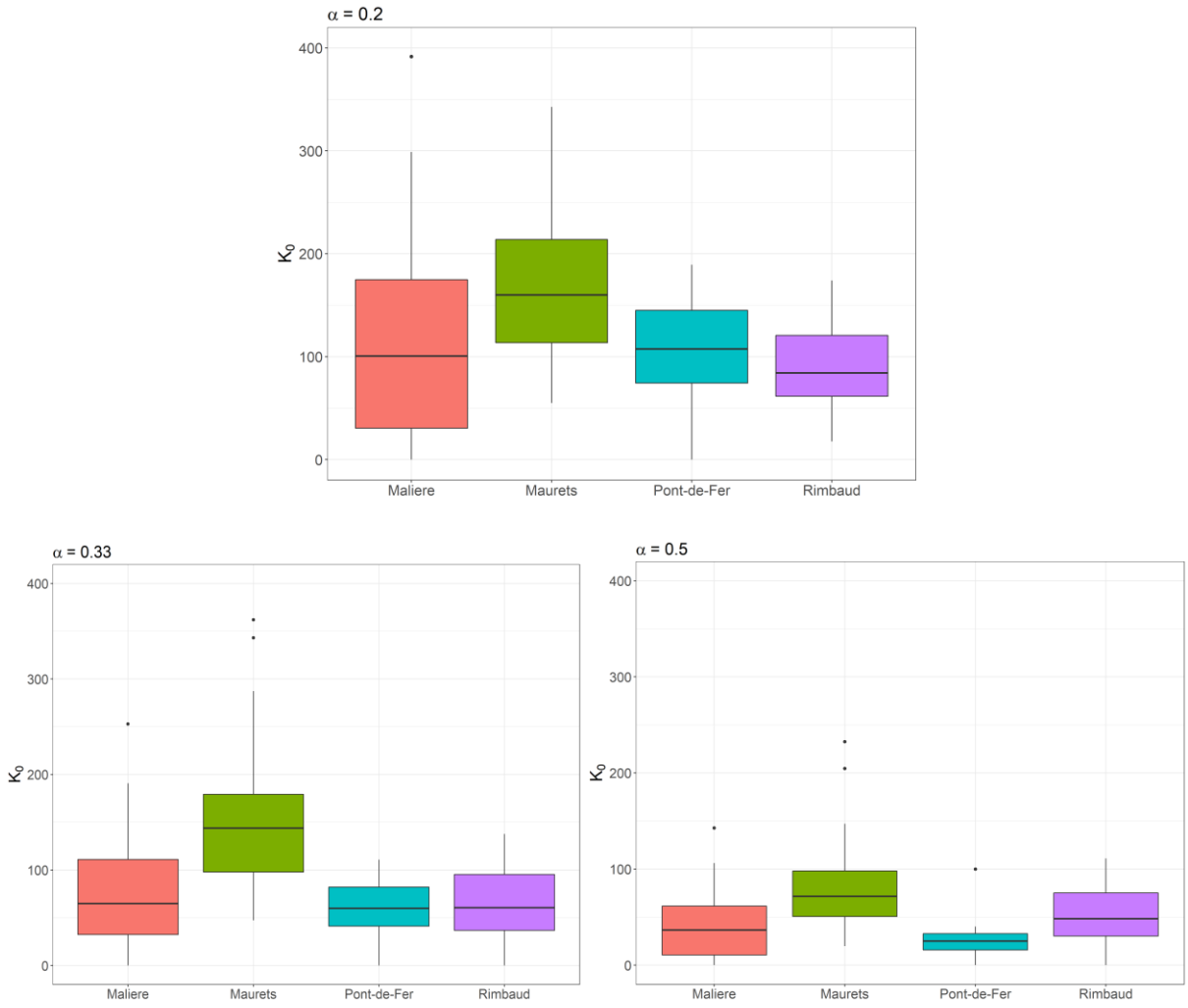

Figure 4.15: Comparison of K_0 *parameters generated using different values of α (α = 0.2, 0.33 and 0.5) across 4 selected sub-catchments.*

4.3. Temporal variability of parameters at sub-catchment scale

In each sub-catchment, *S* was the most variable parameter. As we also indicated in the previous chapter, the variation of K_0 was not significantly correlated with any index as well as could be neglected when comparing with the variation of *S* parameter. Thus, for the temporal variability of parameters at the sub-catchment scale, we have just focused on the *S*

parameter. The temporal variation of parameter *S* was related to the initial condition of these sub-catchments.

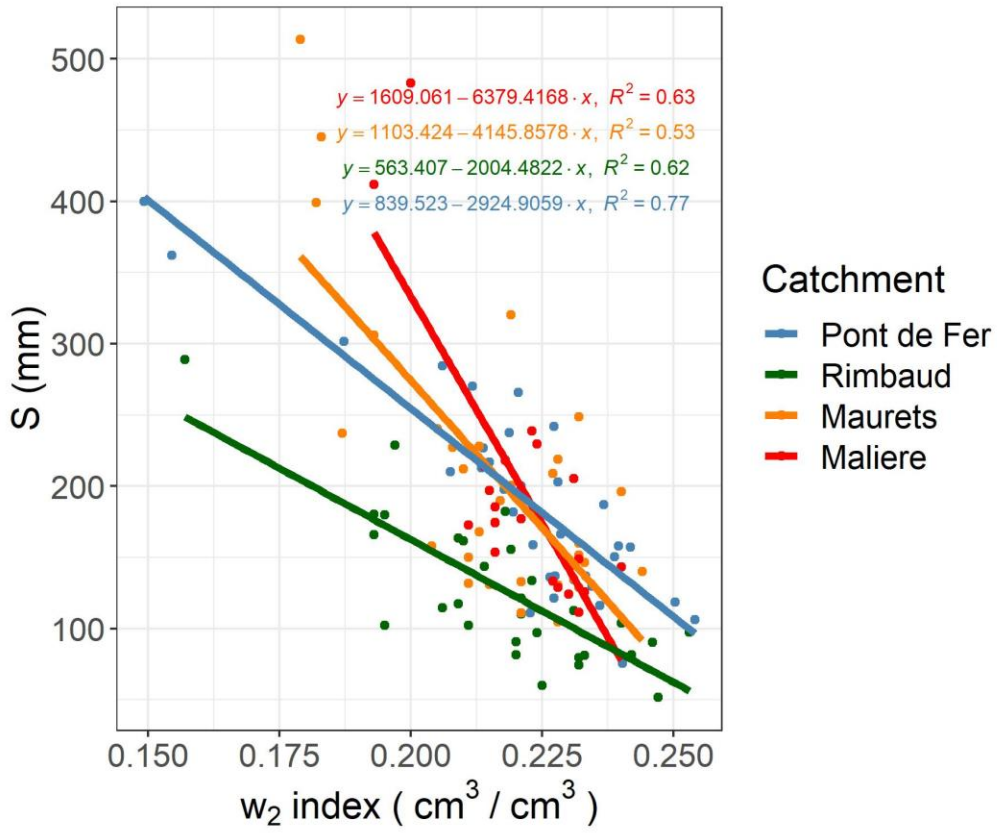

Figure 4.16: The linear relationship between S *parameter and* w_2 *for each of the four selected sub-catchments*

The parameter *S* was firstly related to the w_2 index. Figure 4.16 shows a relatively strong correlation between *S* and w_2 index, as all the correlation coefficients R^2 are more than 0.5. The comparison between the relationships of *S* and w_2 in the catchments divided into two groups with similar slopes, but different intercepts: Pont de Fer and Rimbaud; Maurets and Malière.

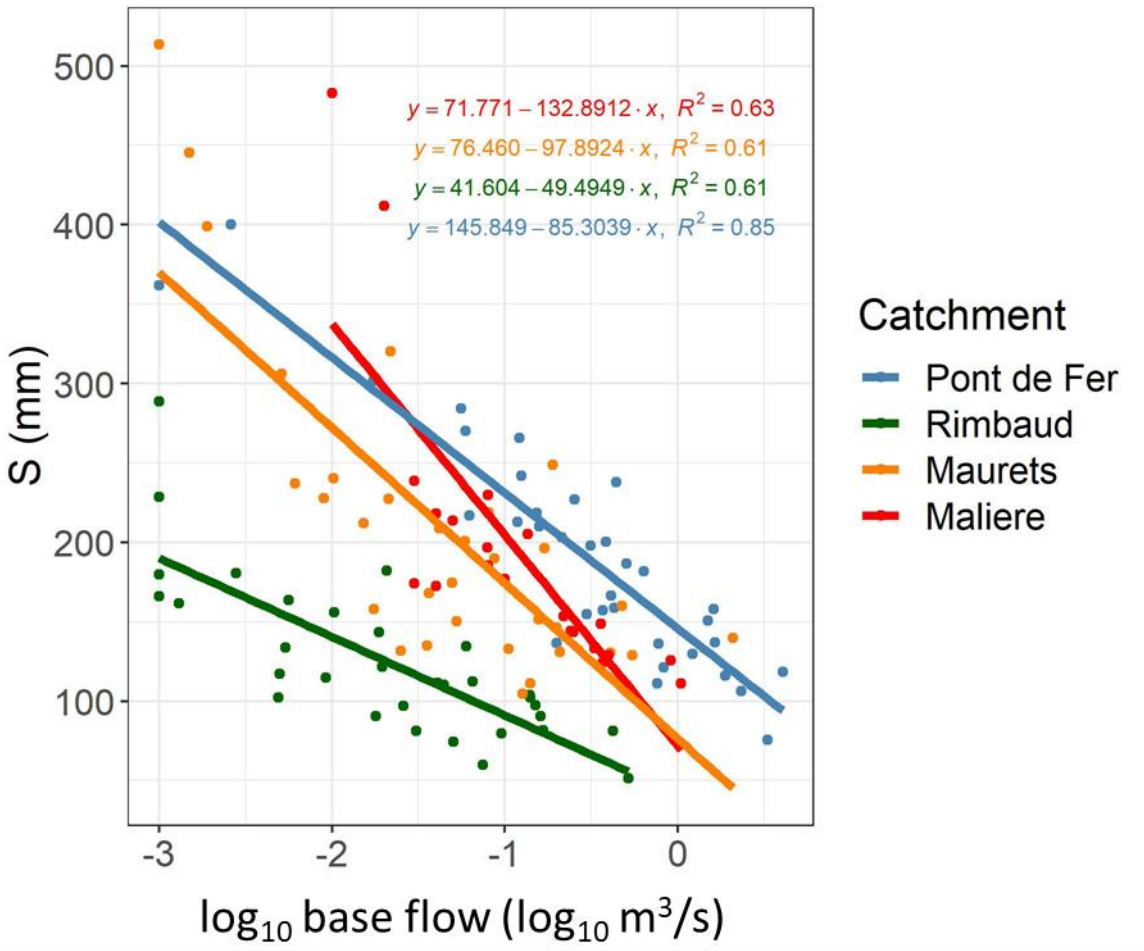

Figure 4.17: The linear relationship between S *parameters and the base flow for each of the four selected sub-catchments*

Maximum water retention *S* was also expected to be correlated with the base flow, as shown for Pont de Fer. In Rimbaud, Malière, and Maurets, the correlation coefficient R^2 between *S* and base flow were less than in Pont de Fer, however, it still implied a relatively strong positive linear correlation (Figure 4.17). The value of R^2 was 0.61 in Rimbaud catchment, 0.61 in Maurets catchment, 0.63 in the Malière catchment. The relationships between *S* and the base flow for all the sub-catchments also divided into two groups: a steeper slope for Pont de Fer and Rimbaud, but different intercept; gentler slopes in Maurets and Malière, and closer intercepts. As the base flow is depended on the area of the catchment, a new predictor was considered: the specific base flow, i.e. the base flow that divides the area of the catchment (Figure 4.18).

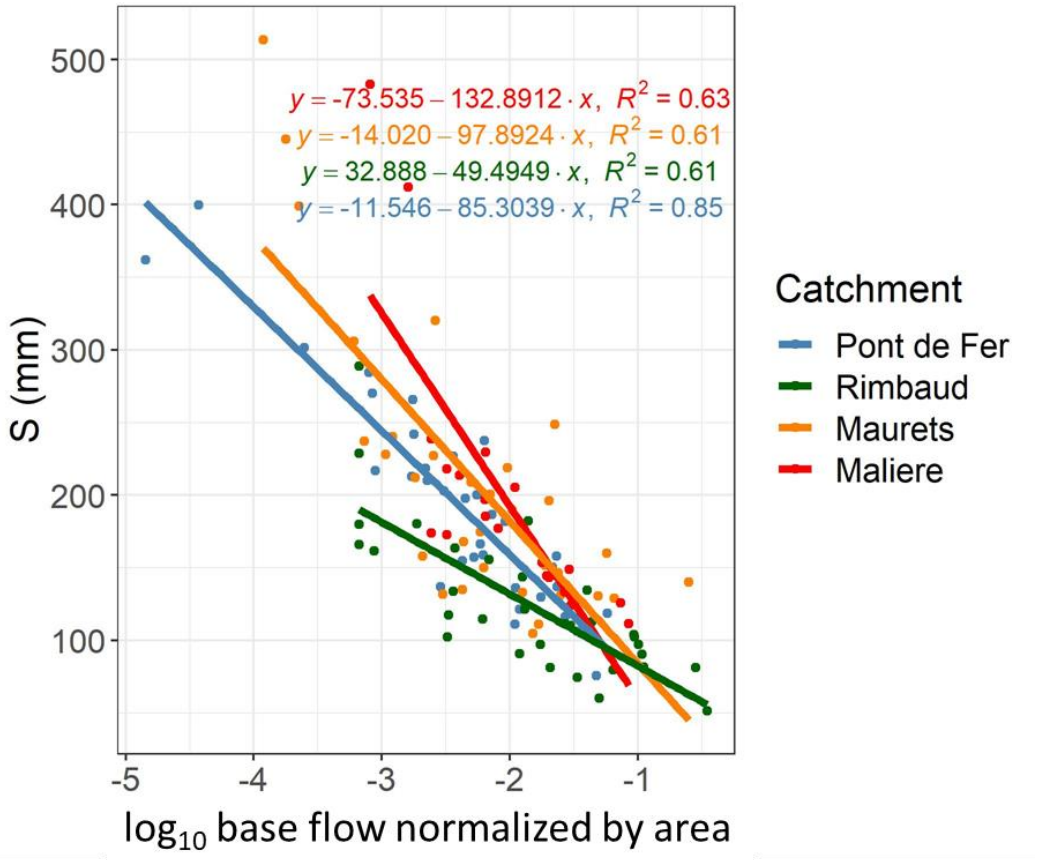

Figure 4.18: The linear relationship between S *parameter (mm) and the base flow normalized by area for each of the four selected sub-catchments.*

This predictor was able to reduce the difference in the intercept so that Rimbaud and Pont de Fer exhibited very near relationships. This should be considered as a positive result, which shows that the same relationship could fit in catchments having very different properties such as areas or runoff coefficients. But the specific base flow failed to explain the difference in the slope among sub-catchments.

4.4. Discussion and conclusion

To summary, the SCS-LR model showed the ability to simulate floods in Rimbaud, Maurets, Malière sub-catchments of the Real Collobrier. Those catchments exhibited similar median runoff coefficients, but previous studies highlighted that hydrological processes could be different not only from a catchment to another but also within a given catchment.

The temporal variability of the *S* parameter was correlated with the base flow and w_2 index, with high values of R^2. It confirms that the event variability of the *S* parameter is mainly explained by the initial soil wetness conditions, whereas rainfall characteristics such as amounts, intensities or durations do not significantly impact the *S* estimations. From this point of view, Real Collobrier catchments are "violent" catchments (Hawkins, 1993). The median predictive NSE from w_2 /baseflow were respectively 0.77 /0.83 in Pont de Fer, 0.65/ 0.5 in Maurets and 0.63/0.65 in Malière; in comparison, the median predictive NSE was higher in Rimbaud, 0.82 /0.83.

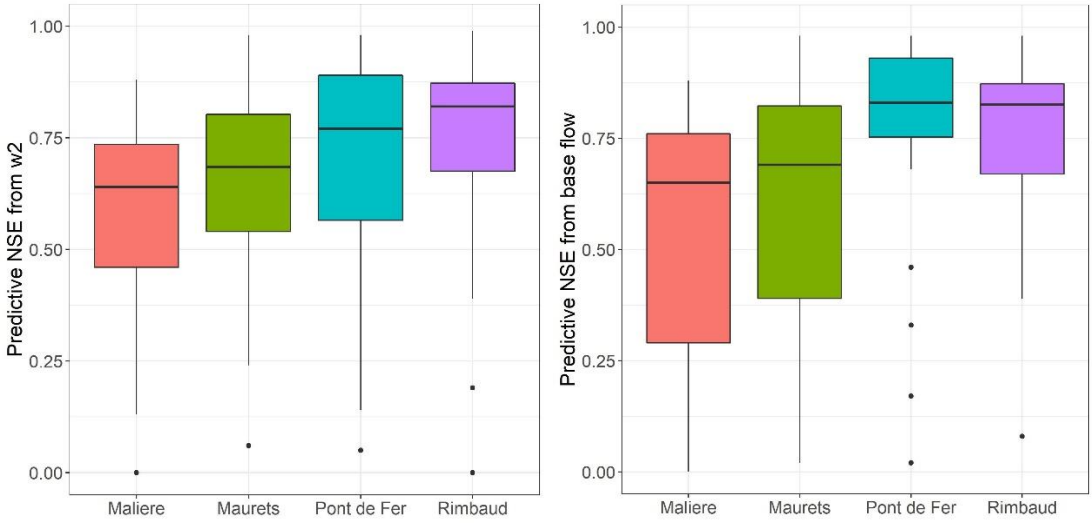

The spatial variability of the K_0 parameter was attributed to an incorrect relationship between the propagation time Tm and the diffusion time Km of the Lag and Route model. Although several other hypotheses could be made about the spatial variability of K_0, we decided to adopt a new relationship, which we will have to be validated *a posteriori* in the next chapter.

The spatial variability of the median *S* parameter was coherent with the spatial variability of the runoff coefficient. The higher the runoff coefficient was, the smaller the *S* parameter. As being the maximum storage capacity, *S* should depend on the soil depths, porosities and water content along with the vertical profile of the soils. As the w_2 index integrated all these data, it was expected that the same relationship between *S* and w_2 could have been convenient for all the catchments. But this was not the case: Pont de Fer and Rimbaud exhibited similar slopes, but different intercepts, as well as Maurets and Malière; but slopes were different in Pont de Fer and Rimbaud on the other hand, in Maurets and Malière on the

other hand; slopes or intercepts, or both of them made that the relationships were different for each catchment. This could be due to the fact that the tiles of the SIM model which supplied the w_2 values were too large for representing the specificities of those small catchments. It could also be due to the fact that the soil properties that SIM used were not really appropriate or accurate enough to represent the actual soil properties. Unfortunately, we could not know what values were used within SIM, and we cannot comment furthermore the convenience of the properties of the soil. We, however, think that improving the knowledge of the soil properties such as soil depths and soil porosities and water content along the vertical profile would greatly help to improve the understanding of the spatial variability of the *S* parameter (Oudin et al., 2010).

The base flow was another predictor expected to integrate all the factors explaining the *S* values so that the relationship between *S* and the base flow could be the same for all the catchments. To avoid scale effects, the base flow had to be turned into the specific base flow. The relationships were close together for Pont de Fer and Rimbaud in the one hand and for Maurets and Malière on the other hand. The possibility to find similar relationships for such different catchments as Rimbaud and Pont de Fer seems to be positive in order to use the specific base flow as an index of not only the spatial variability but also of the spatial variability of the *S* parameter.

Additional hypothesis concerning the failure of finding a unique relationship between *S* and the soil moisture predictors could be that the *S* estimates were biased because the *S* parameter was considered as uniform over the whole catchments. This assumption could hold for a homogeneous headwater catchment like the Rimbaud catchment, but it is not realistic for more heterogeneous catchments such as Maurets, Malière, and Pont de Fer, which contain different geomorphological units. Unfortunately, we did not have time to deepen such hypothesis, but it might be a promising direction for a better understanding of the *S* spatial variability.

Finally, a question arises with the small area of the catchments we considered in this chapter. That's why the next chapter deals with larger Mediterranean catchments.

5. Variability of the parameters in catchment scale

This chapter aims to answer the following questions (i) how do the parameters vary from a catchment to another, for a sample Mediterranean catchments of which areas cover several hundreds of km^2, (ii) is it possible to derive this variability from a few available predictors and to supply a uniform relationship to relate parameters and predictors, at least for Mediterranean catchments that are close together?

The spatial variability in catchment-scale was investigated by considering the results of a set of Mediterranean catchments, including Aille, Ardèche, Allier, Gardon Anduze, Tarnon, Verdouble, and Vidoule. These catchments have been studied in previous works between HSM and SCHAPI, and the data are now available in the ATHYS database "Bassins" http://www.athys-soft.org/bassins. Each catchment was described in the database, as well for the geographic features as for the modeling results when using SCS-LR model. Those data have been processed again to suit the last improvements of the model.

5.1. Presentation of the selected catchments

In the analysis of this chapter, we consider 7 other catchments which locate within the Mediterranean regions. These catchments include Aille (Vibaudan, department Var), Allier (Langogne, department Lozère), Ardèche (Vogüé, department Ardèche), Gardon (Anduze, department Gard), Tarnon (Florac, department Lozère), Verdouble (Tautavel, department Pyrénées-Orientales) and Vidourle (Sommières, department Gard) (Figure 5.1).

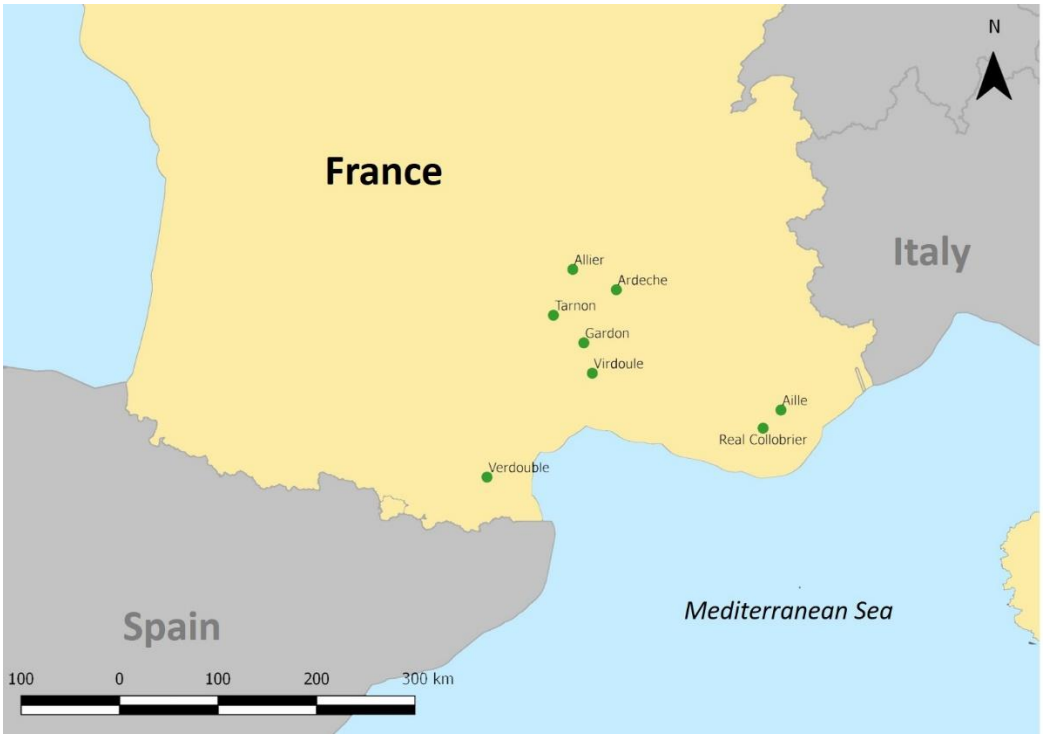

Figure 5.1: Locations of the selected catchments within the Mediterranean region.

All the information about the characteristics of these catchments can be found in detail in the ATHYS database "Bassins". Table 5.1 summarizes the main characteristics of these catchments, including the area of the basins, number of rain gauges and rating curve gauging installed in the catchment, the density of the rain gauges (the area that one rain gauge represents), the elevation, average slope, geology and the component of vegetation presented in the catchment. Each catchment has at least 3 rain gauges. One rain gauge is in charge of representing an area from 37 to 108 km^2. Plus 4 sub-catchments of the Real Collobrier, a total of 11 catchments are analyzed in this section.

Table 5.1: Characteristics of the 7 selected catchments. # rain gauges: the number of rain gauges installed in the catchment; # rating curve gauging: the number of rating curve gauging installed in the catchment

Catchment	Area (km^2)	# rain gauges	Rain gauge density	Elevation (m)		Average slope	# rating curve gauging	Geology	Vegetation
				Range	Average				
Aille	228	5	46	43-731	200	8.47°	48	Sedimentary rocks (68%) (Permian sandstone, dolomites and the sands of the Holocene)	Forest (63%); agriculture uses (29%), artificial purpose, including urban area (5%**)**.
Allier	324	3	108	900 - 1482	1174	8.1°	-	The magmatic, volcanic and metamorphic rocks	Mostly forest and semi-natural zone (82%). 15% used for agriculture purpose
Ardèche	629	7	90	140 – 1535	711	18.7°	2	Northern part: plutonic and magmatic rocks. Central and western part: metamorphic rocks (gneiss and mica schists). Southern part: Jurassic limestone	Mainly covered by forests (70%); vineyards, orchards and some urban areas (5%)
Gardon	544	6	91	124-1202	528	20.3°	7	Mainly metamorphic rocks (shale, gneiss and mica schist); granite (25%) and Jurassic limestone (25%)	Forests and heaths (80%); vineyards and orchards
Tarnon	256	7	37	554 - 1560	954	19°	226	Schists (two-thirds of the area), granite (central and western part), limestone. (Eastern part)	Dominated by coniferous forests and deciduous forests (80%); agriculture activity (5%)
Verdouble	299	6	50	107 - 959	407	14.4°	24	Mostly calcareous soils (Early, Late Cretaceous and Jurassic), early Triassic marl-limestone soil, Devonian, Ordovician, and Late Visean clay and shale soils	Mediterranean scrubland (70%), agricultural activity, (viticulture - 10%), some forests and meadows
Vidourle	600	6	100	20 - 975	135.5	4.9°	7	The Western and North-Western part: Cretaceous marl-limestone and Jurassic limestone. The plain of Bénovie: marly and clay	Agricultural zone, gardens, arboriculture, vineyards; scrubland (the Northern part); riparian forest system along the river.

5.2. Variabilities of the hydrological indexes for all the catchments

Figure 5.2 described the great variability of runoff coefficients across 11 catchments in the Mediterranean region. Among those catchments, Rimbaud and Allier were the catchments with the highest median runoff coefficient, while Pont de Fer, Tarnon and Ardèche were the catchments with lowest median runoff coefficient among all catchments. Especially, there was one event which had the runoff coefficient higher than 100% in Ardèche catchment. This phenomenon was caused by the way of separation of this event and the previous event.

The peak flow strongly depended on the area of the catchments. Figure 5.3 thus reported the variability of specific peak flow, which was calculated as the peak flow divided by area. Indeed, we could see in the figure that catchments with large area (such as Gardon, Ardèche, Verdouble) usually had high values of peak flow. Meanwhile, catchments with small area, such as that of Real Collobrier often had much lower peak flow. The highest median specific peak flow was in Rimbaud, while Allier had the lowest median specific peak flow.

Figure 5.4 indicated the variability of average rainfall across 11 catchments. Similar to the other two parameters, the results showed strong variability of average rainfall. Among all catchments, Gardon was the catchment with the highest median of average rainfall across all flood events, while Vidourle and Aille were the two catchments with the lowest median average rainfall among all catchments.

The complete information about the events and the correlation among indexes can be found in Section C of the Appendix. Besides the great variability across all catchments, the results also showed the variability of these three indexes across all the flood events in each catchment.

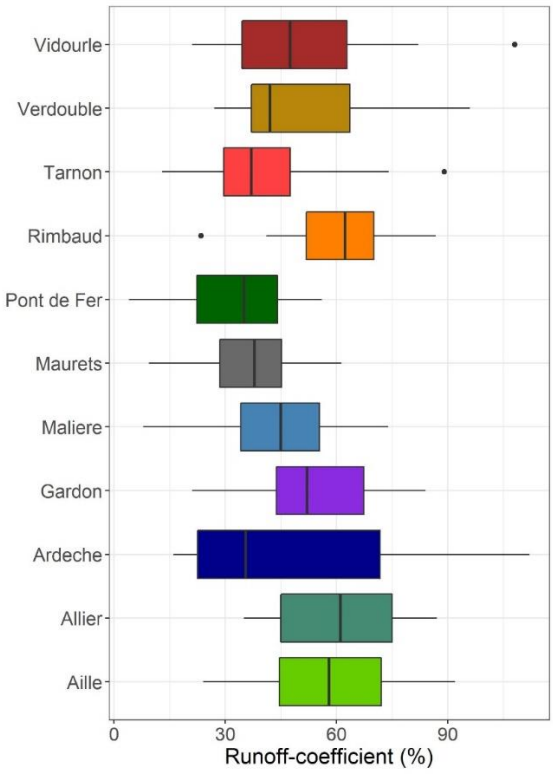

Figure 5.2: The variability of runoff coefficients across 11 catchments

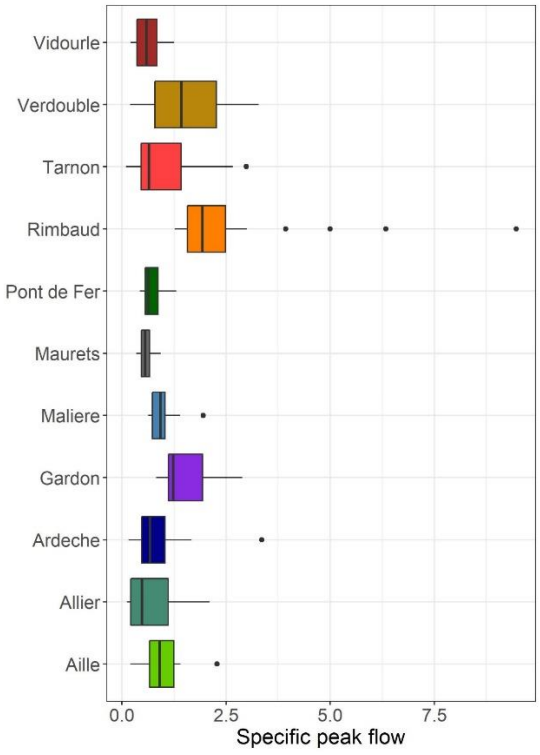

Figure 5.3 : The variability of specific peak flow across 11 catchments

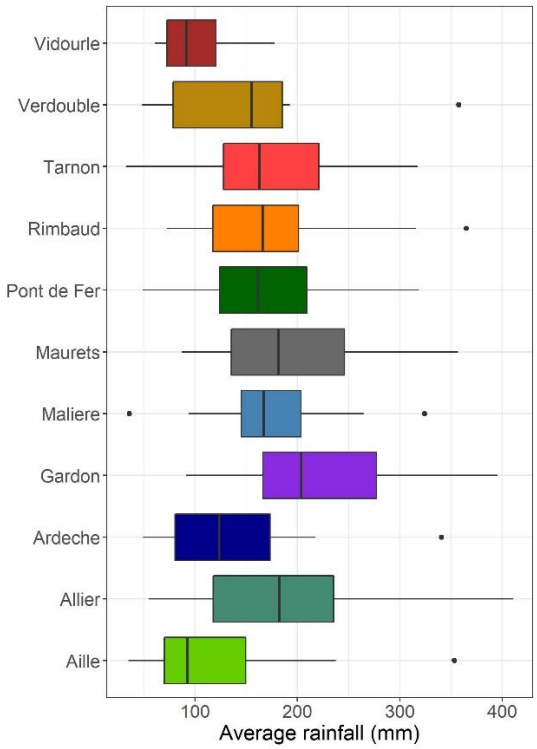

Figure 5.4: The variability of average rainfall across 11 catchments

5.3. Calibration of the model on Mediterranean catchments

The *ds* value was calculated for each catchment as the median value of the recession coefficient, for each event. The *ds* parameter varied between 0.3 and 0.5 d^{-1} for all the catchments Table 5.2. This variability is known to have a small impact on the flood simulation, as shown by the sensitivity tests performed in Chapter 3.

The ω' value was first calibrated at the event scale, at the same time that S and V_0, and then was set to its median value, as it was done in Chapter 4. Doing so, ω' ranged from 10 mm in the Aille catchment to 200 mm in the Allier catchment. This variability was related to the variability of the S parameter.

For the 11 Mediterranean catchments of our sample, the V_0 parameter was not considered as uniform because the landscapes and the slopes could vary a lot, from flat areas in the plains to steep hillslopes in the Cevennes Mountains. To avoid equifinality in estimating the LR model parameters, the K_0 parameter was set to a constant value. A first attempt consisted of using the LR model with Equation 17, by setting $K_0 = 2$, as it was done in the first studies of those catchments in BD ATHYS.

The optimization was then run with the calibration of the two parameters S and V_0 while K_0 was set as 2. Figure 5.5 shows that in this case, V_0 was mainly related to the area of the catchment (R^2=0.78), which seems to confirm that the scale effect influenced the transfer function's parameters.

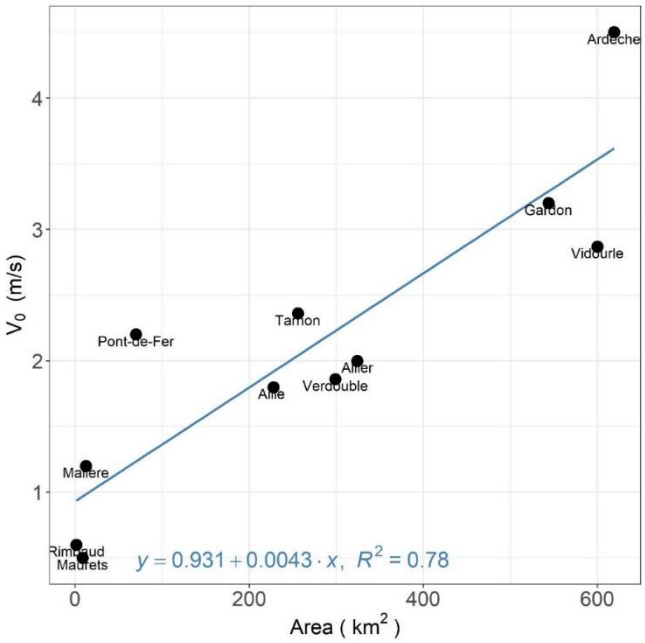

Figure 5.5: Correlation between the median V_0 and the area of all selected catchments with K_0 = 2

Thus, to avoid this scale effect, we changed the relationship $K_m = K_0.T_m$ into $K_m = K_0.{T_m}^{\alpha}$, with α =0.33 as we did in Real Collobrier catchments. The calibration was finally made with 2 parameters S and V_0 while K_0 was set as 60, for all the events of each catchment (Table 5.2).

Table 5.2: The parameters of the calibrated SCS-LR model for each of the selected catchments

Catchment	No of events	S		ω'	V_0	ds	K_0	Median NSE
		Range	Median					
Aille	28	9-164	41	10	2	0.4	60	0.92
Allier	11	193-542	332	200	2.2	0.4	60	0.90
Ardèche	18	120-508	193	160	4.5	0.3	60	0.90
Gardon	19	92-391	210	110	3.6	0.3	60	0.84
Tarnon	22	57-431	136	36	2.9	0.5	60	0.91
Verdouble	11	11-319	87	21	2	0.5	60	0.88

Vidourle	11	0-144	83	60	2.5	0.4	60	0.91
Pont de Fer	34	93-384	165	60	2.5	0.4	60	0.96
Rimbaud	32	52-289	112	70	2.5	0.4	60	0.88
Maurets	32	105-513	182	35	2.5	0.4	60	0.91
Malière	21	111-483	174	90	0.7	0.4	60	0.82

As we can see, the calibration gave positive simulations for these catchments with very high values of NSE (>0.84). However, the values of the set of parameters were not the same for all the catchments and had to be analyzed from a spatial point of view.

5.4. Spatial variability of the parameters

5.4.1. V_0 parameter

In most of the cases, the value of V_0 ranged from 2-2.5 except Maurets, Gardon, Ardèche, and Tarnon. The scale dependency of V_0 was decreased with the use of new formulation with K_0 equal to 60 (Figure 5.6).

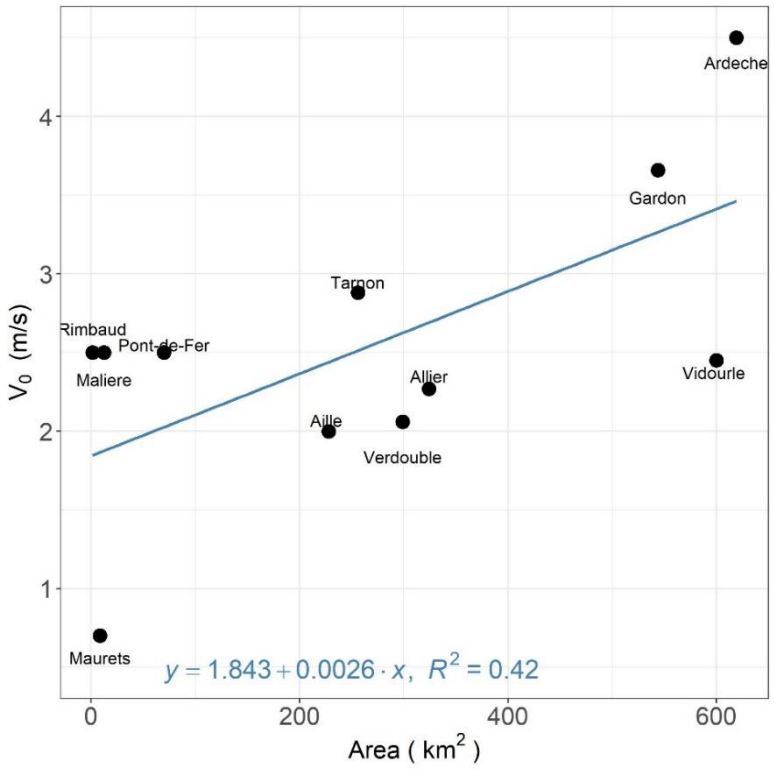

Figure 5.6: Correlation between the median V_0 and the area of all selected catchments with K_0 = 60

As the V_0 parameter denotes the maximal velocity on a cross-section, the spatial variability of this parameter was expected to be depended on the catchment characteristics. We can see in Figure 5.7, the catchment which had a high value of V_0 accompanied by a high value of the average slope. Without the case of Maurets, where the difference of transfer function parameter was explained as the role of subsurface flow, we can see the relationship between V_0 and the average slope of each catchment with a moderate correlation. However, the main issue of variability of the model is about the maximum water retention S parameter.

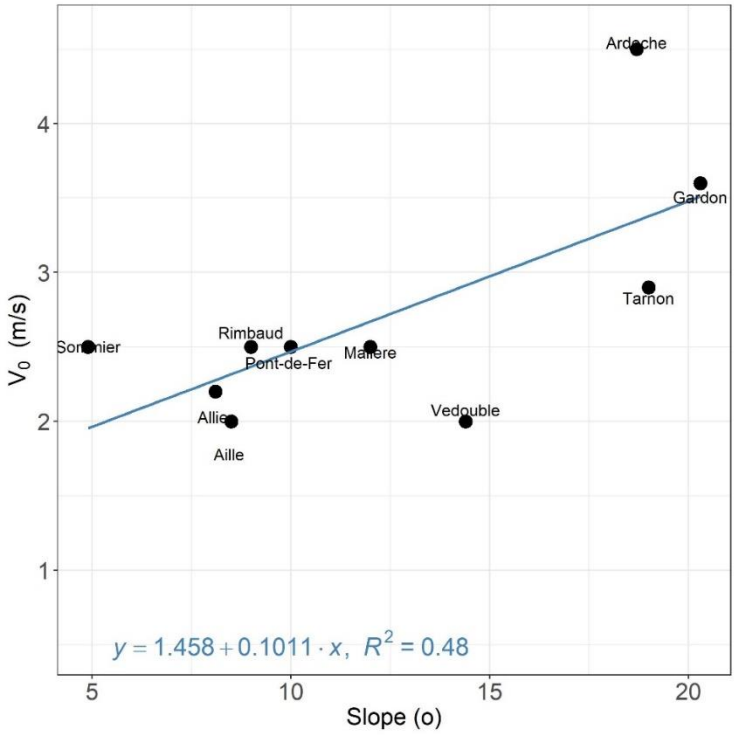

Figure 5.7 : Correlation between the median V_0 and the average slope of all selected catchments with K_0 = 60

5.4.2. S parameter

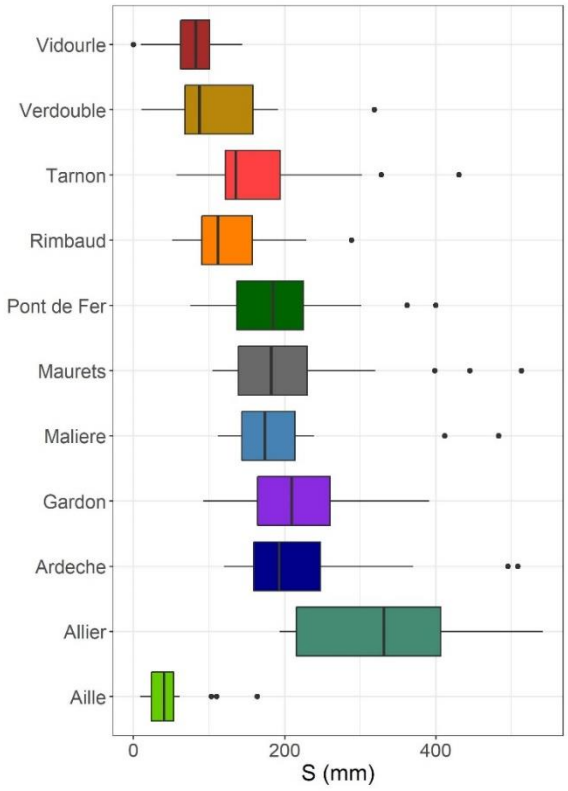

Figure 5.8: The variability of the S *parameter across 11 catchments*

The calibration of *S* the parameter showed that in general, the *S* median value varied between catchments (Figure 5.8). The highest value of *S* belonged to Allier, while the catchment Aille had the lowest *S* value. One of the reason for the high value of *S* parameter in Allier catchment could be due to the soil in this basin is highly permeable, thus it can absorb a high proportion of precipitation and supply deep aquifers. The Aille catchment is the specific catchment, which has different geology than the others: such Permian sandstones are known to generate red impervious soils like in the Lodeve and Salagou area, in the Herault department (Brunet and Bouvier, 2017). But other reasons could be considered: first, it is known that the *S* parameter sometimes depends on the rainfall amounts (Bouvier et al., 2018; Hawkins, 1993). In the Aille catchment, as we showed before, the median rainfall was lower than in the other catchments. So we looked for a possible relationship with the rainfall amount, by considering the *S* calibrated values and the cumulated mean areal rainfall for each event in the Aille catchment and the other catchments (Figure 5.9). The regression coefficient R^2 were small (< 0.25 for 9 out of the

11 catchments), and did not confirm such relationship between *S* and that rainfall amount. It also confirmed that Mediterranean catchments are "violent" catchments.

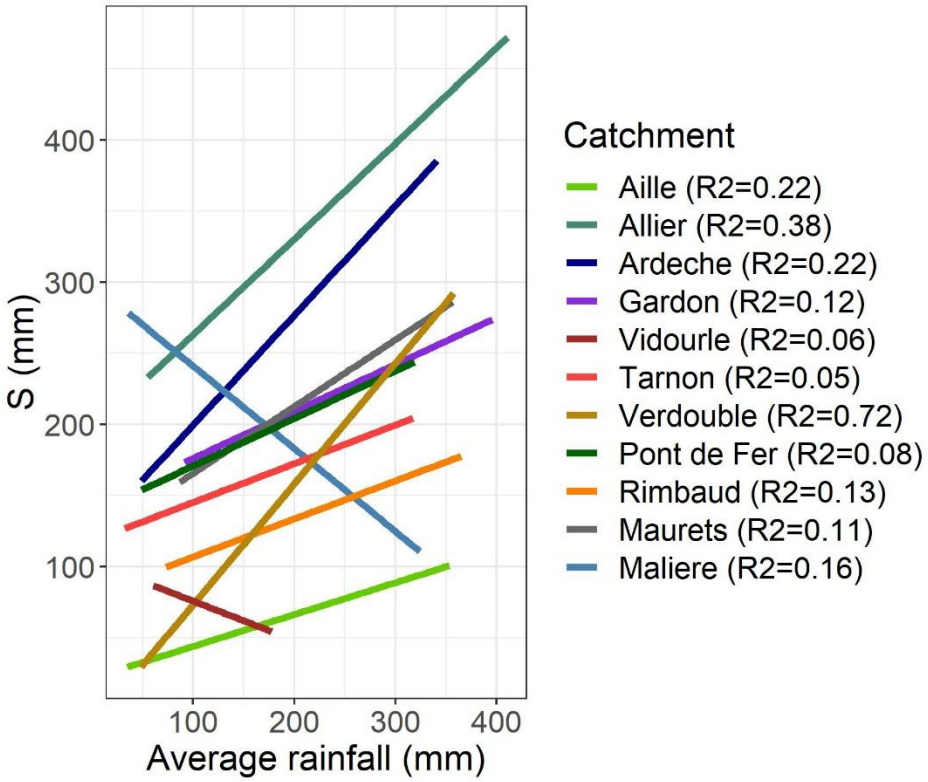

Figure 5.9: Correlation between average rainfall and S *calibrated for all events of each of the selected catchments.*

Then, we compared the median *S* value and the median runoff coefficient for all the catchment (Figure 5.10). There was not any correlation between these two values. This could be explained by the fact that the runoff coefficient can be due to both the fast and slow responses of the catchment, while *S* expresses only the fast response of the catchment. For example, Allier and Aille catchment have similar high runoff coefficient, but for different reasons : soils in Allier were supposed to have a high water storage capacity, but also a high capacity to release runoff in form of delayed runoff, whereas soils in Aille did probably store much water due to their imperviousness, and consequently could not release much water. So one more time, it emphasized the role of subsurface flow contribution in the runoff process. Thus, we concluded that *S* interpretation must account for the kind of runoff generation in the catchment.

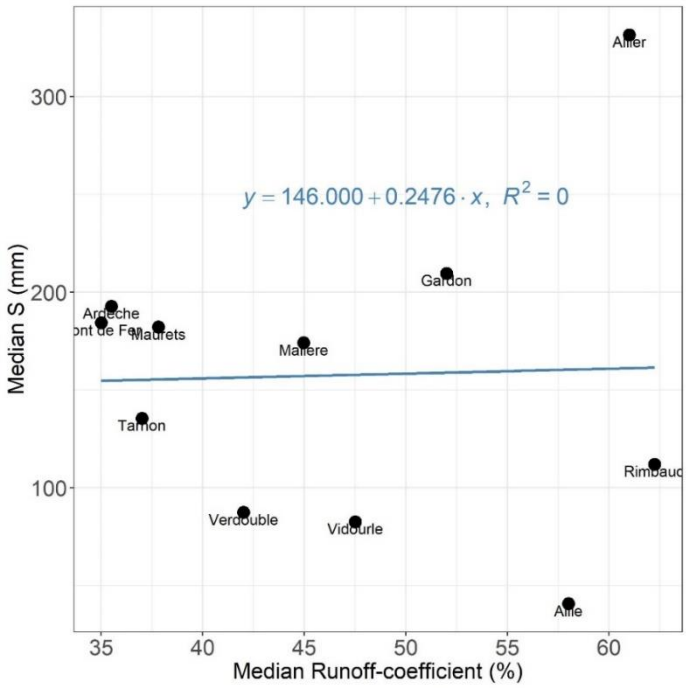

Figure 5.10: The correlation between median runoff-coefficient and median S of all catchments

5.5. Temporal variability of the parameters in catchments scale

Besides the concerns about the quantity of S parameter, we were also interested in considering the relationship between S and external indexes of the catchments. We would like to investigate whether we can have a regional scheme for Mediterranean catchments. Thus we compared the relationships between the S values and the soil moisture predictors in all the catchments.

One problem arose with the w_2 predictor, which was used in Real Collobrier catchments but was not available in our database of the other Mediterranean catchments. Those catchments had used the Hu2 predictor, which is another output index of the Meteo France SIM model, calculated as Equation 19. The Hu2 is the index in the second layer as the same as w_2. This index is available for all the catchments except Real Collobrier, where we only had data for a few years. Thus, we tried to compare these two indexes. Hu2 could be derived from w_2 when knowing θs.

Hu2 and w_2 were thus compared during the year 2001 when both predictors were available (Figure 5.11),

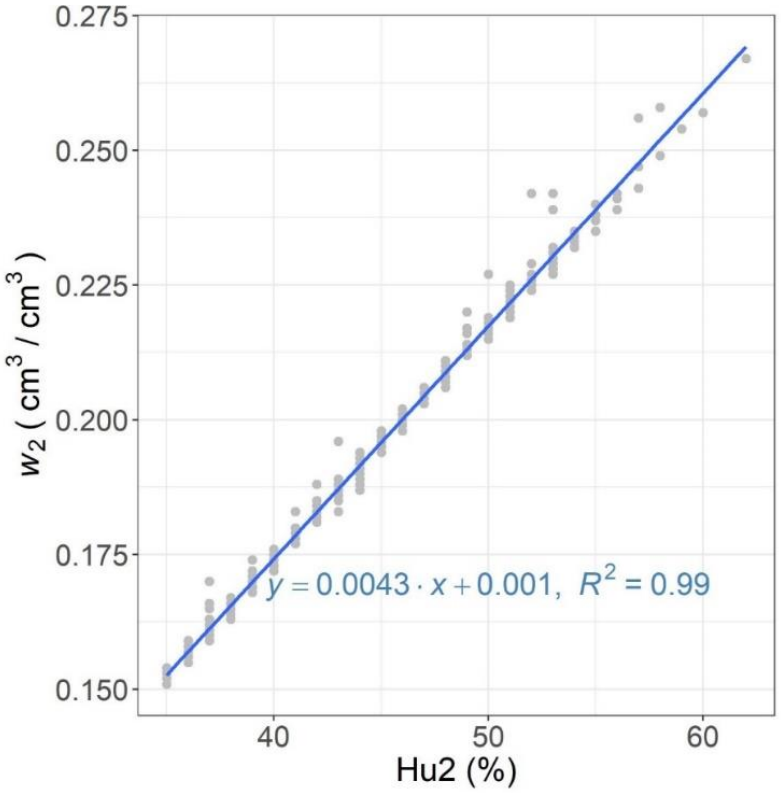

Figure 5.11: Comparison of Hu2 and w_2 index in the year of 2001 for Real Collobrier.

The correlation coefficient (R^2=0.99) claimed that Hu2 and w_2 could be considered as equivalent. Therefore, we derived Hu2 of Real Collobrier from the w_2 index for all the events. In this case, the θs water content at saturation in Real Collobrier should be 0.43, which is coherent within the range reported by Taha et al., 1997.

5.5.1. S and Hu2 correlation for all catchments

We next investigated the correlation between the median *S* and the median Hu2 (Figure 5.12). The result showed that we did not find a strong correlation for all Mediterranean cases. However, for most of the cases, we normally had a high *S* accompanied by the low Hu2 index.

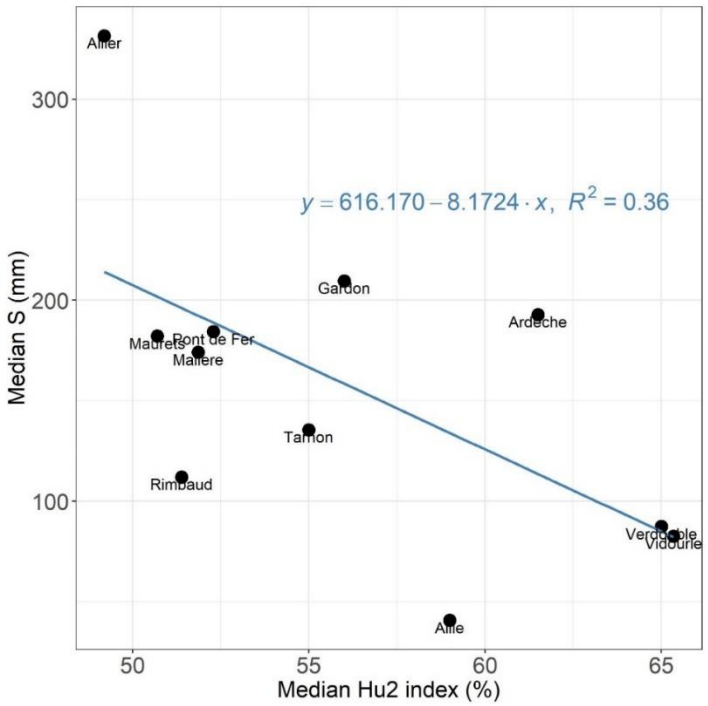

Figure 5.12: The correlation between median Hu2 index and median S *of all catchments*

The regression between *S* and Hu2 index of all events for each catchment was also integrated in Figure 5.13, and the corresponding sets of values for intercept, slope and correlation coefficient were reported in Table 5.3. The calibrated *S* parameter in selected catchments was found to be correlated with Hu2 index. For a piece of evidence, 9/11 had the correlation coefficient R^2 higher than 0.5. We can also see the divergence of both slope and intercept for all the catchments. The regression seems to be divided into 2 groups as we found in the case of Real Collobrier sub-catchments:

Allier, Maurets, and Malière had similar slopes which were gentler compare with the others. The intercepts of these catchments were also not so far together.

The other group with the rest of the catchments which had similar slopes. However, their intercepts varied a lot with the minimum was Aille and the maximum belonged to Ardèche.

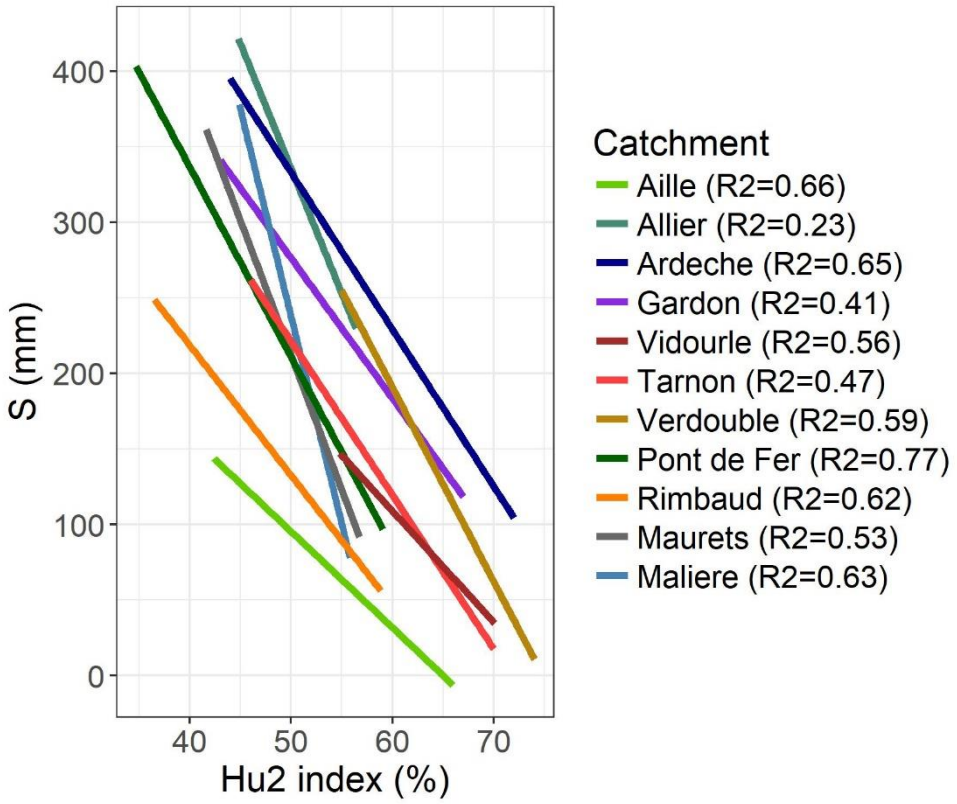

Figure 5.13: The correlation between Hu2 index and S *calibrated of all events for each of the selected catchments.*

Table 5.3: The values of slopes, intercepts and correlation coefficients of the linear regression between S *and Hu2 index and between* S *and base flow for each of the selected catchments*

Catchment	S-Hu2			S-base flow (log)		
	Intercept	Slope	R^2	Intercept	Slope	R^2
Aille	413.34	-6.36	0.66	36.90	-18.20	0.48
Allier	1162.63	-16.54	0.23	508.73	-210.13	0.43
Ardèche	852.01	-10.38	0.65	376.16	-94.79	0.21
Gardon	740.70	-9.29	0.41	345.12	-99.40	0.27
Vidourle	550.56	-7.36	0.56	72.22	4.21	0.00
Tarnon	730.04	-10.18	0.47	150.76	-42.80	0.48
Verdouble	961.83	-12.85	0.59	104.70	-33.33	0.32
Pont de Fer	814.83	-12.39	0.79	131.74	-83.52	0.86
Rimbaud	574.81	-8.74	0.48	41.60	-49.49	0.61
Maurets	1103.42	-17.83	0.53	76.46	-97.89	0.61
Malière	1609.06	-27.43	0.63	71.77	-132.89	0.63

The following reasons can explain the variability of S-Hu2 relationships:

- First, the soil properties which are used within the SIM model derive from synthetic information or relationships that could not retrieve the actual properties of the soils: the hydraulic properties of the soils indeed derive from the percentages of sand and clay, supplied by the FAO map soil; the soil depths depend on the land use and vegetation of Corine Land Cover. Thus, the Hu_2 values could be biased and/or unable to account for the actual spatial variability of the water content.
- Second, the divergence could be due to the rain gauge uncertainty which can affect the *S* parameter (see chapter 3). In most of the catchments, the rain gauge density was low, 1 rain gauge per more than 90 km^2. This was equivalent conditions to those of the Real Collobrier in Pont de Fer when using 1 single rain gauge. It was shown how was able to vary the intercepts, and at a lesser point, the slopes (see Figure 3.28 and Figure 3.29 in Chapter 3). The interesting point is that we had again similar slopes for most of the catchments, but different intercepts.
- Third, the rating curves could be affected by errors in the determination of the high water-levels discharges. In most of the cases indeed, few gauging has been performed and the rating curves must be largely extrapolated. For example, in the cases of Gardon and Vidourle, the calibration curve was established with only 7 gaugings and for Ardèche with 2 gaugings. The highest gauged discharge value was often much lower than the highest observed discharge so that uncertainty could happen in the extrapolation of the rating curve to high flows and affected the model parameters.
- Fourth, the calibration protocol could also be responsible for bias in the estimation of S: for the calibration of all events in each catchment, we used a constant value for almost the parameters excepts *S* and V_0. Although in general, the effects of using median value of these parameters are unremarkable (as we can see in the sensitivity test), it can really affect the estimating of the calibrated parameters in some case. For example, using of initial abstraction Ia/S = 0.2 for all the catchments may be not convenient because, in many previous studies, it was claimed that each catchment have different behavior and the recommendation was to use a specific value for each catchment (Mishra and Singh, 2003).

However, the trend of the high value of *S* accompanied by the low value of Hu2 (in drier condition) can be concluded for the Mediterranean catchments. We can conclude that Hu2 is locally a suitable predictor for the capability of S, but not to create the regional scheme for all Mediterranean catchments.

5.5.2. S and base flow correlation for all catchments

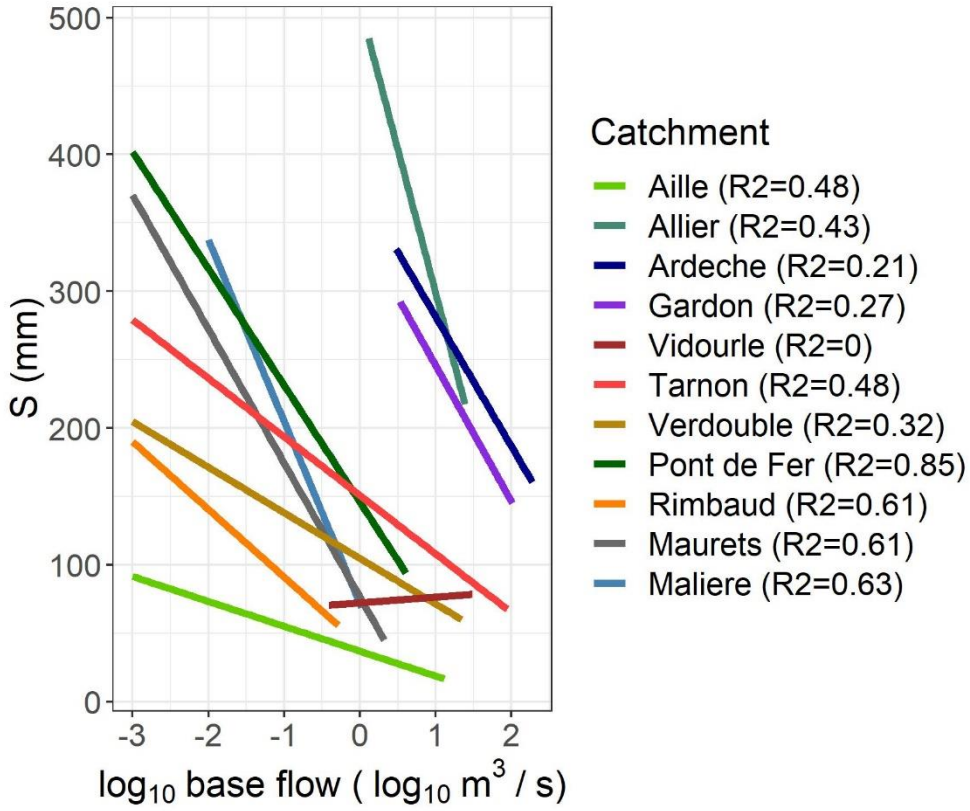

Figure 5.14: The correlation between base flow and S calibrated of all events for each of the selected catchments.

The base flow could be considered as another index to explain the event variability of the *S* parameter. However, we did not have a strong relationship for most of the catchments (Figure 5.14). The worst score was obtained for the Vidourle catchment. The best scores were obtained for the Real Collobrier catchments (0.61 to 0.86), whereas the other Mediterranean catchments had R^2 less than 0.5.

Moreover, the relationships were very different from catchment to another. Regional classification of the relationships would be based on 2 groups of catchments which are geographical neighborhood (except Verdouble which are far from others): the first group contained Allier, Tarnon, Ardèche, and Gardon; Aille and all Real Collobrier belonged to

the second group. For the first group, in spite of the neighbor of location and geographical features, the regressions were only similar in Ardèche and Gardon. The second group was also not stable in all cases.

Other attempts were made for using normalized base flow, reducing the value by the area of the catchment or the mean base flow value. When using the specific base flow (base flow normalized by catchment area -Figure 5.16), or normalizing the base flow with its average base flow value (Figure 5.15), the regressions were closer together than when had not normalized especially for the case of Ardèche and Gardon, but it still failed to create the region scheme for Mediterranean catchments.

Several reasons can be found to explain the scatter of the relationships:

- First, as for the S-Hu2 relationships, the density of rain gauges could originate bias in the estimation of the *S* parameter.
- Second, the base flow as a low flow is subject to many uncertainties due to the erosion or sediment accumulation in the gauging section. In most cases, the number of gauging is not sufficient to characterize such changes.
- Third, it seems that the base flow could be a fair index for relating the *S* parameter at the event scale in a given catchment but could not be significant from a spatial point of view. A higher base flow leads indeed to a lower *S* parameter values at the event scale, but a higher median base flow could suggest that the catchment is prone to dominant subsurface flows, which does not guarantee a low median value of the *S* parameter (rather the opposite). Thus, it is not surprising that normalizing the base flow with the area or with the median value does not improve the scatter of the relationships between *S* and the base flow.
- The bias could also come from the rainfall uncertainty, which made the weak correlation between base flow and *the S* parameter. We need further research on integrating catchments' characteristics on this index.

Finally, the conclusion is that it was not easy to regionalize the parameter with either internal or external indexes of the catchments. The difficulties were that the uncertainty could affect the model, as well as the indexes, could not integrate the information of the important characteristic of the catchments (especially the soil properties).

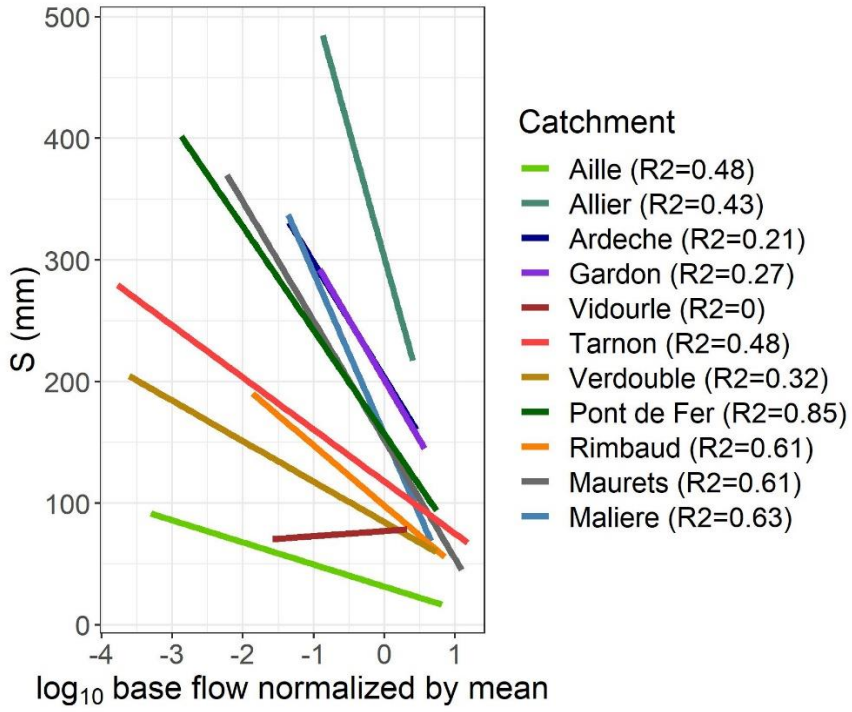

Figure 5.15: The correlation between base flow normalized by average value and S *calibrated of all events for each of the selected catchments.*

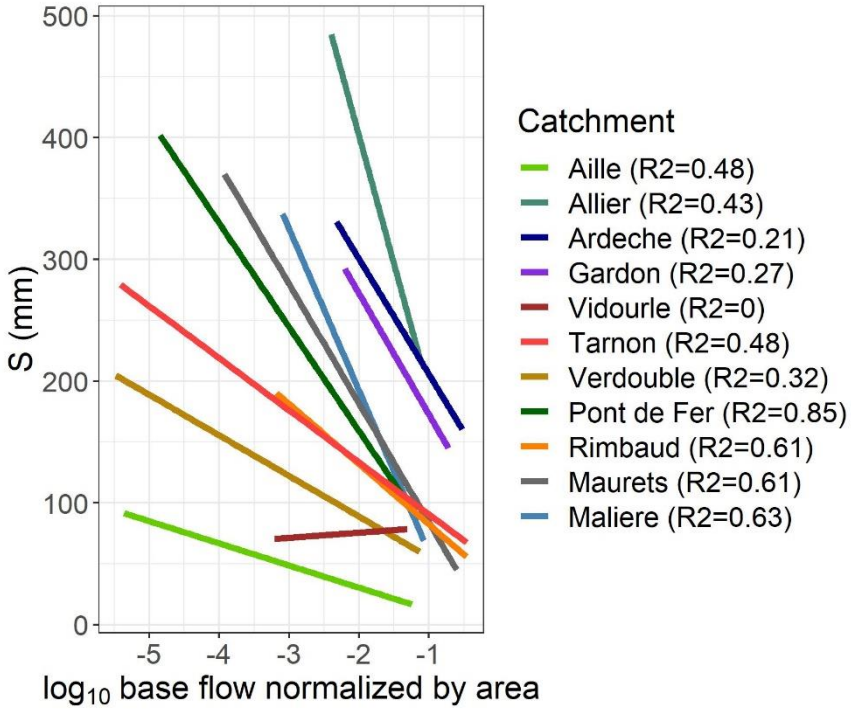

Figure 5.16: The correlation between base flow normalized by the catchment area and S *calibrated of all events for each of the selected catchments.*

5.6. The predictive score of the model

The relationship between Hu2/baseflow and *S* were then used to calculate the predictive score of the model. We used the regression to predicted the parameter, by that calculated the NSE value for each event in each catchment. The values of NSE from Hu2 and baseflow was reported in Figure 5.17 and Figure 5.18. For the predicted NSE from base flow, the median NSE of all events was lowest in Maurets (0.5) and highest in Pont de Fer. In the other case with predicted NSE from Hu2, the median NSE of all events range from 0.63 (in the cases of Ardèche and Malière) to 0.82 (Rimbaud). The case of Vidourle when we had the R^2=0 with the relationship between *S* and baseflow, the predictive NSE value still quite high (0.8). The reason could be due to that because the regression of the S and baseflow have a flat slope, thus, the predicted S was not so far from the calibrated S even the correlation are low. Indeed, the value of calibrated S in Vidourle mainly ranged from 60 mm to 100 mm with the median as 80 mm while predicted S from baseflow ranged from 70 mm to 80 mm with the median as 78mm. Thus, we maybe need more than the using of median predicted NSE to really express the accuracy of the model.

Besides, in general, the predicted NSE from Hu2 had higher values compared with the predicted NSE from baseflow. We also noted that in the case of Ardèche and Allier where had the lowest density of rain gauge, the predicted NSE is generally lower than the others.

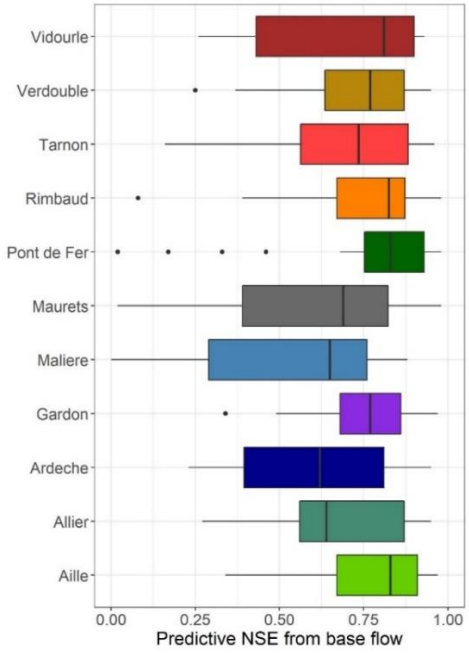

Figure 5.17: The variability of the predictive NSE derived from base flow across 11 catchments

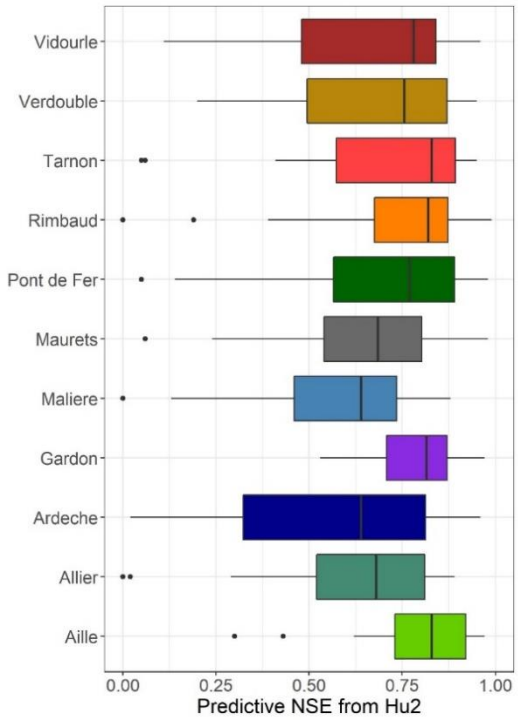

Figure 5.18: The variability of the predictive NSE derived from Hu2 index across 11 catchments

5.7. Conclusion

To summary, the results of this chapter show that the SCS-LR model can simulate the floods in Mediterranean catchments with high efficiency. The variability of the transfer function parameters V_0 in the catchment scale depended on the different characteristics of each catchment. The variability of *the S* parameter was not found to be related to the runoff coefficient of rainfall amount. It could due to the kind of runoff generation in the catchment.

It was not possible to derive the variability of the model parameters from the Hu2/base flow index. Hu2 finally performs better than base flow from a spatial point of view. A uniform relationship between parameters and Hu2/base flow was not possible to obtain for Mediterranean catchment. However, the calibrated *S* parameter in two catchments Allier and Ardèche which are geographical neighbor had a very close regression with the base flow. The case of Aille catchment could be considered as an example for the difficulties of the regionalization of Mediterranean catchments when this case has different behavior with the others but it was not expressed in any hydrological index of the catchment (runoff coefficient, base flow, Hu2).

6. Conclusions and Perspectives

6.1. Summary

In this study, we show the interest in using a parsimonious distributed event-based model in forecasting the Mediterranean floods. The model is under the ATHYS platform and the results contribute to the work of floods forecasting in the HSM-IRD co-ordination. The model is first applied to a very well-documented Mediterranean catchment (Real Collobier) and then enlarge to other catchments. Thanks to the previous work of collecting data in Real Collobrier catchment, we can also measure the rain-gauge uncertainty. Then, the variabilities of the model's parameters are explained by applying the model in Real Collobrier sub-catchments and further Mediterranean catchments. These findings hopefully can contribute to the concept of regionalization for Mediterranean catchments.

6.2. Main results

The present work has allowed a detailed analysis of the Real Collobrier catchment characteristics and hydrological data. The Real Collobrier catchment is highly heterogeneous and gives very different characteristics of floods in these sub-catchments. The high rainfall variabilities across this catchment are highlighted throughout the manuscript. The other Mediterranean catchments hydrological characteristics are also described generally.

To answer the questions that listed in the objective part in Chapter 1, we give here the main conclusions and results, firstly, for Real Collobrier catchment:

1) The improvement of SCS-LR model by integrating Michel's formulation was convenient to use to simulate flash flood.
2) The results of our study proved that adjusted SCS-LR model could simulate Mediterranean flash flood with high accuracy. The model requires a small number of parameters, and it can be set up with accessible data. The calibration of the model based on the rainfall and runoff data corresponding Real Collobrier and other

Mediterranean catchments gave the positive results with high values of NSE as well as high values of R^2 for the correlation between S and the initial condition in most of the cases.

3) Moreover, the dense rainfall data in Real Collobrier gave us the possibility to test the effect of the rain gauge density on the results of the simulation. The results proved that the reduction of the density of the rain gauges affected both the regression with the initial condition and the calibrated parameters of the model. The decrease in the number of rain gauge led to the change of model's parameters and the decrease of correlation coefficient R^2. This result leads to the conclusion that the comparison of the parameters from a catchment to another can be affected by the rain gauge density.
4) The result of the rain gauge density also proved that calibration uncertainty could affect the regression of S parameter and initial condition more than the rainfall uncertainty with the error of special event calibration. However, when using only one gauge in Real Collobrier catchment, we had a large variety of S parameter.

Furthermore, when we applied the model to Real Collobrier sub-catchments and further other Mediterranean catchments (Aille, Allier, Ardèche, Gardon, Tarnon, Verdouble, and Vidourle):

5) The spatial variability of the transfer model's parameter can be due to the scale effect. The solution is to reduce by the relationship between the propagation time T_m and the diffusion time K_m of the Lag and Route model. Besides, it can also be affected by the catchment's characteristic of e.g. the slope of the catchment.
6) The spatial variability of the production model's S parameter in Real Collobrier sub-catchments was concluded to coherent with the spatial variability of the runoff coefficient. Further with other Mediterranean catchments, we generally had a high S accompanied by low SIM output index. We also found that Mediterranean catchments are "violent" catchments according to (Hawkins, 1993) point of view and the S interpretation must account for the kind of runoff generation in the catchment.
7) The temporary variation of S parameter (regression between S and SIM output/base-flow) led to the conclusion that it was difficult to regionalize the parameter of SCS-LR model to predict flash flood in Mediterranean catchments due to the reason that we did not find a stable case despite we had some positive results as the trend of high S –

low value of SIM output or the similarity in the regression S – base flow of Ardèche and Gardon. The output of the SIM model performed worse than the base flow in deriving S parameter in the case of Real Collobrier catchment but better in other Mediterranean catchments. The failure of the regionalization could be due to:

- For the output of the SIM model, the reason could be due to the fact that the tiles of the model supplied too large values for representing the specificities of small catchments or the soil properties that SIM used were not really appropriate or accurate enough to represent the actual soil properties.
- The bias from estimating base flow or its inability to represent the spatial variability between catchments could be the case for the base flow.
- The bias in extrapolating flows could also affect the simulation. In some cases (e.g. Gardon and Ardèche) there were a few gauging to establish the rating curve. Thus, the uncertainty can happen in the extrapolation of the rating curve to high flows and change the model's parameters.
- The reason can also due to the rainfall uncertainty. Except for the case of Real Collobrier, the others had not the very high density of rain gauge. The variation of all the slopes and intercepts for the Mediterranean was quite similar to the case when we use only 1 single gauge in Real Collobrier when the S for minimum and maximum value of initial condition could vary a lot.
- The calibration of the parameters can be the problem. The use of Ia/S = 0.2, the use of constant parameters, the use of uniform S for the whole catchment can also lead to the error in calibrating S parameter, then weaken the correlation between S and initial conditions.

6.3. Perspectives

There are still points to be developed in the framework of this Ph.D. thesis and several perspectives can be proposed. The perspectives enclose the following aspects: developing or finding a descriptor to transpose the parameter from gauged to ungauged Mediterranean catchments; (comparing the event-based model and the continuous model); continuing to apply the model to catchments in various climate.

6.3.1. Developing or finding a descriptor to transpose the parameter from gauged to ungauged Mediterranean catchments

As we showed above, the base-flow and Hu2 (w_2) index were not possible to create a regional scheme for generally Mediterranean catchments. The reason could be due to their own characteristic. Further researches on integrating these indexes with other soil information (soil depth for example) or developing a new index which contains soil information are needed to solve this problem.

In the case of small catchments, the data of Hu2 (w_2) index should have been calculated in a smaller resolution than 8x8 km^2 to have more accurate information.

Another reason for the failure of having a regional scheme for Mediterranean catchments could be the rainfall uncertainty. The benefits of the rainfall radar in case of the low density of rain gauges should be investigated.

6.3.2. Applying SCS-LR to catchments in various climate

The model can be applied on Orgeval, another well-documented catchment which located 70 km from the East of Paris, with a moderate oceanic climate. The catchment includes 7 stream gauges, 8 rain gauges (hourly basis), and soil moisture data (3 TDR stations, hourly basis). The data is also collected by IRSTEA from 1962.

Another catchment which floods can also be simulated is Dong Cao, which located in North Vietnam. This is a tropical watershed which IRD has taken charged for several years on the experiment. This can be the basin which I will work with after the Ph.D. in the contract with the university where I will work when coming back to Vietnam. It is also planned that I can work in collaboration with the IRD and the international laboratory LOTUS, to be in charge of studies carried out for Dong Cao basin.

References

Abbaspour, K. C., Johnson, C. A. and Genuchten, M. T. van: Estimating Uncertain Flow and Transport Parameters Using a Sequential Uncertainty Fitting Procedure, Vadose Zone J., 3(4), 1340–1352, doi:10.2113/3.4.1340, 2004.

Amponsah, W., Ayral, P.-A., Boudevillain, B., Bouvier, C., Braud, I., Brunet, P., Delrieu, G., Didon-Lescot, J.-F., Gaume, E., Lebouc, L., Marchi, L., Marra, F., Morin, E., Nord, G., Payrastre, O., Zoccatelli, D. and Borga, M.: Integrated high-resolution dataset of high-intensity European and Mediterranean flash floods, Earth Syst. Sci. Data, 10(4), 1783–1794, doi:https://doi.org/10.5194/essd-10-1783-2018, 2018.

Anagnostou, E. N.: A convective/stratiform precipitation classification algorithm for volume scanning weather radar observations, Meteorol. Appl., 11(4), 291–300, doi:10.1017/S1350482704001409, 2004.

Anderson, M. G. and Burt, T. P.: Process studies in hillslope hydrology. [online] Available from: http://agris.fao.org/agris-search/search.do?recordID=GB19940060148 (Accessed 2 March 2019), 1990.

Andréassian, V., Perrin, C., Michel, C., Usart-Sanchez, I. and Lavabre, J.: Impact of imperfect rainfall knowledge on the efficiency and the parameters of watershed models, J. Hydrol., 250(1), 206–223, doi:10.1016/S0022-1694(01)00437-1, 2001.

Anon: Geosol / index, [online] Available from: https://webapps.gissol.fr/geosol/ (Accessed 16 October 2018), n.d.

Anquetin, S., Creutin, J.-D., Delrieu, G., Ducroq, V., Gaume, E. and Ruin, I.: Increasing the forecasting lead-time of weather driven flash-floods. [online] Available from: https://halshs.archives-ouvertes.fr/halshs-00382515 (Accessed 3 March 2019), 2004.

Anselmo, V.: Massime portate osservate o indirettamente valutate nei corsi d'acqua subalpini., Atti e Rassegna Tecnica della Società degli Ingegneri e Architetti in Torino, 39(10), 245–275, 1985.

Arnaud, P., Bouvier, C., Cisneros, L. and Dominguez, R.: Influence of rainfall spatial variability on flood prediction, J. Hydrol., 260(1), 216–230, doi:10.1016/S0022-1694(01)00611-4, 2002.

Arnold, J. and Allen, P.: Automated Methods for Estimating Baseflow and Groundwater Recharge From Stream Flow Records, JAWRA J. Am. Water Resour. Assoc., 35, 411–424, doi:10.1111/j.1752-1688.1999.tb03599.x, 2007.

Aron, G., C. Miller, A. and F. Lakatos, D.: Infiltration Formula Based on SCS Curve Number, ASCE J Irrig Drain Div, 103, 1977.

Artan, G., Gadain, H., Smith, J. L., Asante, K., Bandaragoda, C. J. and Verdin, J. P.: Adequacy of satellite derived rainfall data for stream flow modeling, Nat. Hazards, 43(2), 167–185, doi:10.1007/s11069-007-9121-6, 2007.

Aubert, Y., Arnaud, P., Ribstein, P. and Fine, J. A.: La méthode SHYREG débit-application sur 1605 bassins versants en France métropolitaine, Hydrol. Sci. J., 59(5), 993–1005, doi:10.1080/02626667.2014.902061, 2014.

Auzet, A. V., Boiffin, J. and Ludwig, B.: Concentrated flow erosion in cultivated catchments: Influence of soil surface state, Earth Surf. Process. Landf., 20(8), 759–767, doi:10.1002/esp.3290200807, 1995.

Balsamo, G., Albergel, C., Beljaars, A., Boussetta, S., Brun, E., Cloke, H., Dee, D., Dutra, E., Muñoz-Sabater, J., Pappenberger, F., Rosnay, P. de, Stockdale, T. and Vitart, F.: ERA-Interim/Land: a global land surface reanalysis data set, Hydrol. Earth Syst. Sci., 19(1), 389–407, doi:https://doi.org/10.5194/hess-19-389-2015, 2015.

Bardossy, A. and Singh, S. K.: Robust estimation of hydrological model parameters, Hydrol Earth Syst Sci, 11, 2008.

Barnes, B. S.: The structure of discharge-recession curves, Eos Trans. Am. Geophys. Union, 20(4), 721–725, doi:10.1029/TR020i004p00721, 1939.

Barredo, J. I.: Major flood disasters in Europe: 1950–2005, Nat. Hazards, 42(1), 125–148, doi:10.1007/s11069-006-9065-2, 2007.

Bartalis, Z., Wagner, W., Naeimi, V., Hasenauer, S., Scipal, K., Bonekamp, H., Figa, J. and Anderson, C.: Initial soil moisture retrievals from the METOP-A Advanced Scatterometer (ASCAT), Geophys. Res. Lett., 34(20), doi:10.1029/2007GL031088, 2007.

Bastola, S., Ishidaira, H. and Takeuchi, K.: Regionalisation of hydrological model parameters under parameter uncertainty: A case study involving TOPMODEL and basins across the globe, J. Hydrol., 357(3), 188–206, doi:10.1016/j.jhydrol.2008.05.007, 2008.

Bechtold, P. and Bazile, E.: The 12–13 November 1999 flash flood in southern France, Atmospheric Res., 56(1), 171–189, doi:10.1016/S0169-8095(00)00097-1, 2001.

Beck, M. B.: Water Quality Modeling: A Review of the Analysis of Uncertainty, Water Resour. Res. [online] Available from: http://pure.iiasa.ac.at/id/eprint/2913/ (Accessed 21 April 2019), 1987.

Becker, M. W., Georgian, T., Ambrose, H., Siniscalchi, J. and Fredrick, K.: Estimating flow and flux of ground water discharge using water temperature and velocity, J. Hydrol., 296(1), 221–233, doi:10.1016/j.jhydrol.2004.03.025, 2004.

Béguin, E.: Érosion mécanique après l'incendie du massif des Maures. Le bassin versant du Rimbaud., Mémoire de DEA, Universite de Provence., 1993.

Behrangi, A., Khakbaz, B., Jaw, T. C., AghaKouchak, A., Hsu, K. and Sorooshian, S.: Hydrologic evaluation of satellite precipitation products over a mid-size basin, J. Hydrol., 397(3), 225–237, doi:10.1016/j.jhydrol.2010.11.043, 2011.

Bell, V. A. and Moore, R. J.: The sensitivity of catchment runoff models to rainfall data at different spatial scales, Hydrol. Earth Syst. Sci., 4(4), 653–667, doi:https://doi.org/10.5194/hess-4-653-2000, 2000.

Bentura, P. L. F. and Michel, C.: Flood routing in a wide channel with a quadratic lag-and-route method., 1997.

Bergkamp, G., Cammeraat, L. H. and Martinez-Fernandez, J.: Water Movement and Vegetation Patterns on Shrubland and an Abandoned Field in Two Desertification-Threatened Areas in Spain, Earth Surf. Process. Landf., 21(12), 1073–1090, doi:10.1002/(SICI)1096-9837(199612)21:12<1073::AID-ESP640>3.0.CO;2-8, 1996.

Berthet, L., Andréassian, V., Perrin, C. and Javelle, P.: How crucial is it to account for the antecedent moisture conditions in flood forecasting? Comparison of event-based and continuous approaches on 178 catchments, Hydrol. Earth Syst. Sci. Discuss., (13), 819–831, 2009.

Betson, R. P.: What is watershed runoff?, J. Geophys. Res., 69(8), 1541–1552, doi:10.1029/JZ069i008p01541, 1964.

Beven, K.: A manifesto for the equifinality thesis, J. Hydrol., 320(1), 18–36, doi:10.1016/j.jhydrol.2005.07.007, 2006.

Beven, K. and Binley, A.: The future of distributed models: Model calibration and uncertainty prediction, Hydrol. Process., 6(3), 279–298, doi:10.1002/hyp.3360060305, 1992.

Beven, K. and Freer, J.: A dynamic TOPMODEL, Hydrol. Process., 15(10), 1993–2011, doi:10.1002/hyp.252, 2001.

Beven, K. J.: Rainfall-Runoff Modelling: The Primer, John Wiley & Sons., 2012.

Bitew, M. M. and Gebremichael, M.: Evaluation Through Independent Measurements: Complex Terrain and Humid Tropical Region in Ethiopia, in Satellite Rainfall Applications for Surface Hydrology, edited by M. Gebremichael and F. Hossain, pp. 205–214, Springer Netherlands, Dordrecht., 2010.

Bitew, M. M., Gebremichael, M., Ghebremichael, L. T. and Bayissa, Y. A.: Evaluation of High-Resolution Satellite Rainfall Products through Streamflow Simulation in a Hydrological Modeling of a Small Mountainous Watershed in Ethiopia, J. Hydrometeorol., 13(1), 338–350, doi:10.1175/2011JHM1292.1, 2011.

Blöschl, G.: Scaling in hydrology, Hydrol. Process., 15(4), 709–711, doi:10.1002/hyp.432, 2001.

Blöschl, G. and Sivapalan, M.: Scale issues in hydrological modelling: A review, Hydrol. Process., 9(3–4), 251–290, doi:10.1002/hyp.3360090305, 1995.

Blöschl, G., Reszler, C. and Komma, J.: A spatially distributed flash flood forecasting model, Environ. Model. Softw., 23(4), 464–478, doi:10.1016/j.envsoft.2007.06.010, 2008.

Boone, A., Calvet, J.-C. and Noilhan, J.: Inclusion of a Third Soil Layer in a Land Surface Scheme Using the Force–Restore Method, J. Appl. Meteorol., 38(11), 1611–1630, doi:10.1175/1520-0450(1999)038<1611:IOATSL>2.0.CO;2, 1999.

Borga, M., Boscolo, P., Zanon, F. and Sangati, M.: Hydrometeorological Analysis of the 29 August 2003 Flash Flood in the Eastern Italian Alps, J. Hydrometeorol., 8(5), 1049–1067, doi:10.1175/JHM593.1, 2007.

Borga, M., Anagnostou, E. N., Blöschl, G. and Creutin, J.-D.: Flash flood forecasting, warning and risk management: the HYDRATE project, Environ. Sci. Policy, 14(7), 834–844, doi:10.1016/j.envsci.2011.05.017, 2011.

Bosznay, M.: Generalization of SCS Curve Number Method, J. Irrig. Drain. Eng., 115(1), 139–144, doi:10.1061/(ASCE)0733-9437(1989)115:1(139), 1989.

Botterweg, P.: The user's influence on model calibration results: an example of the model SOIL, independently calibrated by two users, Ecol. Model., 81(1), 71–81, doi:10.1016/0304-3800(94)00161-A, 1995.

Boudevillain, B., Delrieu, G., Galabertier, B., Bonnifait, L., Bouilloud, L., Kirstetter, P.-E. and Mosini, M.-L.: The Cévennes-Vivarais Mediterranean Hydrometeorological Observatory database, Water Resour. Res., 47(7), doi:10.1029/2010WR010353, 2011.

Bouvier, C. and Delclaux, F.: ATHYS: a hydrological environment for spatial modelling and coupling with a GIS., 1996.

Bouvier, C., Bouchenaki, L. and Tramblay, Y.: Comparison of SCS and Green-Ampt Distributed Models for Flood Modelling in a Small Cultivated Catchment in Senegal, Geosciences, 8(4), 122, doi:10.3390/geosciences8040122, 2018.

Bracken, L. J., Cox, N. J. and Shannon, J.: The relationship between rainfall inputs and flood generation in south–east Spain, Hydrol. Process., 22(5), 683–696, doi:10.1002/hyp.6641, 2008.

Brocca, L., Melone, F. and Moramarco, T.: On the estimation of antecedent wetness conditions in rainfall–runoff modelling, Hydrol. Process., 22(5), 629–642, doi:10.1002/hyp.6629, 2008.

Brocca, L., Melone, F., Moramarco, T. and Singh, V. P.: Assimilation of Observed Soil Moisture Data in Storm Rainfall-Runoff Modeling, J. Hydrol. Eng., 14(2), 153–165, doi:10.1061/(ASCE)1084-0699(2009)14:2(153), 2009.

Brunet, P. and Bouvier, C.: Retour d'expérience sur la crue du 12 septembre 2015 à Lodève (Hérault, France) : influence du karst sur les débits de pointe de crue, Houille Blanche, (3), 39–46, doi:10.1051/lhb/2017020, 2017.

Brutsaert, W.: Hydrology by Wilfried Brutsaert, Camb. Core, doi:10.1017/CBO9780511808470, 2005.

Bull, L. J., Kirkby, M. J., Shannon, J. and Hooke, J. M.: The impact of rainstorms on floods in ephemeral channels in southeast Spain, CATENA, 38(3), 191–209, doi:10.1016/S0341-8162(99)00071-5, 2000.

Camarasa-Belmonte, A. M.: Flash floods in Mediterranean ephemeral streams in Valencia Region (Spain), J. Hydrol., 541, 99–115, doi:10.1016/j.jhydrol.2016.03.019, 2016.

Cazier, D. J. and Hawkins, R. H.: Regional Application of the Curve Number Method, pp. 710–710, ASCE. [online] Available from: https://cedb.asce.org/CEDBsearch/record.jsp?dockey=0041386 (Accessed 22 April 2019), 1984.

Central Unit for Soil Conservation: Hand book of Hydrology, GOVERNMENT OF INDIA-MINISTRY OF AGRICULTURE CENTRAL UNIT FOR SOIL CONSERVATION (HYDROLOGY AND SEDIMENTATION), New Dlehi., 1972.

Champeaux, J. L., Masson, V. and Chauvin, F.: ECOCLIMAP: a global database of land surface parameters at 1 km resolution, Meteorol. Appl., 12(1), 29–32, doi:10.1017/S1350482705001519, 2005.

Chen, C.: An evaluation of the mathematics and physical significance of the Soil Conservation Service curve number procedure for estimating runoff volume, in Rainfall-Runoff Relationship, edited by V.P. Singh, Water Resour. Pub., Littleton, Colo. 80161., 1982.

Chen, X., Zhang, L., Gippel, C. J., Shan, L., Chen, S. and Yang, W.: Uncertainty of Flood Forecasting Based on Radar Rainfall Data Assimilation, Adv. Meteorol., doi:10.1155/2016/2710457, 2016.

Clapp, R. B. and Hornberger, G. M.: Empirical equations for some soil hydraulic properties, Water Resour. Res., 14(4), 601–604, doi:10.1029/WR014i004p00601, 1978.

Cole, S. J. and Moore, R. J.: Hydrological modelling using raingauge- and radar-based estimators of areal rainfall, J. Hydrol., 358(3), 159–181, doi:10.1016/j.jhydrol.2008.05.025, 2008.

Collischonn, B., Collischonn, W. and Tucci, C. E. M.: Daily hydrological modeling in the Amazon basin using TRMM rainfall estimates, J. Hydrol., 360(1), 207–216, doi:10.1016/j.jhydrol.2008.07.032, 2008.

Collis-George, N.: Infiltration equations for simple soil systems, Water Resour. Res., 13(2), 395–403, doi:10.1029/WR013i002p00395, 1977.

Condie, S. A. and Webster, I. T.: The influence of wind stress, temperature, and humidity gradients on evaporation from reservoirs, Water Resour. Res., 33(12), 2813–2822, doi:10.1029/97WR02405, 1997.

Costa, J. E.: A comparison of the largest rainfall-runoff floods in the United States with those of the People's Republic of China and the world, J. Hydrol., 96(1), 101–115, doi:10.1016/0022-1694(87)90146-6, 1987.

Coustau, M., Bouvier, C., Borrell-Estupina, V. and Jourde, H.: Flood modelling with a distributed event-based parsimonious rainfall-runoff model: case of the karstic Lez river catchment, Nat. Hazards Earth Syst. Sci., 12, 1119–1133, 2012.

Creutin, J. D., Borga, M., Lutoff, C., Scolobig, A., Ruin, I. and Créton-Cazanave, L.: Catchment dynamics and social response during flash floods: the potential of radar rainfall monitoring for warning procedures, Meteorol. Appl., 16(1), 115–125, doi:10.1002/met.128, 2009.

Creutin, J.-D. and Borga, M.: Radar hydrology modifies the monitoring of flash-flood hazard, Hydrol. Process., 17(7), 1453–1456, doi:10.1002/hyp.5122, 2003.

Crockford, R. H. and Richardson, D. P.: Partitioning of rainfall into throughfall, stemflow and interception: effect of forest type, ground cover and climate, Hydrol. Process., 14(16–17), 2903–2920, doi:10.1002/1099-1085(200011/12)14:16/17<2903::AID-HYP126>3.0.CO;2-6, 2000.

Dawdy, D. R. and Bergmann, J. M.: Effect of rainfall variability on streamflow simulation, Water Resour. Res., 5(5), 958–966, doi:10.1029/WR005i005p00958, 1969.

Delrieu, G., Nicol, J., Yates, E., Kirstetter, P.-E., Creutin, J.-D., Anquetin, S., Obled, C., Saulnier, G.-M., Ducrocq, V., Gaume, E., Payrastre, O., Andrieu, H., Ayral, P.-A., Bouvier, C., Neppel, L., Livet, M., Lang, M., du-Châtelet, J. P., Walpersdorf, A. and Wobrock, W.: The Catastrophic Flash-Flood Event of 8–9 September 2002 in the Gard Region, France: A First Case Study for the Cévennes–Vivarais Mediterranean Hydrometeorological Observatory, J. Hydrometeorol., 6(1), 34–52, doi:10.1175/JHM-400.1, 2005.

Deodhar, M. J.: Elementary Engineering Hydrology, Pearson Education India., 2008.

Devia, G. K., Ganasri, B. P. and Dwarakish, G. S.: A Review on Hydrological Models, Aquat. Procedia, 4, 1001–1007, doi:10.1016/j.aqpro.2015.02.126, 2015.

Diakakis, M. and Deligiannakis, G.: Flood fatalities in Greece: 1970–2010, J. Flood Risk Manag., 10(1), 115–123, doi:10.1111/jfr3.12166, 2017.

Dore, A. J., Mousavi-Baygi, M., Smith, R. I., Hall, J., Fowler, D. and Choularton, T. W.: A model of annual orographic precipitation and acid deposition and its application to Snowdonia, Atmos. Environ., 40(18), 3316–3326, doi:10.1016/j.atmosenv.2006.01.043, 2006.

Dorigo, W. A., Wagner, W., Hohensinn, R., Hahn, S., Paulik, C., Xaver, A., Gruber, A., Drusch, M., Mecklenburg, S., Oevelen, P. van, Robock, A. and Jackson, T.: The International Soil Moisture Network: a data hosting facility for global in situ soil moisture measurements,

Hydrol. Earth Syst. Sci., 15(5), 1675–1698, doi:https://doi.org/10.5194/hess-15-1675-2011, 2011.

Drobinski, P., Ducrocq, V., Alpert, P., Anagnostou, E., Béranger, K., Borga, M., Braud, I., Chanzy, A., Davolio, S., Delrieu, G., Estournel, C., Boubrahmi, N. F., Font, J., Grubišić, V., Gualdi, S., Homar, V., Ivančan-Picek, B., Kottmeier, C., Kotroni, V., Lagouvardos, K., Lionello, P., Llasat, M. C., Ludwig, W., Lutoff, C., Mariotti, A., Richard, E., Romero, R., Rotunno, R., Roussot, O., Ruin, I., Somot, S., Taupier-Letage, I., Tintore, J., Uijlenhoet, R. and Wernli, H.: HyMeX: A 10-Year Multidisciplinary Program on the Mediterranean Water Cycle, Bull. Am. Meteorol. Soc., 95(7), 1063–1082, doi:10.1175/BAMS-D-12-00242.1, 2013.

Durand, P., Robson, A. and Neal, C.: Modelling the hydrology of submediterranean montane catchments (Mont-Lozère, France) using TOPMODEL: initial results, J. Hydrol., 139(1), 1–14, doi:10.1016/0022-1694(92)90191-W, 1992.

Durbude, D. G., Jain, M. K. and Mishra, S. K.: Long-term hydrologic simulation using SCS-CN-based improved soil moisture accounting procedure, Hydrol. Process., 25(4), 561–579, doi:10.1002/hyp.7789, 2011.

Eckhardt, K.: How to construct recursive digital filters for baseflow separation, Hydrol. Process., 19(2), 507–515, doi:10.1002/hyp.5675, 2005.

Eckhardt, K. and Arnold, J. G.: Automatic calibration of a distributed catchment model, J. Hydrol., 251(1), 103–109, doi:10.1016/S0022-1694(01)00429-2, 2001.

Estupina-Borrell, V., Dartus, D. and Ababou, R.: Flash flood modeling with the MARINE hydrological distributed model, Hydrol Earth Syst Sci Discuss, 2006, 3397–3438, doi:10.5194/hessd-3-3397-2006, 2006.

Faurès, J.-M., Goodrich, D. C., Woolhiser, D. A. and Sorooshian, S.: Impact of small-scale spatial rainfall variability on runoff modeling, J. Hydrol., 173(1), 309–326, doi:10.1016/0022-1694(95)02704-S, 1995.

Fishman, G. S. and Kiviat, P. J.: The statistics of discrete-event simulation, SIMULATION, 10(4), 185–195, doi:10.1177/003754976801000406, 1968.

Fitzjohn, C., Ternan, J. L. and Williams, A. G.: Soil moisture variability in a semi-arid gully catchment: implications for runoff and erosion control, CATENA, 32(1), 55–70, doi:10.1016/S0341-8162(97)00045-3, 1998.

Folton, N., Tolsa, M. and Arnaud, P.: Le Bassin de recherche du Réal Collobrier - Étude des processus hydrologiques en milieu méditerranéen a échelle fine., in 50 ans de l'Orgeval, p. 7 p., IRSTEA, Paris, France. [online] Available from: https://hal.archives-ouvertes.fr/hal-00779374 (Accessed 1 December 2017), 2012.

Folton, N., Martin, E., Arnaud, P., L'Hermite, P. and Tolsa, M.: A 50-year analysis of hydrological trends and processes in a Mediterranean catchment, Hydrol. Earth Syst. Sci. Discuss., 1–28, doi:10.5194/hess-2018-547, 2018.

Foody, G. M., Ghoneim, E. M. and Arnell, N. W.: Predicting locations sensitive to flash flooding in an arid environment, J. Hydrol., 292(1), 48–58, doi:10.1016/j.jhydrol.2003.12.045, 2004.

Friedenthal, S., Moore, A. and Steiner, R.: A Practical Guide to SysML: The Systems Modeling Language, 3 edition., Morgan Kaufmann, Amsterdam ; Boston., 2014.

Garambois, P.-A., Douinot, A., Roux, H. and Dartus, D.: Méthodes de régionalisation pour un modèle pluie-débit distribué et à base physique dédié aux crues éclair, Houille Blanche, (2), 71–77, doi:10.1051/lhb/2016021, 2016.

Gaume, E., Livet, M., Desbordes, M. and Villeneuve, J.-P.: Hydrological analysis of the River Aude, France, flash flood on 12 and 13 November 1999, J. Hydrol., 286, 135–154, doi:10.1016/j.jhydrol.2003.09.015, 2004.

Gaume, E., Borga, M., Llassat, M. C., Maouche, S., Lang, M. and Diakakis, M.: Mediterranean extreme floods and flash floods, in The Mediterranean Region under Climate Change. A Scientific Update, pp. 133–144, IRD Editions. [online] Available from: https://hal.archives-ouvertes.fr/hal-01465740 (Accessed 2 March 2019), 2016.

Gentine, P., Troy, T. J., Lintner, B. R. and Findell, K. L.: Scaling in Surface Hydrology: Progress and Challenges, J. Contemp. Water Res. Educ., 147(1), 28–40, doi:10.1111/j.1936-704X.2012.03105.x, 2012.

Golding, B. L.: Discussion of "Runoff curve number with varying site moisture, Journal of Irrigation and Drainage Division, ASCE, 105 (IR4), 441-442., 1979.

Gourley, J. J., Hong, Y., Flamig, Z. L., Wang, J., Vergara, H. and Anagnostou, E. N.: Hydrologic Evaluation of Rainfall Estimates from Radar, Satellite, Gauge, and Combinations on Ft. Cobb Basin, Oklahoma, J. Hydrometeorol., 12(5), 973–988, doi:10.1175/2011JHM1287.1, 2011.

Grayson, R. B., Moore, I. D. and McMahon, T. A.: Physically based hydrologic modeling: 2. Is the concept realistic?, Water Resour. Res., 28(10), 2659–2666, doi:10.1029/92WR01259, 1992.

Gregory, K. J.: Palaeohydrology and Environmental Change, 1 edition., edited by G. Benito and V. R. Baker, Wiley, Chichester ; New York., 1998.

Gresillon, J. M., Taha, A., Le Meillour, F., Lavabre, J. and Puech, C.: Analyse temporelle et spatiale des apports de crue sur un bassin méditerranéen: relation avec les processes hydrologiques, in Effects of Scale on Interpretation and Management of Sediment and Water Quality., 1995.

Grimes, D. I. F. and Diop, M.: Satellite-based rainfall estimation for river flow forecasting in Africa. I: Rainfall estimates and hydrological forecasts, Hydrol. Sci. J., 48(4), 567–584, doi:10.1623/hysj.48.4.567.51410, 2003.

Gruntfest, E. and Handmer, J.: Coping With Flash Floods, Springer Science & Business Media. [online] Available from:

https://books.google.fr/books?id=F2JDBAAAQBAJ&printsec=frontcover&hl=vi (Accessed 18 April 2019), 2001.

Guetter, A. K., Georgakakos, K. P. and Tsonis, A. A.: Hydrologic applications of satellite data: 2. Flow simulation and soil water estimates, J. Geophys. Res. Atmospheres, 101(D21), 26527–26538, doi:10.1029/96JD01655, 1996.

Gupta, H. V., Sorooshian, S., Hogue, T. S. and Boyle, D. P.: Advances in Automatic Calibration of Watershed Models, in Calibration of Watershed Models, edited by Q. Duan, H. V. Gupta, S. Sorooshian, A. N. Rousseau, and R. Turcotte, pp. 9–28, American Geophysical Union., 2003.

Habets, F., Boone, A., Champeaux, J.-L., Etchevers, P., Franchisteguy, L., Leblois, E., Ledoux, E., Moigne, P. L., Martin, E., Morel, S., Noilhan, J., Seguí, P. Q., Regimbeau, F. R. and Viennot, P.: The SAFRAN-ISBA-MODCOU hydrometeorological model applied over France, J. Geophys. Res. Atmospheres, 113(D06113), 18, doi:10.1029/2007JD008548, 2008.

Hall, F. R.: Base Flow Recessions—a Review, Water Resour. Res. - WATER RESOUR RES, 4, doi:10.1029/WR004i005p00973, 1968.

Harvey, L. D. D.: Upscaling in Global Change Research, Clim. Change, 44(3), 225–263, doi:10.1023/A:1005543907412, 2000.

Hawkins, R. H.: Runoff Curve Numbers with Varying Site Moisture, J. Irrig. Drain. Div., 104(4), 389–398, 1978.

Hawkins, R. H.: Asymptotic Determination of Runoff Curve Numbers from Data, J. Irrig. Drain. Eng., 119(2), 334–345, doi:10.1061/(ASCE)0733-9437(1993)119:2(334), 1993.

Hawkins, R. H., Woodward, D. E. and Jiang, R.: Invertigation of the runoff curve number abstraction ratio, in : USDA-NRCS Hydraulic Engineering Workshop, Tucson AZ, Nov 2002, pp. 1-12, 2002.

Helming, K., Römkens, M. J. M. and Prasad, S. N.: Surface Roughness Related Processes of Runoff and Soil Loss: A Flume Study, Soil Sci. Soc. Am. J., 62(1), 243–250, doi:10.2136/sssaj1998.03615995006200010031x, 1998.

Heuvelink, G. B. M.: Uncertainty analysis in environmental modelling under a change of spatial scale, Nutr. Cycl. Agroecosystems, 50(1), 255–264, doi:10.1023/A:1009700614041, 1998.

Huang, M., Gallichand, J., Dong, C., Wang, Z. and Shao, M.: Use of soil moisture data and curve number method for estimating runoff in the Loess Plateau of China, Hydrol. Process., 21(11), 1471–1481, doi:10.1002/hyp.6312, 2007.

Huang, P., Li, Z., Yao, C., Li, Q. and Yan, M.: Spatial Combination Modeling Framework of Saturation-Excess and Infiltration-Excess Runoff for Semihumid Watersheds, Adv. Meteorol., doi:10.1155/2016/5173984, 2016.

Huffman, G. J.: Estimates of Root-Mean-Square Random Error for Finite Samples of Estimated Precipitation, J. Appl. Meteorol., 36(9), 1191–1201, doi:10.1175/1520-0450(1997)036<1191:EORMSR>2.0.CO;2, 1997.

Huyck, A. A. O., Pauwels, V. R. N. and Verhoest, N. E. C.: A base flow separation algorithm based on the linearized Boussinesq equation for complex hillslopes, Water Resour. Res., 41(8), doi:10.1029/2004WR003789, 2005.

Imeson, A. C., Verstraten, J. M., van Mulligen, E. J. and Sevink, J.: The effects of fire and water repellency on infiltration and runoff under Mediterranean type forest, CATENA, 19(3), 345–361, doi:10.1016/0341-8162(92)90008-Y, 1992.

Jain, M. K., Kothyari, U. C. and Ranga Raju, K. G.: A GIS based distributed rainfall–runoff model, J. Hydrol., 299(1), 107–135, doi:10.1016/j.jhydrol.2004.04.024, 2004.

Javelle, P., Organde, D., Demargne, J., Saint-Martin, C., De Saint-Aubin, C., Garandeau, L. and Janet, B.: Setting up a French national flash flood warning system for ungauged catchments based on the AIGA method, in 3rd European Conference on Flood Risk Management FLOODrisk 2016, vol. 7, p. 11 p., Lyon, France., 2016.

Javelle, P., Braud, I., Saint-Martin, C., Payrastre, O., Gaume, E., Borga, M., Gourley, J. and Zappa, M.: Sub-chapter 3.4.3. Improving flash flood forecasting and warning capabilities, in The Mediterranean region under climate change : A scientific update, edited by J.-P. Moatti and S. Thiébault, pp. 587–595, IRD Éditions, Marseille. [online] Available from: http://books.openedition.org/irdeditions/23955 (Accessed 18 April 2019), 2018.

Johnson, M. S., Coon, W. F., Mehta, V. K., Steenhuis, T. S., Brooks, E. S. and Boll, J.: Application of two hydrologic models with different runoff mechanisms to a hillslope dominated watershed in the northeastern US: a comparison of HSPF and SMR, J. Hydrol., 284(1), 57–76, doi:10.1016/j.jhydrol.2003.07.005, 2003.

Jonkman, S. N.: Global Perspectives on Loss of Human Life Caused by Floods, Nat. Hazards, 34(2), 151–175, doi:10.1007/s11069-004-8891-3, 2005.

Kelliher, F. M., Leuning, R., Raupach, M. R. and Schulze, E.-D.: Maximum conductances for evaporation from global vegetation types, Agric. For. Meteorol., 73(1), 1–16, doi:10.1016/0168-1923(94)02178-M, 1995.

Kerr, Y. H., Waldteufel, P., Wigneron, J., Delwart, S., Cabot, F., Boutin, J., Escorihuela, M., Font, J., Reul, N., Gruhier, C., Juglea, S. E., Drinkwater, M. R., Hahne, A., Martin-Neira, M. and Mecklenburg, S.: The SMOS Mission: New Tool for Monitoring Key Elements ofthe Global Water Cycle, Proc. IEEE, 98(5), 666–687, doi:10.1109/JPROC.2010.2043032, 2010.

Kirkby, M. J.: Hillslope hydrology, Wiley., 1978.

Kirkby, M. J., Naden, P. S., Burt, T. and Butcher, D. P.: Computer Simulation in Physical Geography, 2nd Edition, 2 edition., Wiley, Chichester ; New York., 1993.

Kitanidis, P. and Bras, R.: Real-Time Forecasting With a Conceptual Hydrologic Model 1. Analysis of Uncertainty, Water Resour. Res. - WATER RESOUR RES, 16, 1025–1033, doi:10.1029/WR016i006p01025, 1980a.

Kitanidis, P. and Bras, R.: Real-time forecasting with a conceptual hydrologic model: 2. Applications and results, Water Resour. Res. - WATER RESOUR RES, 16, 1034–1044, doi:10.1029/WR016i006p01034, 1980b.

Knisel, W. G. (ed): CREAMS: a field scale model for Chemicals, Runoff, and Erosion from Agricultural Management Systems [USA], U. S. Dept Agric. Conserv. Res. Rep. USA [online] Available from: http://agris.fao.org/agris-search/search.do?recordID=US8025878 (Accessed 23 April 2019), 1980.

Koren, V. I., Finnerty, B. D., Schaake, J. C., Smith, M. B., Seo, D.-J. and Duan, Q.-Y.: Scale dependencies of hydrologic models to spatial variability of precipitation, J. Hydrol., 217(3), 285–302, doi:10.1016/S0022-1694(98)00231-5, 1999.

Krajewski, W. F. and Smith, J. A.: Radar hydrology: rainfall estimation, Adv. Water Resour., 25(8), 1387–1394, doi:10.1016/S0309-1708(02)00062-3, 2002.

Krajewski, W. F., Lakshmi, V., Georgakakos, K. P. and Jain, S. C.: A Monte Carlo Study of rainfall sampling effect on a distributed catchment model, Water Resour. Res., 27(1), 119–128, doi:10.1029/90WR01977, 1991.

Lamb, R. and Kay, A. L.: Confidence intervals for a spatially generalized, continuous simulation flood frequency model for Great Britain, Water Resour. Res., 40(7), doi:10.1029/2003WR002428, 2004.

Lasanta, T., García-Ruiz, J. M., Pérez-Rontomé, C. and Sancho-Marcén, C.: Runoff and sediment yield in a semi-arid environment: The effect of land management after farmland abandonment, CATENA, 38, 265–278, doi:10.1016/S0341-8162(99)00079-X, 2000.

Le Moine, N.: Le bassin versant de surface vu par le souterrain : une voie d'amélioration des performances et du réalisme des modèles pluie-débit?, thesis, Paris 6, 1 January. [online] Available from: http://www.theses.fr/2008PA066468 (Accessed 3 March 2019), 2008.

Lee, H., McIntyre, N., Wheater, H. and Young, A.: Selection of conceptual models for regionalisation of the rainfall-runoff relationship, J. Hydrol., 312(1), 125–147, doi:10.1016/j.jhydrol.2005.02.016, 2005.

Lhomme, J., Bouvier, C. and Perrin, J.-L.: Applying a GIS-based geomorphological routing model in urban catchments, J. Hydrol., 299(3), 203–216, doi:10.1016/j.jhydrol.2004.08.006, 2004.

Llasat, M. C., Llasat-Botija, M., Prat, M. A., Porcù, F., Price, C., Mugnai, A., Lagouvardos, K., Kotroni, V., Katsanos, D., Michaelides, S., Yair, Y., Savvidou, K. and Nicolaides, K.: High-impact floods and flash floods in Mediterranean countries: The FLASH preliminary database, Adv. Geosci., 23, 47–55, 2010.

Llasat, M. C., Llasat-Botija, M., Petrucci, O., Pasqua, A. A., Rosselló, J., Vinet, F. and Boissier, L.: Towards a database on societal impact of Mediterranean floods within the framework of the HYMEX project, Nat. Hazards Earth Syst. Sci., 13(5), 1337–1350, doi:10.5194/nhess-13-1337-2013, 2013.

Lundquist, J. D. and Cayan, D. R.: Seasonal and Spatial Patterns in Diurnal Cycles in Streamflow in the Western United States, J. Hydrometeorol., 3(5), 591–603, doi:10.1175/1525-7541(2002)003<0591:SASPID>2.0.CO;2, 2002.

Luo, Y., Weng, E., Wu, X., Gao, C., Zhou, X. and Zhang, L.: Parameter identifiability, constraint, and equifinality in data assimilation with ecosystem models, Ecol. Appl., 19(3), 571–574, doi:10.1890/08-0561.1, 2009.

Maggioni, V., Sapiano, M. R. P. and Adler, R. F.: Estimating Uncertainties in High-Resolution Satellite Precipitation Products: Systematic or Random Error?, J. Hydrometeorol., 17(4), 1119–1129, doi:10.1175/JHM-D-15-0094.1, 2016.

Maidment, D. R.: Handbook of hydrology, McGraw-Hill., 1993.

Marc, V., Travi, Y. and Lavabre, J.: Etude du fonctionnement hydrologique de bassins versants méditerranéens par le traçage naturel chimique et isotopique, in Tracer Technologies for Hydrological System., 1995.

Marchandise, A. and Viel, C.: Utilisation des indices d'humidité de la chaîne Safran-Isba-Modcou de Météo-France pour la vigilance et la prévision opérationnelle des crues, Houille Blanche, (6), 35–41, doi:10.1051/lhb/2009075, 2009.

Marchi, L., Borga, M., Preciso, E. and Gaume, E.: Characterisation of selected extreme flash floods in Europe and implications for flood risk management, J. Hydrol., 394(1), 118–133, doi:10.1016/j.jhydrol.2010.07.017, 2010.

Martin, F., Martin, C., Lavabre, J. and Folton, N.: Fonctionnement hydrologique des bassins versants de roches métamorphiques : exemple du bassin versant des Maurets (massif des Maures, Var, France), Etudes Géographie Phys., XXXI, 39–69, 2004.

Martín-Vide, J. P., Niñerola, D., Bateman, A., Navarro, A. and Velasco, E.: Runoff and sediment transport in a torrential ephemeral stream of the Mediterranean coast, J. Hydrol., 225(3), 118–129, doi:10.1016/S0022-1694(99)00134-1, 1999.

Massari, C., Brocca, L., Moramarco, T., Tramblay, Y. and Didon Lescot, J.-F.: Potential of soil moisture observations in flood modelling: Estimating initial conditions and correcting rainfall, Adv. Water Resour., 74, 44–53, doi:10.1016/j.advwatres.2014.08.004, 2014.

McCuen, R. H.: Approach to Confidence Interval Estimation for Curve Numbers, J. Hydrol. Eng., 7(1), 43–48, doi:10.1061/(ASCE)1084-0699(2002)7:1(43), 2002.

McGuire, K. J., McDonnell, J. J., Weiler, M., Kendall, C., McGlynn, B. L., Welker, J. M. and Seibert, J.: The role of topography on catchment-scale water residence time, Water Resour. Res., 41(5), doi:10.1029/2004WR003657, 2005.

McIntyre, N., Lee, H., Wheater, H., Young, A. and Wagener, T.: Ensemble predictions of runoff in ungauged catchments, Water Resour. Res., 41(12), doi:10.1029/2005WR004289, 2005.

McKane, R., Brookes, A., Djang, K., Stieglitz, M., Abdelnour, A., Pan, F. and Phillips, D: VELMA Version 2.0 User Manual and Technical Documentation, Corvallis, Oregon. [online] Available from: https://www.epa.gov/sites/production/files/2016-01/documents/velma_2.0_user_manual.pdf, 2014.

McNaught, A. D. and Wilkinson, A.: Compendium of Chemical Terminology, 2 edition., Wiley, Oxford England ; Malden, MA, USA., 1997.

Meinzer, O. E.: Outline of ground-water hydrology, with definitions, USGS Numbered Series, U.S. Govt. Print. Off.,. [online] Available from: http://pubs.er.usgs.gov/publication/wsp494 (Accessed 28 February 2019), 1923.

Merz, R. and Blöschl, G.: Regionalisation of catchment model parameters, J. Hydrol., 287(1), 95–123, doi:10.1016/j.jhydrol.2003.09.028, 2004.

Michaelides, K. and Wainwright, J.: Modelling the effects of hillslope–channel coupling on catchment hydrological response, Earth Surf. Process. Landf., 27(13), 1441–1457, doi:10.1002/esp.440, 2002.

Michel, C., Andréassian, V. and Perrin, C.: Soil Conservation Service Curve Number Method: How to mend a wrong soil moisture accounting procedure?, Water Resour. Res. - WATER RESOUR RES, 410, doi:10.1029/2004WR003191, 2005.

Mishra, S. K. and Singh, V. P.: Soil Conservation Service Curve Number (SCS-CN) Methodology. [online] Available from: //www.springer.com/la/book/9781402011320 (Accessed 9 January 2018), 2003.

Mishra, S. K. and Singh, V. P.: Soil Conservation Service Curve Number (SCS-CN) Methodology, Springer Science & Business Media., 2013.

Mishra, S. K., Sahu, R. K., Eldho, T. I. and Jain, M. K.: An Improved IaS Relation Incorporating Antecedent Moisture in SCS-CN Methodology, Water Resour. Manag., 20(5), 643–660, doi:10.1007/s11269-005-9000-4, 2006.

Mockus, V.: Letter to Orrin Ferris, March 5, 6p, In: Rallison, R.E, Origin and evolution of the SCS runoff equation, Proc., A.S.C.E. Symp. Watershed Management, Boise, Idaho, July, 1980, 1964.

Montaldo, N. and Albertson, J. D.: Temporal dynamics of soil moisture variability: 2. Implications for land surface models: DYNAMICS OF MOISTURE VARIABILITY, 2, Water Resour. Res., 39(10), doi:10.1029/2002WR001618, 2003.

Montz, B. E. and Gruntfest, E.: Flash flood mitigation: recommendations for research and applications, Glob. Environ. Change Part B Environ. Hazards, 4(1), 15–22, doi:10.1016/S1464-2867(02)00011-6, 2002.

Moore, I. D. and Grayson, R. B.: Terrain-based catchment partitioning and runoff prediction using vector elevation data, Water Resour. Res., 27(6), 1177–1191, doi:10.1029/91WR00090, 1991.

Moussa, R. and Chahinian, N.: Comparison of different multi-objective calibration criteria using a conceptual rainfall-runoff model of flood events, Hydrol Earth Syst Sci, 13(4), 519–535, doi:10.5194/hess-13-519-2009, 2009.

Nalbantis, I.: Use of multiple-time-step information in rainfall-runoff modelling, J. Hydrol., 165(1), 135–159, doi:10.1016/0022-1694(94)02567-U, 1995.

Nash, J. E. and Sutcliffe, J. V.: River flow forecasting through conceptual models part I — A discussion of principles, J. Hydrol., 10(3), 282–290, doi:10.1016/0022-1694(70)90255-6, 1970.

Nathan, R. J. and McMahon, T. A.: Evaluation of automated techniques for base flow and recession analyses, Water Resour. Res., 26(7), 1465–1473, doi:10.1029/WR026i007p01465, 1990.

Nicótina, L., Alessi Celegon, E., Rinaldo, A. and Marani, M.: On the impact of rainfall patterns on the hydrologic response, Water Resour. Res., 44(12), doi:10.1029/2007WR006654, 2008.

Nie, W., Yuan, Y., Kepner, W., Nash, M. S., Jackson, M. and Erickson, C.: Assessing impacts of Landuse and Landcover changes on hydrology for the upper San Pedro watershed, J. Hydrol., 407(1), 105–114, doi:10.1016/j.jhydrol.2011.07.012, 2011.

Nikolopoulos, E. I., Anagnostou, E. N., Hossain, F., Gebremichael, M. and Borga, M.: Understanding the Scale Relationships of Uncertainty Propagation of Satellite Rainfall through a Distributed Hydrologic Model, J. Hydrometeorol., 11(2), 520–532, doi:10.1175/2009JHM1169.1, 2010.

Nikolopoulos, E. I., Anagnostou, E. N. and Borga, M.: Using High-Resolution Satellite Rainfall Products to Simulate a Major Flash Flood Event in Northern Italy, J. Hydrometeorol., 14(1), 171–185, doi:10.1175/JHM-D-12-09.1, 2012.

Norbiato, D., Borga, M. and Dinale, R.: Flash flood warning in ungauged basins by use of the flash flood guidance and model-based runoff thresholds, Meteorol. Appl., 16(1), 65–75, doi:10.1002/met.126, 2009.

Obled, Ch., Wendling, J. and Beven, K.: The sensitivity of hydrological models to spatial rainfall patterns: an evaluation using observed data, J. Hydrol., 159(1), 305–333, doi:10.1016/0022-1694(94)90263-1, 1994.

Ogden, F. L., Sharif, H. O., Senarath, S. U. S., Smith, J. A., Baeck, M. L. and Richardson, J. R.: Hydrologic analysis of the Fort Collins, Colorado, flash flood of 1997, J. Hydrol., 228(1), 82–100, doi:10.1016/S0022-1694(00)00146-3, 2000.

Olivera, F. and Maidment, D.: Geographic Information Systems (GIS)-Based Spatially Distributed Model for Runoff Routing, Water Resour. Res., 35, doi:10.1029/1998WR900104, 1999.

Oudin, L., Andréassian, V., Perrin, C., Michel, C. and Moine, N. L.: Spatial proximity, physical similarity, regression and ungaged catchments: A comparison of regionalization approaches based on 913 French catchments, Water Resour. Res., 44(3), doi:10.1029/2007WR006240, 2008.

Oudin, L., Kay, A., Andreassian, V. and Perrin, C.: Are seemingly physically similar catchments truly hydrologically similar?, Water Resour. Res., 46, doi:Oudin, Ludovic; Kay, Alison; Andreassian, Vazken; Perrin, Charles. 2010 Are seemingly physically similar catchments truly hydrologically similar? Water Resources Research, 46, W11558. 15, pp. https://doi.org/10.1029/2009WR008887 <https://doi.org/10.1029/2009WR008887>, 2010.

Owe, M., Jeu, R. de and Holmes, T.: Multisensor historical climatology of satellite-derived global land surface moisture, J. Geophys. Res. Earth Surf., 113(F1), doi:10.1029/2007JF000769, 2008.

Papagiannaki, K., Lagouvardos, K. and Kotroni, V.: A database of high-impact weather events in Greece: a descriptive impact analysis for the period 2001–2011, Nat. Hazards Earth Syst. Sci., 13(3), 727–736, doi:https://doi.org/10.5194/nhess-13-727-2013, 2013.

Parkin, G., O'Donnell, G., Ewen, J., Bathurst, J. C., O'Connell, P. E. and Lavabre, J.: Validation of catchment models for predicting land-use and climate change impacts. 2. Case study for a Mediterranean catchment, J. Hydrol., 175(1), 595–613, doi:10.1016/S0022-1694(96)80027-8, 1996.

Patil, S. D., Wigington, P. J., Leibowitz, S. G., Sproles, E. A. and Comeleo, R. L.: How does spatial variability of climate affect catchment streamflow predictions?, J. Hydrol., 517, 135–145, doi:10.1016/j.jhydrol.2014.05.017, 2014.

Pechlivanidis, I. G., McIntyre, N. and Wheater, H. S.: The significance of spatial variability of rainfall on simulated runoff: an evaluation based on the Upper Lee catchment, UK, Hydrol. Res., 48(4), 1118–1130, doi:10.2166/nh.2016.038, 2017.

Penna, D., Tromp-van Meerveld, H. J., Gobbi, A., Borga, M. and Dalla Fontana, G.: The influence of soil moisture on threshold runoff generation processes in an alpine headwater catchment, Hydrol. Earth Syst. Sci., 15(3), 689–702, doi:https://doi.org/10.5194/hess-15-689-2011, 2011.

Pensieri, S., Schiano, M. E., Picco, P., Tizzi, M. and Bozzano, R.: Analysis of the Precipitation Regime over the Ligurian Sea, Water, 10(5), 566, doi:10.3390/w10050566, 2018.

Perrin, C.: Vers une amélioration d'un modèle global pluie-débit au travers d'une approche comparative, thesis, Grenoble INPG, 1 January. [online] Available from: http://www.theses.fr/2000INPG0105 (Accessed 18 April 2019), 2000.

Piñol, J., Beven, K. and Freer, J.: Modelling the hydrological response of mediterranean catchments, Prades, Catalonia. The use of distributed models as aids to hypothesis formulation, Hydrol. Process., 11(9), 1287–1306, doi:10.1002/(SICI)1099-1085(199707)11:9<1287::AID-HYP561>3.0.CO;2-W, 1997.

Pirastru, M. and Niedda, M.: Evaluation of the soil water balance in an alluvial flood plain with a shallow groundwater table, Hydrol. Sci. J., 58(4), 898–911, doi:10.1080/02626667.2013.783216, 2013.

Pitlick, J.: Relation between peak flows, precipitation, and physiography for five mountainous regions in the western USA, J. Hydrol., 158(3), 219–240, doi:10.1016/0022-1694(94)90055-8, 1994.

Ponce, V. M. and Hawkins, R. H.: Runoff Curve Number: Has It Reached Maturity?, J. Hydrol. Eng. - J HYDROL ENG, 1, doi:10.1061/(ASCE)1084-0699(1996)1:1(11), 1996.

Ponce Victor M. and Hawkins Richard H.: Runoff Curve Number: Has It Reached Maturity?, J. Hydrol. Eng., 1(1), 11–19, doi:10.1061/(ASCE)1084-0699(1996)1:1(11), 1996.

Price, K., Jackson, C. R., Parker, A. J., Reitan, T., Dowd, J. and Cyterski, M.: Effects of watershed land use and geomorphology on stream low flows during severe drought conditions in the southern Blue Ridge Mountains, Georgia and North Carolina, United States, Water Resour. Res., 47(2), doi:10.1029/2010WR009340, 2011.

Puech, Ch., Lavabre, J. and Martin, C.: Les feux de forêts de l'été 1990 dans le Massif des Maures: cartographie à l'aide de l'imagerie satellitaire, premières conséquences sur le cycle hydrologique, recherches sur les phénomènes d'érosion, G.I.S. Real Collobrier, Sécheresse, 2, 175–181, 1991.

Quintana Seguí, P., Martin, E., Habets, F. and Noilhan, J.: Improvement, calibration and validation of a distributed hydrological model over France, Hydrol Earth Syst Sci, 13(2), 163–181, doi:10.5194/hess-13-163-2009, 2009.

Rao, S. S.: Engineering optimization: theory and practice, 4th ed., John Wiley & Sons, Hoboken, N.J., 2009.

Rauch, W., Thurner, N. and Harremoës, P.: Required accuracy of rainfall data for integrated urban drainage modeling, Water Sci. Technol., 37(11), 81–89, doi:10.1016/S0273-1223(98)00319-9, 1998.

Rebora, N., Molini, L., Casella, E., Comellas, A., Fiori, E., Pignone, F., Siccardi, F., Silvestro, F., Tanelli, S. and Parodi, A.: Extreme Rainfall in the Mediterranean: What Can We Learn from Observations?, J. Hydrometeorol., 14(3), 906–922, doi:10.1175/JHM-D-12-083.1, 2013.

Recouvreur, R.: Étude de réduction de la vulnérabilité du massif de Bouzaréah aux catastrophes naturelles, Rapport de stage de l'ENGREF, ISL Ingenierie., 2005.

Reid, I. and Frostick, L.: Channel form, flows and sediments in deserts, in Arid Zone Geomorphology: Process, Form and Change in Drylands, pp. 205–229, Wiley, Chichester. [online] Available from: https://www.wiley.com/en-

fr/Arid+Zone+Geomorphology%3A+Process%2C+Form+and+Change+in+Drylands%2C+3rd+Edition-p-9780470519080 (Accessed 19 April 2019), 1997.

Rinderer, M., Seibert, J. and Lin, H.: Soil information in hydrologic models: hard data, soft data, and the dialog between experimentalists and modelers, in Hydropedology: Synergistic Integration of Soil Science and Hydrology, pp. 515–536, Elsevier, Waltham., 2012.

Ronda, R. J., van den Hurk, B. J. J. M. and Holtslag, A. A. M.: Spatial Heterogeneity of the Soil Moisture Content and Its Impact on Surface Flux Densities and Near-Surface Meteorology, J. Hydrometeorol., 3(5), 556–570, doi:10.1175/1525-7541(2002)003<0556:SHOTSM>2.0.CO;2, 2002.

Rossi, G., Harmanciogammalu, N. B. and Yevjevich, V.: Coping with Floods, Springer Science & Business Media., 2012.

Roux, H., Labat, D., Garambois, P.-A., Maubourguet, M.-M., Chorda, J. and Dartus, D.: A physically-based parsimonious hydrological model for flash floods in Mediterranean catchments, Nat Hazards Earth Syst Sci, 11(9), 2567–2582, doi:10.5194/nhess-11-2567-2011, 2011.

Rykiel, E. J.: Testing ecological models: the meaning of validation, Ecol. Model., 90(3), 229–244, doi:10.1016/0304-3800(95)00152-2, 1996.

Saltelli, A., Chan, K. and Scott, E. M.: Sensitivity Analysis, Wiley., 2009.

Sardou, M., Maouche, S. and Missoum, H.: Compilation of historical floods catalog of northwestern Algeria: first step towards an atlas of extreme floods, Arab. J. Geosci., 9(6), 455, doi:10.1007/s12517-016-2490-y, 2016.

Saulnier, G.-M. and Le Lay, M.: Sensitivity of flash-flood simulations on the volume, the intensity, and the localization of rainfall in the Cévennes-Vivarais region (France), Water Resour. Res., 45(10), W10425, doi:10.1029/2008WR006906, 2009.

Savenije, H. H. G.: Equifinality, a blessing in disguise?, Hydrol. Process., 15(14), 2835–2838, doi:10.1002/hyp.494, 2001.

Schick, A. P.: Hydrologic aspects of floods in extreme arid environments, in Flood Geomorphology, pp. 189–203, Wiley, New York. [online] Available from: https://www.researchgate.net/publication/282838829_Hydrologic_aspects_of_floods_in_extreme_arid_environments (Accessed 3 March 2019), 1988.

Scofield, R. A. and Oliver, V. J.: A scheme for estimating convective rainfall from satellite imagery, [online] Available from: https://repository.library.noaa.gov/view/noaa/18514 (Accessed 4 March 2019), 1977.

SCS: Urban hydrology for small watersheds, Tech. Release No. 55, Conservation Service, U.S.D.A., Washington, D.C., 1975.

Sharma, K. D.: The hydrological indicators of desertification, J. Arid Environ., 39(2), 121–132, doi:10.1006/jare.1998.0403, 1998.

Singer, M. J. and Le Bissonnais, Y.: Importance of surface sealing in the erosion of some soils from a mediterranean climate, Geomorphology, 24, 79–85, doi:10.1016/S0169-555X(97)00102-5, 1998.

Singh, V. P.: Hydrologic Systems: Watershed modeling, Prentice Hall., 1988.

Singh, V. P.: Computer Models of Watershed Hydrology, Water Resources Publications., 2012.

Sitterson, J., Knightes, C., Parmar, R., Wolfe, K., Muche, M. and Avant, B.: An Overview of Rainfall-Runoff Model Types, Washington, DC. [online] Available from: https://cfpub.epa.gov/si/si_public_record_report.cfm?dirEntryId=339328&Lab=NERL (Accessed 2 March 2019), 2017.

Skinner, B. J. and Murck, B. W.: The Blue Planet: An Introduction to Earth System Science, Wiley., 2011.

Sloto, R. A. and Crouse, M. Y.: HYSEP: A Computer Program for Streamflow Hydrograph Separation and Analysis, USGS Numbered Series, U.S. Geological Survey, Reston, VA. [online] Available from: http://pubs.er.usgs.gov/publication/wri964040 (Accessed 20 April 2019), 1996.

Smith, M. B., Koren, V., Zhang, Z., Zhang, Y., Reed, S. M., Cui, Z., Moreda, F., Cosgrove, B. A., Mizukami, N. and Anderson, E. A.: Results of the DMIP 2 Oklahoma experiments, J. Hydrol., 418–419, 17–48, doi:10.1016/j.jhydrol.2011.08.056, 2012.

Springer, E. P., McGurk, Hawkins, R. H. and Coltharp, G. B.: Curve Numbers from Watershed Data, in Proceedings of Symposium on Watershed Management, p. 938–950, Boise, Idaho., 1980.

Srinivasulu, S. and Jain, A.: Rainfall-Runoff Modelling: Integrating Available Data and Modern Techniques, in Practical Hydroinformatics: Computational Intelligence and Technological Developments in Water Applications, edited by R. J. Abrahart, L. M. See, and D. P. Solomatine, pp. 59–70, Springer Berlin Heidelberg, Berlin, Heidelberg., 2008.

Steenhuis, T., Winchell, M., Rossing, J., Zollweg, J. and Walter, M.: SCS Runoff Equation Revisited for Variable-Source Runoff Areas, J. Irrig. Drain. Eng.-Asce - J IRRIG DRAIN ENG-ASCE, 121, doi:10.1061/(ASCE)0733-9437(1995)121:3(234), 1995.

Stephens, C. M., Johnson, F. M. and Marshall, L. A.: Implications of future climate change for event-based hydrologic models, Adv. Water Resour., 119, 95–110, doi:10.1016/j.advwatres.2018.07.004, 2018.

Stransky, D., Bares, V. and Fatka, P.: The effect of rainfall measurement uncertainties on rainfall-runoff processes modelling, Water Sci. Technol. J. Int. Assoc. Water Pollut. Res., 55(4), 103–111, 2007.

Su, F., Hong, Y. and Lettenmaier, D. P.: Evaluation of TRMM Multisatellite Precipitation Analysis (TMPA) and Its Utility in Hydrologic Prediction in the La Plata Basin, J. Hydrometeorol., 9(4), 622–640, doi:10.1175/2007JHM944.1, 2008.

Sun, J.: Convective-scale assimilation of radar data: progress and challenges, Q. J. R. Meteorol. Soc., 131(613), 3439–3463, doi:10.1256/qj.05.149, 2005.

Sun, X., Mein, R. G., Keenan, T. D. and Elliott, J. F.: Flood estimation using radar and raingauge data, J. Hydrol., 239(1), 4–18, doi:10.1016/S0022-1694(00)00350-4, 2000.

Syed, K. H., Goodrich, D. C., Myers, D. E. and Sorooshian, S.: Spatial characteristics of thunderstorm rainfall fields and their relation to runoff, J. Hydrol., 271(1), 1–21, doi:10.1016/S0022-1694(02)00311-6, 2003.

Tague, C. and Grant, G. E.: Groundwater dynamics mediate low-flow response to global warming in snow-dominated alpine regions, Water Resour. Res., 45(7), doi:10.1029/2008WR007179, 2009.

Taha, A., M. Gresillon, J. and Clothier, B.: Modelling the link between hillslope water movement and stream flow: Application to a small Mediterranean forest watershed, J. Hydrol. - J HYDROL, 203, 11–20, doi:10.1016/S0022-1694(97)00081-4, 1997.

Tallaksen, L. M.: A review of baseflow recession analysis, J. Hydrol., 165(1), 349–370, doi:10.1016/0022-1694(94)02540-R, 1995.

Tarboton, D.: Rainfall Runoff Processes. [online] Available from: https://digitalcommons.usu.edu/cee_facpub/2570, 2003.

Tarolli, P., Borga, M., Morin, E. and Delrieu, G.: Analysis of flash flood regimes in the North-Western and South-Eastern Mediterranean regions, Nat. Hazards Earth Syst. Sci., 12(5), 1255–1265, doi:https://doi.org/10.5194/nhess-12-1255-2012, 2012.

Tramblay, Y., Bouvier, C., Martin, C., Didon-Lescot, J.-F., Todorovik, D. and Domergue, J.-M.: Assessment of initial soil moisture conditions for event-based rainfall–runoff modelling, J. Hydrol., 387(3), 176–187, doi:10.1016/j.jhydrol.2010.04.006, 2010.

Tramblay, Y., Bouaicha, R., Brocca, L., Dorigo, W., Bouvier, C., Camici, S. and Servat, E.: Estimation of antecedent wetness conditions for flood modelling in northern Morocco, Hydrol Earth Syst Sci, 16(11), 4375–4386, doi:10.5194/hess-16-4375-2012, 2012.

Travi, Y., Lavabre, J., Blavoux, B. and Martin, C.: Traçage chimique et isotopique (Cl", lsO) d'une crue d'automne sur un petit bassin versant Méditerranéen incendié, Journal des Sciences Hydrologiques, 39(6), 605–619, 1994.

Troutman, B. M.: Runoff prediction errors and bias in parameter estimation induced by spatial variability of precipitation, Water Resour. Res., 19(3), 791–810, doi:10.1029/WR019i003p00791, 1983.

Tsintikidis, D., Georgakakos, K. P., Artan, G. A. and Tsonis, A. A.: A feasibility study on mean areal rainfall estimation and hydrologic response in the Blue Nile region using METEOSAT images, J. Hydrol., 221(3), 97–116, doi:10.1016/S0022-1694(99)00071-2, 1999.

Tukey, J. W.: Exploratory Data Analysis, Addison-Wesley Publishing Company., 1977.

UNESCO and World Meteorological Organization: Results of the International Hydrological Programme of UNESCO, 1993-1998 - UNESCO Digital Library, p. 10, Geneva. [online] Available from: https://unesdoc.unesco.org/ark:/48223/pf0000114617 (Accessed 28 February 2019), 1999.

Vannier, O., Braud, I. and Anquetin, S.: Regional estimation of catchment-scale soil properties by means of streamflow recession analysis for use in distributed hydrological models, Hydrol. Process., 28(26), 6276–6291, doi:10.1002/hyp.10101, 2014.

Vaze, J., Jordan, P., Beecham, R., Frost, A. and Summerell, G.: Guidelines for rainfall-runoff modelling: towards best practice model application. [online] Available from: https://publications.csiro.au/rpr/pub?list=BRO&pid=csiro:EP117631 (Accessed 2 March 2019), 2011.

Vinogradov, Y. B., Semenova, O. M. and Vinogradova, T. A.: An approach to the scaling problem in hydrological modelling: the deterministic modelling hydrological system, Hydrol. Process., 25(7), 1055–1073, doi:10.1002/hyp.7901, 2011.

Vischel, T. and Lebel, T.: Assessing the water balance in the Sahel: Impact of small scale rainfall variability on runoff. Part 2: Idealized modeling of runoff sensitivity, J. Hydrol., 333(2), 340–355, doi:10.1016/j.jhydrol.2006.09.007, 2007.

Vischel, T., Pegram, G. G. S., Sinclair, S., Wagner, W. and Bartsch, A.: Comparison of soil moisture fields estimated by catchment modelling and remote sensing: a case study in South Africa, Hydrol. Earth Syst. Sci., 12(3), 751–767, doi:https://doi.org/10.5194/hess-12-751-2008, 2008.

Viviroli, D., Mittelbach, H., Gurtz, J. and Weingartner, R.: Continuous simulation for flood estimation in ungauged mesoscale catchments of Switzerland – Part II: Parameter regionalisation and flood estimation results, J. Hydrol., 377(1–2), 208–225, doi:10.1016/j.jhydrol.2009.08.022, 2009.

Vivoni, E. R., Entekhabi, D. and Hoffman, R. N.: Error Propagation of Radar Rainfall Nowcasting Fields through a Fully Distributed Flood Forecasting Model, J. Appl. Meteorol. Climatol., 46(6), 932–940, doi:10.1175/JAM2506.1, 2007.

Wagner, W., Blöschl, G., Pampaloni, P., Calvet, J.-C., Bizzarri, B., Wigneron, J.-P. and Kerr, Y.: Operational readiness of microwave remote sensing of soil moisture for hydrologic applications, Hydrol. Res., 38(1), 1–20, doi:10.2166/nh.2007.029, 2007.

Wainwright, J. and Mulligan, M.: Environmental Modelling: Finding Simplicity in Complexity, John Wiley & Sons., 2013.

Wang, M. and Hjelmfelt, A. T.: DEM Based Overland Flow Routing Model, J. Hydrol. Eng., 3(1), 1–8, doi:10.1061/(ASCE)1084-0699(1998)3:1(1), 1998.

Watson, F. G. R., Grayson, R. B., Vertessy, R. A. and McMahon, T. A.: Large-scale distribution modelling and the utility of detailed ground data, Hydrol. Process., 12(6), 873–888, doi:10.1002/(SICI)1099-1085(199805)12:6<873::AID-HYP660>3.0.CO;2-A, 1998.

Weiler, M. and McDonnell, J.: Virtual experiments: a new approach for improving process conceptualization in hillslope hydrology, J. Hydrol., 285(1), 3–18, doi:10.1016/S0022-1694(03)00271-3, 2004.

Western, A. W. and Blöschl, G.: On the spatial scaling of soil moisture, J. Hydrol., 217(3–4), 203–224, doi:10.1016/S0022-1694(98)00232-7, 1999.

Western, A. W., Grayson, R. B. and Blöschl, G.: Scaling of Soil Moisture: A Hydrologic Perspective, Annu. Rev. Earth Planet. Sci., 30(1), 149–180, doi:10.1146/annurev.earth.30.091201.140434, 2002.

Wetzel, P. J. and Chang, J.-T.: Concerning the Relationship between Evapotranspiration and Soil Moisture, J. Clim. Appl. Meteorol., 26(1), 18–27, doi:10.1175/1520-0450(1987)026<0018:CTRBEA>2.0.CO;2, 1987.

Wilk, J., Kniveton, D., Andersson, L., Layberry, R., Todd, M. C., Hughes, D., Ringrose, S. and Vanderpost, C.: Estimating rainfall and water balance over the Okavango River Basin for hydrological applications, J. Hydrol., 331(1), 18–29, doi:10.1016/j.jhydrol.2006.04.049, 2006.

Williams, J. R. and LaSeur, W. V.: Water Yield Model Using SCS Curve Numbers, J. Hydraul. Div., 102(9), 1241–1253, 1976.

Wilson, C. B., Valdes, J. B. and Rodriguez-Iturbe, I.: On the influence of the spatial distribution of rainfall on storm runoff, Water Resour. Res., 15(2), 321–328, doi:10.1029/WR015i002p00321, 1979.

Winkler, R., Moore, D. R., Redding, T. E., Spittlehouse, D. L., Carlyle-Moses, D. E. and Smerdon, B. D.: Hydrologic Processes and Watershed Response Chapter 6., 2010.

Winter, T. C., Rosenberry, D. O. and LaBaugh, J. W.: Where Does the Ground Water in Small Watersheds Come From?, Groundwater, 41(7), 989–1000, doi:10.1111/j.1745-6584.2003.tb02440.x, 2003.

Wittenberg, H.: Effects of season and man-made changes on baseflow and flow recession: case studies, Hydrol. Process., 17(11), 2113–2123, doi:10.1002/hyp.1324, 2003.

Wittenberg, H. and Sivapalan, M.: Watershed groundwater balance estimation using streamflow recession analysis and baseflow separation, J. Hydrol., 219(1), 20–33, doi:10.1016/S0022-1694(99)00040-2, 1999.

Woods, R.: Hydrologic Concepts of Variability and Scale, in Encyclopedia of Hydrological Sciences, American Cancer Society., 2006.

Woodward, D. E. and Gburek, W. J.: Progress Report ARS/SCS Runoff Curve Number Work Group, pp. 378–382, ASCE. [online] Available from: https://cedb.asce.org/CEDBsearch/record.jsp?dockey=0077547 (Accessed 23 April 2019), 1992.

Woolhiser, D. A.: KINEROS: A Kinematic Runoff and Erosion Model : Documentation and User Manual, U.S. Department of Agriculture, Agricultural Research Service., 1989.

Wu, H., Adler, R. F., Hong, Y., Tian, Y. and Policelli, F.: Evaluation of Global Flood Detection Using Satellite-Based Rainfall and a Hydrologic Model, J. Hydrometeorol., 13(4), 1268–1284, doi:10.1175/JHM-D-11-087.1, 2012.

Xie, H., Shen, Z., Chen, L., Lai, X., Qiu, J., Wei, G., Dong, J., Peng, Y. and Chen, X.: Parameter Estimation and Uncertainty Analysis: A Comparison between Continuous and Event-Based Modeling of Streamflow Based on the Hydrological Simulation Program–Fortran (HSPF) Model, Water, 11(1), 171, doi:10.3390/w11010171, 2019.

Xu: Textbook of Hydrologic Models, Uppsala University, Sweden. [online] Available from: https://www.scribd.com/document/170746718/Hydrology-Textbook (Accessed 2 March 2019), 2002.

Yair, A. and Kossovsky, A.: Climate and surface properties: Hydrological response of small and and semi-arid watersheds, Geomorphology, 42, 43–57, doi:10.1016/S0169-555X(01)00072-1, 2002.

Yair, A. and Raz-Yassif, N.: Hydrological processes in a small arid catchment: scale effects of rainfall and slope length, Geomorphology, 61(1–2), 155–169, doi:10.1016/j.geomorph.2003.12.003, 2004.

Yao, C., Zhang, K., Yu, Z., Li, Z. and Li, Q.: Improving the flood prediction capability of the Xinanjiang model in ungauged nested catchments by coupling it with the geomorphologic instantaneous unit hydrograph, J. Hydrol., 517, 1035–1048, doi:10.1016/j.jhydrol.2014.06.037, 2014.

Yapo, P. O., Gupta, H. V. and Sorooshian, S.: Multi-objective global optimization for hydrologic models, J. Hydrol., 204(1), 83–97, doi:10.1016/S0022-1694(97)00107-8, 1998.

Young, A. R.: Stream flow simulation within UK ungauged catchments using a daily rainfall-runoff model, J. Hydrol., 320(1), 155–172, doi:10.1016/j.jhydrol.2005.07.017, 2006.

Yu, B.: Theoretical Justification of SCS Method for Runoff Estimation, J. Irrig. Drain. Eng., 124(6), 306–310, doi:10.1061/(ASCE)0733-9437(1998)124:6(306), 1998.

Yu, D., Xie, P., Dong, X., Hu, X., Liu, J., Li, Y., Peng, T., Ma, H., Wang, K. and Xu, S.: Improvement of the SWAT model for event-based flood simulation on a sub-daily timescale, Hydrol. Earth Syst. Sci., 22(9), 5001–5019, doi:https://doi.org/10.5194/hess-22-5001-2018, 2018.

Zech, Y., Sillen, X., Debources, C. and Van Hauwaert, A.: Rainfall-Runoff Modelling of Partly Urbanized Watersheds: Comparison Between a Distributed Model Using GIS and Other Models Sensitivity Analysis, Water Sci. Technol., 29(1–2), 163–170, doi:10.2166/wst.1994.0662, 1994.

Zehe, E. and Blöschl, G.: Predictability of hydrologic response at the plot and catchment scales: Role of initial conditions, Water Resour. Res., 40(10), doi:10.1029/2003WR002869, 2004.

Zehe, E., Becker, R., Bárdossy, A. and Plate, E.: Uncertainty of simulated catchment runoff response in the presence of threshold processes: Role of initial soil moisture and precipitation, J. Hydrol., 315(1), 183–202, doi:10.1016/j.jhydrol.2005.03.038, 2005.

Zhang, X., Drake, N. A. and Wainwright, J.: Spatial Modelling and Scaling Issues, in Environmental Modelling - Finding Simplicity in Complexity, pp. 69–90, John Wiley & Sons., 2013.

Zimmermann, H.-J.: An application-oriented view of modeling uncertainty, Eur. J. Oper. Res., 122(2), 190–198, doi:10.1016/S0377-2217(99)00228-3, 2000.

Appendix

A. Supplementary results for model calibration on Real Collobrier catchment (chapter 3)

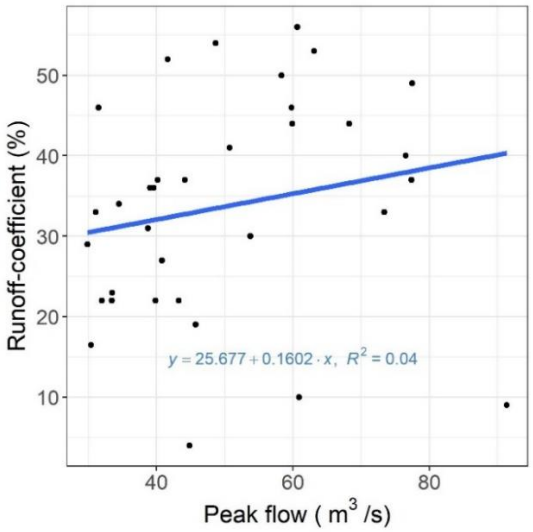

Figure A 1: Correlation between runoff coefficient and peak flow of the events in Pont de Fer catchment

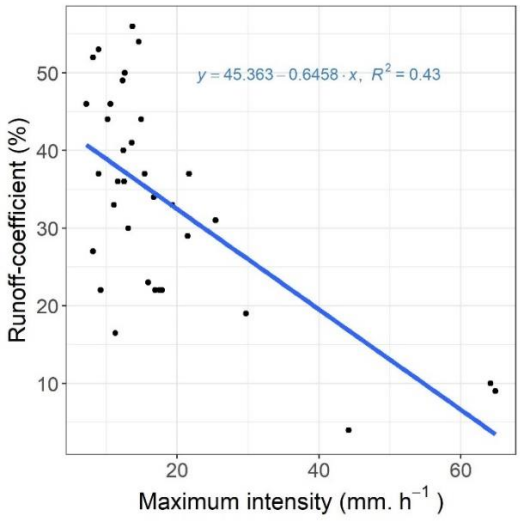

Figure A 2: Correlation between runoff coefficient and maximum rainfall intensity of the events in Pont de Fer catchment

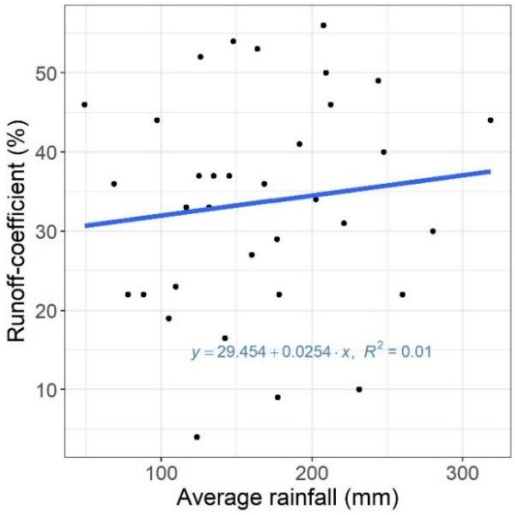

Figure A 3: Correlation between runoff coefficient and average rainfall of the events in Pont de Fer catchment

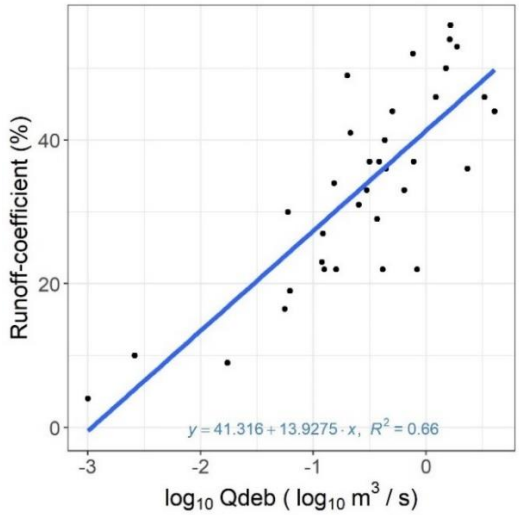

Figure A 4: Correlation between runoff coefficient and base flow of the events in Pont de Fer catchment

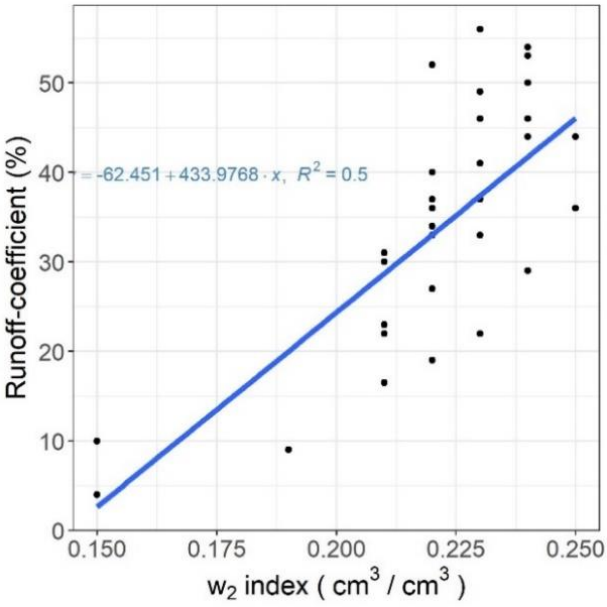

Figure A 5: Correlation between runoff coefficient and volumetric water content of the events in Pont de Fer catchment

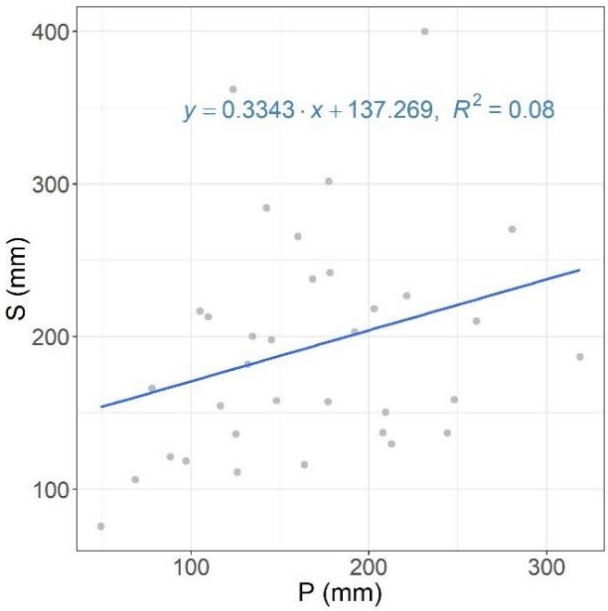

Figure A 6: Correlation between S and average rainfall of the events in Pont de Fer catchment.

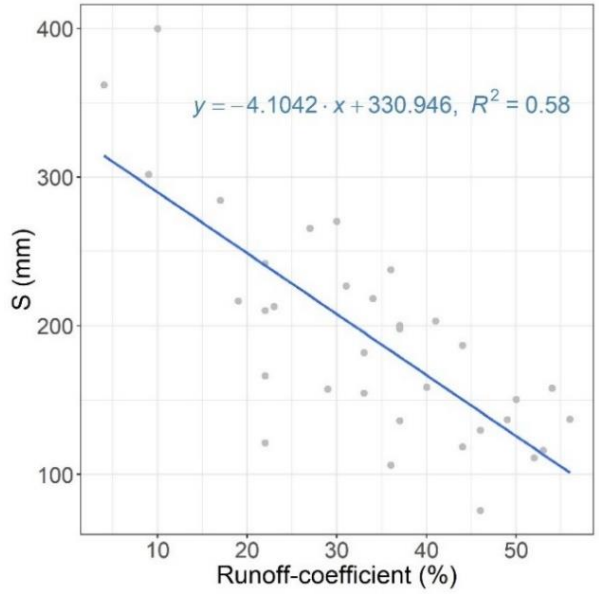

Figure A 7: Correlation between S and runoff coefficient of the events in Pont de Fer catchment.

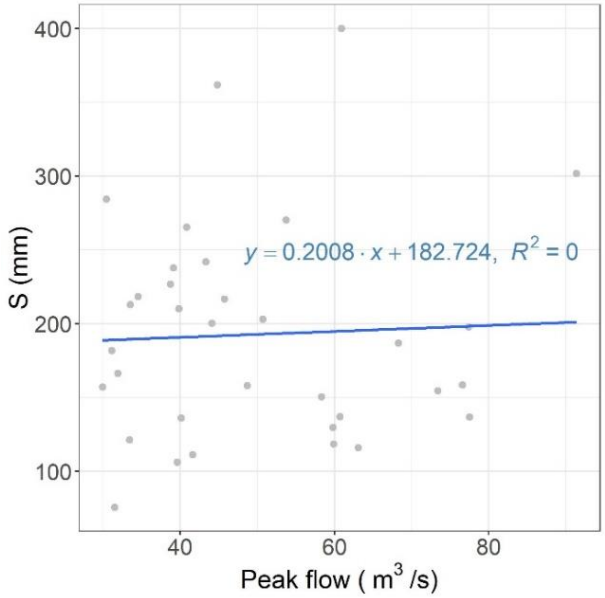

Figure A 8: Correlation between S and peak flow of the events in Pont de Fer catchment

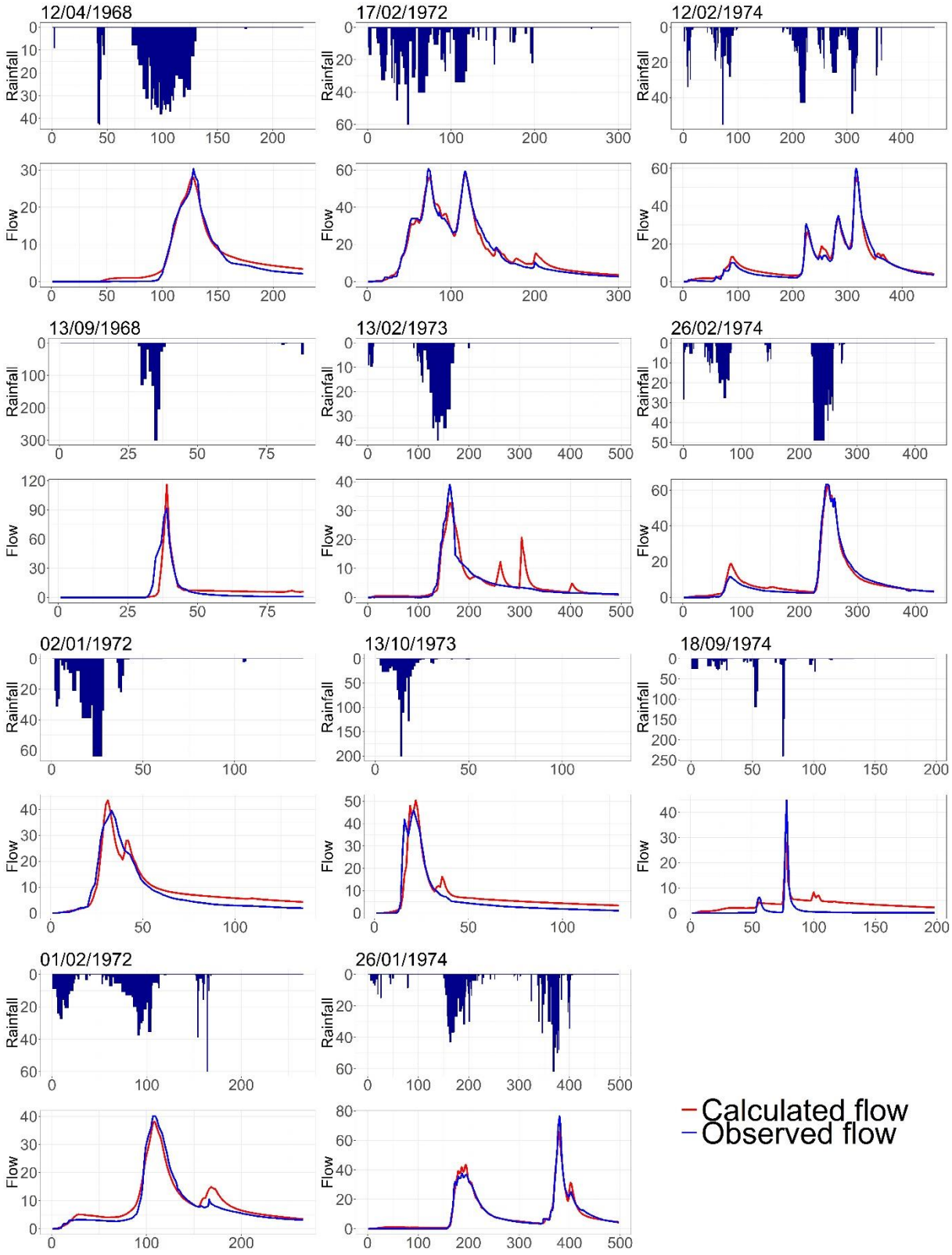

Figure A 9 : Observed and simulated hydrographs at the 30-minutes time step for the first 11 events, the plotted rain corresponded to the rainfall measured in gauge 4 (Guérin) located near the center of the catchment.

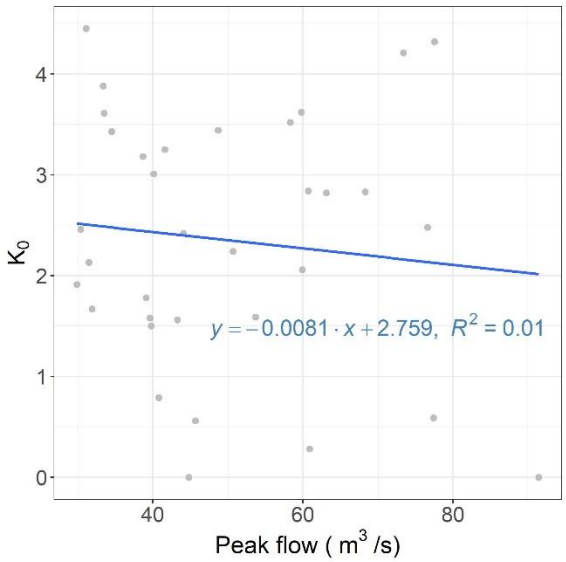

Figure A 10: Correlation between K_0 and peak flow of the events in Pont de Fer catchment.

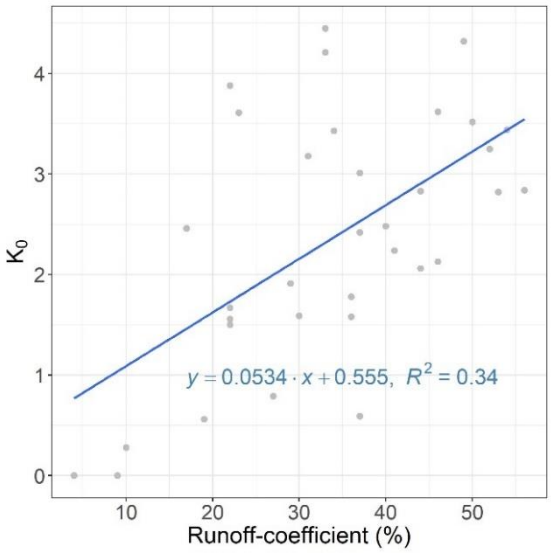

Figure A 11: Correlation between K_0 and runoff coefficient of the events in Pont de Fer catchment.

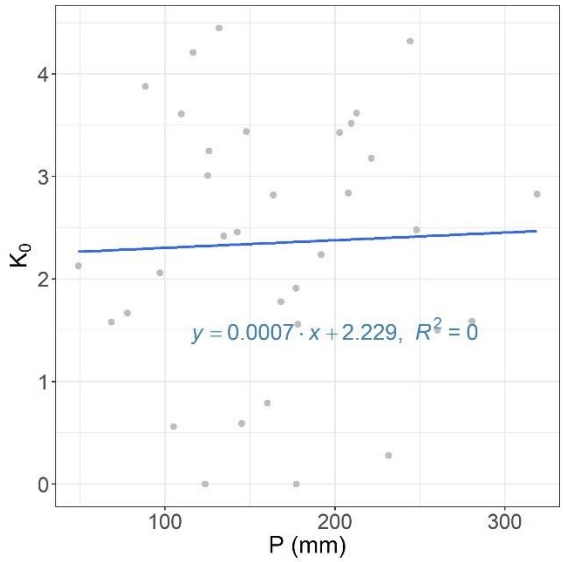

Figure A 12: Correlation between K_0 and average rainfall of the events in Pont de Fer catchment.

B. Supplementary results for spatial variability on sub-catchment scale (chapter 4)

Table A 1: The characteristics of all flood events in Rimbaud sub-catchment. P: cumulated precipitation; Vr: runoff volume; Rc: runoff coefficient; w_2*: volumetric water content of the root layer.*

Event	Starting date	Finishing date	P (mm)	Vr ($10^3.m^3$)	Rc (%)	Peak flow ($m^3.s^{-1}$)	w_2 ($cm^3.cm^{-3}$)	Base flow ($m^3.s^{-1}$)
1	13/09/1968 19:45	17/09/1968 23:45	187.6	110.7	41.0	14.2	0.20	0.00
2	01/01/1972 00:00	05/01/1972 03:00	80.5	100.5	86.7	1.9	0.25	0.52
3	01/02/1972 19:45	07/02/1972 05:15	177.7	174.7	68.3	2.2	0.22	0.04
4	26/12/1972 01:00	31/12/1972 00:00	315.8	299.6	65.9	3.4	0.22	0.01
5	14/01/1973 21:30	19/01/1973 19:15	170.7	159.5	64.9	2.9	0.23	0.07
6	02/10/1973 14:30	05/10/1973 03:00	150.6	50.7	23.4	7.5	0.16	0.00
7	13/10/1973 07:30	15/10/1973 23:00	139.7	98.2	48.8	2.7	0.21	0.00
8	02/02/1974 00:45	05/02/1974 15:45	149.6	154.0	71.5	2.9	0.25	0.15
9	16/02/1974 11:15	21/02/1974 10:00	178.3	175.2	68.2	2.9	0.24	0.14
10	04/02/1976 07:00	06/02/1976 17:00	119.5	107.6	62.5	2.9	0.25	0.16
11	15/04/1976 14:45	18/04/1976 06:45	161.3	142.3	61.3	4.2	0.21	0.02
12	24/10/1976 02:45	31/10/1976 21:30	364.9	370.1	70.4	2.9	0.23	0.06
13	01/01/1977 08:00	03/01/1977 16:00	73	45.7	43.4	2.0	0.23	0.42
14	06/12/1977 03:00	10/12/1977 21:45	245.6	219.4	62.0	2.4	0.22	0.01
15	26/10/1979 00:30	30/10/1979 14:00	241.9	240.7	69.1	3.4	0.22	0.02
16	28/01/1986 22:45	01/02/1986 23:45	200.6	144.1	49.9	2.9	0.21	0.01
17	09/11/1987 16:30	12/11/1987 07:00	112.1	84.8	52.5	2.6	0.22	0.02
18	24/11/1990 08:15	01/12/1990 02:30	120.7	110.7	63.7	2.7	0.21	0.00
19	08/12/1990 23:00	13/12/1990 18:15	98.4	104.5	73.7	5.9	0.22	0.03
20	12/10/1991 10:30	17/10/1991 09:30	81.7	69.0	58.6	2.2	0.20	0.14
21	17/10/1992 02:00	19/10/1992 09:00	75.6	61.5	56.5	2.8	0.22	0.03
22	30/10/1992 12:00	04/11/1992 04:15	136.7	137.5	69.9	3.7	0.22	0.02
23	24/04/1993 15:45	04/05/1993 13:30	208.1	240.5	80.3	2.8	0.21	0.01
24	06/01/1994 02:45	09/01/1994 08:15	122.9	100.4	56.7	2.2	0.21	0.01
25	10/01/1996 04:45	14/01/1996 15:30	189.6	215.6	79.0	2.9	0.23	0.10
26	20/01/1996 10:45	27/01/1996 20:00	224.8	276.0	85.3	2.0	0.23	0.05
27	17/09/1996 19:15	24/09/1996 18:30	199.9	119.1	41.4	2.1	0.19	0.00
28	16/11/1996 05:30	19/11/1996 23:30	99.2	116.5	81.6	3.8	0.23	0.08
29	06/01/1997 21:15	11/01/1997 05:30	110.4	74.8	47.1	2.2	0.24	0.17
30	29/04/1998 15:15	04/05/1998 17:15	202.4	173.1	59.4	4.5	0.19	0.00
31	17/01/1999 07:30	20/01/1999 06:00	189.5	151.4	55.5	4.3	0.23	0.04
32	09/10/2002 02:00	13/10/2002 00:30	253.6	169.3	46.4	9.5	0.20	0.00

Table A 2: The characteristics of all flood events in Maurets sub-catchment. P: cumulated precipitation; Vr: runoff volume; Rc: runoff coefficient; w_2*: volumetric water content of the root layer.*

Event	Starting date	Finishing date	P (mm)	Vr ($10^3.m^3$)	Rc (%)	Peak flow ($m^3.s^{-1}$)	w_2 ($cm^3.cm^{-3}$)	Base flow ($m^3.s^{-1}$)
1	08/01/1970 12:30	17/01/1970 17:30	261.0	635.7	29.0	2.9	0.232	0.189
2	25/12/1970 10:15	31/12/1970 20:15	179.3	269.3	17.9	3.3	0.193	0.0051
3	01/01/1972 01:15	06/01/1972 12:30	87.0	280.2	38.3	6.5	0.244	2.09
4	01/02/1972 16:30	07/02/1972 08:00	135.9	583.2	51.1	3.7	0.221	0.14
5	17/02/1972 13:15	23/02/1972 19:45	249.8	1285.8	61.3	7.3	0.228	0.409
6	19/12/1973 11:30	27/12/1973 21:30	242.4	574.7	28.2	3.9	0.19	0.0061
7	26/01/1974 07:15	05/02/1974 16:00	258.1	809.2	37.3	4.8	0.217	0.087
8	26/02/1974 12:45	07/03/1974 15:00	196.1	694.4	42.2	5.3	0.232	0.478
9	24/10/1976 01:30	01/11/1976 01:30	356.7	1401.8	46.8	7.1	0.228	0.0806
10	11/01/1978 12:00	23/01/1978 16:45	313.9	1515.5	57.5	7.8	0.211	0.0251
11	08/02/1978 22:00	13/02/1978 08:15	159.4	704.2	52.6	6.2	0.215	0.208
12	23/10/1979 11:45	31/10/1979 4:00	245.8	590.6	28.6	4.1	0.219	0.0219
13	30/11/1984 11:15	03/12/1984 23:00	101.8	198.2	23.2	4.5	0.219	0.059
14	04/03/1985 12:15	14/03/1985 08:45	101.3	457.8	53.8	4.6	0.228	0.127
15	13/01/1988 13:15	17/01/1988 07:00	139.7	434.9	37.1	5.4	0.216	0.0494
16	24/04/1993 13:00	04/05/1993 15:30	233.4	774.3	39.5	5.3	0.208	0.0212
17	04/01/1994 15:00	09/01/1984 13:15	109.2	308.8	33.7	5.2	0.204	0.0175
18	03/02/1994 16:15	08/02/1994 01:45	133.9	478.1	42.5	3.6	0.211	0.0527
19	19/10/1994 14:00	25/10/1994 12:15	218.0	250.8	13.7	3.7	0.183	0.0015
20	10/01/1996 04:00	18/01/1996 09:15	163.9	685.9	49.8	6.2	0.232	0.157
21	20/01/1996 10:45	31/01/1996 10:00	250.9	1039.1	49.3	3.5	0.233	0.2
22	10/11/1996 09:00	29/11/1996 19:00	175.6	378.4	25.6	3.3	0.21	0.0153
23	01/01/1997 00:30	11/01/1997 13:45	183.9	639.6	41.4	6.5	0.232	0.546
24	17/01/1999 06:30	20/01/1999 08:15	132.8	338.9	30.4	6.0	0.227	0.0418
25	17/10/1999 13:15	27/10/1999 01:30	246.1	308.5	14.9	3.9	0.182	0.0019
26	05/11/2000 22:00	12/11/2000 06:00	105.9	151.4	17.0	4.4	0.213	0.009
27	12/11/2000 07:15	25/11/2000 21:30	165.4	468.7	33.7	4.7	0.231	0.0356
28	24/12/2000 05:15	31/12/2000 01:45	145.9	547.1	44.6	4.2	0.213	0.0364
29	24/01/2001 03:15	31/01/2001 09:30	113.9	387.5	40.5	4.9	0.221	0.105
30	09/10/2002 01:15	13/10/2002 07:30	223.4	176.3	9.4	4.4	0.179	0.0001
31	26/01/2006 12:30	01/02/2006 23:45	255.0	823.9	38.5	5.2	0.205	0.0102
32	12/12/2008 18:15	18/12/2008 13:15	185.8	565.0	36.2	4.7	0.24	0.17

Table A 3: The characteristics of all flood events in Malière sub-catchment. P: cumulated precipitation; Vr: runoff volume; Rc: runoff coefficient; w_2*: volumetric water content of the root layer.*

Event	Starting date		Finishing date		Pmoy (mm)	Vr ($10^3.m^3$)	Rc (%)	Peak flow ($m^3.s^{-1}$)	w_2 ($cm^3.cm^{-3}$)	Base flow ($m^3.s^{-1}$)
1	10/2/1966	23:15	15/02/1966	17:15	159.4	776.8	39	24.2	0.215	0.079
2	30/10/1966	18:00	08/11/1996	13:00	133.5	741.9	45	13	0.221	0.1
3	17/02/1972	13:15	23/02/1972	20:00	213.5	1674.2	63	11.4	0.228	0.4
4	11/01/1973	11:15	20/01/1973	04:15	166.65	1014.6	49	8.2	0.216	0.22
5	12/02/1974	02:15	21/02/1974	15:45	246.3	1692	55	7.8	0.227	0.33
6	26/02/1974	12:45	07/03/1974	15:15	177.3	1626.2	74	12.8	0.23	0.37
7	05/02/1975	02:00	09/02/1975	06:15	155.5	868.4	45	10.3	0.216	0.03
8	24/10/1976	01:30	01/11/1976	01:30	324.25	1964.8	49	12.7	0.231	0.136
9	01/01/1977	03:00	09/01/1977	03:45	143.6	1143.8	64	8.1	0.233	0.91
10	06/12/1977	02:00	11/12/1977	15:15	244.6	1008.4	33	17.3	0.223	0.03
11	13/01/1988	13:15	17/01/1988	07:00	109.9	425.4	31	9.1	0.216	0.08
12	08/12/1990	23:00	13/12/1990	18:45	93.6	291.1	25	8.7	0.224	0.08
13	24/04/1993	13:00	04/05/1993	15:30	203.6	1082.7	43	8.1	0.218	0.04
14	10/01/1996	04:00	18/01/1996	09:15	167.4	1126.2	54	11.4	0.232	0.36
15	20/01/1996	10:45	31/01/1996	10:00	264.6	1808.2	55	10.5	0.231	0.24
16	10/11/1996	09:00	29/11/1996	19:00	164.6	698.2	34	13.6	0.211	0.04
17	01/01/1997	00:30	11/01/1997	13:45	200.1	1596.4	64	12.2	0.232	1.05
18	29/04/1998	14:00	05/05/1998	17:30	185.7	581.9	25	13.9	0.193	0.02
19	17/01/1999	06:30	20/01/1999	08:15	164.2	736.2	36	9.6	0.232	0.09
20	24/12/2000	05:15	31/12/2000	01:45	145.3	764.1	42	25.6	0.214	0.05
21	13/12/2008	18:15	18/12/2008	13:15	185.8	1308.7	57	14.5	0.24	0.25

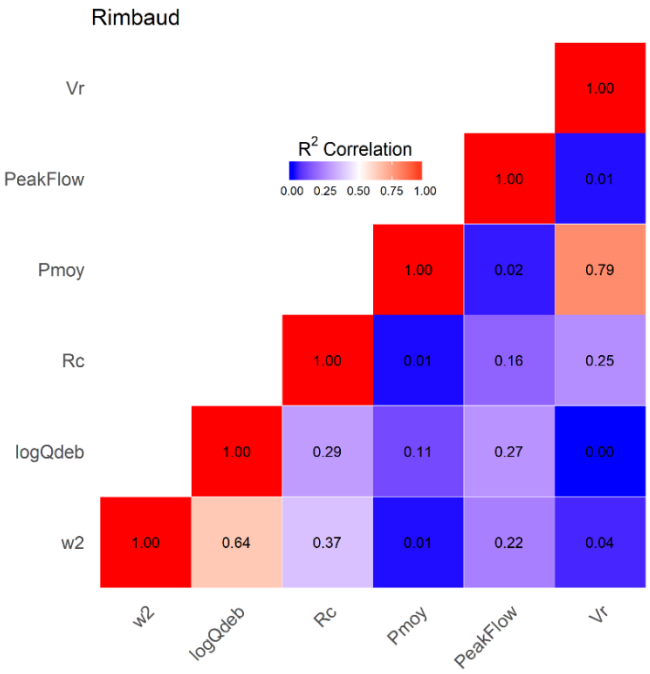

Figure A 13: Correlation between each pair of indexes in the Rimbaud catchment. w_2: volumetric water content ($cm^3.cm^{-3}$); logQdeb: log_{10} base flow (log_{10} $m^3.s^{-1}$); Rc: runoff coefficient (%); Pmoy: average areal cumulated precipitation (mm); PeakFlow: peak flow ($m^3.s^{-1}$); Vr: runoff volume ($10^3.m^3$).

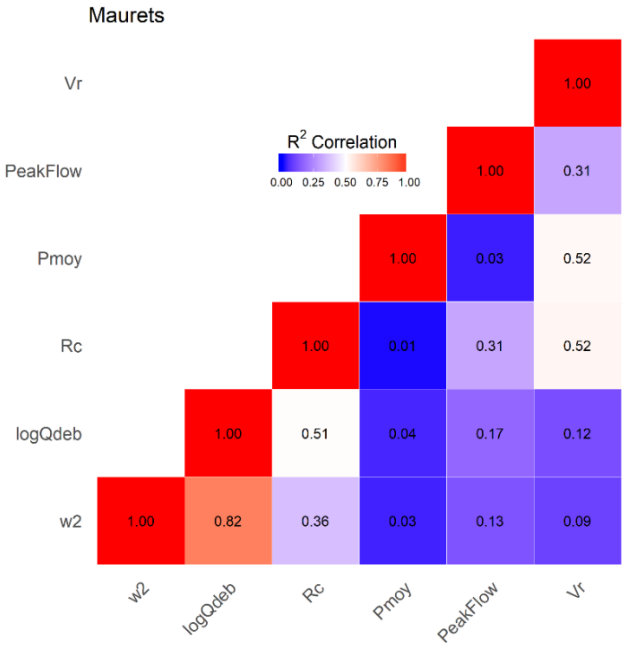

Figure A 14: Correlation between each pair of indexes in the Maurets catchment. w_2: volumetric water content ($cm^3.cm^{-3}$); logQdeb: log_{10} base flow (log_{10} $m^3.s^{-1}$); Rc: runoff coefficient (%); Pmoy: average areal cumulated precipitation (mm); PeakFlow: peak flow ($m^3.s^{-1}$); Vr: runoff volume ($10^3.m^3$).

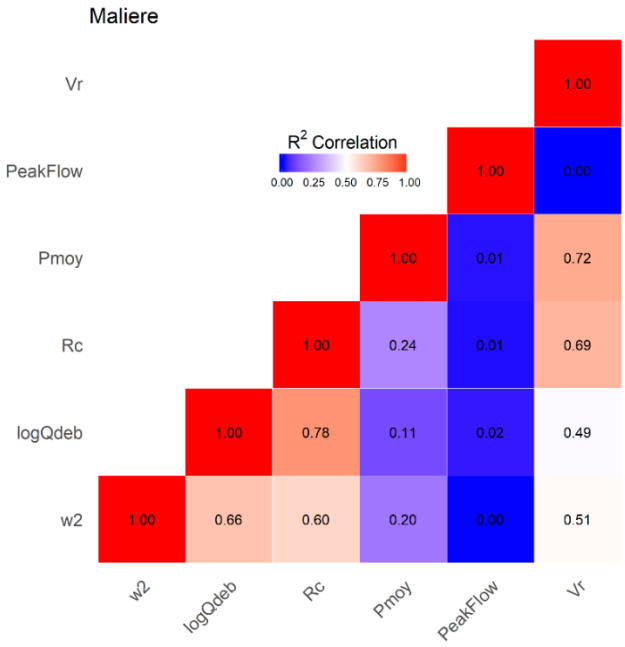

Figure A 15: Correlation between each pair of indexes in the Malière catchment. w_2: volumetric water content ($cm^3.cm^{-3}$); logQdeb: log_{10} base flow (log_{10} $m^3.s^{-1}$); Rc: runoff coefficient (%); Pmoy: average areal cumulated precipitation (mm); PeakFlow: peak flow ($m^3.s^{-1}$); Vr: runoff volume ($10^3.m^3$).

C. Supplementary results for spatial variability on catchment scale (chapter 5)

Table A 4: The characteristics of all flood events in Aille catchment. P: cumulated precipitation; Vr: runoff volume; Rc: runoff coefficient.

Event	Starting date	Finishing date	P (mm)	Vr ($10^3.m^3$)	Rc (%)	Base flow ($m^3.s^{-1}$)	Hu2 index (%)	Peak flow ($m^3.s^{-1}$)
1	07/01/1997 00:00	13/01/1997 22:00	46.8	8485.2	0.79	11	66	194
2	17/01/1999 00:00	23/01/1999 00:00	93.3	12055	0.56	1	61.7	260
3	18/10/1999 01:00	27/10/1999 23:00	231.6	21155.4	0.4	0	56	278
4	22/12/2000 00:00	31/12/2000 23:00	139.5	19705	0.62	1	58.4	291
5	26/01/2001 00:00	04/02/2001 00:00	75.7	10245.4	0.59	3	59.4	152
6	19/01/2003 23:00	29/01/2003 00:00	35.1	3010.4	0.37	1	59	46
7	01/09/2005 00:00	17/09/2005 23:00	203.9	11189.1	0.24	0	42.4	168
8	02/12/2005 00:00	07/12/2005 23:00	60.6	5498.2	0.4	1	59.3	119
9	20/01/2006 00:00	09/02/2006 23:00	115	17143.8	0.65	1	57.1	112
10	03/11/2008 00:00	08/11/2008 22:00	90.2	11909.1	0.58	13	60	237
11	09/12/2008 00:00	20/12/2008 21:00	159.4	33730.8	0.92	1	60.1	207
12	21/10/2009 01:00	28/10/2009 19:00	99.5	9745.9	0.43	0	52.7	320
13	14/06/2010 00:00	21/06/2010 23:00	237.5	28681.6	0.53	0	50.4	520
14	01/11/2011 23:00	11/11/2011 23:00	353.2	62469.8	0.77	0	53.9	306
15	25/10/2012 23:00	27/10/2012 23:00	86.9	9467.2	0.47	1	55.9	312
16	09/11/2012 00:00	13/11/2012 00:00	47.5	5039.1	0.46	1	60.4	106
17	26/11/2012 12:00	30/11/2012 11:00	92.7	14839.2	0.7	1	59.3	278
18	12/12/2012 23:00	15/12/2012 23:00	64.7	10962	0.74	1	59.1	193
19	19/01/2013 00:00	25/01/2013 12:00	85.6	14522.4	0.74	1	58.3	149

Table A 5: The characteristics of all flood events in Allier catchment. P: cumulated precipitation; Vr: runoff volume; Rc: runoff coefficient.

Event	Starting date	Finishing date	P (mm)	Vr ($10^3.m^3$)	Rc (%)	Base flow ($m^3.s^{-1}$)	Hu2 index (%)	Peak flow ($m^3.s^{-1}$)
1	11/11/1996 00:00	14/11/1996 00:00	321.5	36682	0.35	2.79	48.7	436.01
2	17/05/1999 00:00	22/05/1999 12:00	338.8	47122	0.43	7.2	51.8	360.2
3	20/10/1999 00:00	26/10/1999 00:00	182.1	23910	0.41	4.8	49.2	156.47
4	10/10/2000 00:00	22/10/2000 00:00	105.5	15577	0.46	7.8	51.1	37.5
5	29/11/2000 00:00	11/12/2000 00:00	89.3	22360	0.77	17.6	56.4	60.5
6	17/10/2001 00:00	26/10/2001 00:00	228.2	38566	0.52	1.3	44.8	393.17
7	20/11/2002 00:00	30/11/2002 00:00	135.7	33336	0.76	14.7	53.6	129.3
8	26/12/2002 00:00	01/01/2003 00:00	55.3	12016	0.67	18.5	52.8	67.7
9	21/11/2003 00:00	29/11/2003 00:00	196	47453	0.75	9.7	49	334.3
10	29/11/2003 00:00	09/12/2003 00:00	235.4	66454	0.87	24.4	55.4	335.9
11	30/03/2004 00:00	08/04/2004 00:00	117.8	24329	0.64	8.3	48.2	68.3
12	18/10/2006 00:00	23/10/2006 00:00	138.1	20084	0.45	4.2	48.3	153.32
13	30/10/2008 00:00	08/11/2008 00:00	410.8	81425	0.61	4	46.7	682

Table A 6: The characteristics of all flood events in Verdouble catchment. P: cumulated precipitation; Vr: runoff volume; Rc: runoff coefficient.

Event	Starting date	Finishing date	P (mm)	Vr ($10^3.m^3$)	Rc (%)	Base flow ($m^3.s^{-1}$)	Hu2 index (%)	Peak flow ($m^3.s^{-1}$)
1	08/03/1987 12:30	13/03/1987 19:00	48.4	6805.5	0.47	3.3	64	58.1
2	14/12/1995 22:30	17/12/1995 23:30	83.2	23904.4	0.96	2.6	69	754.1
3	01/02/1996 03:30	05/02/1996 23:30	74.4	19578.7	0.88	22	74	426
4	05/12/1996 21:30	08/12/1996 07:00	130.1	16341.7	0.42	2.5	71	600.8
5	09/11/1999 21:30	16/11/1999 17:00	357.5	43132.9	0.4	0.2	55	898.8
6	20/12/2000 19:30	26/12/2000 22:30	192.7	19190.9	0.33	0.1	62	258.8
7	08/04/2002 21:30	14/04/2002 00:00	164.2	17950.7	0.36	0.001	68	285.3
8	01/12/2003 21:30	05/12/2003 22:30	155.5	12422	0.27	0.001	65	212.6
9	19/02/2004 23:00	23/02/2004 22:00	63.3	7239.9	0.38	1.7	63	127.7
10	14/11/2005 00:30	16/11/2005 00:00	192.7	34075.1	0.59	8.7	70	979.9
11	28/01/2006 15:30	31/01/2006 08:00	177.7	36380.9	0.68	3.5	64	594.3

Table A 7: The characteristics of all flood events in Ardèche catchment. P: cumulated precipitation; Vr: runoff volume; Rc: runoff coefficient.

Event	Starting date	Finishing date	P (mm)	Vr ($10^3.m^3$)	Rc (%)	Base flow ($m^3.s^{-1}$)	Hu2 index (%)	Peak flow ($m^3.s^{-1}$)
1	21/09/1992 08:00	23/09/1992 08:00	340.8	35928	0.17	49	46	2111
2	18/05/1993 23:00	22/05/1995 08:00	78.5	17982	0.37	29	56	271
3	09/10/1993 23:00	13/10/1993 12:00	99.6	20314.6	0.33	153	71	379.2
4	13/10/1993 12:00	16/10/1993 00:00	54.8	15086.5	0.45	188	72	311.7
5	15/10/1993 23:00	18/10/1993 08:00	75.5	7899.1	0.17	145	71	97.2
6	18/09/1999 23:00	22/09/1999 00:00	188	19104.2	0.16	7	44	418.3
7	22/09/1999 23:00	24/09/1999 12:00	49.3	5134.5	0.17	41	61	102.2
8	18/10/1999 00:00	22/10/1999 08:00	154.4	41659.8	0.44	42	60	679.7
9	22/10/1999 08:00	24/10/1999 03:00	96.5	19278.2	0.32	165	70	366.9
10	27/09/2000 23:00	06/10/2000 00:00	145.9	22095.4	0.24	30.1	50	329.9
11	08/11/2000 23:00	19/11/2000 23:00	203.5	122712	0.97	77	62	1049.1
12	15/10/2001 23:00	19/10/2001 19:00	140.1	19140.1	0.22	14	56	456
13	19/10/2001 19:00	27/10/2001 11:00	119.4	52880.6	0.72	122	66	813.6
14	07/09/2002 23:00	13/09/2002 00:00	69.6	11174.6	0.26	6.3	53	164.6
15	11/11/2002 23:00	19/11/2002 22:00	179.6	78662	0.71	7.6	57	294.9
16	19/11/2002 22:00	23/11/2002 05:00	86.5	25794.7	0.48	80	65	498.6
17	23/11/2002 05:00	05/12/2002 00:00	181.4	126278	1.12	132	68	569.3
18	21/11/2003 02:00	29/11/2003 07:00	127.6	72785	0.92	43	62	428
19	16/08/2004 23:00	19/08/2004 09:00	142	14487.2	0.16	3	47	707.5
20	24/10/2004 23:00	27/10/2004 11:00	70	14592.4	0.34	9.6	57	216
21	27/10/2004 11:00	01/11/2004 23:00	217.6	102288	0.76	52	64	869.1
22	01/11/2004 23:00	08/11/2004 12:00	114.3	68901.1	0.97	72	70	520.9

Table A 8: The characteristics of all flood events in Gardon catchment. P: cumulated precipitation; Vr: runoff volume; Rc: runoff coefficient.

Event	Starting date	Finishing date	P (mm)	Vr ($10^3.m^3$)	Rc (%)	Base flow ($m^3.s^{-1}$)	Hu2 index (%)	Peak flow ($m^3.s^{-1}$)
1	22/09/1994 01:00	26/09/1994 11:00	268.2	39802.3	0.27	9.7	49	663.5
2	19/10/1994 06:00	24/10/1994 11:00	317.9	80019	0.46	16.3	56	843.7
3	02/11/1994 09:00	09/11/1994 04:00	304.4	94644	0.57	34	62	666
4	18/09/1995 05:00	22/09/1995 01:00	169	41763.6	0.45	41	56	909
5	03/10/1995 02:00	06/10/1995 20:00	261.2	71553.6	0.5	38	56	1572
6	13/10/1995 02:00	15/10/1995 03:00	195.3	47559.6	0.45	27	61	1383
7	03/11/1997 04:00	10/11/1997 00:00	340.3	100247.4	0.54	4.5	54	805.5
8	16/12/1997 11:00	24/12/1997 05:00	395.7	177134	0.82	10.6	56	1139.4
9	14/04/1998 23:00	19/04/1998 22:00	117.4	25315.6	0.4	3.9	55	466.1
10	29/04/1998 13:00	06/05/1998 12:00	130.6	47206.1	0.66	19.2	58	480.8
11	17/05/1999 05:00	25/05/1999 11:00	174.5	64375.9	0.68	13.5	55	606.5
12	19/10/1999 21:00	27/10/1999 06:00	201.5	41299.4	0.38	37	57	622.6
13	28/09/2000 10:00	01/10/2000 04:00	213.3	32379.8	0.28	3.4	51	1186.6
14	09/10/2002 02:00	13/10/2002 16:00	201.2	52527.6	0.48	35	53	445
15	23/11/2002 13:00	27/11/2002 07:00	91.4	33284	0.67	103	62	605.4
16	09/12/2002 07:00	16/12/2002 15:00	233.1	89557.2	0.71	45	57	605
17	30/09/2003 12:00	04/10/2003 02:00	145.1	16902.7	0.21	9.3	43	510.7
18	15/11/2003 11:00	20/11/2003 10:00	158	52147.1	0.61	21.2	58	668.8
19	21/11/2003 08:00	27/11/2003 20:00	206.1	84165	0.75	40	63	1028.8
20	29/11/2003 18:00	06/12/2003 08:00	318.1	144968.5	0.84	46	67	1112.6

Table A 9: The characteristics of all flood events in Tarnon catchment. P: cumulated precipitation; Vr: runoff volume; Rc: runoff coefficient.

Event	Starting date	Finishing date	P (mm)	Vr ($10^3.m^3$)	Rc (%)	Base flow ($m^3.s^{-1}$)	Hu2 index (%)	Peak flow ($m^3.s^{-1}$)
1	22/04/1993 06:00	03/05/1993 06:00	236.5	29652.5	0.49	0.8	52	108.5
2	20/09/1994 23:00	29/09/1994 06:00	281.2	27986	0.39	0.2	50	568.9
3	17/10/1994 19:00	23/10/1994 23:00	197.4	19165.2	0.38	1	56	127.8
4	24/11/1995 05:00	30/11/1995 23:00	145.9	18327.7	0.49	3.3	57	205.4
5	19/01/1996 16:00	24/01/1996 17:00	279.5	63965.7	0.89	8	62	681.4
6	27/01/1996 02:00	31/01/1996 22:00	124.5	13466.3	0.42	30	69	119.1
7	14/10/1996 02:00	17/10/1996 12:00	128.9	9888.5	0.3	2	55	99
8	10/11/1996 22:00	14/11/1996 23:00	169.5	18785.2	0.43	1.2	56	335.8
9	03/12/1996 07:00	09/12/1996 01:00	206.5	24118.3	0.46	2.9	60	120.1
10	17/12/1997 10:00	21/12/1997 09:00	180.1	34152.8	0.74	1	56	559
11	17/05/1999 11:00	22/10/1999 11:00	145.1	14970.2	0.4	0.8	56	389.2
12	19/10/1999 17:00	22/10/1999 04:00	126.9	7536.4	0.23	0.3	51	165
13	11/11/1999 22:00	16/11/1999 22:00	154.3	10327	0.26	0	54	80
14	26/09/2000 23:00	02/10/2000 05:00	231.1	8142.3	0.14	0	47	258.3
15	17/10/2001 23:00	25/10/2001 00:00	304.1	25969.4	0.33	0	46	504.6
16	09/10/2002 05:00	11/10/2002 13:00	230.1	11358.6	0.19	0	46	235
17	19/11/2002 23:00	01/12/2002 02:00	163.1	14782.3	0.35	0.8	57	183.4
18	15/11/2003 22:00	19/11/2003 06:00	105.3	7856.9	0.29	0	54	116
19	20/11/2003 08:00	27/11/2003 08:00	317.1	58822.1	0.72	3	58	763.8
20	30/11/2003 20:00	03/12/2003 01:00	123.8	11887.2	0.37	5	64	119
21	02/12/2003 10:00	06/12/2003 05:00	168.1	31884.3	0.74	88	70	593.9
22	30/03/2004 09:00	04/04/2004 13:00	211.6	20086.9	0.37	0.5	53	120.5
23	29/04/2004 06:00	01/05/2004 16:00	141.4	12771	0.35	1	55	315
24	30/10/2005 22:00	02/11/2005 22:00	47.6	3716	0.3	3	53	74.6
25	03/11/2005 23:00	06/11/2005 07:00	32.7	1374.6	0.16	4.2	56	24.7
26	27/01/2006 22:00	31/01/2006 05:00	110.6	14507.3	0.51	0.3	53	109.7
27	22/09/2006 21:00	26/09/2006 15:00	151.7	4871	0.13	1.4	52	164.7

Table A 10: The characteristics of all flood events in Vidourle catchment. P: cumulated precipitation; Vr: runoff volume; Rc: runoff coefficient.

Event	Starting date	Finishing date	P (mm)	Vr ($10^3.m^3$)	Rc (%)	Base flow ($m^3.s^{-1}$)	Hu2 index (%)	Peak flow ($m^3.s^{-1}$)
1	19/10/1994 17:00	26/10/1994 23:00	139.4	72244	0.82	3.94	64.8	566.76
2	21/09/1994 23:00	26/09/1994 12:00	178	38593	0.34	0.39	60.9	562.31
3	02/10/1995 21:00	07/10/1995 10:00	103	26863	0.41	5.89	61.9	406.81
4	24/11/1995 16:00	29/11/1995 05:00	76	17394	0.36	19.56	67.6	327.64
5	13/10/1995 08:00	17/10/1995 21:00	126.3	42579	0.54	5.21	65.5	480.99
6	18/12/1996 23:00	22/12/1996 01:00	136.9	56321	0.65	25.57	70.1	790.43
7	17/12/1997 08:00	23/12/1997 00:00	92.8	63267	1.08	0.81	67.4	549.99
8	28/05/1998 06:00	30/05/1998 00:00	73.2	9908	0.21	3.94	59.1	181.3
9	20/10/1999 19:00	23/10/1999 01:00	72.4	15356	0.34	25.57	66.4	219.6
10	17/05/1999 05:00	21/05/1999 18:00	72.1	19252	0.42	30.89	63.6	131.31
11	24/12/2000 10:00	27/12/2000 00:00	96.9	34298	0.56	20.7	67.3	485.6
12	28/09/2000 07:00	02/10/2000 20:00	90.3	14756	0.26	13.31	54.8	185.79
13	28/01/2001 02:00	02/02/2001 00:00	61.3	25231	0.65	25.57	67.9	277.79
14	08/03/2001 01:00	12/03/2001 00:00	60.8	20381	0.53	24.31	65.2	249.17

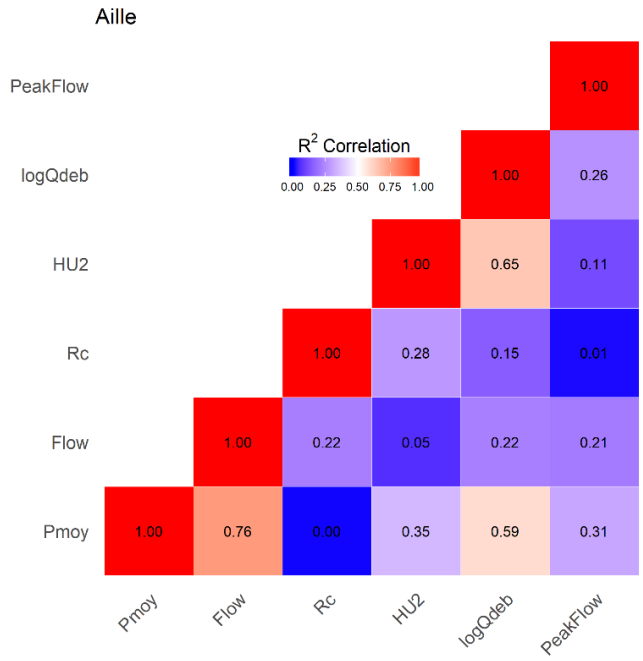

Figure A 16: Correlation between each pair of indexes in the Aille catchment. Pmoy: average areal cumulated precipitation (mm); Flow: runoff volume ($10^3.m^3$); Rc: runoff coefficient (%); HU2: Hu2 soil moisture index (%); logQdeb: log_{10} base flow (log_{10} $m^3.s^{-1}$); PeakFlow: peak flow ($m^3.s^{-1}$)

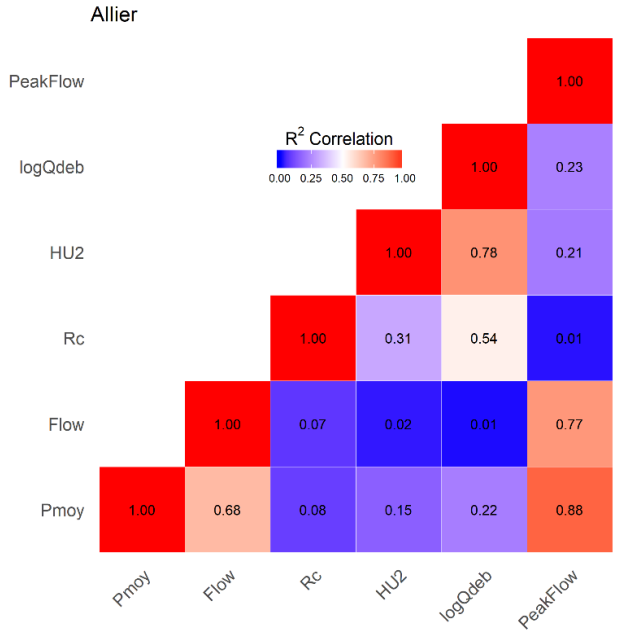

Figure A 17: Correlation between each pair of indexes in the Allier catchment. Pmoy: average areal cumulated precipitation (mm); Flow: runoff volume ($10^3.m^3$); Rc: runoff coefficient (%); HU2: Hu2 soil moisture index (%); logQdeb: log_{10} base flow (log_{10} $m^3.s^{-1}$); PeakFlow: peak flow ($m^3.s^{-1}$)

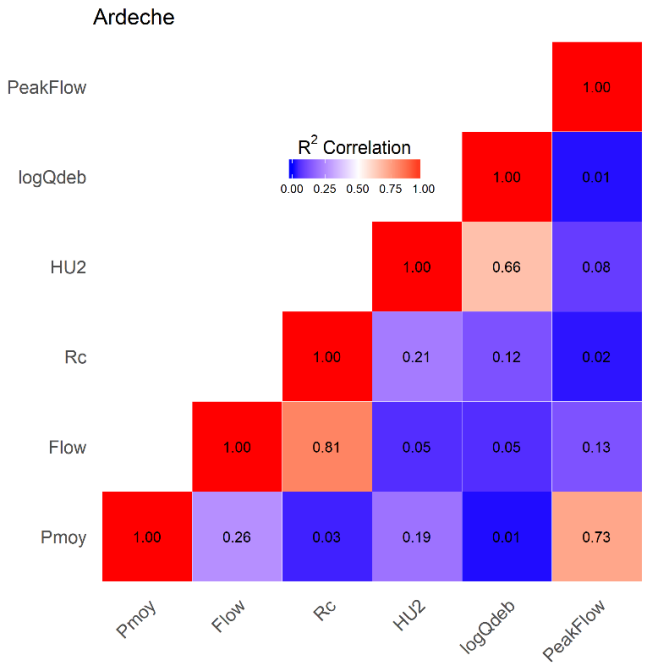

Figure A 18: Correlation between each pair of indexes in the Aille catchment. Pmoy: average areal cumulated precipitation (mm); Flow: runoff volume ($10^3.m^3$); Rc: runoff coefficient (%); HU2: Hu2 soil moisture index (%); logQdeb: log_{10} base flow (log_{10} $m^3.s^{-1}$); PeakFlow: peak flow ($m^3.s^{-1}$)

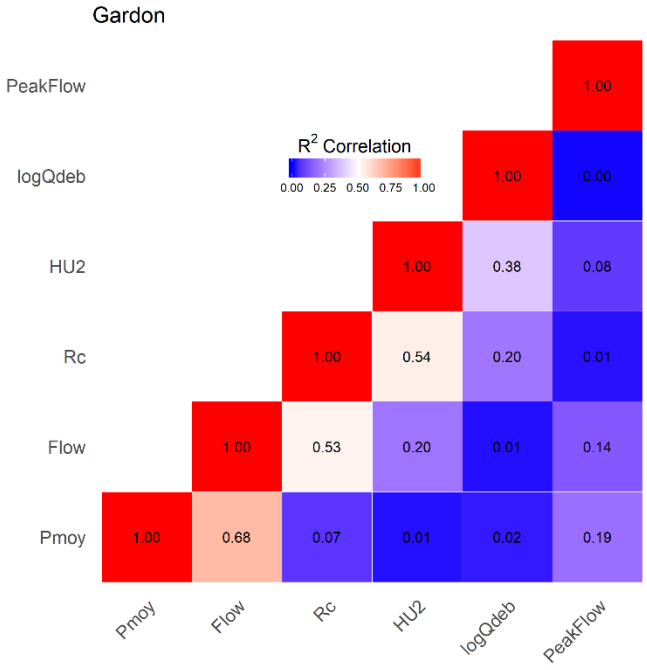

Figure A 19: Correlation between each pair of indexes in the Gardon catchment. Pmoy: average areal cumulated precipitation (mm); Flow: runoff volume ($10^3.m^3$); Rc: runoff coefficient (%); HU2: Hu2 soil moisture index (%); logQdeb: log_{10} base flow (log_{10} $m^3.s^{-1}$); PeakFlow: peak flow ($m^3.s^{-1}$)

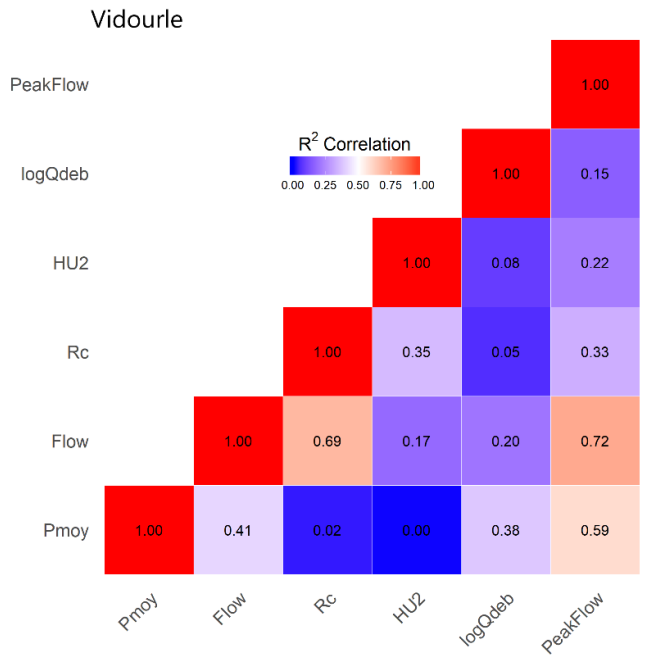

Figure A 20: Correlation between each pair of indexes in the Vidourle catchment. Pmoy: average areal cumulated precipitation (mm); Flow: runoff volume ($10^3.m^3$); Rc: runoff coefficient (%); HU2: Hu2 soil moisture index (%); logQdeb: log_{10} base flow (log_{10} $m^3.s^{-1}$); PeakFlow: peak flow ($m^3.s^{-1}$)

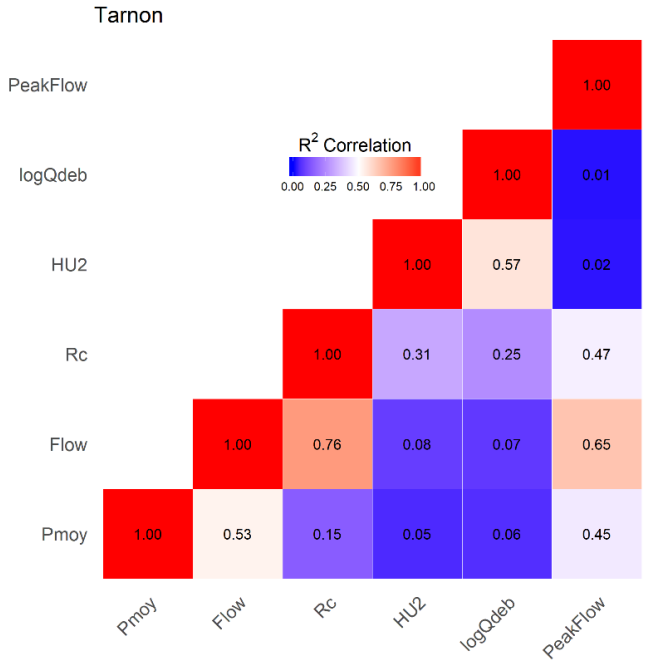

Figure A 21: Correlation between each pair of indexes in the Tarnon catchment. Pmoy: average areal cumulated precipitation (mm); Flow: runoff volume ($10^3.m^3$); Rc: runoff coefficient (%); HU2: Hu2 soil moisture index (%); logQdeb: log_{10} base flow (log_{10} $m^3.s^{-1}$); PeakFlow: peak flow ($m^3.s^{-1}$)

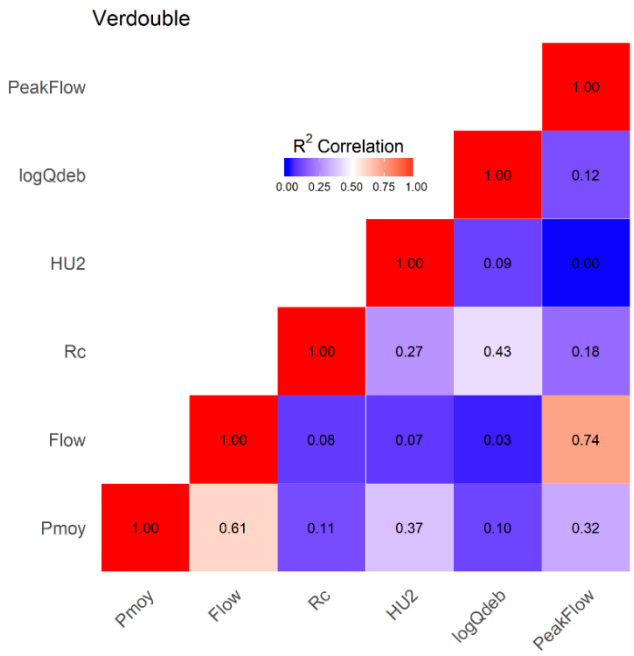

Figure A 22: Correlation between each pair of indexes in the Verdouble catchment. Pmoy: average areal cumulated precipitation (mm); Flow: runoff volume ($10^3.m^3$); Rc: runoff coefficient (%); HU2: Hu2 soil moisture index (%); logQdeb: log_{10} base flow (log_{10} $m^3.s^{-1}$); PeakFlow: peak flow ($m^3.s^{-1}$)

D. Publication specific to the PhD study

Flood modeling using the distributed event-based SCS-LR model in the Mediterranean Real Collobrier catchment

Son Nguyen[a], Christophe Bouvier[b*]

[a]*USTH, Ph.D., Hanoi, Vietnam*

[b]*IRD, UMR 5569 HydroSciences, Montpellier, France*

* Corresponding author: Christophe Bouvier (bouvier@msem.univ-montp2.fr)

(This manuscript has been accepted by Hydrological Science Journal)

Flood modeling using the distributed event-based SCS-LR model in the Mediterranean Real Collobrier catchment

Abstract

Event-based models are often used for flood prediction because they require fewer data than more complex models and account for few parameters. Here we present the performance of such model in simulating Mediterranean floods, with a focus on the initialization and the impact of the rainfall uncertainties on the calibration of the model. The distributed event-based parsimonious Soil Conservation Service Lag-and-Route model was applied in the Real Collobrier catchment, which contains a very high density of rain gauges. The initial condition of the model was highly correlated with predictors such as the base-flow or the soil water content. The reduction of the rain gauges density can change remarkably the calibration of the model. As the density of rain gauge is generally low in most catchments, the uncertainties associated with the rainfall measurement are thus expected either to mask the actual accuracy of the model or to alter the model parameters.

Keywords: Flash flood, model SCS-LR, Event-based model initialization, Mediterranean catchment, Precipitation uncertainty

1. Introduction

The Mediterranean area is prone to flash floods, generating heavy damages and losses of human lives (Amponsah et al., 2018). The water levels can rise more than a dozen meters in less than a few hours, because of rainfalls exceeding some hundreds of millimeters a day (Delrieu et al., 2005). The most effective way to mitigate risk due to flash floods may be to implement real-time flood forecast systems. As a result, rainfall-runoff models are crucial tools. Several models have already been tested for flash floods modelling (Durand et al., 1992; Piñol et al., 1997; Blöschl et al., 2008; Moussa and Chahinian, 2009; Saulnier and Le Lay, 2009; Vincendon et al., 2010; Roux et al., 2011). Those models are either event-based models or continuous models. The event-based models have advantages such as using limited data or reducing the complexity of the model and the number of parameters. However, they need to be initialized for each event, and the initial condition of the model has to be derived from an external variable, which expresses the state of the catchment at the beginning of the rain event. A comparison of event-based and continuous models was performed by Berthet et al., 2009. It showed that both types

of model were more or less equivalent. However, event-based models are often the only option in many cases, when a complete series of data are not available. Recently, another study also compared continuous and event-based models and showed that event-based models are suitable for climate change impact (Stephens et al., 2018).

When using event-based models, the relationship between the initial condition of the model and the external predictors remains critical. For example, it is known that cumulated rainfalls occurring in some previous days are often inefficient for predicting the S –or CN parameter- of the SCS model (Huang et al., 2007; Tramblay et al., 2010; Durbude et al., 2011). Alternative predictors have been proposed in order to improve the assessment of the initial condition of event-based models: antecedent discharge (Tramblay et al., 2012), piezometric levels (Coustau et al., 2012), output soil wetness of the Safran-Isba-Modcou (SIM) model of Meteo-France (Tramblay et al., 2010; Roux et al., 2011), output of the daily SWAT continuous model embedded in an event-based sub-daily SWAT model (Yu et al., 2018). Field monitoring of soil moisture was also used (Tramblay et al., 2010) and satellite soil moisture data were suggested (Tramblay et al., 2012). At this point, the relationship between the initial condition of the model and the external predictors remains however little known and needs further exploration. As a matter of fact, the relationship can be affected as well by the structure of the model as by uncertainties associated to the input data, and it is not possible yet to estimate their respective influence. Thus, testing the models with highly documented input data was necessary to get a reliable estimation of the goodness of the models.

The question this paper addresses is to assess the performance of a distributed event-based parsimonious rainfall-runoff model in simulating Mediterranean floods. Namely, it focuses on two main aspects: firstly, the impact of the initial soil water content in the response of the catchment, and secondly, the impact of the rainfall uncertainties on both the goodness and the calibration of the model. In order to deal with these questions, the SCS-LR model has been used within a highly documented Mediterranean catchment, the Real Collobrier, which contains 17 rain gauges over 70 km2. This rain gauge density indeed allows efficiently grabbing the typical spatial variability of the Mediterranean storms (Anquetin et al., 2010). The SCS-LR model is a parsimonious event-based distributed model, which combines the SCS runoff model and the Lag and Route routing model, both operating within a grid mesh of cells over the catchment. The model accounts for the spatial distribution of the rain without increase of complexity (i.e. without increase of the number of the parameters). Both runoff and routing parameters can vary in space, but using uniform parameters makes the model parsimonious, and the calibration easier (Willems et al., 2014). The Real Collobrier provides the opportunity to assess the accuracy

of the model within a dense network of rain gauges, reducing the uncertainties of the areal rainfall. The paper also intends to give an example of the event-based model calibration, which is not a trivial task (Awol et al., 2018). In addition, the impact of the density of rain gauges on the calibration and the goodness of the model was assessed by reducing the density of rain gauges. Because many catchments are monitored with a low density of rain gauges, the sensitivity of the model to the rainfall uncertainties will help to compare the results in several catchments, within the scope of a regionalization study for example.

The paper was organized as follows : section 1 described the characteristics of the model, emphasizing the assumptions which were expected to bring an optimal result in simulating floods, as well as the calibration protocol of the model; section 2 presented the geographical and hydrological characteristics of the study site; section 3 dedicated to the results of the calibration and the goodness of the model, when using all the rain gauges available in the catchment, i.e. 17 rain gauges; section 4 assessed the impact of the rain gauges density on the goodness and the calibration of the model, evaluated by considering each gauge as a single gauge in the catchment; section 5 discussed the results comparing to other studies dealing with the initialization of event-based models.

2. Methodology

2.1.Runoff model

The Soil Conservation Service (SCS) model was established in the mid-1950s by the United State Department of Agriculture (USDA), aiming to demonstrate and evaluate the design and construction of soil and water conservation project. To date, the SCS method is one of the most popular runoff models and was the object of many improvements as well in the formulation of the model as in the interpretation of its parameters (Mishra and Singh, 2013; Ponce Victor M. and Hawkins Richard H., 1996).

Although it was first defined to relate cumulated runoff and rainfall at the event scale, it is possible to integrate time into this model to predict infiltration rates (Aron et al., 1977; Gaume et al., 2004). Coustau et al. (2012) implemented drainage of the cumulated rainfall and delayed runoff within the SCS model: the drainage of the cumulated rainfall led to a decrease in the runoff coefficient within a period without rain, whereas the delayed runoff performed more accurate recession of the floods. Michel et al. (2005) proposed a direct relationship between the runoff coefficient and the storage in a soil reservoir (instead of the cumulated rainfall), which made easier to account for the decrease of the runoff coefficient and the delayed runoff in SCS (Michel et al. 2005).

Figure 1 - HERE

The model used here was the formulation of the SCS given by Michel et al. (2005), in which were added the drainage and delayed runoff proposed by Coustau et al. (2012). Although it was not within the scope of this paper, such formulation was also adapted to run the model in continuous mode. The model was run within the ATHYS platform modeling www.athys-soft.org, as described hereafter.

The effective rainfall (or runoff) intensity $R(t)_{[L/T]}$ at a given time t can be calculated as followed (Fig. 1):

$$R(t) = C(t).i(t) \quad (1)$$

in which, $i(t)_{[L/T]}$ denotes the rain intensity at time t, and $C(t)_{[-]}$ is the runoff coefficient, as (Michel et al., 2005):

$$C(t) = \frac{H(t) - Sa}{S}.\left(2 - \frac{H(t) - Sa}{S}\right) when\ S(t) > Sa \quad (2)$$

$C(t) = 0$ otherwise

In the equation above, t is the time, $H_{[L]}$ denotes the level of the soil reservoir; $S_{[L]}$ the maximum water capacity of the reservoir; $S_{a[L]}$ the Michel's initial abstraction, equal to the sum of the initial water level in the soil reservoir $H_{0[L]}$ and the $I_{a[L]}$ abstraction in the classical SCS:

$$S_a = H_0 + I_a \quad (3)$$

S_a should be independent of the event, which means that I_a is event-dependent, and that the variability of I_a is compensated by the variability of H_0.

The water level in the soil reservoir is governed by the infiltration and the drainage: the infiltration fills the reservoir, and the drainage makes that the runoff coefficient decreases when it does not rain (due to water evaporation near the soil surface, lateral sub-surface flow or deep drainage at lower layers). The infiltration $f(t)$ equals:

$$f(t) = \big(1 - C(t)\big).i(t) \quad (4)$$

The drainage $Vid(t)_{[L/T]}$, so-called "the vertical flow", is assumed to be a linearly dependent on the level $H(t)$ in the reservoir:

$$Vid(t) = ds.H(t) \quad (5)$$

where $ds_{[1/T]}$ is a proportionality coefficient.

The level of the reservoir is finally computed by:

$$\frac{dH(t)}{dt} = f(t) - Vid(t)$$

$$H(t_0) = H_0 \quad (6)$$

Moreover, a delayed runoff provided by sub-surface runoff or exfiltration is generated as a part of the drainage of the soil reservoir. This runoff, $Exf(t)_{[L/T]}$, so-called the "lateral flow", is assumed to be a constant fraction ω of the drainage:

$$Exf(t) = \omega . Vid(t) \quad (7)$$

Thus, the total runoff $Rtot(t)_{[L/T]}$ produced by a cell at time t is given by:

$$Rtot(t) = R(t) + Exf(t) \quad (8)$$

Finally, the SCS model operates in distributed mode over a grid mesh of regular cells. Each cell is thus able to produce runoff, according to the selected parameters S, ω and ds, which can vary for each cell, or not.

Coustau et al. (2012) pointed out an important point concerning the drainage. They argued that using the same reservoir discharge ds before and after the rain was not convenient, because the discharge mostly comes from the groundwater before the flood, from the near-surface layers during the recession of the flood. The corresponding discharge rates are supposed to be different, slow before the flood, fast during the recession. Thus, the drainage should be differentiated before and after the rain/flood. For event-based models, several solutions can be proposed to represent the dual discharge of the soil reservoir, such as considering two ds coefficients instead of one or introducing a threshold of the amount of the rain or the level in the reservoir, which activated either the slow or the fast drainage. Finally, the adopted solution was here to consider as Coustau et al. (2012) that the initial storage H_0 was always 0 at the beginning of the event, making that the drainage is null before the rainfall started and the reservoir filled up. The hypothesis that there is no drainage of the soil reservoir before the rain starts seems to be convenient in most cases. This hypothesis also makes it possible to reduce the number of parameters of the model by removing H_0, whereas the other solutions require additional parameters. Consequently, according to the hypothesis $H_0 = 0$, i) S is no longer the maximal storage capacity of the reservoir soil, but the initial water deficit of the reservoir, which should vary from an event to another, ii). S_a is similar to I_a, which is set as a function of S: $I_a = 0.2S$.

Coustau et al. (2012) also indicated that ω and S were linked by a linear regression, with a negative slope. That means the higher S, the lower ω. In other terms, the delayed runoff was low when the soil was initially dry, and high when the soil was initially wet. This is coherent with the fact that free water in the soil depends on the water content. In order to reduce the equifinality, it was thus decided to express ω as the ratio of a water storage threshold $\omega'_{[L]}$ and the S water storage capacity of the soil at the beginning of the event, $\omega = \omega'/S$ when $S > \omega'$, and $\omega = 1$ when $S < \omega'$. The ω' parameter substituted to the ω parameter in the calibration of the model and was expected to be uniform for all the events.

2.2. *Routing model*

Figure 2 - HERE

The runoff from each cell was then routed to the outlet by a linear lag-and-route model (Bouvier and Delclaux 1996). From each cell m, the runoff at time t_0 generated an elementary hydrograph $Q_m(t)$ at the outlet of the catchment:

$$Q_m(t) = \frac{q(t_0)}{K_m} exp\left(-\frac{t-(to+T_m)}{K_m}\right) * A \quad (9)$$

where $q(t_0)$ denotes the runoff from the cell at the date t_0, T_m and K_m represent respectively the travel time (route) and the diffusion time (lag) of the initial input along the travel paths, and A is the area of the cell (Fig. 2).

The travel time T_m was computed by

$$T_m = \Sigma_k \frac{l_k}{V_0} \quad (10)$$

in which, l_k is the length of the k^{th} cells between the cell m and the outlet; V_0 denotes the velocity of travel, which was considered here as uniform over the whole catchment. The diffusion time K_m was assumed to be proportional to the travel time T_m, with the slope equal to K_0, as follows:

$$K_m = K_0.T_m \quad (11)$$

Finally, all the elementary hydrographs derived from any time and any cell were added to obtain the total hydrograph (Olivera and Maidment, 1999). The model, although not physically based, has several advantages: short computation times, slight dependence on the spatial resolution (because it does not rely on cells slopes), possibility to give a physical interpretation to the parameters. However, the concept only retrieves the hydrograph at the outlet of the catchment, but not the internal flows at the cell scale. This is due to the fact that the elementary hydrographs are only added at the outlet of the catchment, but not in the upstream cells. For this reason, the model cannot work for any storage in the cells, which requires an actual budget at any time in the given cells.

The complete model finally dealt with three parameters for the production function: S (initial water deficit), ds (drainage coefficient of the reservoir), ω' (related to the fraction $\omega = \omega'/S$ of the drainage corresponding to the delayed runoff), and two parameters for the transfer function: V_0 (velocity of travel), K_0 (coefficient of the linear relationship between the travel time and the diffusion time).

2.3.Base flow

The base flow is the "memory" of the catchment, due to the previous rainfalls, before the event. In the SCS-LR event-based model used as above, no base flow could be simulated, because the initial water level in the reservoir was 0 so that the drainage and delayed runoff were also null

until the rainfall begins during the event. The simulated flow was only due to the rainfall of the event. Thus, the simulated discharges must be compared to the total observed discharges, minus the base flow. This base flow was estimated by fitting an exponential decrease with time, between the first discharge of the event Q_0 and the last continuously decreasing discharge Q_i (i.e. Q_i such as $Q_k<Q_{k-1}$, for any 1<k<i), before the rising of the flood: $Q_k=Q_0.exp(-\alpha(t_i-t_0))$, with $\alpha = Ln((Q_i-Q_0)/(t_i-t_0))$. The base flow was then computed with this exponential decrease for the whole event, and subtracted to the observed discharge, to be compared to the simulated discharge.

2.4.Water content predictors

In addition to the base flow, the *w* volumetric water content output of the SIM model (Habets et al., 2008; Quintana Seguí et al., 2009) was used as another predictor of the initial condition of the model. The SIM model supplied water content *w* computed once a day at 6 TU, over an 8x8 km² grid mesh of France, for three layers (Boone et al., 1999): surface layer (1cm deep), root layer and deep layer (depths depending on the type of vegetation), according the soil hydraulic properties (water content at saturation w_{sat}, water content at wilting point, w_{wilt}, water content at field capacity w_{fc}). The latter derives from the percentages of sand and clay, supplied by the 1-km resolution INRA soil map. In the scope of this study, we only considered the indicator from the second soil layer, w_2, because of the shallow depth of the soils in the catchment.

2.5.Model calibration

The calibration of the model was driven event-by-event, aiming to maximize the Nash–Sutcliffe Efficiency (NSE, Nash and Sutcliffe, 1970) value for each event:

$$NSE = 1 - \frac{\sum_{t=1}^{T}(Q_0^t - Q_c^t)^2}{\sum_{t=1}^{T}(Q_0^t - \overline{Q_0})^2} \qquad (12)$$

where $\overline{Q_0}$ is the mean of observed discharges during the event, Q_c^t is the calculated discharge and Q_0^t is the observed discharge at time t during the event.

Nash–Sutcliffe efficiency can take values from −∞ to 1. An efficiency of 1 (*NSE* = 1) implies a perfect match of modeled discharge to the observed data. An efficiency of 0 (*NSE* = 0) indicates that the model predictions are as accurate as the mean of the observed data, whereas an efficiency less than zero (NSE < 0) occurs when the observed mean during the event is a better predictor than the model or, in other words, when the residual variance is larger than the data variance. Essentially, the closer the model efficiency is to 1, the more accurate the model is. Note that NSE was computed only for the time steps corresponding strictly positive observed discharge during the event (after subtraction of the base flow, see above).

Some parameters were kept constant for all the events, whereas others were allowed to vary from one event to another (see section 4.1). The algorithm used for the maximization of NSE was the simplex algorithm (Rao, 2009).

2.6.Model efficiency

When using an event-based model, the calibration of the model event-by-event leads to the optimal NSE of the model, i.e. the NSE obtained with the optimal values of the calibrated parameters. But the predictive score of the model must account either for the best adjustment of the simulated floods to the observed one and for the better adjustment of the relationship between the initial condition of the model and the external predictors. In other terms, the predictive NSE of the model should be the NSE constrained by the predicted value of the initial condition of the model. The so-called predictive NSE thus assesses the accuracy of the event-based model. The goodness of the model will be thus expressed by the quartiles (upper, median, lower) of the predictive NSE values of all the events, the initial condition being predicted by the relationship with the external predictors (base flow, the output of the SIM model). The model efficiency will also be controlled by split-sample cross-validation, in order to check the stability of both the calibration and goodness of the model. For the event-based models, note that the split-sample cross-validation needs to compare the predictive NSE of both calibration and validation samples.

3. Study site and data

3.1.Real Collobrier catchment

Real Collobrier is located in the South of France, near the Mediterranean Sea, and has been monitored since 1968 by IRSTEA. Discharge data are available for 11 sub-basins, with areas ranging from 0.7 km^2 to 70 km^2. In the larger catchment, at Pont de Fer (Fig. 3), the altitudes decrease from the east (770m maximum) to the west (80m at the outlet). The geological formations are mainly crystalline, with metamorphism increasing from east to west: gneiss, schists, phyllites (Folton et al., 2012). Vegetation includes chestnut, cork or green oaks, pines forests; vineyards are grown in a small portion of the area. The average proportions in sand and clay in Real Collobrier are 633 g/kg and 162 g/kg (from Geosol https://webapps.gissol.fr/geosol/). Parkin et al. (1996) gave a description of the soil in the Rimbaud sub-catchment: the soils are generally sandy, and contain a significant proportion of gravel and broken rock; there is considerable local variation in soil depth from nothing (at bedrock outcrops) to a meter or more in bedrock depressions, but depths are generally less than 1 m; the deepest and most homogeneous soils occur in the chestnut plantation near the catchment

outlet, where soil depths may reach 2 m; plant roots generally extend over the full depth of the shallow soils. The shallow soils seem to have high hydraulic conductivities at saturation, up to 100 $mm.h^{-1}$ (Parkin et al., 1996), and low water retention (Taha et al., 1997) .

The climate of this area is typically Mediterranean with a dry and hot summer, heavy rainstorms in autumn, generated by south winds coming from the Mediterranean Sea (rainfall intensities up to 100 mm per hour), and rainy winter and spring. The annual average rainfall ranges from 750 mm to 1200 mm depending on the elevation.

Figure 3 - HERE

3.2.Rainfall-runoff data

Both rainfall and runoff data were obtained from IRSTEA (https://bdoh.irstea.fr/REAL-COLLOBRIER/), and were used with 30 minutes time step. We considered here the discharges at Pont-de-Fer station, which controls a catchment of 70 km^2. In this catchment, 17 rain gauges were available for the rainfall data. The events were delimited by considering several conditions: i) a new event was defined when occurred a period of 48 hours without amount exceeding 0.5 mm during a 30minutes-time step; a 48 hours period was enough to consider that discharge came back to the initial value before the rain, ii) the rainfall during the event had to exceed 50 mm in at least one rain gauge; ; the threshold 50 mm was found necessary for flood triggering, iii) the peak flow during the event had to exceed 30 m^3/s, which corresponded to the 1-year return period peak flow.

The method led to select 34 events from 1968 to 2006 (Table 1). All the rain gauges did not always work together, as shown in Table 1, but 31 out of 34 events have more than 12 rain gauges working together. The cumulated mean areal rainfall of the events ranged from 49 to 318 mm, with an average of 166 mm. The spatial variability of the rainfall during the event was expressed by the coefficient of variation CV (ratio of the spatial standard deviation and the spatial average) of the cumulated rainfalls at the rain gauges, CV's varying from 0.11 to 0.84. The ratio between the maximal and the minimal cumulated rainfalls at the rain gauges were more than 2 for 25 events out of 34, more than 3 for 10 events out of 34. The correlation coefficients between the cumulated rainfalls of the events at the different gauges ranged from 0.14 to 0.97 (Table 2). They regularly decreased with the distances between gauges (Fig. 4), but gauges 6 and 8 were less correlated to some others. As a matter of fact, these gauges are located in the upper northeastern part of the catchment and seem to be sensitive to local orographic effects. As an example of a median case, the correlation coefficient between the cumulated rainfalls at gauges Mouton (gauge 5) and Portaniére (gauge 12) was $r = 0.69$, the distance between the gauges being 10.7 km.

Figure 4 - HERE

The maximal peak flow was 91 m^3/s. The response time was computed for some single-peak floods and ranged between 1 and 2 hours, considering the time between the main rainfall intensity and the peak flow. The runoff coefficients ranged between 4 and 56%, 34% on average. The lowest runoff coefficients (≤10%) corresponded to the events which occurred right after long dry periods. In spite of their low runoff coefficients, these events gave high peak flow, e.g. the maximum value 91 m^3/s on the 13/09/1968. The initial moisture of the catchment was expressed for each event firstly by the baseflow and secondly by the w_2 volumetric water content derived from the SIM model. Those two indexes are closely related with a linear correlation between the logarithm of the base flow and w_2 (R^2 = 0.75, the points with null base flow were not taken into account).

4. Calibration and goodness of the model when using all the rain gauges

4.1.Sensitivity of the model to the parameters

Sensitivity tests were performed in order to detect the most influential or independent parameters. The event n°5 has been selected for this test, as a multi-peak event. The *a priori* values and boundaries of the parameters for this event have been set as far as possible from physical or empirical methods. The reference set of parameters used for the sensitivity test was finally S =140 mm, ω'=60 mm, ds = 0.4 d^{-1}, V_0= 2.5 $m.s^{-1}$, K_0 = 3, which led to a good simulation of the observed flood.

S is equivalent to CN as usual, $S_{(mm)} = 25400/CN - 254$ and can be derived from the Soil Conservation Service (SCS) National Engineering Handbook Section 4: Hydrology (NEH-4) and Technical Release 20 (TR-20). CN is known to be related to the land use, the hydrologic condition, the type of soil and the antecedent moisture condition. However, as shown in further discussion, the optimal values of S - or CN can be very different than those supplied by the SCS Handbook. The sensitivity analysis was performed by using S = 75 mm and S = 400 mm as probable boundaries of the S parameter in the Mediterranean area. The model was very sensitive to the range of variation of S (Fig. 5a), so this parameter was calibrated for each event.

There is no physical evidence for the ω' parameter. However, $\omega = \omega'/S$ should be close to 0 in driest condition, and close to 1 in the highest moisture condition. As the range of S parameter was a posteriori found between 75 and 400 mm, the value $\omega' = 60$ mm was set in the first approximation. The sensitivity test was applied with the reference set of parameters, by using ω' = 30, 60 and 90 mm, respectively. The result showed that the ω' parameter mainly affected the recession of the flood, in a range 40% for the low flows, while the peak flows were less impacted, less than 20% (Fig. 5b). As we were mainly interested in the peaks, the ω' parameter was set constant for all the events in the first approximation, ω'= 60 mm.

Figure 5 - HERE

As a mathematical property of the model, the discharge coefficient of the reservoir, *ds*, is equivalent to the recession coefficient α used in the Maillet's law:

$$Q(t) = Q_0.e^{-\alpha * t} \qquad (13)$$

where α is the drainage coefficient and Q_0 initial base flow. The recession coefficient ds was calculated for all the events, fitting an exponential recession on the terminal part of the floods (see Eq.13). The mean value was 0.4 d^{-1}, with a 0.1 d^{-1} standard deviation. The min and max values were respectively 0.2 and 0.7 d^{-1}. The sensitivity test was thus performed with the reference set of parameters, by using *ds* = 0.2, 0.4, 0.7 d^{-1}. The first peak was not sensitive to *ds* (<1%) but the second one was much more (more than 20% between the min and max). That showed that the ds parameter was important in case of multiple peaks flood (Fig. 5c), but most of the events exhibit single peak, so the *ds* parameter was set constant in first approximation, *ds* = 0.4 d^{-1}.

The V_0 parameter should be interpreted as the maximal velocity in a cross-section. Thus, V_0 can be derived from the slope, friction and hydraulic radius of the streams or channels. Although the velocity in a cross section is far to be constant in space (and time) at small scale, it is not unrealistic to assume that V_0 is globally constant over the catchment: roughly speaking, it results from the fact that the slopes are steep and the hydraulic radius low upstream, whereas the slopes are low and the hydraulic radius high downstream. In other terms, the variability of the slopes compensates the variability of the hydraulic radius for stabilizing the velocity values. In addition, V_0 was used to compute the travel time *Tm* between a given cell and the outlet of the catchment (Eq.10) and must be seen as a mean value along this trajectory: this is another reason why the hypothesis of V_0 uniform in space could be reasonable.

The transfer parameters V_0 and K_0 were found to be strongly dependent (Fig. 6). In this example (event n°5), it can be seen that there is a very wide range of pairs (V_0, K_0) which satisfy *NSE* > 0.8, the other parameters being *S* = 140 mm, ω' = 60 mm, *ds* = 0.4 d^{-1}. Thus, it is necessary to set one of these two parameters to avoid their artificial variation. As the V_0 parameter was somewhat more physically-based, we chose to set V_0 = 2.5 $m.s^{-1}$: this is indeed close to the value that would give the Manning-Strickler formula used in a rectangular cross-section with a Strickler friction coefficient 20 $m^{1/3}.s^{-1}$, a slope 0.015 $m.m^{-1}$, a width 20 m, a water level 1 m high, which seems to be realistic according to the available observations.

Figure 6 - HERE

The K_0 parameter governs the relationship between the translation time T_m and the diffusion time K_m. The diffusion time K_m displays a complex role and serves both as a real diffusion since the velocity through a cross-section is not uniform, and as an artificial way to make the real velocity varies in time, whereas V_0 does not. Therefore, there is no physical evidence to set *a priori*

the K_0 value, and it was necessary to calibrate K_0. To know more about the influence of K_0, the sensitivity test was performed with the reference set of parameters, by using K_0 = 0, 2.and 4.5, which were respectively the a posteriori minimal, median and maximal values of the calibrated K_0. K_0 mainly acted in the reduction of the peak flow, and to some extent, in the time position. However, the sensitivity of the model to K_0 seemed to be less than the sensitivity to *S.*

4.2.Model calibration

Then, the parameters *S* and K_0 had to be calibrated for the 34 events. An optimized set of values was found for each event, by optimization of the NSE computed with the observed and computed discharges (Fig. 7a). The *S* calibrated parameter values ranged from 75 to 400 mm (median = 181 mm), K_0 between 0 and 4.5 (median =2.4), and the NSE ranged from 0.27 to 0.99 (median = 0.96, lower quartile = 0.87). The simulated hydrographs indeed proved to be very similar to the observed one (Fig. 7b). The two worst values of NSE corresponded to events occurring in the driest initial soil conditions (18/09/74 and 05/09/2005). In these cases, the low flow values were overestimated, whereas the peak flow values were underestimated.

Figure 7 - HERE

The sensitivity test performed in section 4.1 gave an idea of the impact of such variabilities, and the model was supposed to be more sensitive to *S* than to K_0, at the event scale. Another test was performed to answer the question of the actual impact of the parameter's variability over the whole range of the events. The analysis was led by using the median value of each parameter (*S* then K_0) and by recalibrating the other parameter of the model (Fig. 8). For each calibration, the loss in NSE and the differences in *S* or K_0 expressed the sensitivity of the model to a given parameter. The highest loss in NSE was found when using the median *S* parameter and calibrating K_0: in this case, the median NSE decreased to 0.78 instead of 0.96 when calibrating both *S* and K_0, and the median K_0 increased to 3 instead of 2.4. Meanwhile, using the median parameter K_0 resulted in marginal changes of the median NSE (0.94 instead of 0.96) and median *S* (178 instead of 181 mm). Thus, the parameter *S* can be considered as the key parameter of the model, of which the variability at the event scale must absolutely be accounted for. The variability of the K_0 parameter seemed to have less impact on the flood simulations, although the impact could be important for some events. It is, however, worth to note that the K_0 low value normally appears in dry condition (high value of *S*) while the high value of K_0 is often in wet condition (low value of *S*). In dry initial condition, the shape of the flood would be sharper because the delayed runoff should be smaller (see comment on ' in section 2.1); thus, Ko will tend to be reduced in order to fit the shape of the flood. Finally, the fact that the model was not very sensitive

to K_0 made that we could use the median value to simulate floods without significant loss of accuracy.

Figure 8 - HERE

4.3. Relating S to initial conditions

After the calibration of the model, it appeared that *S* was the most variable and most influential parameter for the simulations. *S* corresponds here to the water deficit at the beginning of the event, so that it is expected to be highly dependent on the previous events and the initial state of saturation of the soil. Therefore, we tried to find relationships between *S* and two indexes supposed to express the initial water content: the base flow and the w_2 volumetric water content at the beginning of the simulated event.

Both indexes gave rise to a relatively strong correlation with maximum water retention, presented by the correlation coefficient R^2 (0.85 between *S* and $log_{10}(Qb)$ and 0.77 between *S* and w_2, Fig. 9). To allow the computation of the logarithms, the null base flows were changed to 0.001 m^3/s.

Figure 9 - HERE

These relationships should be used to assess the actual accuracy that could have the model in calibration mode. The actual accuracy of the model should be indeed estimated by the NSE computed with the predicted values of *S* instead of the optimized values of *S*, i.e. the predictive NSE (see section 2.6). Figure 10 showed that using the predicted values of *S* instead of the optimized one reduced the NSE values (for all the events, the median value of K_0 was used): the median predictive NSE was 0.83 when using the relationship between *S* and the base flow and 0.77 when using the relationship between *S* and the water content w_2 (instead of 0.94 for the median optimal NSE, derived from optimal values of *S* and median value of K_0). This shows that the *S*-base flow relationship performs better than the *S*-w_2 relationship, in order to simulate the flood.

Figure 10 - HERE

4.4.Validation of the model

The validation of the model was performed using cross-validation. Firstly, all the events were split into three samples: sample 1 included the 11 first events; sample 2 contained the events 12 to 22 and sample 3 was constituted of the 12 last events. For each predictor (w_2 or base flow), the model was first calibrated (*S* and K_0) on the set containing the calibration events, and the regression between *S* and 2 predictors was designed from the calibrated values of *S*. Then the model was applied on the set containing the remaining events (Table 3), by using the *S* values

derived from the regression previously designed in the calibration phase and the median value of K_0 obtained with the calibration sample. The median predictive NSE were finally computed for both calibration and validation events (the median value of K_0 was also used for the calibration sample to calculate the median predictive NSE).

The correlation coefficient R^2 were the highest for the second sample (0.9 for w_2 and 0.87 for base flow). One possible reason is that this sample contains all the dry events (i.e. events that occurred in dry soil conditions), and the corresponding extremely low values of S could artificially increase the correlation coefficient R^2. However, the other R^2 values were also very good (≥0.69), that showed a good correlation between the S parameter and the predictors. The coefficients a and b of the relationships did not differ a lot and were also very close to those obtained for the whole sample of events (see Fig.9), meaning that a stable relationship could be used for estimating S whatever the calibration sample was. The median predictive NSE were closed for the calibration and the validation samples, even sometimes higher for the validation sample than for the calibration sample. There was no significantly better sample for the comparison of the median predictive NSE for calibration and validation. Besides, the median predictive NSE were better for the base flow than the w_2, for both the calibration and the validation samples. Finally, to summarize, these results gave acceptable confidence for the performance and the robustness of the model, and for the possibility to apply it for other events than those used in this study.

4.5.Sensitivity of the model to rain gauges density

The rainfall uncertainty was then tested by using only one gauge at a time for model calibration. We implemented the calibration of the model following the method mentioned above (S and K_0 were the parameters to be calibrated for each event, whereas we kept ω' = 60 mm, ds = 0.4 d^{-1}, V_0 = 2.5 $m.s^{-1}$). The results were given in table 4, in which the regression and the predictive score were calculated for two predictors (w_2 and base flow):

The median S values ranged from 112 to 252 mm when using only one rain gauge for calibrating the model (it was 181 mm when using all the rain gauges). The R^2 of the relationship between S and w_2 (resp. S and Qb) ranged from 0.87 to 0.23 (resp. 0.91 to 0.39). The results also indicated that there were differences in both slope and intercept when we considered the regression of the calibrated S parameter and predictors in each rain gauge and in all gauges (Fig. 11). Figure 11 also showed the possible bias of the S parameter estimates, at a given density of rain gauges (here, 1 out of 70 km^2). It showed that for dry soil, let's say w_2 = 0.18 $cm^3.cm^{-3}$ or Qb = 0.01 m^3/s, the S estimates could range from nearly 250 mm to more than 600 mm, even more for w_2, depending on the selected rain gauge used for the calibration of the model. For a wet soil, let's

say w_2 = 0.24 $cm^3.cm^{-3}$ or Qb = 10 m^3/s, the S estimates could range between nearly 50 and 150, even 200 mm.

This is consistent with the fact that a higher number of rain gauges could improve the performance of the model, in other words, more rain data would help the model become more predictive. As seen above, insufficient data affected both the performance of the model (predictive NSE) and the parameters of the model (median, dry and wet values of S).

Figure 11 - HERE

The effect of the rain gauges did depend on their position in the catchment so that the best R^2 were obtained for the gauges Bonnaux and Bourjas. Bonnaux can be considered as the most central gauge in the catchment. Bourjas exhibited the best R^2, probably because only half of the events could be recorded (18/34), which could artificially increase the R^2. In addition, most of the gauges led to equivalent both R^2 and slopes in the relationships between S and the saturation index (base flow or w_2), but different intercepts. This is due to the fact that all these gauges are correlated (as shown in Table 2 and Figure 4), but that rainfalls have different mean values, probably due to orographic effects. Conversely, the worst R^2 were found for the gauges Fourches and Louviere, which were known to be poorly representative of the whole catchment (see Table 2 and Figure 4).). In addition, relationships S-w_2 or S-$log(Qb)$ exhibited different slopes for gauges Fourches, Mouton and Vaudreches, which are close together (Figure 11). Such slopes were the consequence of uncertainties in calibrating S for a single event occurring in extremely dry conditions, for these gauges. If we did not consider the S values for this event and for these gauges, the slopes would have been quite similar to the others. Thus, these slopes should be considered to be due to the calibration uncertainty rather than to the rainfall uncertainty.

.

5. Discussion

The S parameter was first compared to the estimated value that can be derived from the SCS Handbook. Real Collobrier can be described as mostly forestall, with pines, chestnuts, and oaks, in fair hydrologic condition. The most appropriate hydrologic soil group according to the high hydraulic conductivity of the shallow soil (> 100 $mm.h^{-1}$) was A, therefore the S value in medium conditions of soil moisture should be 459 mm when referring the SCS method guide. This

value is far above the median calibrated value, S = 210 mm. As the calibration of S was shown to be robust, this difference should not result from equifinality or any other bias generated by the values of the other parameters, and there should be a more physical explanation. This is probably due to the fact that shallow soil does not have sufficient depth to allow such higher water storage capacity. The hydrological soil group D would be preferable to account for this limited capacity, but in this case, the S value in medium conditions of soil moisture would be 68 mm, which highly underestimates the actual calibrated S value.

Moreover, S was poorly correlated with the classical previous 5-days cumulated rainfall (Huang et al., 2007), P5D, as shown in Fig. 12, and the large and continuous variability of the calibrated S also shows that the predicted values of S cannot be reduced to only three values corresponding to antecedent moisture conditions (AMC) AMC_I, $AMC_{II,}$ and AMC_{III}, as proposed in the SCS guide. The above comments illustrate the difficulty of predicting S from the method guide.

Figure 12 - HERE

Similar relationships between S and the water content estimates have been found before when modeling floods at sub-daily time step. In the small Mediterranean Valescure catchment (4 km^2, Δt = 30 minutes), Tramblay et al. (2010) found a high correlation ($R^2 > 0.7$) between S and either the field monitoring of water content, the base flow, the previous rainfalls or the output of the SIM model. In the Mdouar catchment in Morocco (635 km^2, Δt = 1 h), Tramblay et al. (2012) also found a high correlation (R^2 ~0.8-0.9) between S and either the antecedent precipitation index or the output of the GR4J daily model, whereas only 4 rain gauges operated over the catchment. This high correlation was probably due to the local oceanic climate, generating large-extended spatial rainfall. The correlation between the event cumulative rainfalls of 2 sites distant from 50 km was estimated to r = 0.96, which is much higher than in the Mediterranean climate. In a larger catchment such as the Wangjiaba catchment in China (30630 km^2, 139 operative rain gauges), under Moonson climate, Yu et al. (2018) found predictive NSE values varying between 0.66 and 0.95 for 24 flood events (Δt = 2 h), when using predicted values of S. But in several Mediterranean catchments, weak correlations or predictive NSE have been found between S and the water content predictors (see in the ATHYS catchment database http://www.athys-soft.org/bassins). It seems to be due to the high spatial variability of the rainfall, and the low density of rain gauges in these catchments. As an example, the Gardon at Anduze (545 km^2, Δt = 1 h) indeed exhibited a weak correlation between S and the SIM output or the base flow ($R^2 < 0.5$). The present study indicates that it could be due to the relatively low density of rain gauges (7 rain gauges) on the catchment.

The R^2 of the relationship between S and w_2 or the base flow is not only affected by the rainfall uncertainties, but also by many other uncertainties, such as the ones related to the base

flow, the w_2, the calibration protocol and the accuracy of the model. As the discharge at the Pont-de-Fer stream gauge was controlled by a downstream spillway, the low flow rating curve was assumed to be stable, and the base flow correctly measured. The calibration of the model was performed in different conditions which showed that the calibrated S values were stable whatever the other parameters values were. The uncertainty on the medium and high flows rating curve could also affect the S values, but this kind of uncertainty should generate a rather systematic than a randomized error, which should not affect the R^2 of the relationships between S and the base flow or w_2. Thus, it was reasonable to assume that the main uncertainty which could affect the relationships between S and the base flow or w_2 was due to the rainfall and that the R^2 mainly reflected this uncertainty.

6. Conclusion

The results of our study proved that SCS-LR model could simulate Mediterranean flash flood with good accuracy. The calibration and the validation of the model were mainly based on the rainfall and runoff data corresponding to 34 events of Real Collobrier catchment in the period of 1968 – 2006. The sensitivity test and parameters dependency test allowed reducing the number of parameters to be calibrated. Some parameters could be set constant for all the events, by considering either numerical properties of the parameters (in case of ds or V_0) or empirical assumptions (for ω'). The maximum water retention S and diffusion time K_0 were calibrated for each event, and the variability of S exhibited a wider impact on the simulated flows than the variability than K_0. K_0 could be set to its median value without significant loss of quality in NSE values, nor change in S values. The variability of S was significantly correlated with the predictors of the basin wetness state: the soil water content and the base flow. The regression coefficient values (R^2) were high for both cases (0.85 and 0.77). The calibration protocol showed that the estimated S values were robust and that the variability of these values was not dependent on the other parameters of the model. The median NSE equals 0.94 when using the optimal calibrated values and reduces to respectively 0.83 and 0.77 when using the predicted S values given by respectively the relationship with the base flow or w_2. These latter values are representative of the accuracy of the model at the event scale, as it can be expected for any further application of the model.

Moreover, the dense rainfall data gave us the possibility to test the effect of the rain gauge density on the calibration and the goodness of the model. The results proved that the reduction of the density of the rain gauges affected both the predictive scores of the model and the calibrated parameters of the model. When using a single rain gauge for the calibration of the model, the estimates of S can vary from 250 to more than 600 mm for initially dry soils, and from 50 to more

than 150 mm for initially wet soils, depending on the selected rain gauge. This result shows that the calibrated parameters could be strongly biased by the density of rain gauges so that the comparison of the calibrated parameters between two catchments would be significant if both catchments have an equivalent density of rain gauges.

The model requires a small number of parameters, and it can be set up with accessible data. Although more research is needed to have a better understanding and to test the ability to apply the model in the other Mediterranean or other types of catchments, this study shows a promising application for flash flood prediction. Further objectives would be to assess the model in other catchments, in the Mediterranean or other climates. Such model has also to be compared to other models, including continuous models. The benefits of the rainfall radar in case of the low density of rain gauges should be investigated.

Acknowledgments

M. Nguyen Quoc Son's Ph.D. grant was funded by the Vietnamese Government and completed by the Service Central de Prévision Hydrométéorologique pour l'Annonce et la Prévision des Inondations (SCHAPI). This work contributed to the Hymex program. The authors are very grateful to IRSTEA for providing the Real Collobrier data through the BDOH database. The authors also thank Meteo-France for having supplied the soil moisture data w_2 over the Real Collobrier.

References

Amponsah, W., Ayral, P.-A., Boudevillain, B., Bouvier, C., Braud, I., Brunet, P., Delrieu, G., et al. (2018) Integrated high-resolution dataset of high-intensity European and Mediterranean flash floods. Earth System Science Data 10(4), 1783–1794. doi:https://doi.org/10.5194/essd-10-1783-2018

Anquetin, S., Braud, I., Vannier, O., Viallet, P., Boudevillain, B., Creutin, J.-D. & Manus, C. (2010) Sensitivity of the hydrological response to the variability of rainfall fields and soils for the Gard 2002 flash-flood event. Journal of Hydrology Flash Floods: Observations and Analysis of Hydrometeorological Controls 394(1), 134–147. doi:10.1016/j.jhydrol.2010.07.002

Aron, G., C. Miller, A. & F. Lakatos, D. (1977) Infiltration Formula Based on SCS Curve Number. ASCE J Irrig Drain Div 103.

Awol, F. S., Coulibaly, P. & Tolson, B. A. (2018) Event-based model calibration approaches for selecting representative distributed parameters in semi-urban watersheds. Advances in Water Resources 118, 12–27. doi:10.1016/j.advwatres.2018.05.013

Berthet, L., Andréassian, V., Perrin, C. & Javelle, P. (2009) How crucial is it to account for the antecedent moisture conditions in flood forecasting? Comparison of event-based and continuous approaches on 178 catchments. Hydrology and Earth System Sciences Discussions (13), 819–831.

Blöschl, G., Reszler, C. & Komma, J. (2008) A spatially distributed flash flood forecasting model. Environmental Modelling & Software 23(4), 464–478. doi:10.1016/j.envsoft.2007.06.010

Boone, A., Calvet, J.-C. & Noilhan, J. (1999) Inclusion of a Third Soil Layer in a Land Surface Scheme Using the Force–Restore Method. J. Appl. Meteor. 38(11), 1611–1630. doi:10.1175/1520-0450(1999)038<1611:IOATSL>2.0.CO;2

Bouvier, C. & Delclaux, F. (1996) ATHYS: a hydrological environment for spatial modelling and coupling with a GIS.

Coustau, M., Bouvier, C., Borrell-Estupina, V. & Jourde, H. (2012) Flood modelling with a distributed event-based parsimonious rainfall-runoff model: case of the karstic Lez river catchment. Natural Hazards and Earth System Sciences 12, 1119–1133.

Delrieu, G., Nicol, J., Yates, E., Kirstetter, P.-E., Creutin, J.-D., Anquetin, S., Obled, C., et al. (2005) The Catastrophic Flash-Flood Event of 8–9 September 2002 in the Gard Region, France: A First Case Study for the Cévennes–Vivarais Mediterranean Hydrometeorological Observatory. J. Hydrometeor. 6(1), 34–52. doi:10.1175/JHM-400.1

Durand, P., Robson, A. & Neal, C. (1992) Modelling the hydrology of submediterranean montane catchments (Mont-Lozère, France) using TOPMODEL: initial results. Journal of Hydrology 139(1), 1–14. doi:10.1016/0022-1694(92)90191-W

Durbude, D. G., Jain, M. K. & Mishra, S. K. (2011) Long-term hydrologic simulation using SCS-CN-based improved soil moisture accounting procedure. Hydrol. Process. 25(4), 561–579. doi:10.1002/hyp.7789

Folton, N., Tolsa, M. & Arnaud, P. (2012) Le Bassin de recherche du Réal Collobrier - Étude des processus hydrologiques en milieu méditerranéen a échelle fine. 50 ans de l'Orgeval, 7 p. Paris, France: IRSTEA. Retrieved from https://hal.archives-ouvertes.fr/hal-00779374

Gaume, E., Livet, M., Desbordes, M. & Villeneuve, J.-P. (2004) Hydrological analysis of the River Aude, France, flash flood on 12 and 13 November 1999. Journal of Hydrology 286, 135–154. doi:10.1016/j.jhydrol.2003.09.015

Geosol / index. (n.d.) . Retrieved October 16, 2018, from https://webapps.gissol.fr/geosol/

Habets, F., Boone, A., Champeaux, J.-L., Etchevers, P., Franchisteguy, L., Leblois, E., Ledoux, E., et al. (2008) The SAFRAN-ISBA-MODCOU hydrometeorological model applied over France. Journal of Geophysical Research: Atmospheres 113(D06113), 18. doi:10.1029/2007JD008548

Huang, M., Gallichand, J., Dong, C., Wang, Z. & Shao, M. (2007) Use of soil moisture data and curve number method for estimating runoff in the Loess Plateau of China. Hydrol. Process. 21(11), 1471–1481. doi:10.1002/hyp.6312

Michel, C., Andréassian, V. & Perrin, C. (2005) Soil Conservation Service Curve Number Method: How to mend a wrong soil moisture accounting procedure? Water Resources Research - WATER RESOUR RES 410. doi:10.1029/2004WR003191

Mishra, S. K. & Singh, V. P. (2013) Soil Conservation Service Curve Number (SCS-CN) Methodology. Springer Science & Business Media.

Moussa, R. & Chahinian, N. (2009) Comparison of different multi-objective calibration criteria using a conceptual rainfall-runoff model of flood events. Hydrol. Earth Syst. Sci. 13(4), 519–535. doi:10.5194/hess-13-519-2009

Nash, J. E. & Sutcliffe, J. V. (1970) River flow forecasting through conceptual models part I — A discussion of principles. Journal of Hydrology 10(3), 282–290. doi:10.1016/0022-1694(70)90255-6

Olivera, F. & Maidment, D. (1999) Geographic Information Systems (GIS)-Based Spatially Distributed Model for Runoff Routing. Water Resources Research - WATER RESOUR RES 35. doi:10.1029/1998WR900104

Parkin, G., O'Donnell, G., Ewen, J., Bathurst, J. C., O'Connell, P. E. & Lavabre, J. (1996) Validation of catchment models for predicting land-use and climate change impacts. 2. Case study for a Mediterranean catchment. Journal of Hydrology 175(1), 595–613. doi:10.1016/S0022-1694(96)80027-8

Piñol, J., Beven, K. & Freer, J. (1997) Modelling the hydrological response of mediterranean catchments, Prades, Catalonia. The use of distributed models as aids to hypothesis formulation. Hydrol. Process. 11(9), 1287–1306. doi:10.1002/(SICI)1099-1085(199707)11:9<1287::AID-HYP561>3.0.CO;2-W

Ponce Victor M. & Hawkins Richard H. (1996) Runoff Curve Number: Has It Reached Maturity? Journal of Hydrologic Engineering 1(1), 11–19. doi:10.1061/(ASCE)1084-0699(1996)1:1(11)

Quintana Seguí, P., Martin, E., Habets, F. & Noilhan, J. (2009) Improvement, calibration and validation of a distributed hydrological model over France. Hydrol. Earth Syst. Sci. 13(2), 163–181. doi:10.5194/hess-13-163-2009

Rao, S. S. (2009) Engineering optimization: theory and practice, 4th ed. Hoboken, N.J: John Wiley & Sons.

Roux, H., Labat, D., Garambois, P.-A., Maubourguet, M.-M., Chorda, J. & Dartus, D. (2011) A physically-based parsimonious hydrological model for flash floods in Mediterranean catchments. Nat. Hazards Earth Syst. Sci. 11(9), 2567–2582. doi:10.5194/nhess-11-2567-2011

Saulnier, G.-M. & Le Lay, M. (2009) Sensitivity of flash-flood simulations on the volume, the intensity, and the localization of rainfall in the Cévennes-Vivarais region (France). Water Resour. Res. 45(10), W10425. doi:10.1029/2008WR006906

Stephens, C. M., Johnson, F. M. & Marshall, L. A. (2018) Implications of future climate change for event-based hydrologic models. Advances in Water Resources 119, 95–110. doi:10.1016/j.advwatres.2018.07.004

Taha, A., M. Gresillon, J. & Clothier, B. (1997) Modelling the link between hillslope water movement and stream flow: Application to a small Mediterranean forest watershed. Journal of Hydrology - J HYDROL 203, 11–20. doi:10.1016/S0022-1694(97)00081-4

Tramblay, Y., Bouaicha, R., Brocca, L., Dorigo, W., Bouvier, C., Camici, S. & Servat, E. (2012) Estimation of antecedent wetness conditions for flood modelling in northern Morocco. Hydrol. Earth Syst. Sci. 16(11), 4375–4386. doi:10.5194/hess-16-4375-2012

Tramblay, Y., Bouvier, C., Martin, C. & Didon-Lescot, J.-F. (2009) Assessment of soil moisture to set the initial conditions of a event-based rainfall-runoff model, Plinius11-35. Presented at the 11th Plinius Conference on Mediterranean Storms, held September 7-10, 2009 in Barcelona, Spain. http://meetings.copernicus.org/plinius11, id.Plinius11-35. Retrieved from http://adsabs.harvard.edu/abs/2009pcms.confE..35T

Tukey, J. W. (1977) Exploratory Data Analysis. Addison-Wesley Publishing Company.

Vincendon, B., Ducrocq, V., Saulnier, G.-M., Bouilloud, L., Chancibault, K., Habets, F. & Noilhan, J. (2010) Benefit of coupling the ISBA land surface model with a TOPMODEL hydrological model version dedicated to Mediterranean flash-floods. Journal of Hydrology Flash Floods: Observations and Analysis of Hydrometeorological Controls 394(1), 256–266. doi:10.1016/j.jhydrol.2010.04.012

Willems, P., Mora, D., Vansteenkiste, T., Taye, M. T. & Van Steenbergen, N. (2014) Parsimonious rainfall-runoff model construction supported by time series processing and validation of hydrological extremes – Part 2: Intercomparison of models and calibration approaches. Journal of Hydrology 510, 591–609. doi:10.1016/j.jhydrol.2014.01.028

Yu, D., Xie, P., Dong, X., Hu, X., Liu, J., Li, Y., Peng, T., et al. (2018) Improvement of the SWAT model for event-based flood simulation on a sub-daily timescale. Hydrology and Earth System Sciences 22(9), 5001–5019. doi:https://doi.org/10.5194/hess-22-5001-2018

Table 1: Main characteristics of the rainfall-runoff events in Pont de Fer. P: cumulated precipitation; CV: coefficient of spatial variation of the precipitation; Vr: runoff volume; Rc: runoff coefficient; Imax: maximal rainfall intensity during one-time step; w_2: volumetric water content of the root layer.

Event	Starting date	Finishing date	P (mm)	No of gauges	CV	Vr ($10^3.m^3$)	Rc (%)	Imax ($mm.h^{-1}$)	Peak flow ($m3.s^{-1}$)	w_2 ($cm^3.cm^{-3}$)	Base flow ($m^3.s^{-1}$)
1	12/4/1968	17/04/1968	142.4	16	0.27	2082.7	17	11.3	30.4	0.21	0.06
2	13/09/1968	15/09/1968	177.2	14	0.18	1025.3	9	64.9	91.4	0.19	0.02
3	2/1/1972	5/1/1972	68.5	11	0.29	1961.5	36	11.6	39.6	0.25	2.33
4	1/2/1972	7/2/1972	125.1	16	0.40	3948.3	37	8.9	40.1	0.23	0.77
5	17/02/1972	23/02/1972	207.8	15	0.25	8864.3	56	13.7	60.7	0.23	1.64
6	13/02/1973	23/02/1973	168.2	15	0.84	3850.8	36	12.5	39.1	0.22	0.44
7	13/10/1973	15/10/1973	104.9	15	0.21	1512.7	19	29.7	45.7	0.22	0.06
8	26/01/1974	5/2/1974	247.8	13	0.32	8920.6	40	12.4	76.6	0.22	0.43
9	12/2/1974	21/02/1974	212.6	13	0.25	8286.4	46	10.6	59.8	0.23	1.22
10	26/02/1974	7/3/1974	163.6	16	0.16	7321.0	53	8.9	63.1	0.24	1.88
11	18/09/1974	22/09/1974	123.6	15	0.27	373.5	4	44.2	44.8	0.15	0
12	5/2/1975	9/2/1975	160.1	12	0.18	3395.4	27	8.1	40.8	0.22	0.12
13	29/01/1976	8/2/1976	260.3	15	0.15	5095.0	22	16.9	39.8	0.21	0.16
14	15/04/1976	19/04/1976	145	12	0.35	4288.4	37	15.4	77.4	0.22	0.31
15	24/10/1976	31/10/1976	318.7	15	0.31	11191.6	44	14.9	68.3	0.24	0.50
16	1/1/1977	3/1/1977	49.1	13	0.25	1966.9	46	7.2	31.5	0.24	3.30
17	6/12/1977	11/12/1977	178.1	13	0.11	3142.4	22	17.5	43.3	0.23	0.13
18	11/1/1978	19/01/1978	244.1	13	0.30	10043.5	49	12.3	77.5	0.23	0.20
19	8/2/1978	13/02/1978	125.9	15	0.26	5467.2	52	8.1	41.6	0.22	0.76
20	25/10/1979	31/10/1979	191.8	12	0.13	6182.4	41	13.6	50.7	0.23	0.21
21	30/11/1984	4/12/1984	77.9	13	0.22	1488.4	22	17.9	31.9	0.23	0.41
22	28/01/1986	7/2/1986	280.5	13	0.23	7037.4	30	13.1	53.7	0.21	0.06
23	13/01/1988	17/01/1988	116.4	14	0.37	3325.5	33	11.1	73.4	0.23	0.30
24	20/04/1993	4/5/1993	221.2	10	0.16	6106.0	31	25.4	38.7	0.21	0.25
25	5/1/1994	9/1/1994	109.6	14	0.16	2400.7	23	15.9	33.5	0.21	0.12
26	1/2/1994	8/2/1994	131.8	15	0.12	4192.2	33	19.3	31.1	0.22	0.64
27	10/1/1996	19/01/1996	147.9	14	0.28	5646.6	54	14.6	48.7	0.24	1.62
28	20/01/1996	31/01/1996	209.4	14	0.29	8816.0	50	12.6	58.3	0.24	1.50
29	6/1/1997	13/01/1997	97.1	13	0.27	3266.7	44	10.2	59.9	0.25	4.05
30	13/11/2000	28/11/2000	176.9	13	0.23	4388.0	29	21.5	29.9	0.24	0.37
31	24/12/2000	29/12/2000	134.6	14	0.22	4107.1	37	21.7	44.1	0.22	0.39
32	24/01/2001	31/01/2001	88.3	13	0.19	2749.5	22	9.2	33.4	0.23	0.83
33	5/9/2005	12/09/2005	231.4	8	0.35	2541.8	10	64.2	60.9	0.15	0.003
34	26/01/2006	1/2/2006	202.7	13	0.32	5760.2	34	16.7	34.5	0.22	0.15

Table 2: Correlation matrix calculated with rain-gauge data of events. NA = not available when there is no common event at both gauges.

Gauge	1	2	3	4	5	6	7	8	9	10	11	12	13	14	15	16	17
1	1.00																
2	0.91	1.00															
3	0.92	0.89	1.00														
4	0.93	0.96	0.91	1.00													
5	0.83	0.88	0.89	0.89	1.00												
6	0.88	0.92	0.69	0.81	0.73	1.00											
7	0.95	0.89	0.94	0.86	0.93	0.70	1.00										
8	0.82	0.77	0.48	0.58	0.42	0.90	0.49	1.00									
9	0.94	0.97	0.76	0.91	0.59	0.47	0.91	0.14	1.00								
10	0.91	0.90	0.63	0.81	0.75	0.61	0.87	0.29	0.95	1.00							
11	0.84	0.83	0.51	0.67	0.75	0.61	0.88	0.36	0.92	0.84	1.00						
12	0.90	0.90	0.75	0.82	0.69	0.59	0.83	0.37	0.94	0.90	0.91	1.00					
13	0.90	0.84	0.76	0.75	0.71	0.89	0.82	0.84	0.72	0.71	0.69	0.67	1.00				
14	0.85	0.90	0.69	0.86	0.88	0.64	0.89	0.36	0.93	0.84	0.87	0.88	0.66	1.00			
15	0.96	0.94	0.97	0.95	0.91	0.80	0.93	0.62	0.78	0.82	0.72	0.80	0.81	0.81	1.00		
16	0.77	0.78	0.60	0.70	0.68	0.51	0.72	0.35	0.79	0.80	0.78	0.89	0.61	0.85	0.68	1.00	
17	0.91	0.85	0.97	0.85	0.94	0.93	0.96	0.94	NA	NA	0.72	0.79	0.95	0.82	0.97	0.47	1.00

1 – Babaou, 2 – Bonnaux, 3 – Anselme, 4 – Guerin, 5 – Mouton, 6 – Fourches, 7 – Lambert, 8 – Louviere, 9 – Martels, 10 – Bourjas, 11 – Peyrol, 12 – Portaniere, 13 – Rimbaud, 14 – Vaudreches, 15 – Bourdins, 16 – Davids, 17 – Boussic

Table 3: Results of the split sample tests performed with the two predictors (w_2 index, base flow Qb). "a", "b" and "R^2" are respectively the slope, the intercept and the determination coefficient of the regression designed between the initial condition S and the given predictor using the events of the calibration sample.

Predictors	Calibration events	Validation events	a	b	R^2	Median predictive NSE for calibration	Median predictive NSE for validation
w_2	1-22	23-34	-2429.9	835	0.71	0.78	0.83
	1-11,23-34	12-22	-2740.2	797.45	0.90	0.88	0.76
	12-34	1-11	-2680.4	788.36	0.69	0.71	0.71
Log_{10}Qdeb	1-22	23-34	-81.77	140.73	0.85	0.89	0.76
	1-11,23-34	12-22	-77.49	153.51	0.87	0.9	0.78
	12-34	1-11	-88.91	146.05	0.83	0.81	0.92

Table 4: Results of using each rain gauge performed with the three predictors (w_2 index, base flow Qb). "a", "b" and "R2" are respectively the slope, the intercept and the determination coefficient of the regression established between the initial condition S and the given predictor using the events of the calibration sample.

Gauge	# Events available	Median *S*	*W2*			Base flow		
			a	b	R^2	a	b	R^2
All	34	181.0	-2924.91	839.52	0.77	-85.30	145.85	0.85
Babaou	28	197.8	-2961.43	858.72	0.65	-90.49	154.05	0.76
Bonnaux	27	191.7	-3324.64	919.27	0.72	-97.20	129.07	0.79
Anselme	24	244.8	-2027.36	692.43	0.27	-64.51	207.92	0.42
Guerin	28	215.5	-2782.46	827.45	0.59	-79.37	167.31	0.61
Mouton	25	225.1	-5479.90	1465.77	0.27	-148.82	169.17	0.41
Fourches	27	197.4	-5204.81	1385.53	0.23	-135.17	156.16	0.39
Lambert	26	184.1	-2328.31	704.18	0.51	-66.07	153.42	0.63
Louviere	27	252.7	-2124.46	724.16	0.29	-68.85	215.55	0.39
Martels	15	153.6	-2421.10	683.62	0.64	-69.67	113.06	0.77
Bourjas	18	182.4	-4423.16	1152.60	0.87	-113.00	115.49	0.91
Peyrol	25	119.6	-2020.89	571.91	0.6	-55.28	95.13	0.68
Portaniére	26	143.6	-3365.36	890.62	0.71	-85.63	99.40	0.74
Rimbaud	29	221.9	-2321.87	735.02	0.41	-73.25	181.66	0.52
Vaudreches	26	136.6	-5648.03	1412.75	0.63	-140.77	79.17	0.68
Bourdins	21	233.4	-2557.44	798.06	0.41	-69.58	194.86	0.47
Davids	28	111.8	-2124.44	586.36	0.52	-59.78	83.17	0.64
Boussic	11	233.8	-2304.99	743.57	0.67	-74.80	199.50	0.69

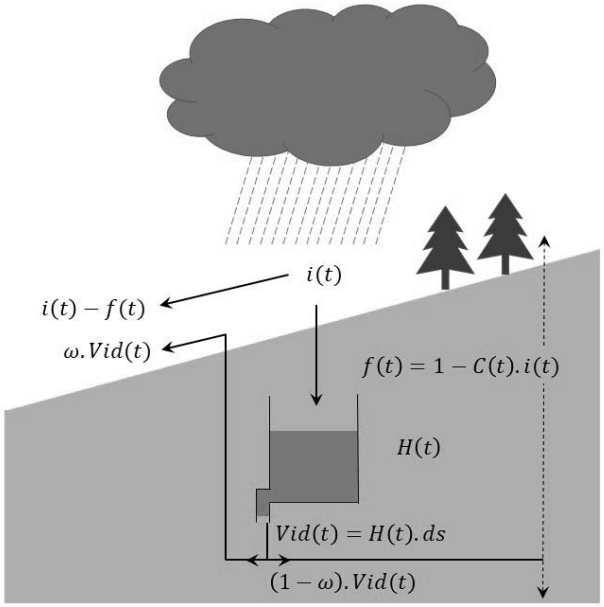

Figure .1: Modified Soil Conservation Service (SCS) model operating for each mesh of the basin (from www.athys-soft.org).

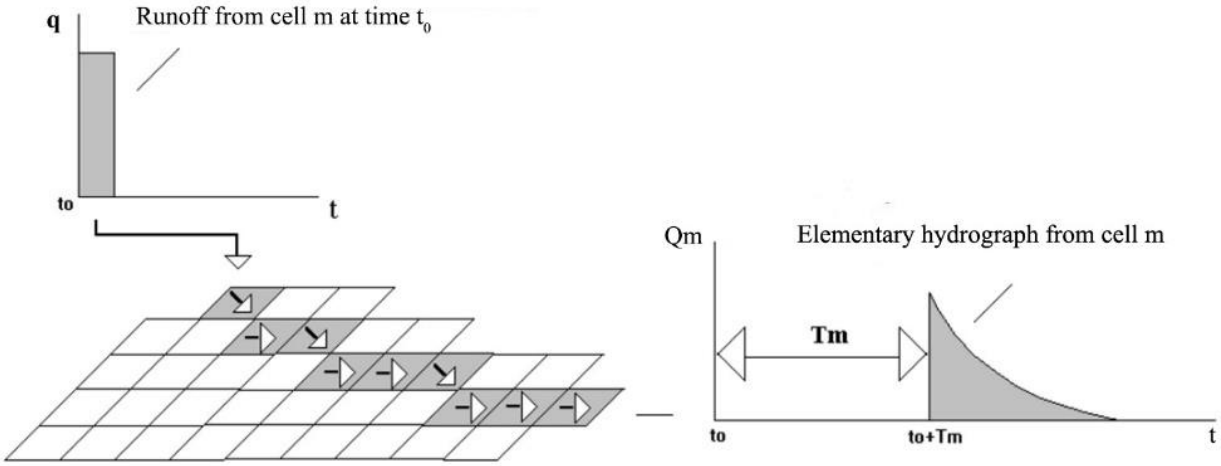

Figure 2: Lag-and-Route model operating for each mesh of the basin.

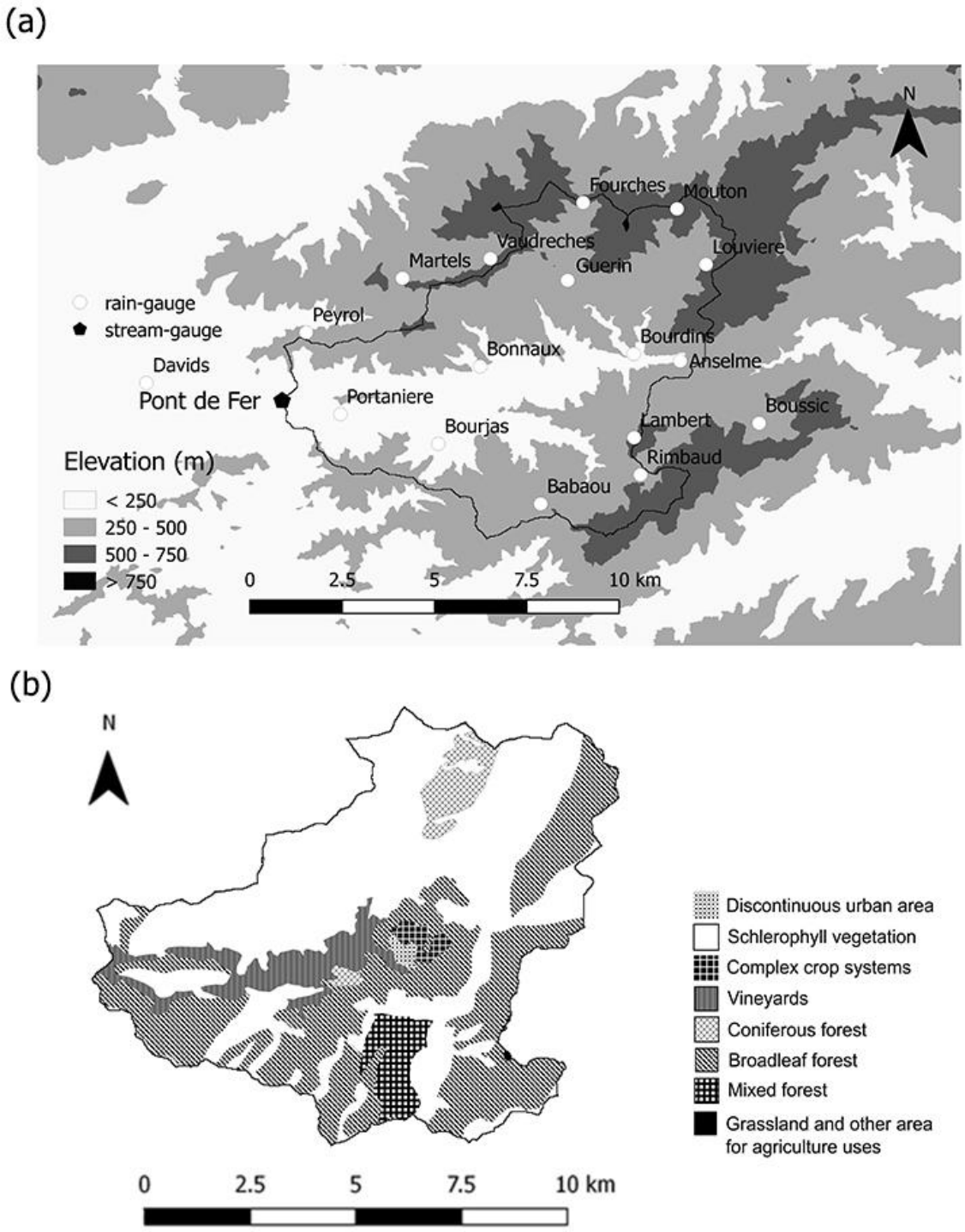

Figure 3: Maps of the Real Collobrier catchment: (a) Relief (from IGN ALTI database at 25m spatial resolution) and rain gauges location, (b) Land use (from Corine Land Cover database).

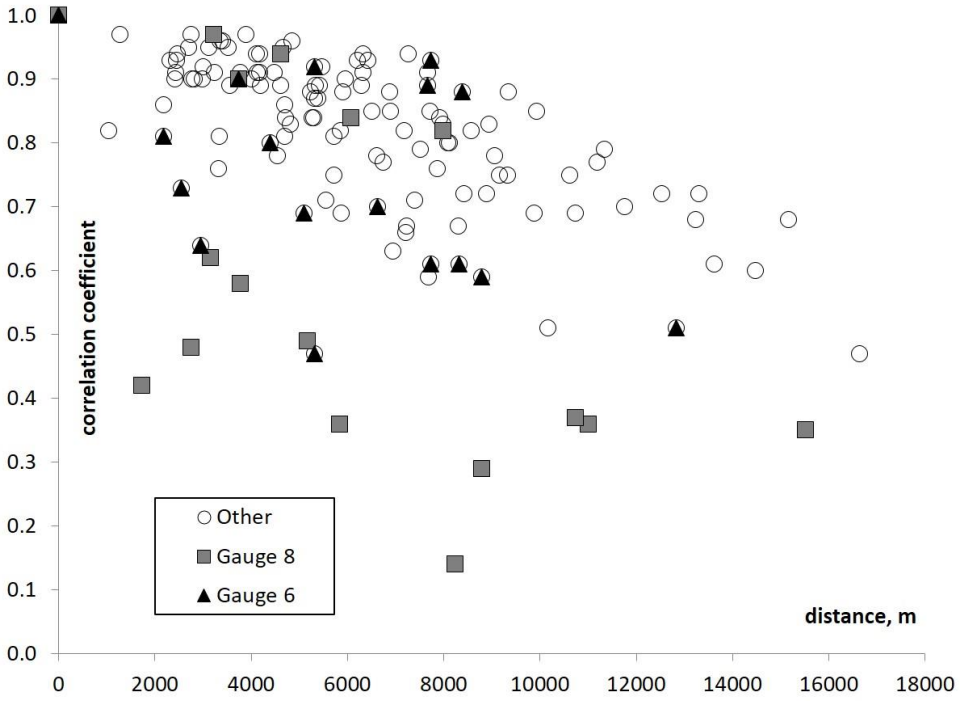

Figure 4: Correlation coefficients between the rainfall amounts measured for the 34 events at each rain gauge. Gauges 6 and 8 were the worst correlated gauges to the other ones.

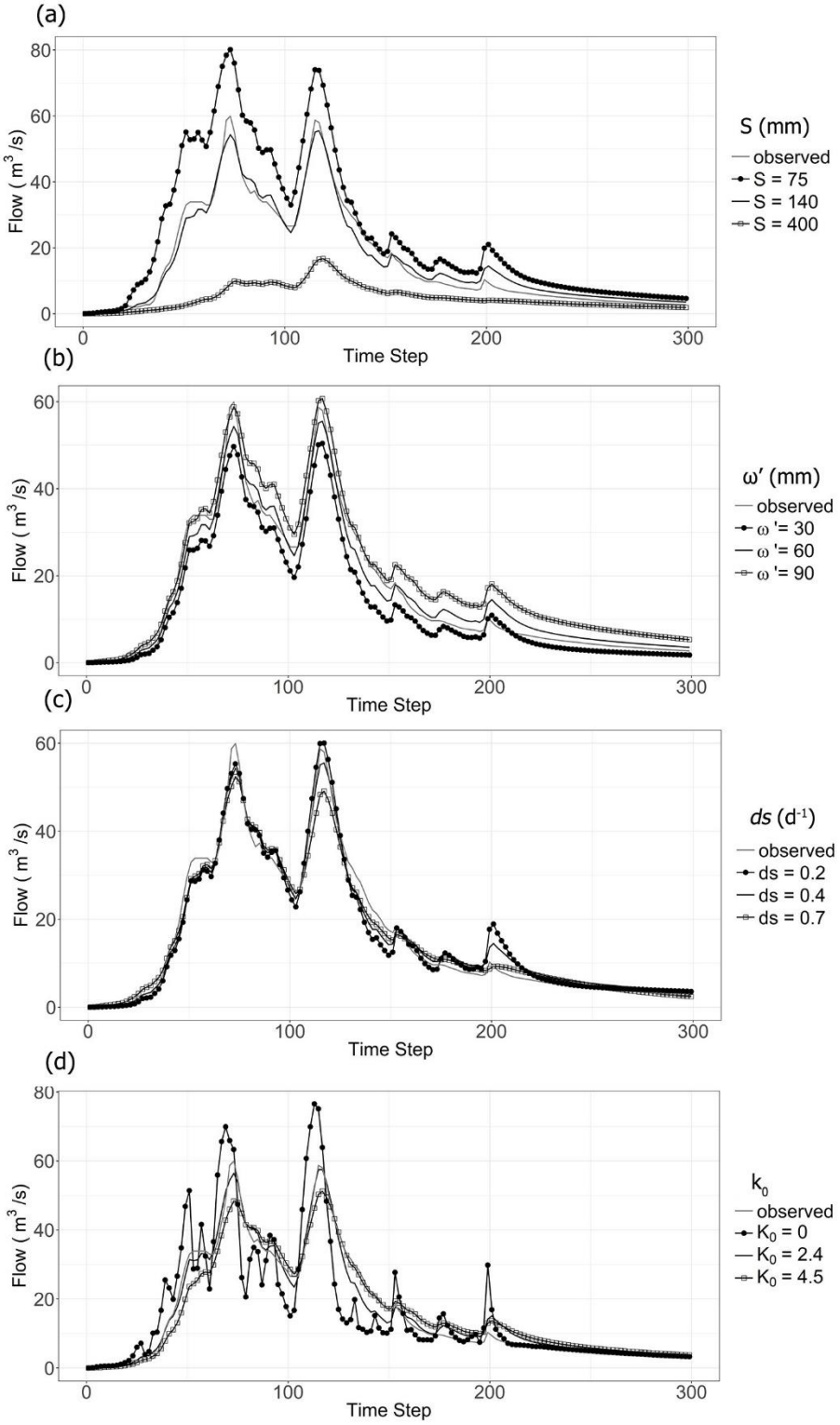

Figure 5: Sensitivity of the model to the parameters S, ’, ds, K_0, event n°5. (a): S parameter, (b): ω’ parameter, (c): ds parameter, (d): K_0 parameter. The plotted hydrographs were obtained by modifying each parameter from a reference set of parameters (S =140 mm, ω’=60 mm, ds = 0.4 d-1, V_0 = 2.5 m.s-1, K_0= 3).

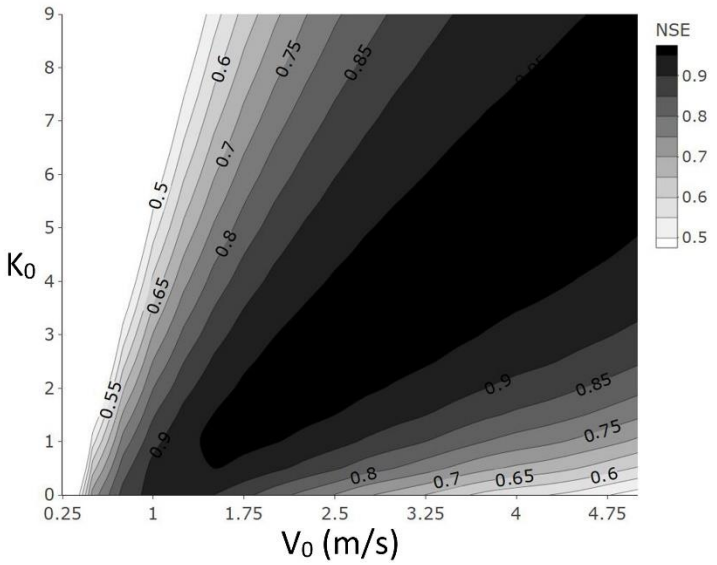

Figure 6 : NSE values depending on V_0 and K_0 (the other parameters were S = 140 mm, ω' = 60 mm, ds = 0.4 d^{-1}), event n°5. The wide area where NSE > 0.8 showed a high dependency between V_0 and K_0 parameters.

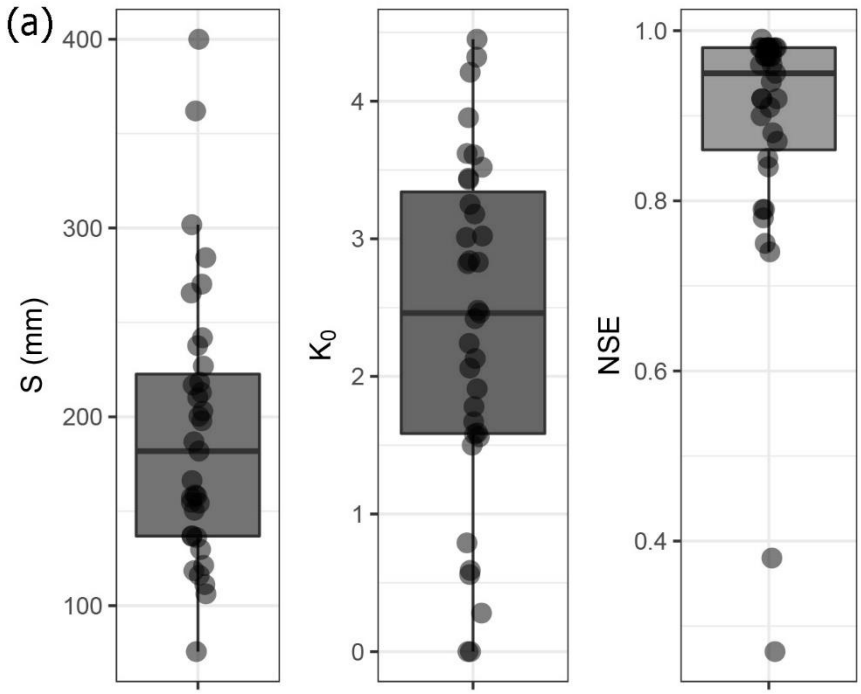

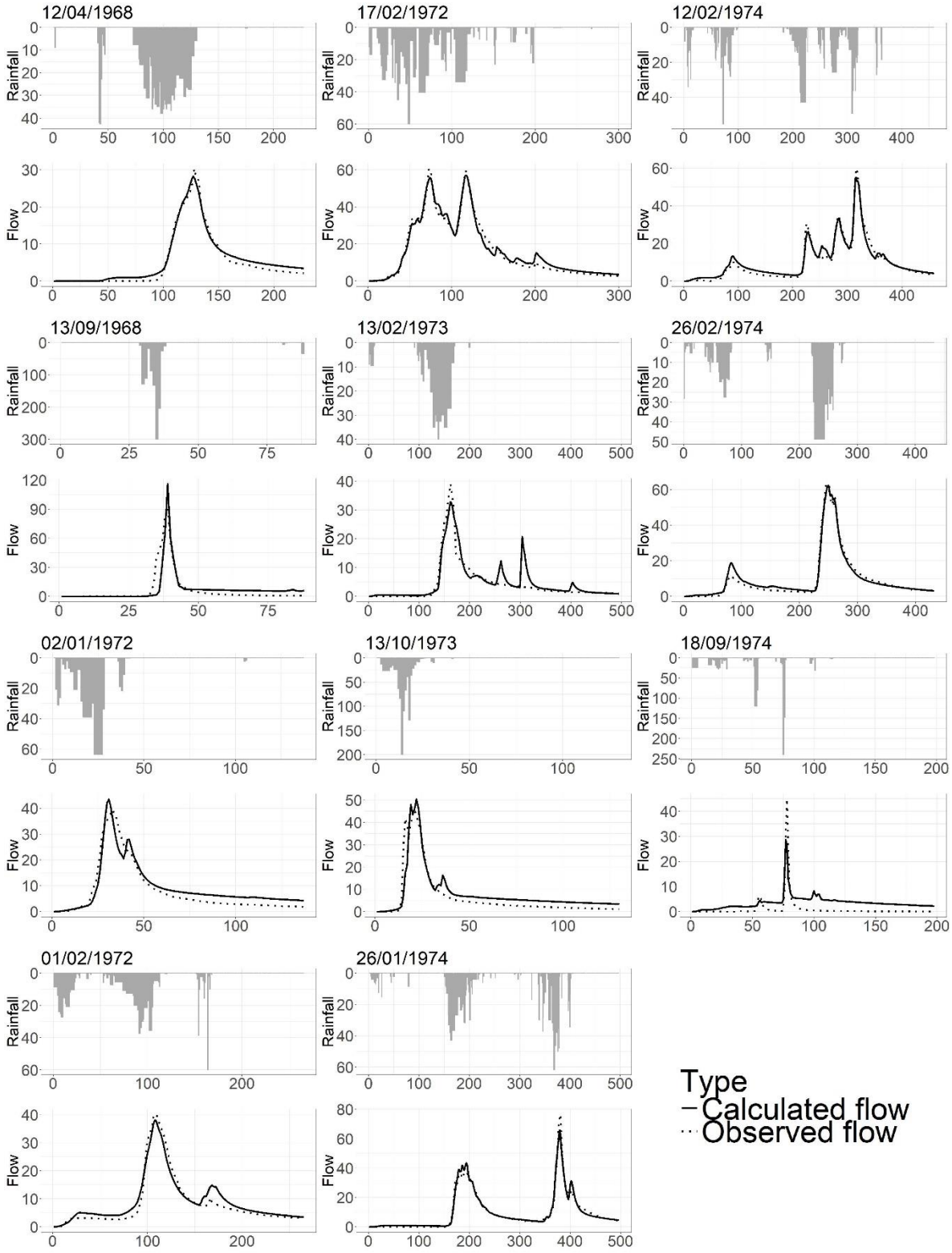

Figure 7 : Calibration results (a): Calibrated values of S and K_0 and corresponding NSE for the events, (b): Observed and simulated hydrographs at the 30-minutes time step for the first 11 events, the plotted rain corresponded to the rainfall measured in gauge 4 (Guérin) located near the center of the catchment.

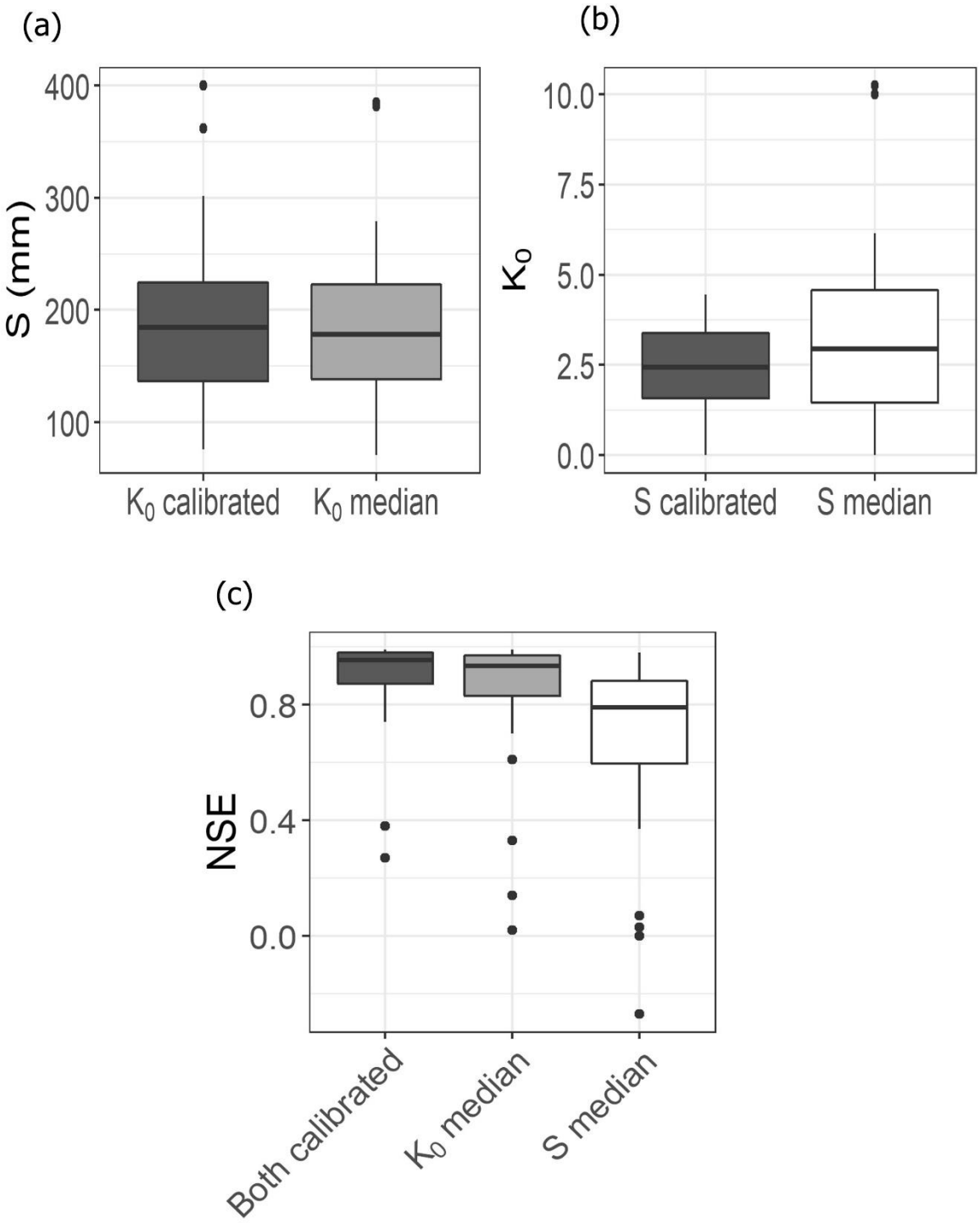

Figure 8: Sensitivity of the model to the variability of each parameter. (a): calibrated S when using either median or calibrated K_0, (b): calibrated K_0 when using either median or calibrated S, (c): corresponding NSE values. The box plots feature median, upper and lower quartiles, (Q_3 and Q_1, respectively), minimum and maximum values without outliers, and outliers (outliers are defined as data points that fall out of the range [Q_1-1.5(Q_3-Q_1), Q_3+1.5*(Q_3-Q_1)] (Tukey, 1977)*

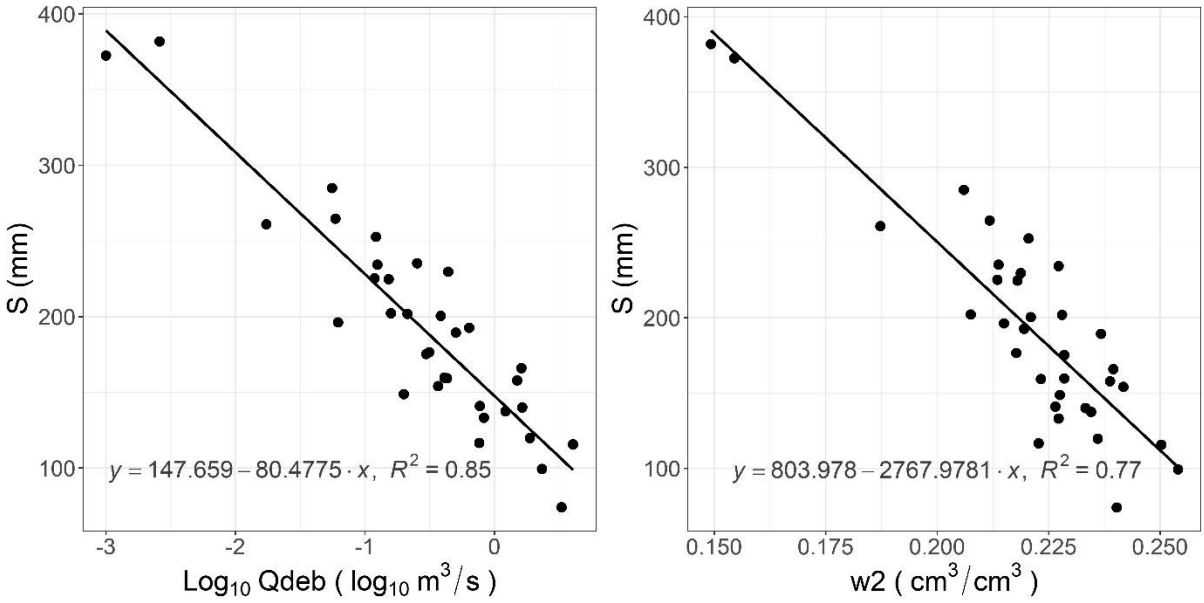

Figure 9: Relationship between S calibrated values and base flow (a), between S calibrated values and volumetric water content w_2 (b).

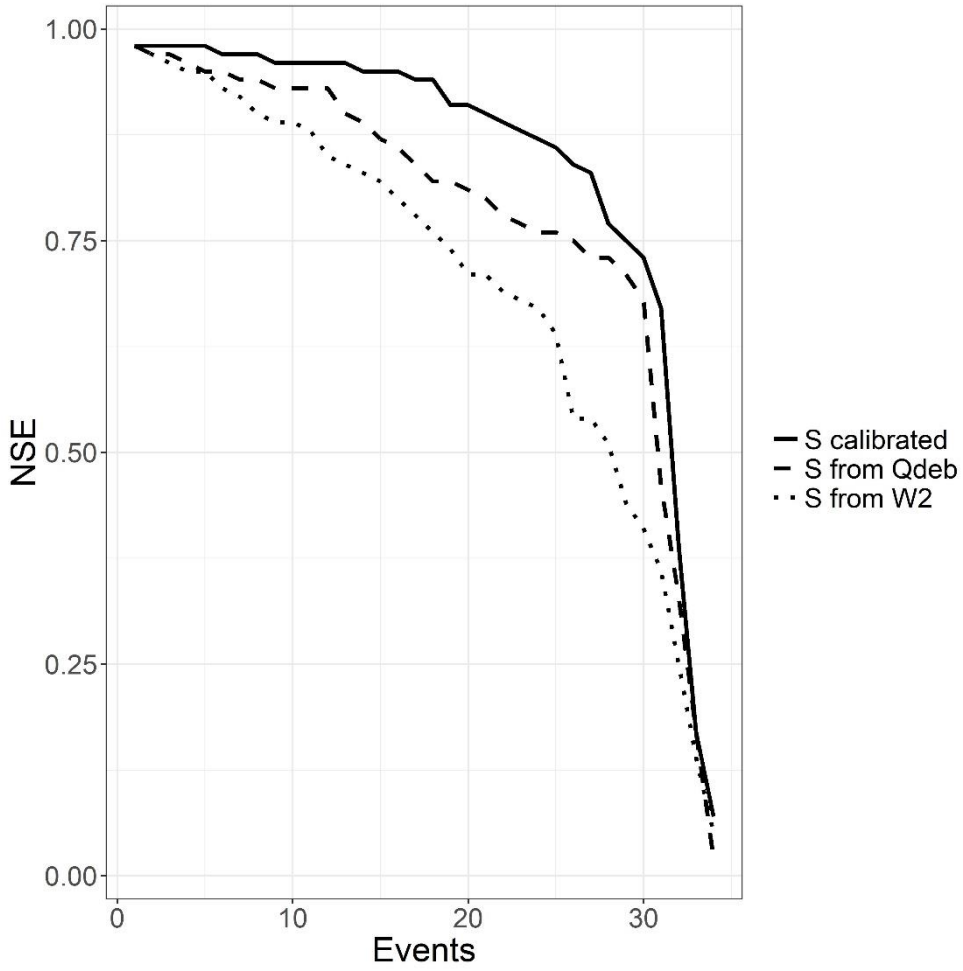

Figure 10: NSE value when using either S calibrated, S derived from w_2 index or from base flow. The NSE values are sorted in descendant order for the 34 events.

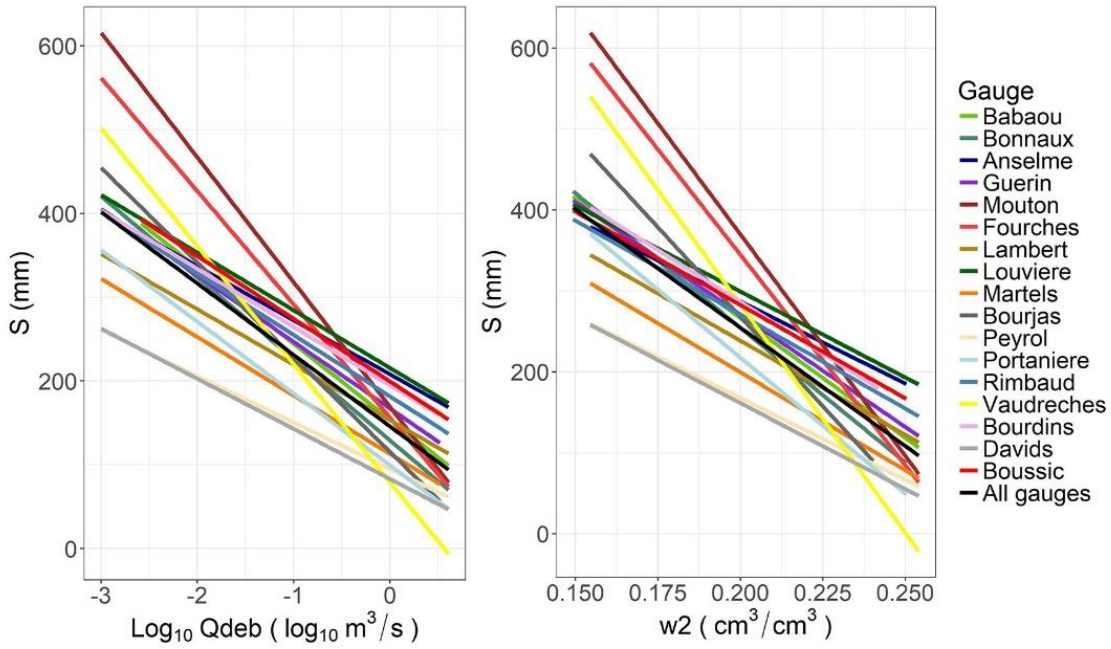

Figure 11: Relationship between S and base flow (a) and between S and w_2 (b) when using all gauges or only one gauge for the model calibration. The regression obtained when using all the gauges was presented in black, while the regression obtained by using each single gauge were shown in colors.

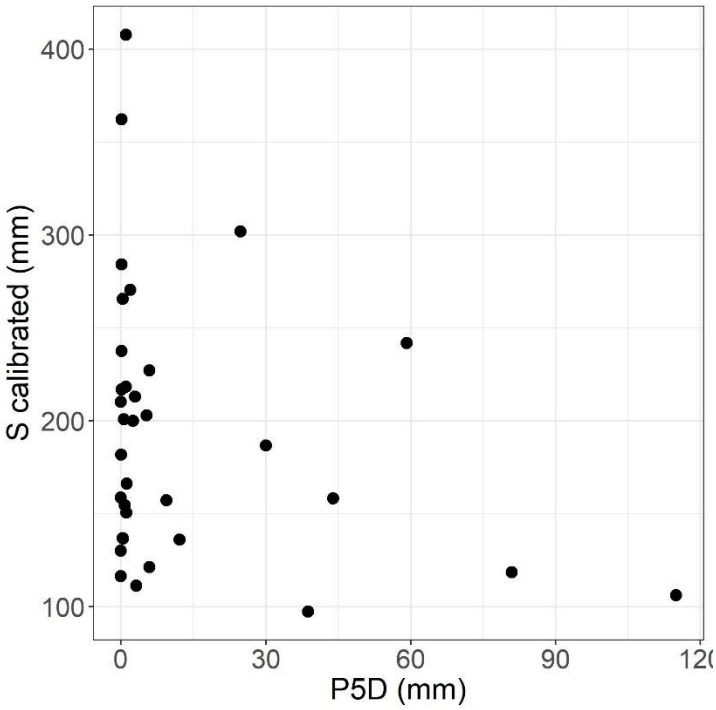

Figure 12: Comparison between calibrated S values and 5-days previous rainfall amounts P5D, for the 34 events